NASA-CR-166,089

NASA Contractor Report 166089
FAA Report DOT/FAA/CT-83-23

Analytical Modeling of Transport Aircraft Crash Scenarios To Obtain Floor Pulses

NASA-CR-166089
1983 00 16217

Gil Wittlin
Dave Lackey

LOCKHEED-CALIFORNIA COMPANY
BURBANK, CALIFORNIA

CONTRACT NO. NAS1-16083
April 1983

LIBRARY COPY

MAY 16 1983

LANGLEY RESEARCH CENTER
LIBRARY, NASA
HAMPTON, VIRGINIA

NASA
National Aeronautics and
Space Administration

Langley Research Center
Hampton, Virginia 23665

U.S. Department
of Transportation

Federal Aviation
Administration

Technical Center
Atlantic City Airport, N.J. 08405

NF02218

NASA Contractor Report 166089
FAA Report DOT/FAA/CT-83-23

Analytical Modeling of Transport Aircraft Crash Scenarios To Obtain Floor Pulses

Gil Wittlin
Dave Lackey

LOCKHEED-CALIFORNIA COMPANY
BURBANK, CALIFORNIA

CONTRACT NO. NAS1-16083
April 1983

National Aeronautics and
Space Administration

Langley Research Center
Hampton, Virginia 23665

U.S. Department
of Transportation

Federal Aviation
Administration

Technical Center
Atlantic City Airport, N.J. 08405

N83-24488#

This Page Intentionally Left Blank

FOREWORD

This report was prepared by the Lockheed-California Company, under contract NAS1-16083, sponsored by the Federal Aviation Administration Technical Center and NASA Langley. The report describes the effort performed from November 1981 through July 1982. The work was administered under the direction of C. Caiafa (FAA) and Dr. R. Thomson (NASA).

The Lockheed-California Company effort was performed by Gil Wittlin with support from D. Lackey. The Lockheed effort was performed within the Dynamics and Vibration Group, supervised by R.E. Donham.

This Page Intentionally Left Blank

SUMMARY

Transport aircraft candidate crash scenarios were analyzed with Program KRASH. Aircraft floor pulses and seat occupant responses are presented. The study included 1) an evaluation of L1649 measured floor pulses during a six-degree slope impact test, 2) an assessment of mass and size effects on the peak responses, 3) analyses to determine responses of wide-body aircraft candidate crash scenarios, 4) an evaluation of FAA-CAMI passenger seat test results and, 5) an assessment of seat performance during potential crash environments. A procedure by which crash environment dynamic pulses can be related to equivalent step pulses and to static loads is demonstrated.

Results of the study lead to the following conclusions:

1. Longitudinal-only pulses can be represented by equivalent step inputs and/or static requirements. Equivalences for vertical-only and combined loading need to be determined. A prime occurrence of failure for seats subjected to lateral loads is at the seat leg attachment to the seat track.

2. The L1649 crash test floor longitudinal pulse for the aft direction (forward inertia) is less than 9g static or an equivalent 5g step pulse. The larger widebody floor pulse magnitudes are expected to be lower than for the corresponding smaller narrow-body aircraft. Aft inertia accelerations are extremely small (<3g transient) for representative crash scenarios. Floor transient acceleration pulses in the vertical, lateral and combined loading directions need to be analyzed with regard to seat-occupant performance using calibrated analytical models.

3. A viable procedure to relate crash scenario floor pulses to standard laboratory test data using current state-of-the-art analysis and test procedures has been demonstrated.

Recommendations are presented with regard to extending current analysis capability and performing additional tests to support and verify analytical methodology.

This Page Intentionally Left Blank

TABLE OF CONTENTS

Section		Page
	FOREWORD	iii
	SUMMARY	v
	LIST OF FIGURES	ix
	LIST OF TABLES	xv
1	INTRODUCTION	1-1
2	CANDIDATE CRASH SCENARIOS	2-1
3	TRANSPORT CATEGORY AIRPLANE FLOOR PULSE DATA	3-1
3.1	Full-Scale Crash Test Conditions	3-1
3.2	L1649 Floor Pulse Test Data	3-4
4	FLOOR PULSE ANALYSIS	4-1
4.1	KRASH Models	4-1
4.2	L1649 Crash Test Analyses	4-13
4.3	Comparison of Wide-Body and Narrow-Body Analysis Results	4-24
5	WIDE-BODY CANDIDATE CRASH ANALYSIS	5-1
5.1	Candidate Crash Scenarios	5-1
5.2	Fuselage Structural Arrangement	5-6
5.3	KRASH Model	5-8
5.4	Ground-to-Ground Overrun (GGO) Scenario	5-12
5.5	Air-to-Ground Hard Landing (AGHL) Scenario	5-22
5.6	Air-to-Ground Impact (AGI) Scenario	5-33
6	MASS AND SIZE SCALING TRENDS	6-1
7	TRANSPORT SEAT TEST PERFORMANCE	7-1
7.1	FAA CAMI Test/Seat Configuration Description	7-1
7.2	Evaluation of Test Results	7-1
7.3	Seat Test versus Analysis Results	7-21
8	SEAT-OCCUPANT PERFORMANCE IN A CRASH ENVIRONMENT	8-1
9	SUMMARY OF RESULTS	9-1
9.1	Overall Program	9-1
9.2	Existing Floor Pulse Data	9-1

TABLE OF CONTENTS (Continued)

Section		Page
9.3	Analysis of L-1649 Six Degree Slope Impact	9-3
9.4	Wide-Body Airplane Candidate Crash Scenario Analysis	9-7
9.5	Mass-Size Scaling Trends	9-11
9.6	Transport Seat Test Evacuation	9-11
9.7	Seat/Occupant Performance	9-12
9.8	Limitations of Analyses	9-19
9.9	Proposed Verification Program	9-20
10	CONCLUSIONS AND RECOMMENDATIONS	10-1
	REFERENCES	R-1

LIST OF FIGURES

Figure		Page
1-1	NTSB and worldwide accident summary data	1-2
1-2	Injury distribution as related to airplane design, airport off-runway hazards and accident avoidance procedures	1-5
1-3	Transportation fatalities, 1980-81	1-6
1-4	Trend of accidents rates, USA versus the world and jet vs. nonjets	1-7
1-5	Input pulse amplitude and duration to produce a 9 g peak response for a single degree of freedom system	1-9
1-6	Task V program flow diagram	1-10
2-1	Comparison of crash scenario parameters	2-4
3-1	Comparison of peak decelerations	3-2
3-2	Effect of airplane configuration on variation of maximum longitudinal acceleration with impact angle	3-3
3-3	L-1649 crash test velocity - time history	3-5
3-4	Location of floor level accelerometers for X, Y and Z recordings, L1649 crash test	3-6
3-5	Floor longitudinal accelerations, L1649 test, 6° slope impact	3-7
3-6	Floor vertical accelerations, L1649 test, 6° slope impact	3-8
3-7	Floor longitudinal acceleration, L1649 tests, 20° slope impact	3-9
3-8	Floor vertical accelerations, L1649 test, 20° slope impact	3-10
3-9	First-order KRASH filter response characteristics	3-11
3-10	L1649 floor longitudinal pulse at FS685, filtered and unfiltered	3-12
3-11	L1649 floor vertical pulse at FS685, filtered and unfiltered	3-13

LIST OF FIGURES (Continued)

Figure		Page
4-1	Effect of position in airplane and airplane configuration on maximum normal accelerations during unflared landing crashes	4-2
4-2	Transport category airplane analytical airframe model concept	4-4
4-3	Variation in number of airframe fuselage masses	4-5
4-4	Single-row floor analytical models	4-7
4-5	Triple-row floor analytical model	4-8
4-6	Seat/occupant models for 1 and 3 passenger representations	4-9
4-7	Two passenger seat/occupant model	4-9
4-8	Deceleration forces on the body	4-14
4-9	Longitudinal acceleration versus fuselage location, 6-degree slope impact, narrow-body airplane	4-15
4-10	Vertical acceleration versus fuselage location, 6-degree slope impact, narrow-body airplane	4-16
4-11	Longitudinal acceleration versus fuselage location, 20 degree slope impact, narrow-body airplane	4-19
4-12	Vertical acceleration versus fuselage location, 20 degree slope impact, narrow-body airplane	4-20
4-13	Longitudinal acceleration versus fuselage location, 20 degree slope impact, narrow-body airplane	4-21
4-14	Vertical acceleration versus fuselage location, 20 degree slope impact, narrow-body airplane	4-22
4-15	Longitudinal acceleration versus fuselage location, 6 degree slope impact, wide-body airplane, rigid ground	4-25
4-16	Vertical acceleration versus fuselage location, 6 degree slope impact, wide-body airplane, rigid ground	4-26
4-17	Longitudinal acceleration versus fuselage location, 6 degree slope impact, wide-body airplane, flexible ground	4-27
4-18	Vertical acceleration versus fuselage location, 6 degree slope impact, wide-body airplane, flexible ground	4-28
4-19	Fuselage shear and bending loads, 6-degree slope, wide-body airplane	4-29

LIST OF FIGURES (Continued)

Figure		Page
4-20	Comparison of wide-body and narrow-body fuselage configurations	4-33
5-1	Ground-to-ground, overrun crash scenario sequence	5-2
5-2	Air-to-ground, hard landing crash scenario sequence	5-3
5-3	Air-to-ground, impact crash scenario sequence	5-4
5-4	Fuselage structural arrangement	5-6
5-5	Forward sections structure	5-9
5-6	Fuselage mid-section structure	5-10
5-7	Wing center section FS 983-1163	5-11
5-8	Keelson structure	5-11
5-9	KRASH model arrangement showing beam and mass identification	5-15
5-10	Airframe responses, ground-to-ground overrun GGO-328-2	5-16
5-11	Airframe responses, ground-to-ground overrun GGO-328-3	5-17
5-12	Airframe responses, ground-to-ground overrun GGO-328-6	5-18
5-13	Longitudinal acceleration versus fuselage location, overrun	5-19
5-14	Vertical acceleration versus fuselage location, overrun	5-20
5-15	Fuselage shear and bending loads, overrun	5-21
5-16	Airframe responses, air-to-ground hard landings, AGHL-358-1	5-25
5-17	Airframe responses, air-to-ground hard landings, AGHL-358-2	5-26
5-18	Airframe responses, air-to-ground hard landings, AGHL 358-3	5-27
5-19	Airframe responses, air-to-ground hard landings, AGHL 358-4	5-28
5-20	Airframe response, air-to-ground hard landings, AGHL 358-5	5-29
5-21	Longitudinal acceleration versus fuselage location, 20 ft/sec hard landing, 0-degree, 6-degree, 15-degree pitch	5-31
5-22	Vertical acceleration versus fuselage location, 20 ft/sec hard landing, 0-degree, 6-degree, 15-degree pitch	5-32
5-23	Envelope of sink speed versus roll angle	5-33

LIST OF FIGURES (Continued)

Figure		Page
5-24	Airframe responses, air-to-ground impact AGI-358-2	5-36
6-1	Transport airplane vs takeoff G.W.	6-2
6-2	Peak acceleration versus airplane size and weight	6-6
6-3	Airframe response, stub wing configuration F.S. 460	6-7
6-4	Airframe response, stub wing configuration, F.S. 600	6-8
6-5	Airframe response, stub wing configuration, F.S. 685	6-8
6-6	Airframe response, stub wing configuration, F.S. 923	6-9
7-1	FAA-CAMI planned test conditions	7-2
7-2	Comparison of KRASH results for different dynamic pulses	7-8
7-3	Comparison of seat-occupant test and analysis results, $-6G_x$ step pulse	7-22
7-4	Comparison of test and analysis longitudinal reaction forces, $-6G_x$ ramped (.030) step pulse	7-23
7-5	Comparison of test and analysis vertical reaction forces, $-6G_x$ ramped (.030) step pulse	7-24
7-6	Comparison of test and analysis lap belt loopoads $-6G_x$ ramped (.030) step pulse	7-25
7-7	Comparison test and analysis pelvis and chest accelerations, $-6G_x$ ramped (.030) step pulse	7-26
7-8	Occupant motion history, analysis of $-6G_x$ step pulse	7-27
8-1	Longitudinal pulses, classes "B", "C" and "E" stub wing configurations, 6-degree slope impact	8-2
8-2	Longitudinal pulses, ground-to-ground overruns, GGO-328-1, -3, -5, flexible ground	8-2
8-3	Longitudinal pulses, ground-to-ground overruns GGO-328-2, -4, -6, rigid ground	8-3
8-4	Longitudinal pulse, L1649 6-degree slope impact test, F.S. 925	8-3
8-5	Equivalent $-G_x$ ramped step input for analytically obtained ground overrun pulses	8-4
8-6	Floor vertical pulses, AGHL-358-1	8-7
8-7	Floor vertical pulses, AGHL 358-2	8-7
8-8	Floor vertical pulses, AGHL 358-3	8-8
8-9	Floor vertical pulses, AGHL 358-4	8-8

LIST OF FIGURES (Continued)

Figure		Page
8-10	Floor vertical pulses, AGHL 358-5	8-9
8-11	Floor vertical pulse, L1649 stub wing	8-9
8-12	Equivalent $-G_z$ ramped step input for analytically obtained hard landing pulses	8-10
8-13	Floor vertical pulse, ground-to-ground overruns GGO-328-1, -5 and -6	8-12
8-14	Fuselage shear and bending moment versus allowables as a function of passenger region, ground-to-ground overruns	8-13
8-15	Fuselage shear and bending moment versus allowables, as a function of passenger region, air-to-ground hard landings	8-14
9-1	Overall program summary	9-2
9-2	L1649 unfiltered & filtered floor pulse test data, longitudinal direction	9-4
9-3	L1649 floor pulse unfiltered and filtered test data, vertical direction	9-5
9-4	Comparison of unfiltered passenger floor peak accelerations as a function of ground and crushing presentations	9-6
9-5	Simultaneous accelerations, ground-to-ground symmetrical overruns	9-8
9-6	Simultaneous accelerations, air-to-ground symmetrical hard landings	9-9
9-7	Simultaneous accelerations, unsymmetrical impact conditions	9-10
9-8	Acceleration versus time duration, longitudinal $-G_x$ loading (test no. 3) condition	9-13
9-9	Acceleration versus time duration, 30 degree yaw (test no. 8) condition	9-14
9-10	Acceleration versus time duration, 9:4.5:1.5 loading (test no. 10) condition	9-15
9-11	Potential improved body block design	9-16
9-12	Dynamic response factor curves for triangular pulse	9-18
9-13	Dynamic response factor curves for ramped step pulse	9-18
9-14	Flow diagram - proposed verification program	9-21
10-1	Crash Environment Analyses Conclusions	10-3/4
10-2	Seat - Occupant Performance Conclusions	10-5/6

This Page Intentionally Left Blank

LIST OF TABLES

Table		Page
1-1	Comparison of Fatal Accident Percentages for NTSB and Worldwide Accident Summaries	1-3
2-1	Identification of Candidate Crash Scenarios	2-2
3-1	Summary of Transport Category Aircraft Full-Scale Crash Test Conditions	3-2
3-2	L1649 Test Floor Pulse Data	3-15
4-1	Model Size and Costs	4-10
4-2	Range of Model Requirements	4-10
4-3	Matrix of Analysis Conditions, 6 and 20-degree slope impacts	4-12
4-4	L1649 6-Degree Slope Impact Unfiltered Responses	4-18
4-5	Summary of Narrow-Body and Wide-Body Analytically Obtained Responses, 6-Degree Slope Impact, Rigid Ground	4-30
4-6	Comparison of Narrow-Body and Wide-Body Analytically Obtained Responses, 6-Degree Slope Impact, Flexible Ground	4-31
5-1	Matrix of Candidate Crash Scenario Conditions	5-5
5-2	Matrix of Analysis Conditions, Wide-Body Ground-to-Ground Candidate Crash Scenario	5-13
5-3	Summary of Ground-to-Ground Analysis Results	5-14
5-4	Matrix of Analysis Conditions, Wide-Body Hard Landing Crash Scenarios	5-23
5-5	Summary of Air-to-Ground Hard Landings Analysis Results	5-24
5-6	Matrix of Analysis Conditions, Wide-Body Air-to-Ground Impact Crash Scenarios	5-34
5-7	Summary of Air-to-Ground Impact Analysis Results	5-35
6-1	Airplane Size and Weight Characteristics	6-3
7-1	FAA-CAMI Test Seat Configurations	7-3
7-2	Summary of FAA-CAMI Seat Configuration/Test Condition Combinations	7-4

LIST OF TABLES (Continued)

Table		Page
7-3	Summary of Loads, Test Conditions 1 and 3, Static versus Dynamic $-G_x$	7-6
7-4	Comparison of Test Results, Test Conditions 1 and 3, static versus dynamic $-G_x$	7-7
7-5	Summary of Loads, Test Conditions 1 and 2, Static Undeformed versus Deformed Floor	7-10
7-6	Comparison of Test Results, Test Conditions 1 and 2, Static Undeformed versus Deformed Floor	7-11
7-7	Summary of Loads, Test Conditions 3 and 5, Dynamic $-G_x$, Undeformed versus Deformed Floor	7-12
7-8	Comparison of Test Results, Test Conditions 3 and 5, Dynamic $-G_x$, Undeformed versus Deformed Floor	7-13
7-9	Summary of Loads Test Conditions 3 and 8, Dynamic, $-G_x$ versus 30° Yaw	7-15
7-10	Comparison of Test Results, Test Conditions 3 and 8, Dynamic, $-G_x$ versus 30° Yaw	7-16
7-11	Summary of Loads, Test Conditions 3 and 10, Dynamic, $-G_x$ versus Combined 9:4.5:1.5	7-17
7-12	Comparison of Test Results, Test Conditions 3 and 10, Dynamic, $-G_x$ versus Combined 9:4.5:1.5	7-18
7-13	Summary of Loads, Test Conditions 8 and 9, Dynamic 30° Yaw, Undeformed versus Deformed Floor	7-19
7-14	Comparison of Test Results, Test Conditions 8 and 9, Dynamic 30° Yaw, Undeformed versus Deformed Floor	7-20
8-1	Peak $-G_z$ Acceleration and Pulse Velocities for Hard Landing Cases Analyzed	8-6

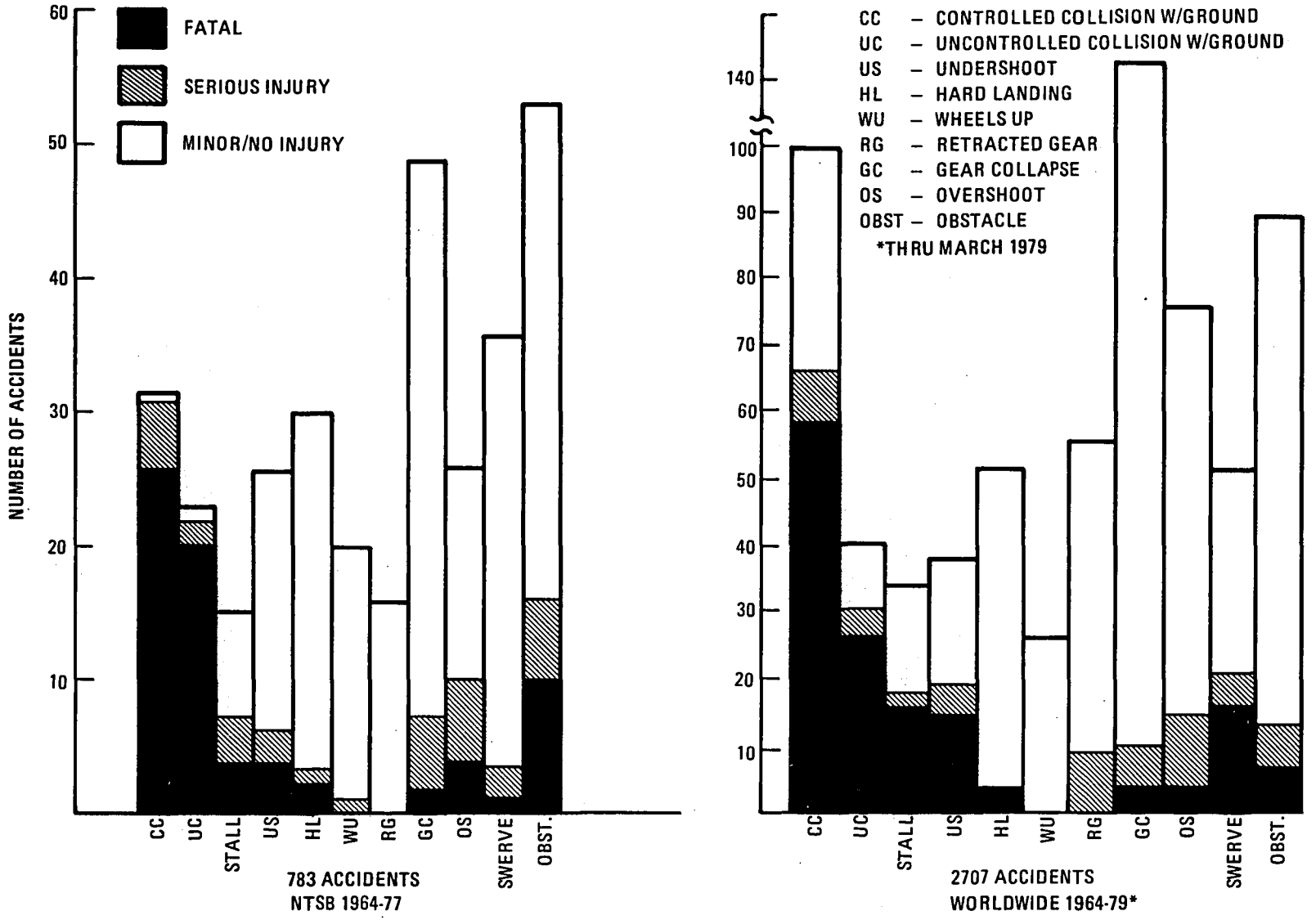

Figure 1-1. - NTSB and worldwide accident summary data.

1. INTRODUCTION

The results of a recent investigation of transport airplane accidents (Reference 1) during the 1964-79 period resulted in the formulation of candidate crash scenarios. From Figure 1-1 it can be seen that the injury potential in transport accidents determined from both National Transportation Safety Board (NTSB) and Worldwide accident data is related to the accident condition. Accidents that are initiated when the aircraft is on the ground or near the runway, and where no hazards are involved, are not likely to be fatal. When the impact occurs at high speed and at a large impact angle, the accident has a high probability of fatality. In between the extremes, the outcome in terms of occupant survivability depends on the surrounding hazards and post-impact behavior. While no accidents are alike in every respect, there are broad similarities for groups of accidents. From Figure 1-1 and Table 1-1 it can be seen that some accident types; i.e., controlled and uncontrolled collisions with the ground, stalls and undershoots, and collisions with obstacles, result in a relatively high percentage of fatal accidents. Accidents, that occur on the airport runway or in the proximity of the airport runway, rarely result in fatalities. Interestingly enough, several of these latter types of accidents such as wheels-up and gear collapse accidents have never resulted in a fatal accident. These accident types are addressed in the Federal Aviation Regulations (FAR 25) (Reference 2) in Sections 25.561 and 25.721.

Of major importance are the conditions under which airplane accidents occur. In particular, location of the accident relative to the runway, hazards and/or obstructions surrounding the airport, operating procedures on and around the airport, and warning systems on aircraft are significant. The following grouping is possible:

- Airplane Design Related - accidents which occur around airports; i.e., on the runway or within 350 m of the runway are only moderately influenced by hazards and surrounding obstructions.

TABLE 1-1. - COMPARISON OF FATAL ACCIDENT PERCENTAGES FOR NTSB AND WORLDWIDE ACCIDENT SUMMARIES

Accident Type	NTSB 1964 – 77			Worldwide (1964 – 79)*		
	No. Fatal Accidents	No. Total Accidents	% Fatal:	No. Fatal Accidents	No. Total Accidents	% Fatal:
Controlled collision	26	32	81.3	58	100	58
Uncontrolled collision	20	23	87	27	40	67.5
Stall	4	15	26.7	16	33	48.5
Undershoot	4	26	15.4	14	37	37.8
Hard landing	2	30	6.7	2	51	3.9
Wheels up	0	20	0	0	27	0
Retracted gear	0	16	0	0	57	0
Gear collapse	2	47	4.3	4	152	2.6
Swerve	1	37	2.7	8	88	9
Overshoot	4	46	8.7	4	75	5.3
Collision with obstacle	10	52	19.2	16	51	31.4

*Thru March 1979

The terrain is easy to define and the airplane configuration readily prescribed. The performance of the airplane for this type of crash scenario is indicative of modern day jet transport crash capability and an indication of the merits of current design requirements.

- Airport Environs Related - accidents which occur in the vicinity of the airport, either on the runway or beyond the runway, and the resultant damage is significantly influenced by hazards and terrain conditions. The performance of the airplane for these scenarios is to a large degree dependent on the airport surroundings. Additional effort is needed to determine how improved design of airport environs and operating procedures can be incorporated to reduce severity of this type of accident.

- Warning System Related - accidents that occur away from the airport, result from loss of airplane control, are a result of pilot disorientation or are caused by unreliable warning systems generally involving impact at high speed, with a wide range of possible impact attitudes and amongst hazardous terrain. The performance of the airplane for these scenarios to a great extent is influenced by the severity of the impact conditions, which in turn, results from the pilot's inability to control the situation. Quite often this inability on the part of the pilot is directly related to his "unawareness of the situation" until it is too late to react in a manner to reduce the vulnerability of the aircraft to the impact conditions.

Figure 1-2 shows the accident data organized into three areas: airplane design-related such as aborts/overruns, airport off-runway hazards, and accident avoidance or warning system related.

Accident avoidance or "warning system related" improvements have resulted in a substantial reduction in the ratio of accidents to departures in the past 20 years. These include cockpit design and communication, improved simulators and trainers, improved system redundancy and improved air/ground traffic control systems. Further improvements in the use of ground proximity warning systems (GPWS) and early detection devices could have a significant effect on reducing the number of severe impact accidents. Preventing airplanes from crashing into hillsides and mountains appears to be more prudent than designing the airplane to resist the crash loads from such inadvertent and severe accidents.

By the same token, "airport environs related" improvements can be made to standardize airport surroundings, to minimize the prospect of airplanes in overrun and/or overshoot situations from impacting embankments, vehicles, steel fences or going over ravines. Reasonable clearances up to 1,000 meters beyond the runway should be considered.

"Airplane design related" improvements involving the design and performance of the airplane structural systems under mild to moderately severe crash conditions are of paramount concern. Overrun and hard/landing crash scenarios have been presented in which impact and terrain conditions are specified which are considered "survivable" in light of current airplane capability. Extending the airplane capability beyond this current range of conditions to unsymmetrical attitude, higher sink speeds, and hazardous terrain requires additional analytical effort and empirical verification for what amounts to a new definition of a "survivable crash environment."

Notwithstanding the fact that the overall safety record of transport aircraft is excellent as measured in relative terms, Figure 1-3, and is in an improving trend, Figure 1-4, there is a need to assure the safety of occupants for as wide a range of crash environments, as is practical. In addition, it is important to maintain the industry's enviable safety record

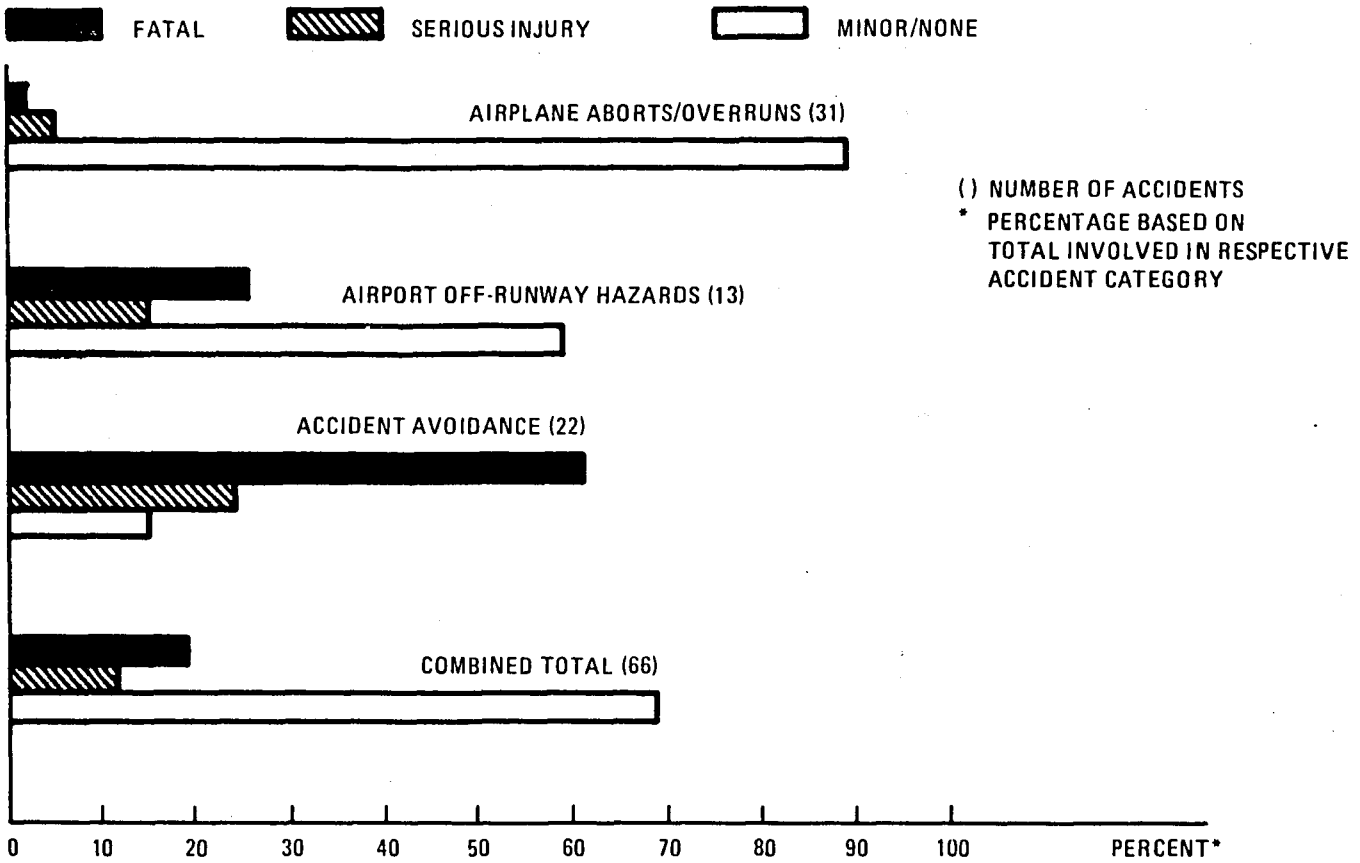

Figure 1-2. - Injury distribution as related to airplane design, airport off-runway hazards and accident avoidance procedures.

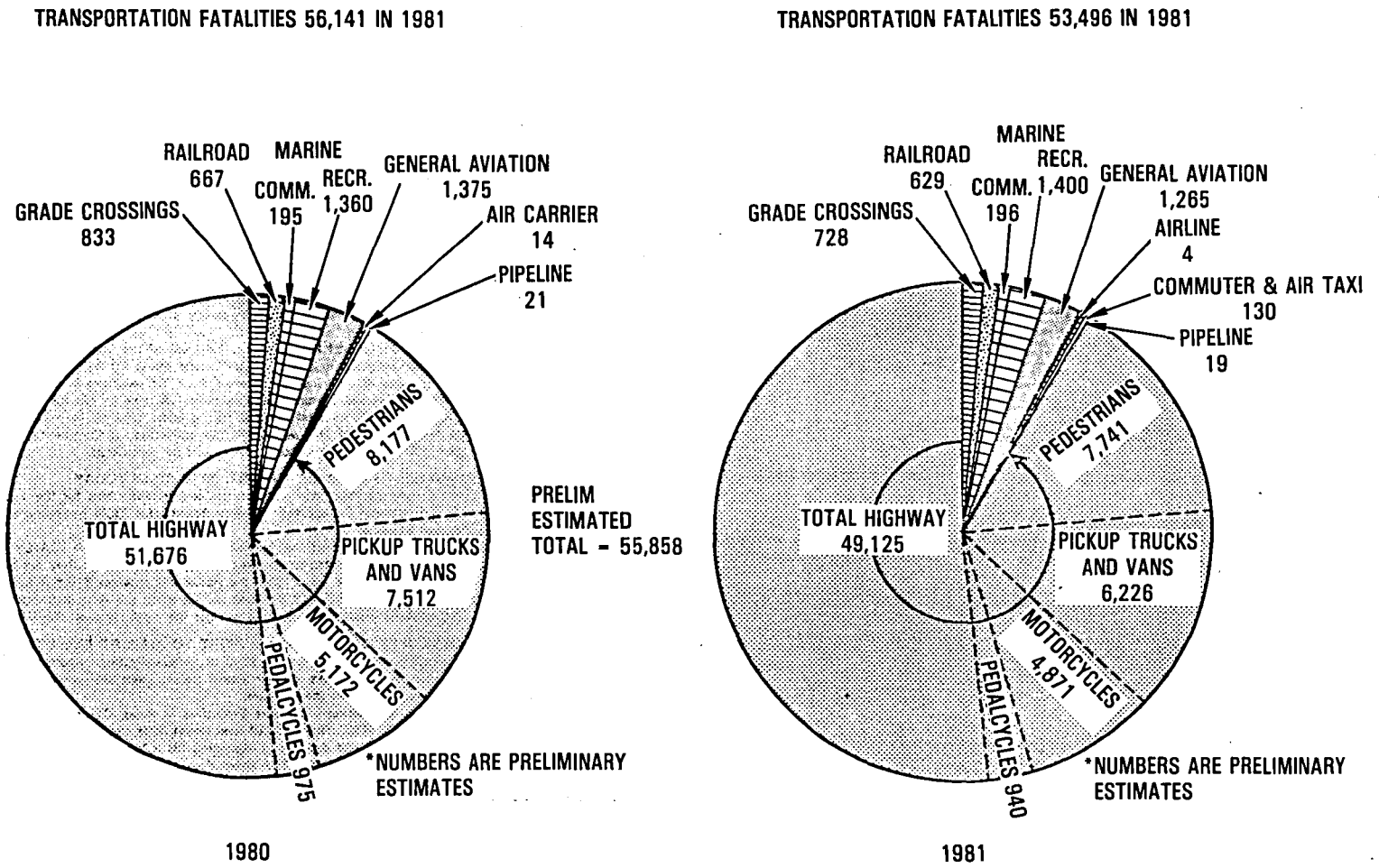

Figure 1-3. - Transportation fatalities, 1980-1981

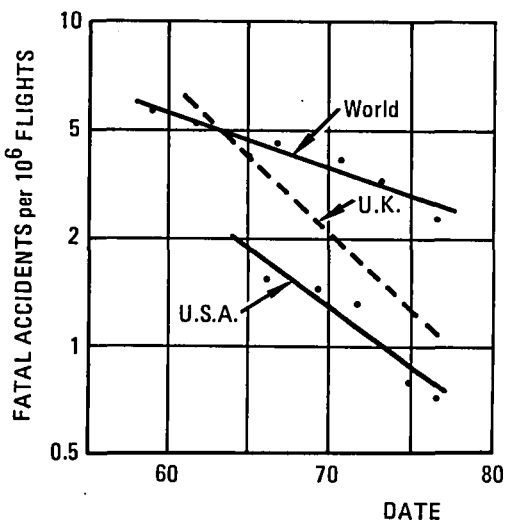

(A) U.S.A. VERSUS THE WORLD

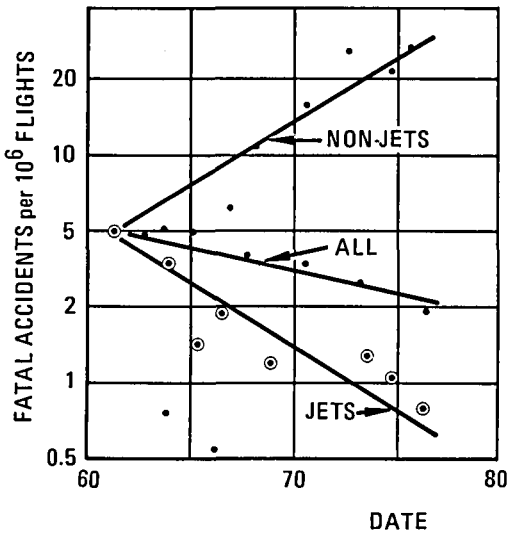

(B) JETS VERSUS NONJETS

Figure 1-4. - Trend of accidents rates, USA versus the world and jets vs nonjets.

as advanced materials replace conventional metals, having improved strength to weight ratios, but with possibly lesser energy absorption capability. This could be particularly applicable with regard to seat qualification tests where current practice is a FAR requirement for a specified inertia (g) loading in the longitudinal (9 forward), vertical (4.5 down, 2.0 up), and lateral (1.5) directions (Reference 2). In order to assess the adequacy of current requirements, it is necessary to ascertain structural responses during each of the candidate crash scenarios. In the case of seat/occupant exposure, the floor dynamic pulses need to be obtained and compared to equivalent static requirements. The formulation of static-dynamic relationships have to be understood before a valid assessment of the current requirements can be performed. Figure 1-5 illustrates that in a simple representation, depending on the characteristic properties of the system being excited and the excitation pulse amplitude and duration, an equivalence to a static response can be developed. Since crash scenarios can produce a wide range of floor pulses it is necessary to determine floor pulse amplitudes, shapes, and durations as well as seat/occupant responses to such pulses.

The effort (Task V) described in this report is directed toward defining floor pulses that can be anticipated for a wide range of crash conditions and configurations. The overall task effort is shown in the flow diagram of Figure 1-6.

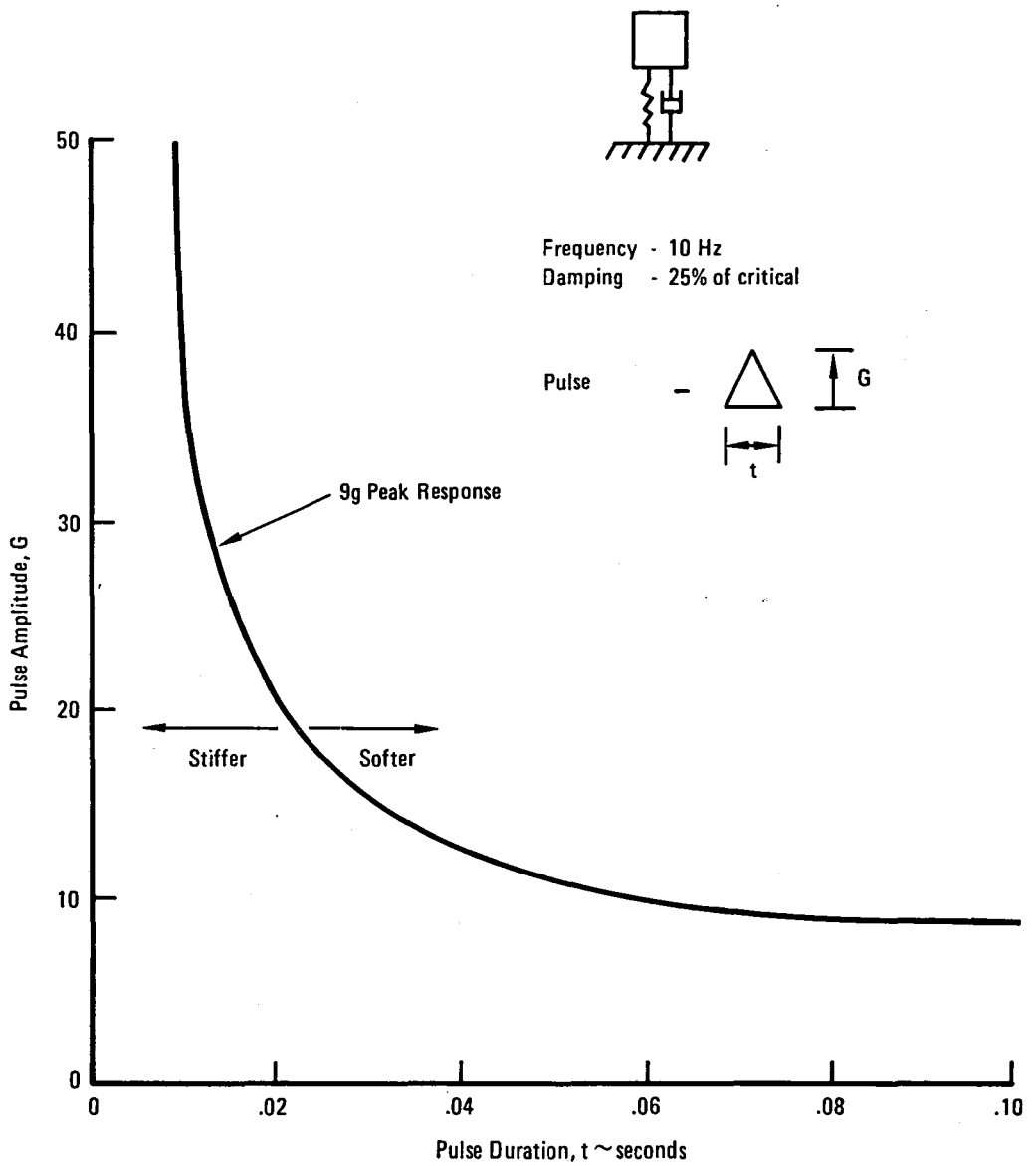

Figure 1-5. - Input pulse amplitude and duration to produce a 9 g peak response for a single degree of freedom system.

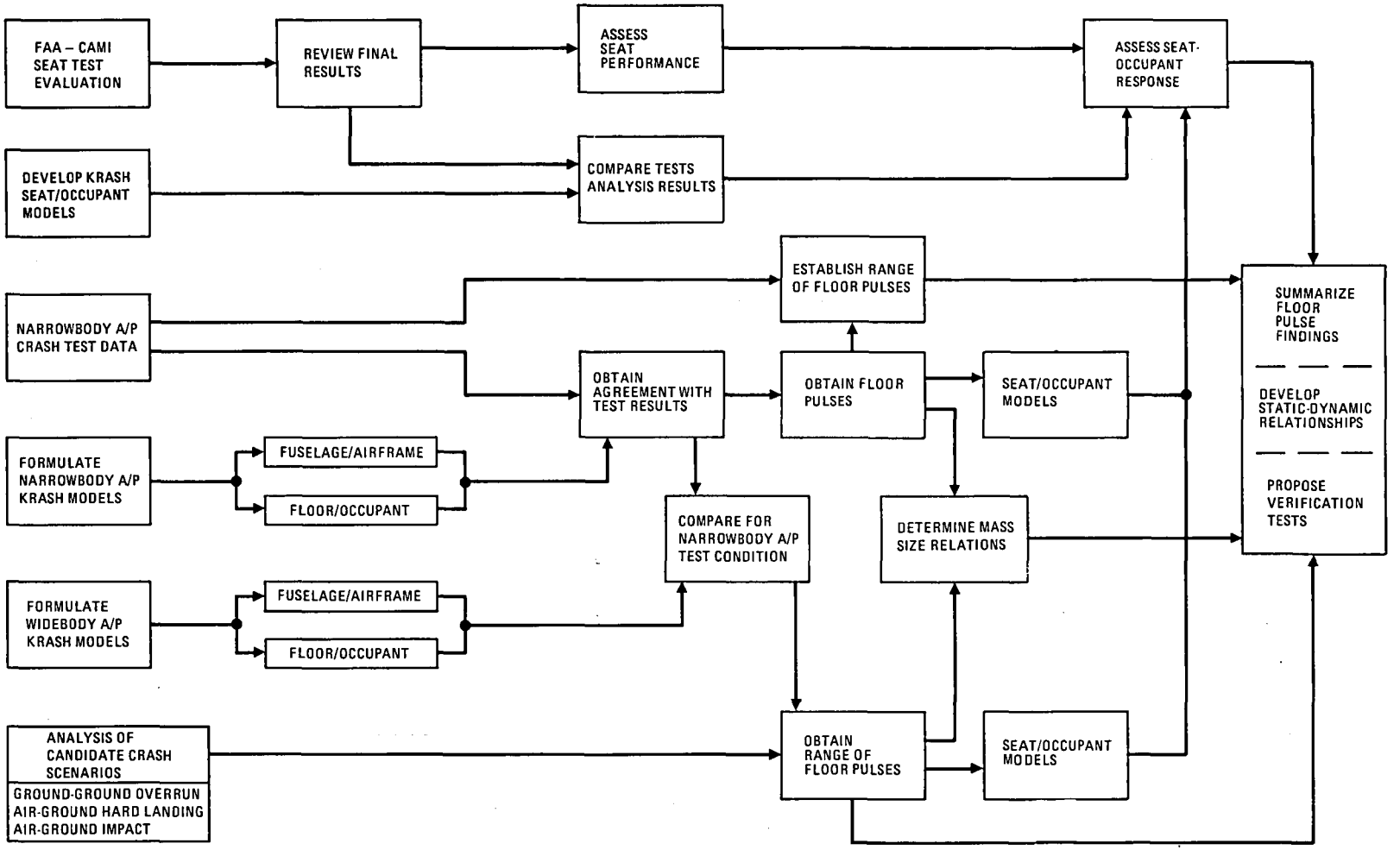

Figure 1-6. - Task V program flow diagram.

2. CANDIDATE CRASH SCENARIOS

The concept of defining crash conditions in terms of scenarios is not new to transport aircraft. In fact, the emergency landing conditions (Reference 2, Paragraph 25.561) describe a scenario for protecting an occupant from serious injury in a minor crash condition. In this scenario the airplane configuration (retracted wheels, design landing weight), airplane velocities (descent velocity of 5 ft/sec, landing touchdown speed), and airplane attitude (pitch, roll, yaw), are either stated directly or implied. For example, for this scenario there are five different gear arrangements which are applicable:

- All gears retracted
- Main gears retracted
- Nose gear retracted

} symmetrical

- Nose and one main gear retracted
- One main gear retracted.

} asymmetrical

The scenario also specifies the ultimate-inertia forces that the occupant can experience.

The review of the transport accident data from the previous tasks reported in Reference 1 and illustrated in Figure 1-1 indicates that occupant safety for the conditions described in FAR 25.561 has been achieved. Of concern now is whether additional scenarios should be specified, and if so, in what manner. From the study described in Reference 1 it was noted that there are several candidate crash scenarios which should be evaluated. These scenarios are described as follows:

- Ground-to-Ground overrun type accident, such as take-off abort or landing overrun, which occurs at a low forward speed (40-130 knots), with the landing gears extended and the airplane in a level and

symmetrical attitude. The accident occurs on paved runway or hard ground. Damage is sustained by the airplane as it traverses a ditch, road or mound. The effective normal velocity as a result of gear collapse or terrain impact, is 1.5 m/sec (5 ft/sec). The availability of pilot action to control impact severity is assumed to exist. Airplane weight can range between landing and maximum take-off.

- Air-to-Ground hard landing accident such as touchdown just short of or on the runway. On the average the sink speed is in the vicinity of 5.2 m/sec (17 ft/sec). Forward velocity is in the range of 126 to 160 knots. The airplane lands with landing gear extended in a nose-up symmetrical attitude ranging from 0 to 14°. These accidents occur on a rigid flat surface with no obstacles or hazards. Analysis should be performed for maximum landing weight.

- Air-to-Ground Impact accident type on hard ground on or off the runway. Sink speed can range up to 10 m/sec (33 ft/sec). Forward velocity is in the range of 126 to 160 knots. Airplane can land with gears retracted or extended in an unsymmetrical attitude. Range of unsymmetry is $\pm 10^{\circ}$ for roll and yaw, with pitch attitude variations from 0° to $+14^{\circ}$.

In general terms, the candidate crash scenarios, in addition to those already defined in the regulations, can be grouped as shown in Table 2-1.

TABLE 2-1. - IDENTIFICATION OF CANDIDATE CRASH SCENARIOS

Candidate Crash Scenario	Impact Conditions	Accident Type	Terrain	Hazard
Ground-to-ground, overrun	Low sink speed Low, forward velocity Sym. A/P attitude Gears extended	Takeoff abort Landing overrun	Runway Hard ground	Ditch Mound Slope Slab Light stanchion
Air-to-ground, hard landing	High sink speed Landing velocity Sym. A/P attitude Gears extended	Hard landing Undershoot	Runway Hard ground	None
Air-to-ground, impact	High sink speed Landing velocity Unsym. A/P attitude Gears extended/ret.	Uncont/controlled Grd collision Stall Undershoot	Wooded Hilly	Trees Slopes Bldgs

A comparison of the crash scenario parameters is shown in Figure 2-1. For each of the candidate scenarios there are several sequences of failure modes or events that can occur. As noted earlier, the current emergency landing conditions for transport airplanes (Reference 2) have provisions which are designed to provide the occupants a reasonable chance of escaping a serious injury in a minor crash. Paragraph 25.561 of Reference 2 specifies the emergency landing condition as retracted wheels and an ultimate descent velocity of five fps at design landing weight. Furthermore, Paragraph 25.721 states that the main landing gear must be designed so that if it fails due to an overload (due to up and aft loads) during taxi and landing, the failure is not likely to cause spillage of enough fuel to constitute a fire hazard. During emergency landing conditions, seats (Paragraph 25.785) and supporting structure for major mass items (Paragraph 25.789) are to maintain integrity under the inertia forces specified in (Paragraph 25.561).

This study is directed solely to the determination of transport aircraft response to those crash scenarios which can be described as "airframe design related."

CANDIDATE CRASH SCENARIO	TAKEOFF ABORT	LANDING OVERRUN	HARD LANDING	UNDERSHOOT	STALL	COLLISION WITH OBSTACLE	CONTROLLED OR UNCONTROLLED GROUND COLLISION	LOW FWD SPEED 40 – 130 KTS	HIGH FWD SPEED 120 – 160 KTS	LOW SINK SPEED <5 FPS	HIGH SINK SPEED 12 – 27 F/PS	EXCESSIVE SINK SPEED 30 FDS	YAW	ROLL ANGLE	LEVEL PITCH	HIGH PITCH ANGLE	PAVED RUNWAY	HARD GROUND	GRASSY DIRT	SOFT GROUND MUD, SAND, WATER	TREES	RAVINE, EMBANKMENT	HILLY SLOPE	BUILDINGS, VEHICLES	POST FENCE LIGHT	DITCH, CONTOUR SLAB, MOUND	MOUNTAIN HILLSIDE	GEARS EXTENDED	RETRACTED	TAKE-OFF WEIGHT	LANDING WEIGHT
GROUND-TO-GROUND OVERRUN (GGD)																															
GG1	O	O						O		O					O		O	O							O	O	O		O	O	
GG2															O							O			O	O	O		O	O	
AIR-TO-GROUND HARD LANDING (AGHL)																															
AG1			O	O					O		O					O	O	O									O			O	
AIR-TO-GROUND IMPACT (AGI)																															
AG2				O					O			O				O		O				O			O		O			O	
AG3					O	O	O		O			O	O	O		O			O	O			O	O	O		O	O	O		O	
AG4					O	O	O		O			O	O	O		O			O	O			O	O	O		O	O	O		O	

Figure 2-1. - Comparison of crash scenario parameters.

3. TRANSPORT CATEGORY AIRPLANE FLOOR PULSE DATA

3.1 Full-Scale Crash Test Conditions

A summary of transport category aircraft full scale crash tests which have been conducted to date is shown in Table 3-1. All the tests were conducted utilizing an airplane guided along a track and impacted into a sloping dirt mound.

A comparison was made in Reference 3, using four aircraft (FH-1 fighter, C-82 Cargo, unpressurized LodeStar, and a pressurized C-46) to compare longitudinal deceleration pulse magnitudes and durations. To that comparison was added L1649 transport crash test data.

The results plotted in Figure 3-1 indicate that the longitudinal deceleration pulse magnitude might decrease as airplane mass and size increases. Figure 3-2 shows the peak longitudinal acceleration as a function of impact angle. Since the data are plotted in relation to aircraft size it appears to also support the possibility of an inverse relationship between peak acceleration and aircraft size.

The following observations have been made with regard to available transport crash pulse data:

- The available test pulse data for transport airplanes are for one particular accident situation, e.g., airplane impact onto sloping dirt terrain.
- The pulse definition, as was shown in Reference 1, is very dependent on the manner in which the test data are reduced and interpreted.
- The acceleration level and pulse shape are dependent upon such variables as airplane attitude, airplane structure, airplane velocity, type of surface, and/or obstacles the airplane hits. Different

TABLE 3-1. - SUMMARY OF TRANSPORT CATEGORY AIRCRAFT FULL-SCALE CRASH TEST CONDITIONS

Airplane	Approximate Weights		Velocity				Slope (degrees)
			Longitudinal		Vertical		
	Kg	(lbs)	m/sec	(ft/sec)	m/sec	(ft/sec)	
C-82	19,026	(42,000)	40.8	(133.8)	11.4	(37.3)	16
Lodestar	9,739	(21,500)	39.0	(127.9)	8.1	(26.7)	12
			48.8	(160.2)	13.6	(44.7)	16
C-46	18,120	(40,000)	41.4	(136.7)	10.90	(35.7)	14
			43.7	(142.6)	22.0	(72.0)	27
L1649	72,027	(159,000)	52.4	(172.0)	5.50	(18.0)	6
			39.0	(103.0)	10.0	(34.7)	20
DC-7	55,266	(122,000)*	67.2	(220.5)	9.4	(30.9)	8
			49.3	(161.7)	16.5	(53.9)	20

*Max. Takeoff Weights, Test Weight Not Stated

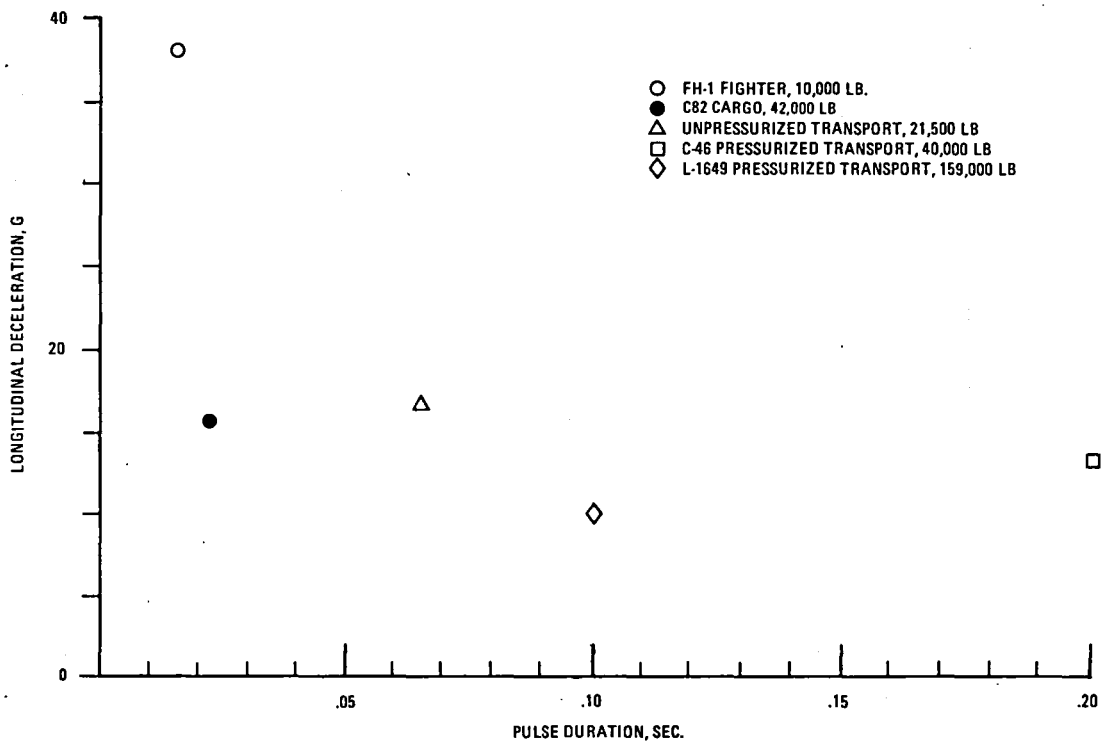

Figure 3-1. - Comparison of peak decelerations.

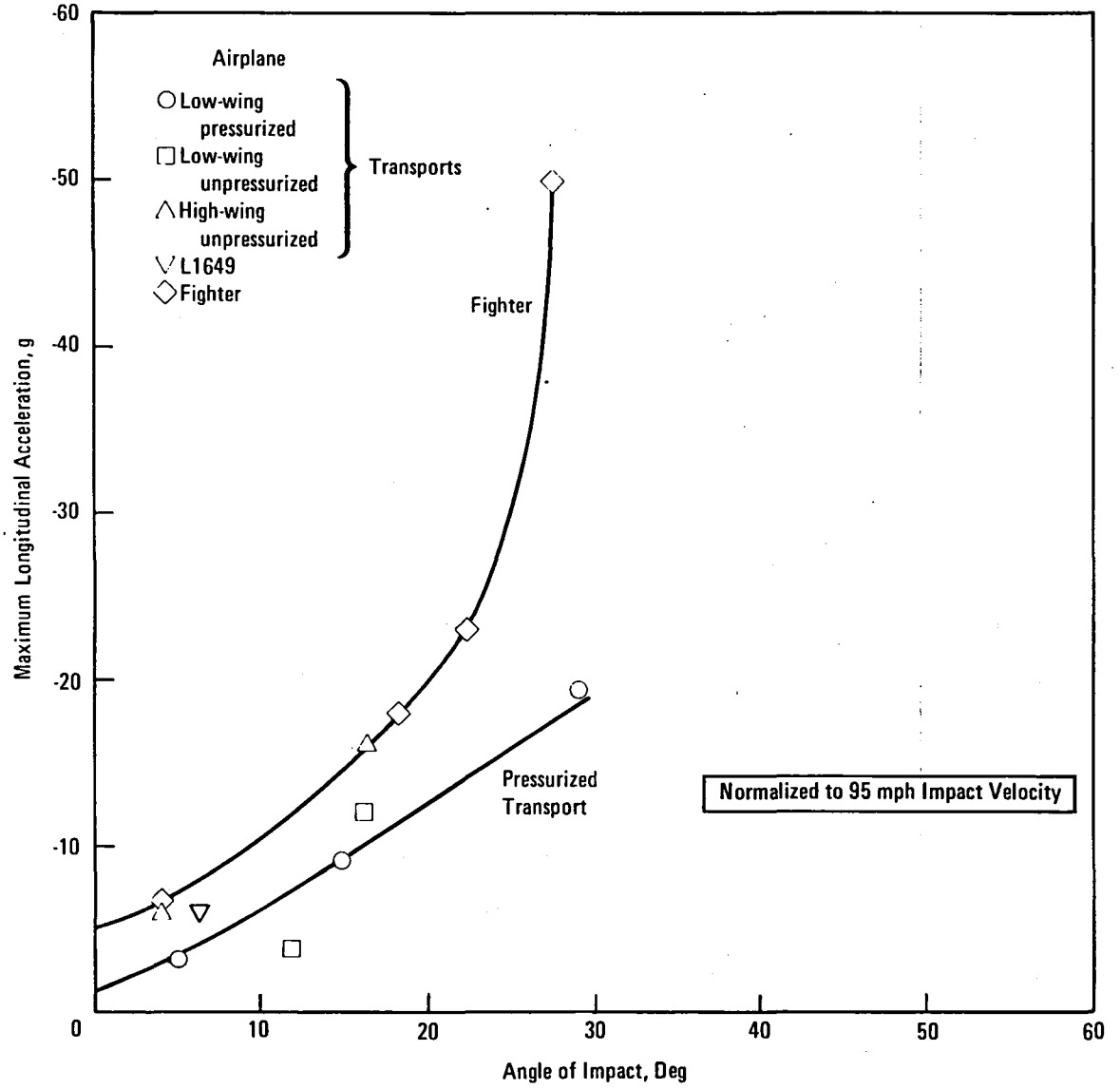

Figure 3-2. - Effect of airplane configuration on variation of maximum longitudinal acceleration with impact angle.

accident conditions; i.e., hard landing on the runway versus an overrun off the runway, will produce different pulses. The pulse varies as a function of location along the fuselage and the relative distance from the impact point.

- The trend with larger jet transports indicates an anticipation of deceleration levels of lesser magnitude and longer duration than the earlier vintage transports and lighter aircraft despite the increase in weight and operating speed. The reasons for this are: (1) the larger wider body jets accelerate over a longer period of time and (2) there is more crushable structure between the impact point and the floor location of the occupants.

3.2 L1649 Floor Pulse Test Data

Unfortunately, there is a limited amount of crash data available on transport aircraft of substantial size. The loss of data channels on the DC-7 test[4] leaves only the L1649[5] crash test with any measured data. This test was performed almost two decades ago and most of the available data comes from published data which have been reduced in many different fashions. The L1649 test involved two sloping terrain impacts. On the initial impact the aircraft hits a slope of six degrees at a forward velocity of 172 ft/sec (sink speed ≅ 18 ft/sec) and the structure appears to remain intact. As a result of the subsequent impact onto a 20 degree slope at 103 ft/sec (~35 ft/sec sink speed) the aircraft fuselage breaks aft of the cabin (~FS 334) immediately and at the aft fuselage (~FS 1014) later on. Figure 3-3 shows the crash test velocity time history and depicts some significant events. Figure 3-4 depicts the fuselage break-up locations. Longitudinal and vertical acceleration time histories obtained from Reference 5 for both the 6° and 20° slope impacts are shown in Figures 3-5 through 3-8.*

The ultimate usage of the L1649 floor pulse data will be to help establish a range of magnitude and duration values of floor pulses for transport aircraft which encompass a wide spectrum of design, size and weight. An objective of this task is to analytically determine, with program KRASH,

*Inertial loads are opposite those shown on these and subsequent figures.

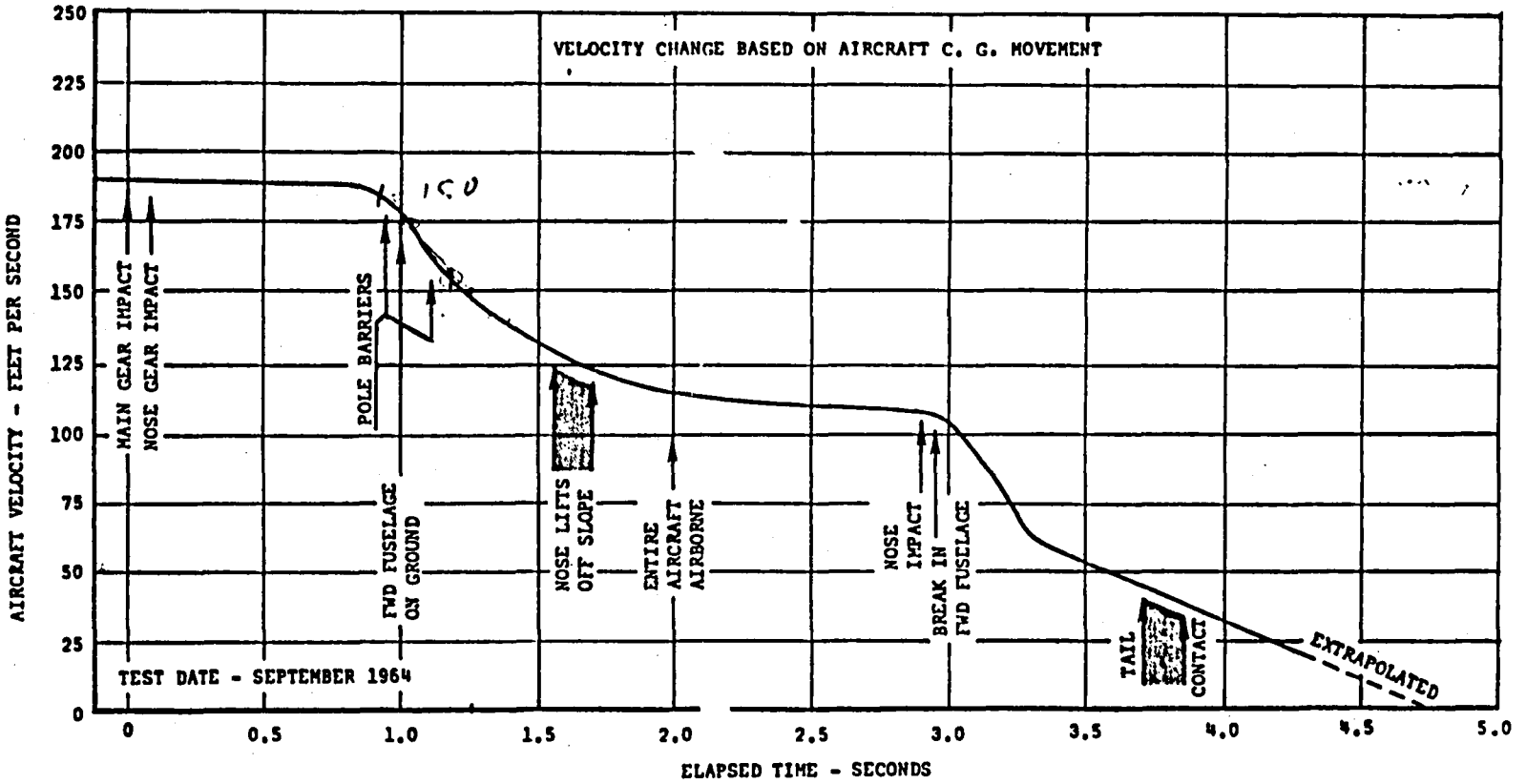

Figure 3-3. - L-1649 crash test velocity - time history.

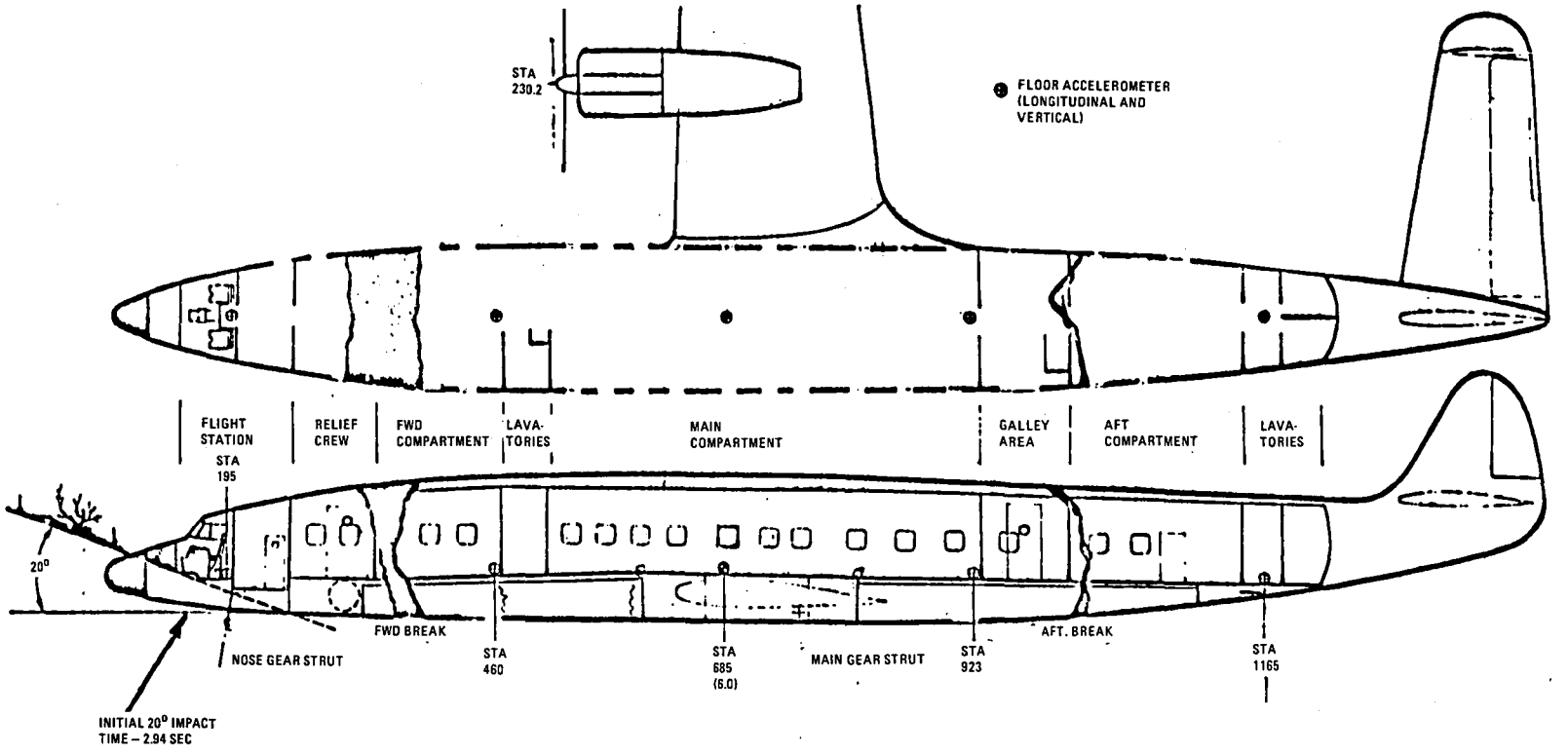

Figure 3-4. - Location of floor level accelerometers for X, Y and Z recordings, L1649 crash test.

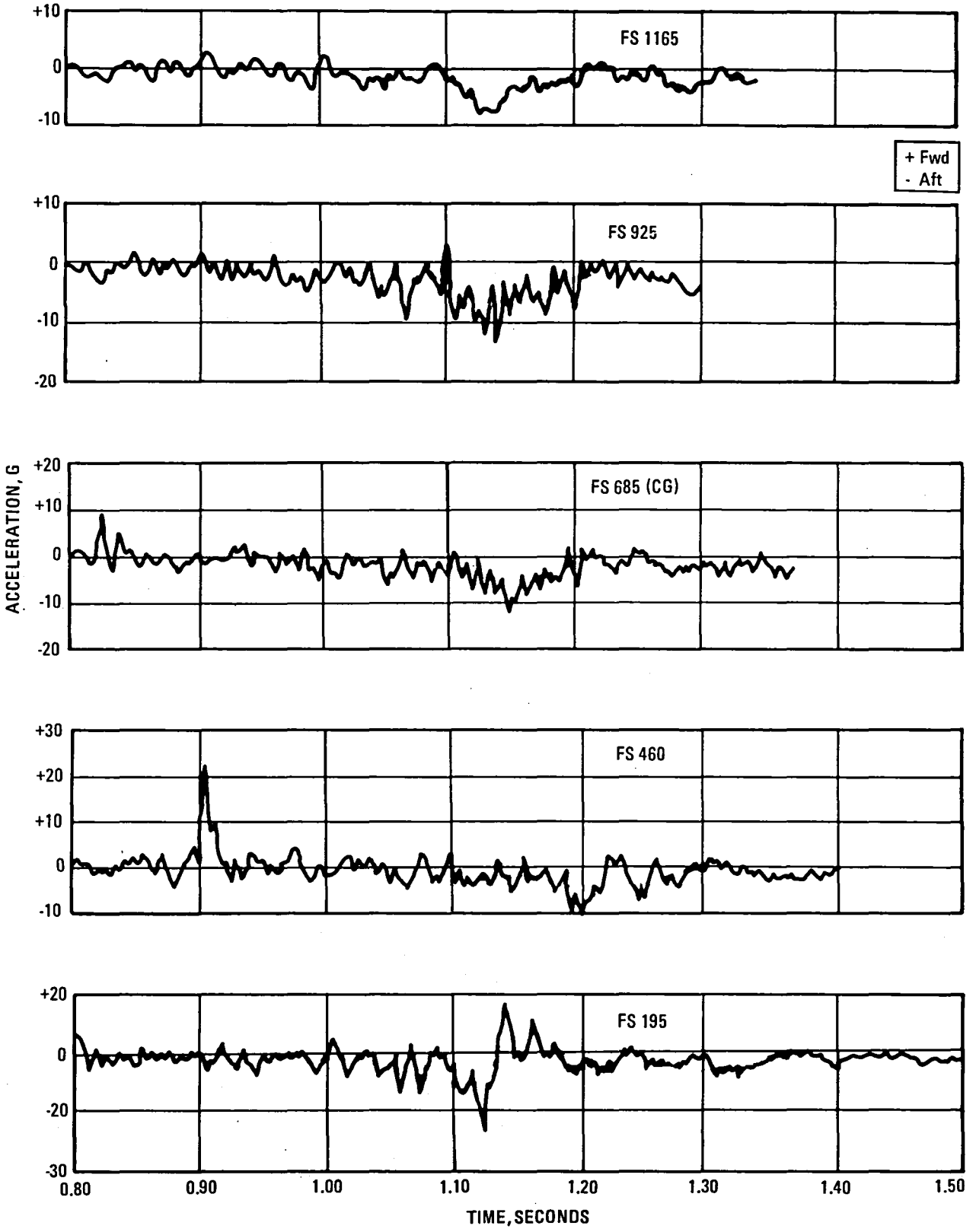

Figure 3-5. - Floor longitudinal accelerations, L1649 test, 6° slope impact.

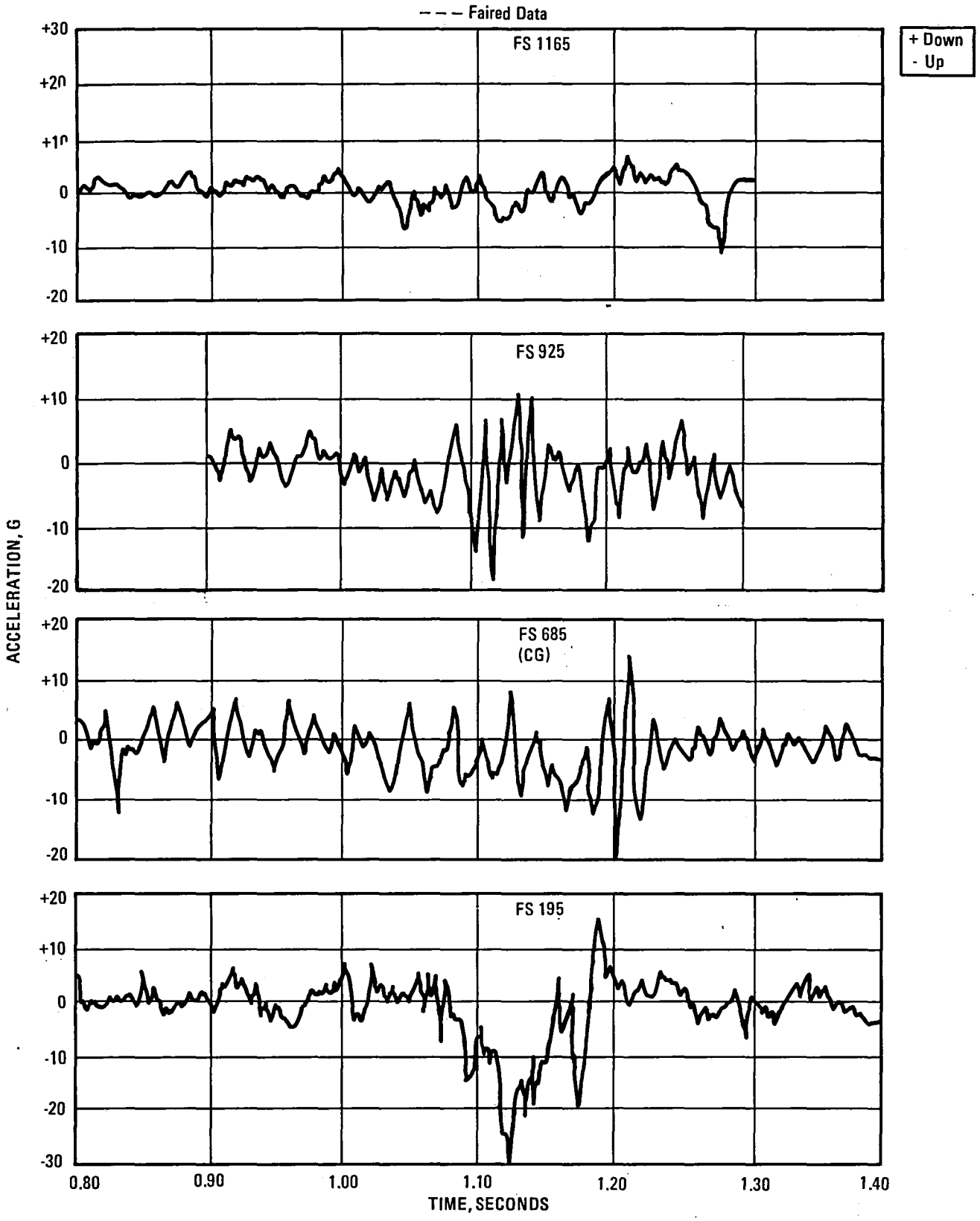

Figure 3-6. - Floor vertical accelerations, L1649 test, 6° slope impact.

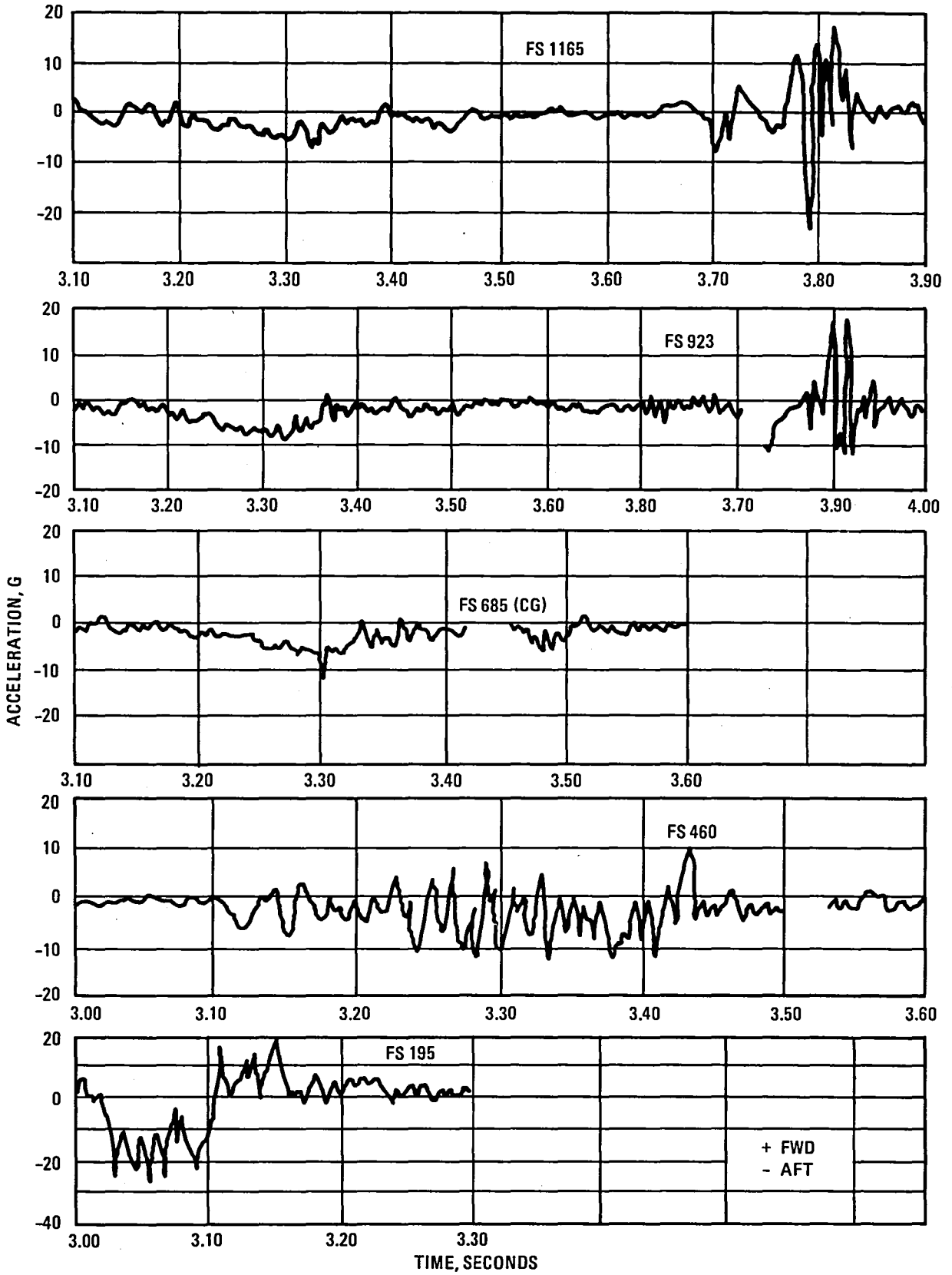

Figure 3-7. - Floor longitudinal acceleration, L1649 tests, 20° slope impact.

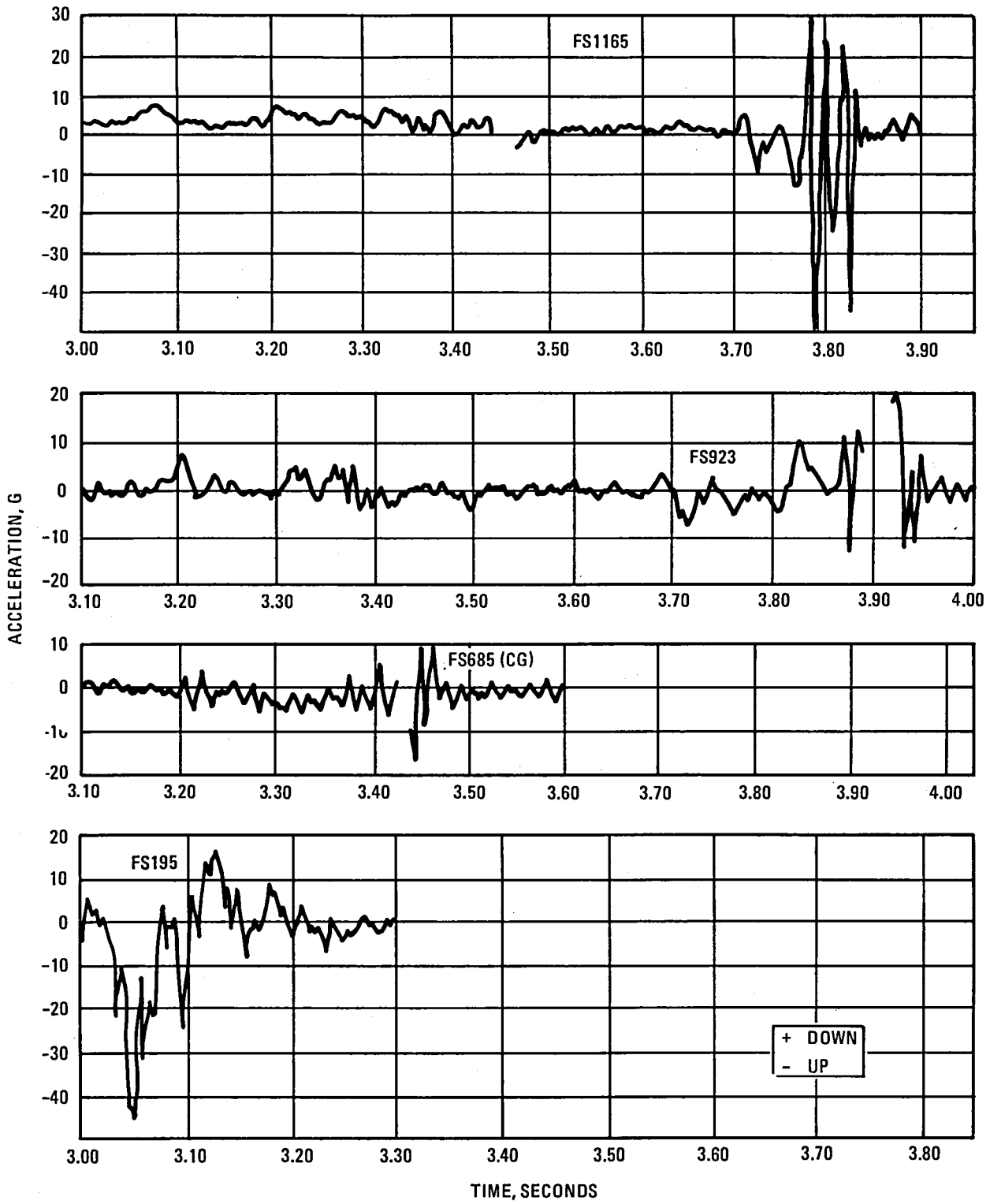

Figure 3-8. - Floor vertical accelerations, L1649 test, 20° slope impact.

floor pulses resulting from potential crash scenarios. The approach in assessing L1649 floor pulse data consists of:

- Digitizing the reported L1649 time histories in selected regions of time for both the 6° and 20° slope impacts.

- Inputting the digitized data into program KRASH as unfiltered data and obtaining filtered response at selected cut-off frequencies (20 Hz, 50 Hz). This will allow comparison between L1649 test data and analytical data generated by the use of program KRASH, since both will be filtered in the same way.

The characteristics of a KRASH simple first order filter is shown in Figure 3-9. Attenuation at the cut-off frequency, 100 Hz in the illustration, is 3 dB. The amplitude reduction varies with the ratio of response frequency to cut-off frequency (W/Wc) and may differ from that of a 2nd order system or test filters.

Figures 3-10 and 3-11 illustrate the test data filtered and unfiltered for the six-degree slope impact at FS685 which is the approximate airplane

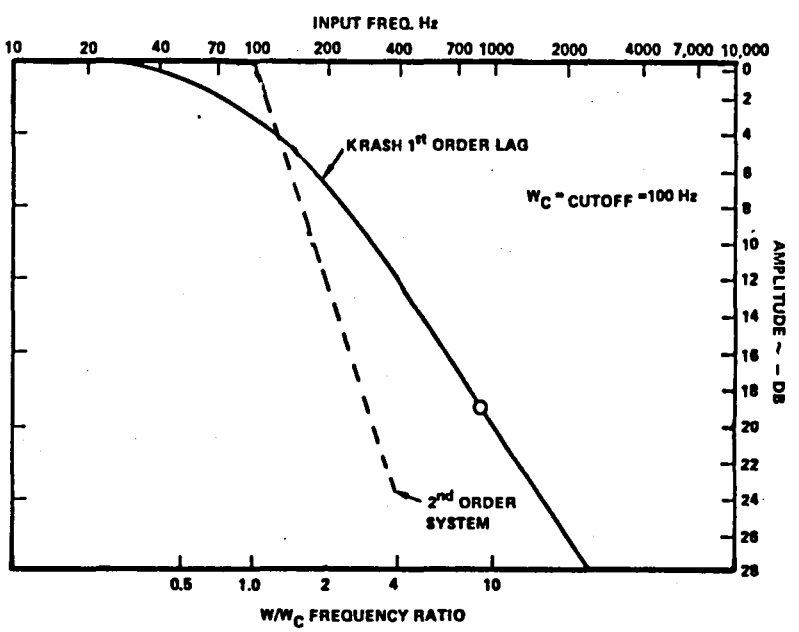

Figure 3-9. - First-order KRASH filter response characteristics.

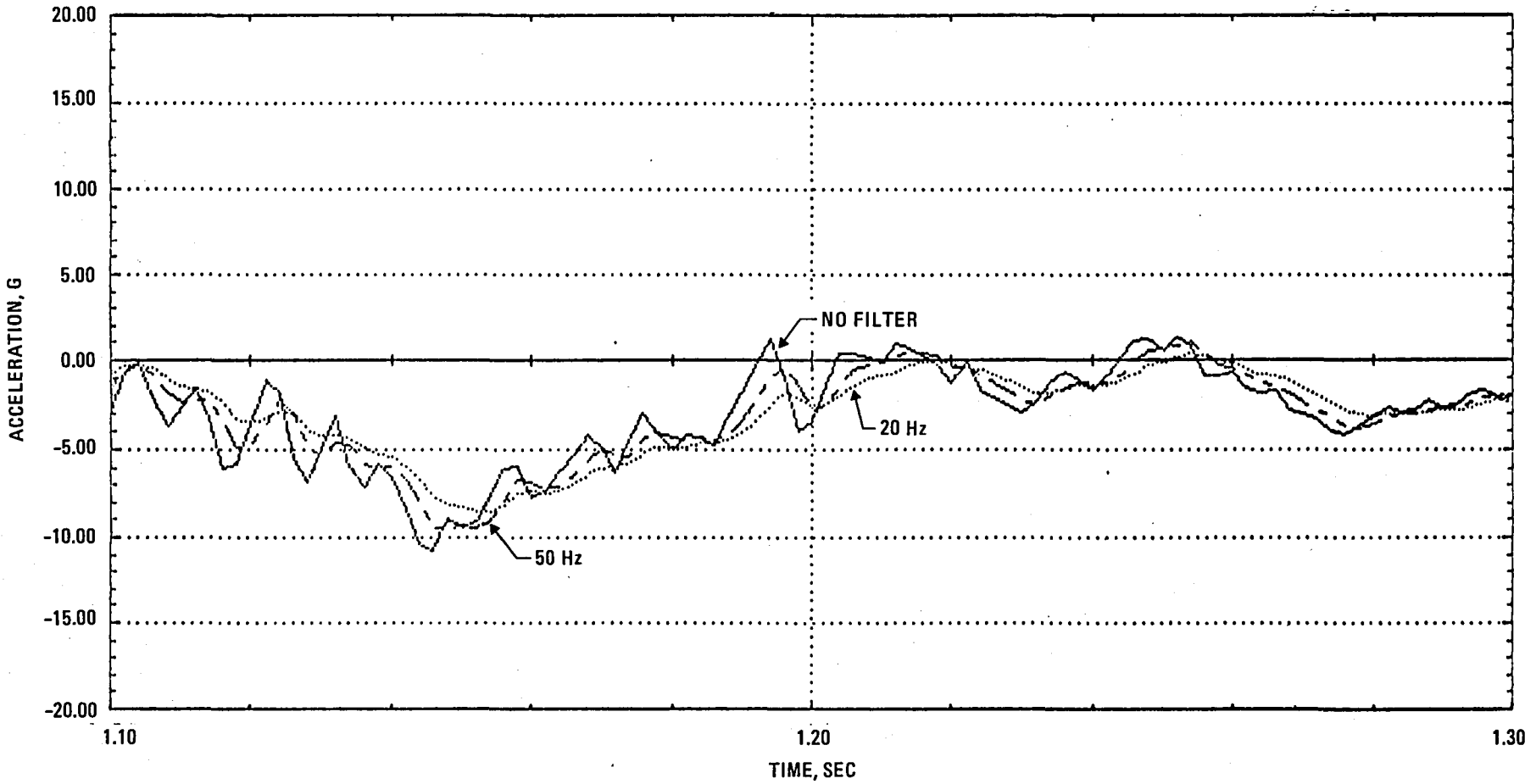

Figure 3-10. - L1649 floor longitudinal pulse at FS685, filtered and unfiltered.

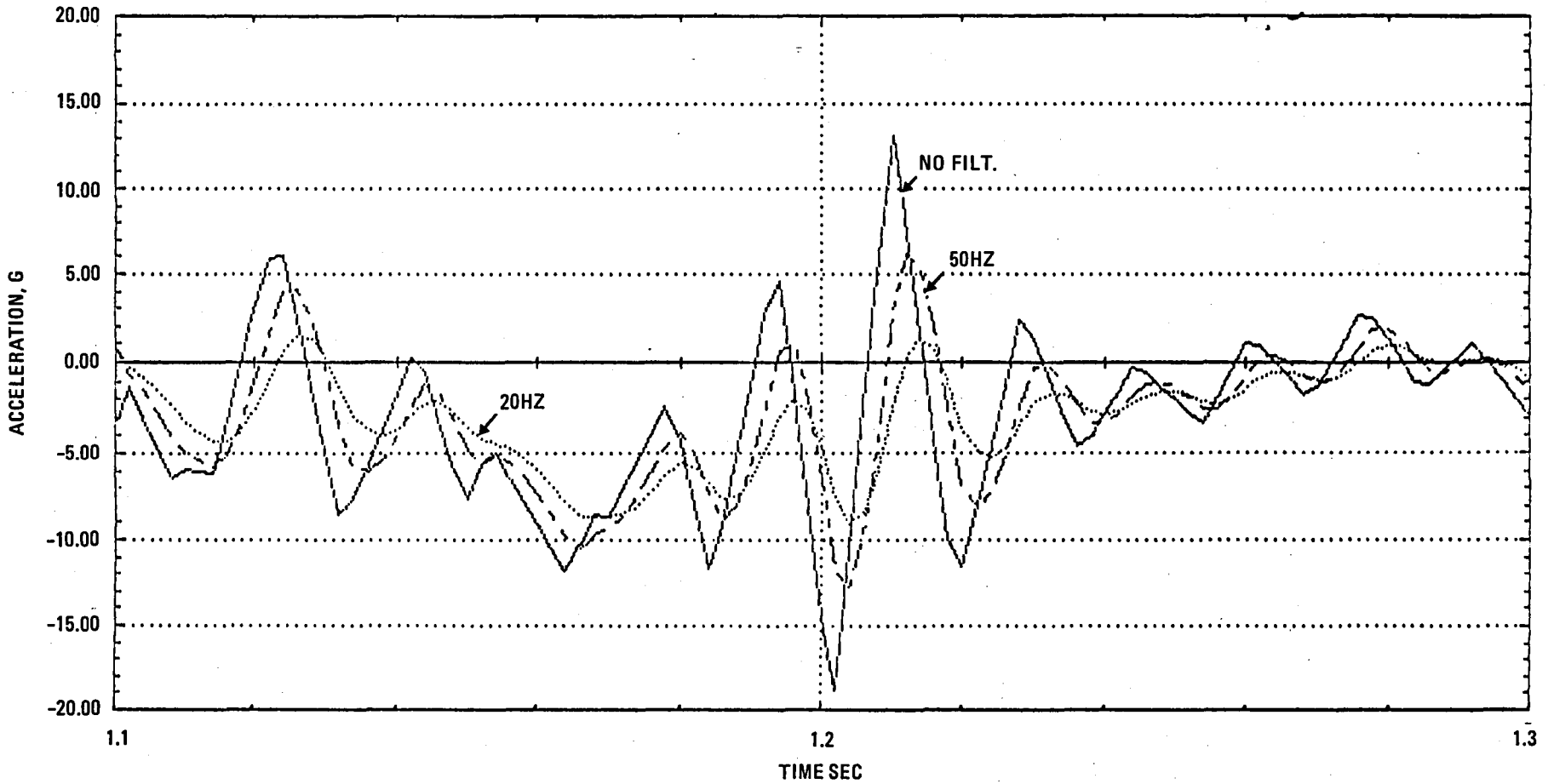

Figure 3-11. - L1649 floor vertical pulse at FS685, filtered and unfiltered.

center of gravity (cg). The duration of the longitudinal pulse is longer for the unfiltered data than for the filtered data (100-120 milliseconds versus 80 milliseconds). The peak amplitude shows a 20 percent reduction (from 10 g to 8 g). The filtered vertical floor pulse shows a reduction of approximately 27 percent (from 11 g to 8 g) in the broad range response from time = 1.1 to 1.3 seconds. A higher, shorter duration (<0.020 second) vertical floor pulse was reduced from 19 g to 8 g with the use of a 20 Hz filter. The longer duration floor pulses (~0.080 seconds duration) should be of more concern for the low frequency occupant response and, thus, will be emphasized in the evaluation of L1649 crash test data and in comparisons with analytical results.

Table 3-2 summarizes the L1649 floor pulse unfiltered data as well as the 20 Hz and 50 Hz KRASH filtered data. The higher peaks are generally associated with shorter duration responses. The data for the vertical pulses are more limited and more difficult to assess than for the longitudinal pulses. Within the cabin region (F.S. 460 to 923) the longitudinal aft responses are triangular, ranging from 8 g filtered to 12 g unfiltered and with corresponding triangular pulse durations of 0.040 to 0.120 seconds. There is practically no forward response (<1 g). The vertical response would appear to decrease from 26 g at the cockpit to 9 g at the cg to 5 g at the aft end based on a triangular pulse of approximately 0.030 seconds duration.

TABLE 3-2. L1649 TEST FLOOR PULSE DATA

FORWARD FUSELAGE	LONGITUDINAL (1)		VERTICAL (1)	
	AFT	FORWARD	UP	DOWN
FS 195				
UNFILTERED	22 < 0.010	15 ~ 0.02	30 < 0.01	15 ~ 0.02
50 Hz	17 ~ 0.040	12 ~ 0.02	26 ~ 0.04	11 ~ 0.02
20 Hz	12.5 ~ 0.050	8 ~ 0.04	22 ~ 0.10	8 ~ 0.04
FS 460				
UNFILTERED	10 ~ 0.025	<1	(3)	(3)
50 Hz	9 ~ 0.030	–		
20 Hz	8 ~ 0.040	–		
FS 685				
UNFILTERED	11 ~ 0.060	<1	19 < 0.01	13 ~ 0.02
50 Hz	10 ~ 0.080	–	12.5 < 0.02	6 ~ 0.02
20 Hz	8 ~ 0.120	–	9 ~ 0.04	<2
FS 923				
UNFILTERED	12 < 0.01	<1	(2)	(2)
50 Hz	10 ~ 0.08	–		–
20 Hz	8 ~ 0.120	–		–
FS 1165				
UNFILTERED	8 ~ 0.100	<1	5 ~ 0.03 10 < 0.01	<5 ~ 0.04
50 Hz	8 ~ 0.100	–	–	–
20 Hz	8 ~ 0.100	–	–	–

(1) Values shown are in peak g and approximate duration in seconds

(2) Questionable

(3) Not available

4. FLOOR PULSE ANALYSIS

4.1 KRASH Models

Analysis of aircraft crash dynamics using hybrid* techniques, particularly program KRASH, has shown favorable results for light fixed-wing and rotary wing aircraft application. Full-scale crash tests (References 6, 7) have provided data from which successful correlation and, consequently, verification of the method have been achieved. Program KRASH has been used by many helicopter manufacturers to assist in showing compliance with the U.S. Army crash requirements (Reference 8).

Advances in computer technology have facilitated the development of programs to analyze structural crash nonlinear behavior which, in turn, has maximized the utilization of data obtained from costly full-scale crash tests. The techniques that have been accepted for crash analyses of the lighter, smaller aircraft are applicable to the larger aircraft, but possibly with some modifications. Smaller aircraft, such as helicopters and general aviation airplanes, have lower longitudinal velocities but higher vertical rates of descent during a crash condition which can include stall/spin and emergency landings on prepared terrain. The percentage of occupiable space in large transport greatly exceeds that of smaller aircraft. Furthermore, occupants of small aircraft are much closer to the airframe/terrain impact point due to obvious airframe construction differences. The crash pulses experienced by transport occupants vary along the length of the fuselage more so than do the pulses of smaller aircraft. Figure 4-1, based on reported crash test data, shows the variation in peak normal acceleration as a function of distance along fuselage length, as well as impact angle (and sink speed).

*Providing the user the flexibility of utilizing available data, experimental and analytical, in developing a structural representation.

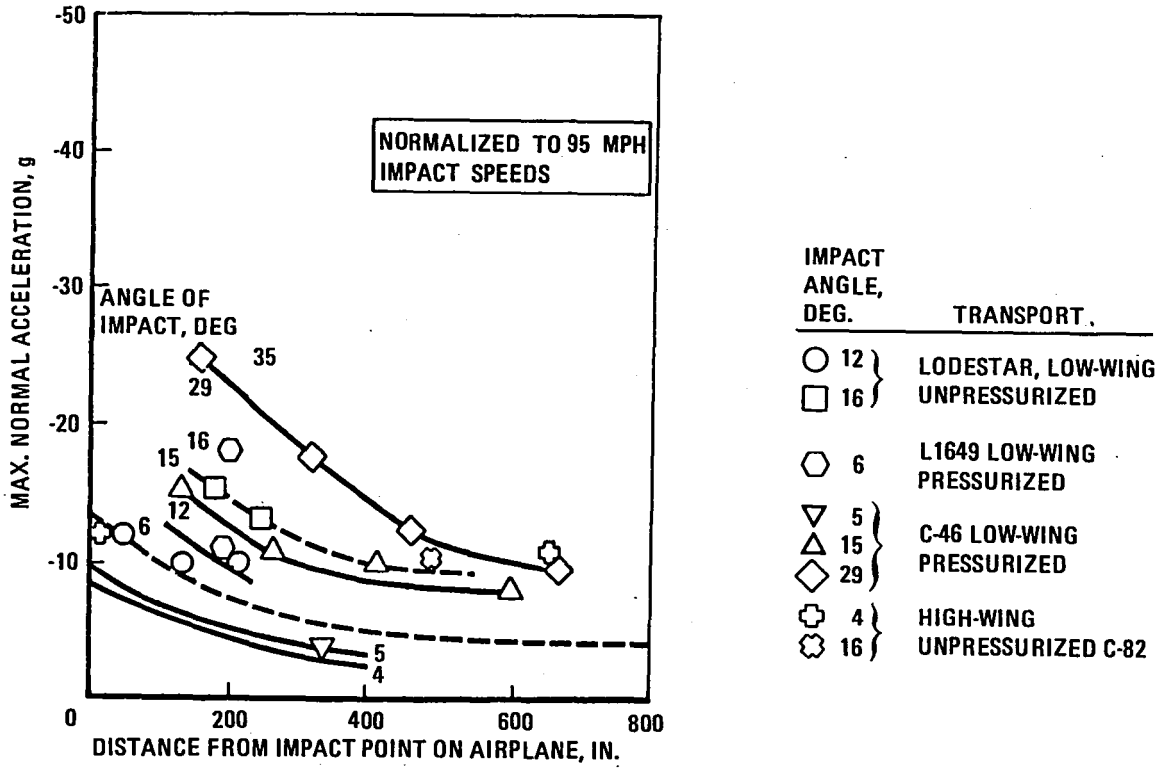

Figure 4-1. - Effect of position in airplane and airplane configuration on maximum normal accelerations during unflared landing crashes.

Prior to this program no full-scale transport airplane crash test data have been correlated with state-of-the-art computer analysis either hybrid, finite element or modal. This is understandable since the last transport airplane crash test was performed in 1964 and the most significant crash dynamics analyses achievements have been accomplished within the past several years. It is unlikely that transport aircraft will be modeled in their entirety with the detail that small aircraft have been, simply because the cost of preparing and performing such an analysis would be prohibitive and may be unnecessary. A modal analysis (Reference 9) of transport aircraft emergency landing conditions was accomplished based on the following fundamental assumptions:

- The overall vehicle remains intact and, to a first approximation behaves linearly.
- Nonlinear behavior is restricted to localized areas on the lower extremities of the airplane in direct contact with the ground.
- Since the local crushing and nonlinear behavior is not sufficiently widespread throughout the airplane to alter the basic linear behavior of the overall structure, normal modes of vibration are used to predict the dynamic response of the overall airplane structure.

- These normal modes are driven by crash forces which are applied at selected descrete locations and represent the local fuselage crushing behavior.

The major drawback to the current modal approach is that it does not treat plastic deformation or post failure behavior. However, the modal approach implies that the analytical approach for transport airplane crash dynamics does not warrant a fully detailed mathematical model. The approach that is followed in this task is outlined as follows:

- Establish three independent transport airplane KRASH models:
  - o Fuselage/airframe
  - o Floor
  - o Seat/occupant
- Investigate the feasibility of performing each separately but dependent on previous model results as well as combining the models.
- Establish a current wide-body representation since the structural data and the form of the data are more readily available.
- Formulate an L1649 narrow body representation based on available data and where L1649 data are not readily accessible scale down from wide-body information. The L1649 crash test was performed in 1964. The design of the aircraft occurred in the mid fifties. It is difficult to obtain characteristic load-deformation stiffness and crushing characteristics in readily usable form, particularly since the aircraft was not modeled for the test.
- Compare the L1649 KRASH model(s) with the reported test data (six degree and 20 degree slope condition) including the filter results described in Section 3. Establish model and terrain conditions for which test and analysis show reasonable agreement.
- Analyze the wide-body aircraft for a crash condition similar to that for which L1649 analysis results seem reasonable.
- Extend wide-body analysis to include responses to the candidate crash scenarios.

Initial analyses were performed with individual airframe, floor, and occupant models to obtain information regarding potential size and cost requirements. Figure 4-2 shows the basic airframe model and Figure 4-3 depicts the increasing detail in a region of a fuselage section. The floor-seat-occupant

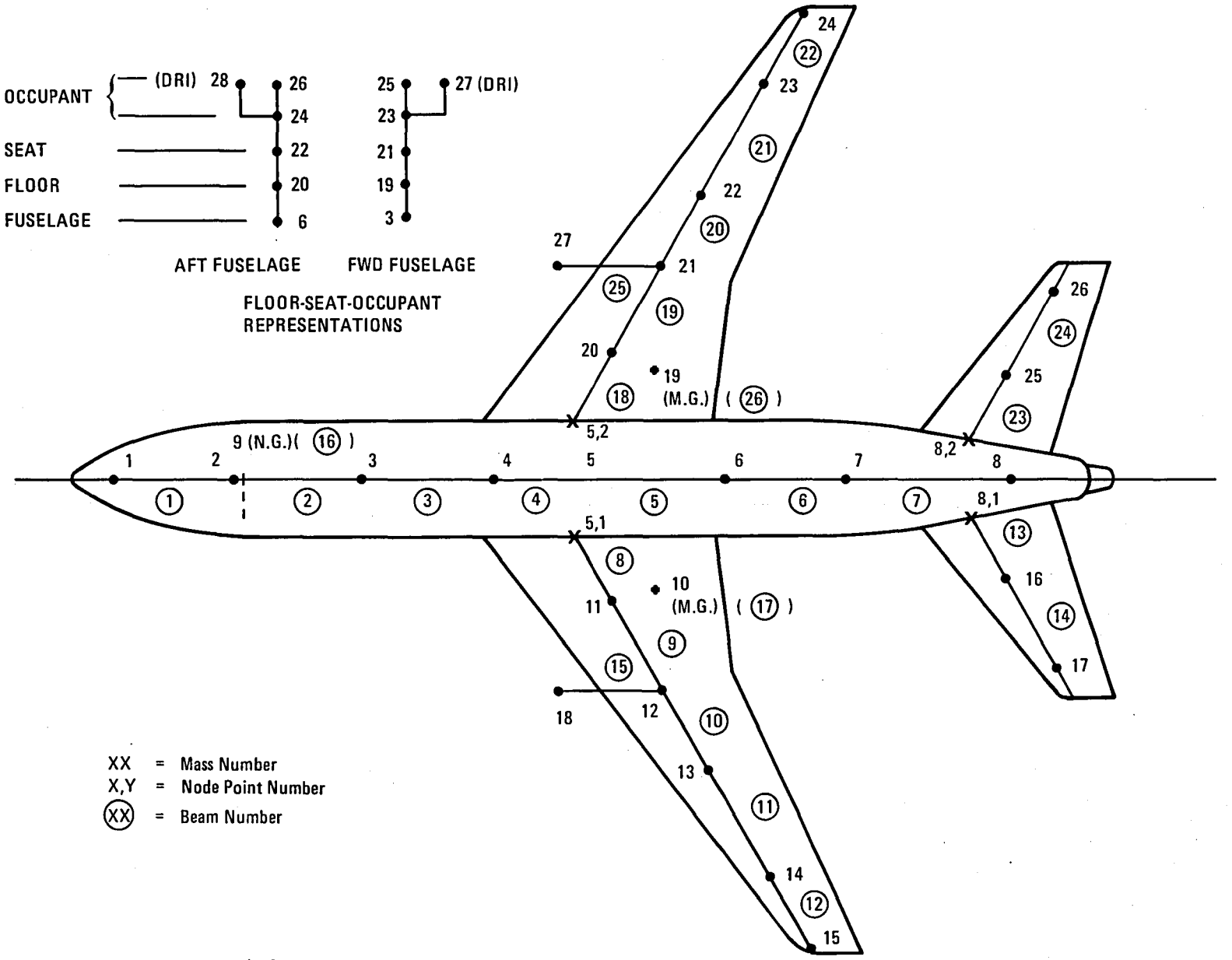

Figure 4-2. - Transport category airplane analytical airframe model concept.

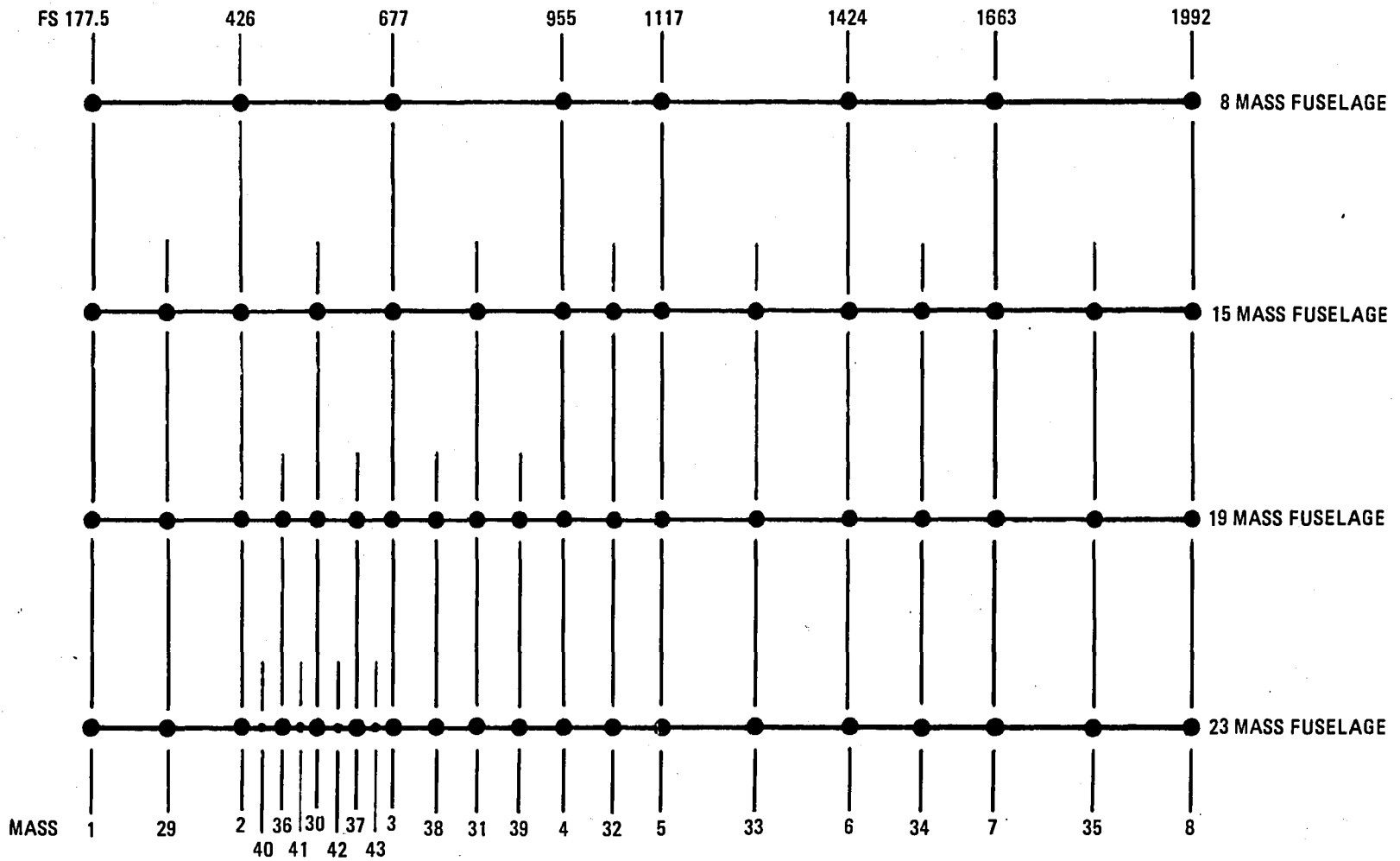

Figure 4-3. - Variation in number of airframe fuselage masses.

representation in two locations (FS677 forward, FS1424 rear) account for interaction between the fuselage shell and interior masses. The mass and stiffness of the floor-seat-occupant representation in the fuselage/airframe model are associated with a floor length of from 30 to 300 inches (depending on detail) and assumes eight seats across a full length. The seat occupancy is assumed to be 50 percent loaded with 90th percentile males. The location of the floor-seat-occupant representations were varied from masses three (FS677) and six (FS1424) to two (FS426) and seven (FS1663) and four (FS955) and five (FS1117) to determine if the fuselage responses would be affected. The fuselage responses were not significantly affected since the occupant masses are relatively small compared with the fuselage segment. As additional detail was developed for the fuselage the weight and stiffness of the affected masses and beams were modified, accordingly. The fuselage crushing springs (masses 1-8) were maintained for each model. As anticipated, the integration step size had to be reduced as the detail increased. However, the acceleration response and beam forces were not significantly affected as the model detail increased, thus the initial fuselage studies are conducted with the basic eight mass fuselage model.

One and three-row floor models, Figures 4-4 and 4-5 respectively, were developed for the purpose of transmitting fuselage response through to the inboard floor and outboard floor seat locations. Each of the models was pulsed with accelerations obtained from a fuselage model analysis. Little difference in floor and occupant responses was noted between the one and three-row floor models. It was, therefore, decided to use the simpler of the two models. Seat/occupant models for 1 and 3 passenger representations, Figure 4-6, as well as a two passenger representation, Figure 4-7, were formulated to obtain comparative responses and computing costs. These models are to be used later in the assessment of the Federal Aviation Administration Civic Aero-medical Institute (FAA-CAMI) seat tests results.

Table 4-1 compares the size and cost results for the models that were evaluated. From Table 4-1 it can be deduced that if the KRASH model requirements of each of the individual types of models were combined the result would be an extremely large model.

Table 4-2 has been prepared to indicate the range of model requirements based on minumum size airframe, and depending on the number of floor row 36 representations and seat-occupant representation. For a symmetrical

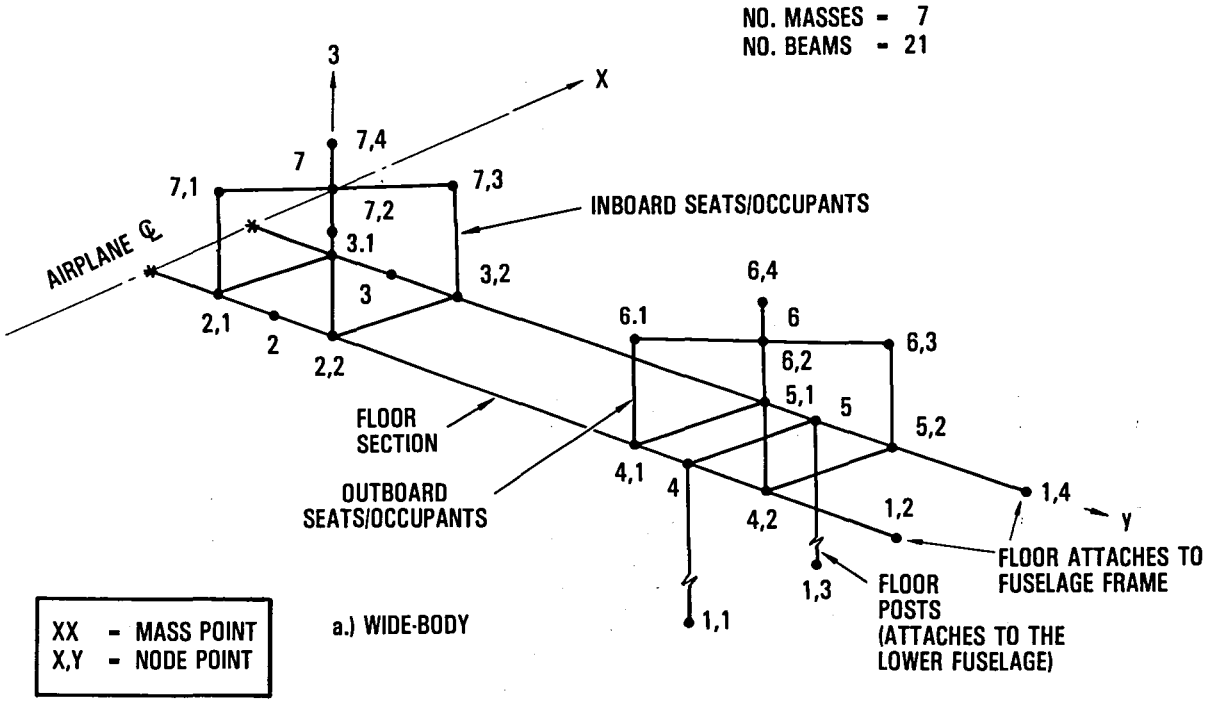

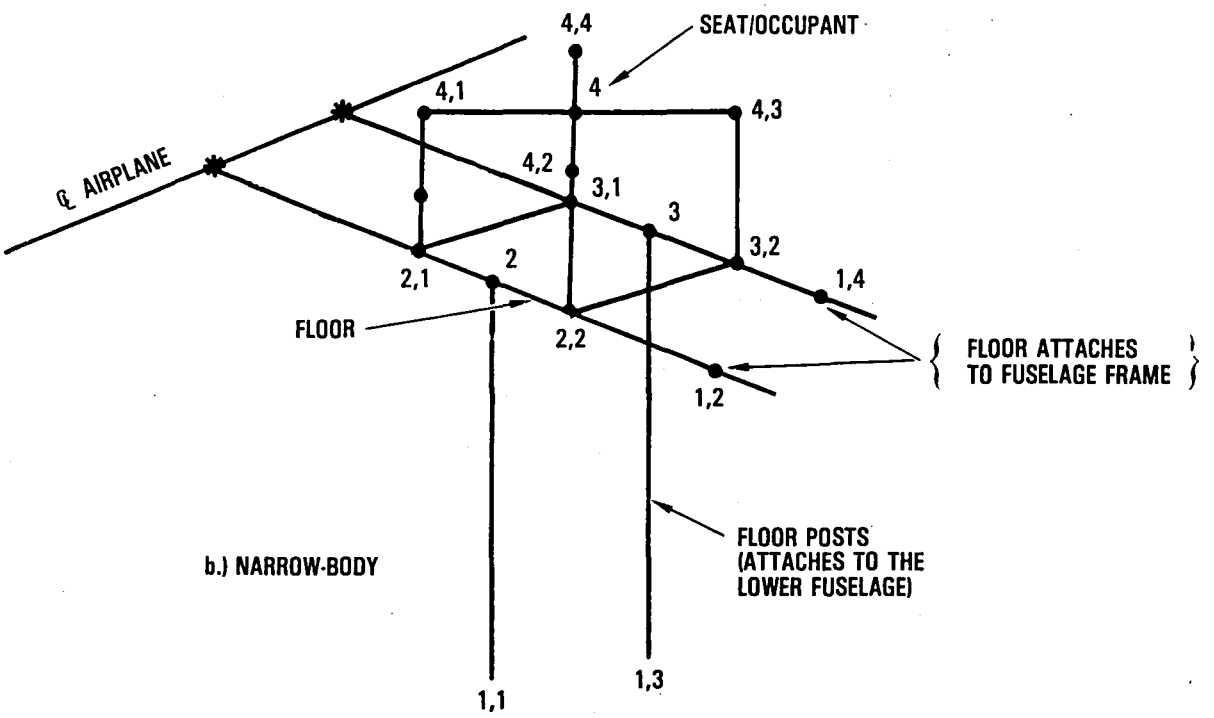

Figure 4-4. Single-row floor analytical models.

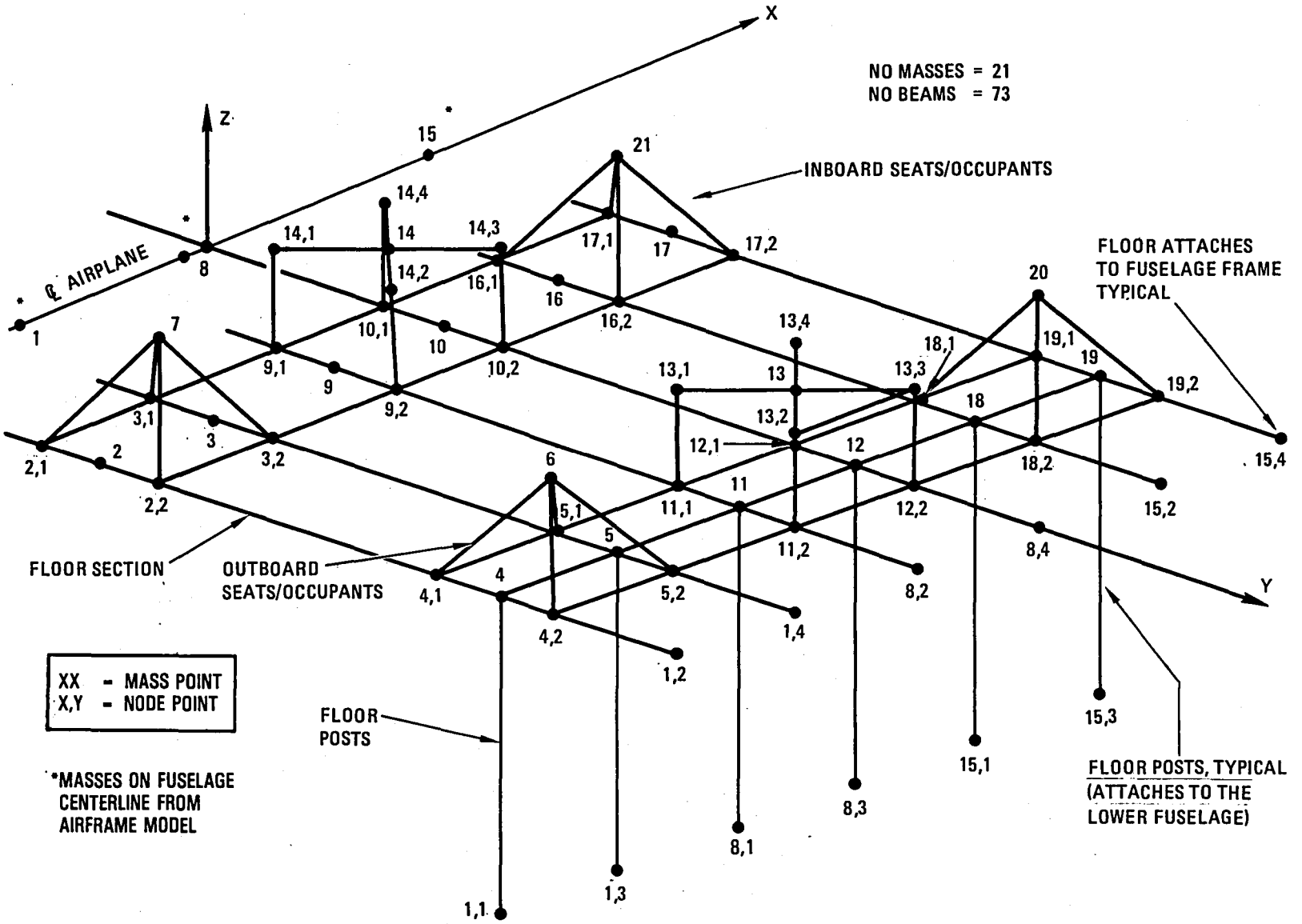

Figure 4-5. - Triple-row floor analytical model.

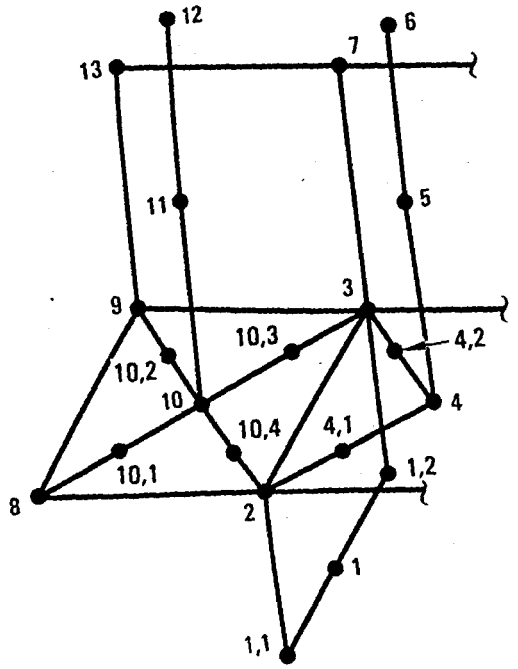

Figure 4-6. Seat/occupant models for 1 and 3 passenger representations.

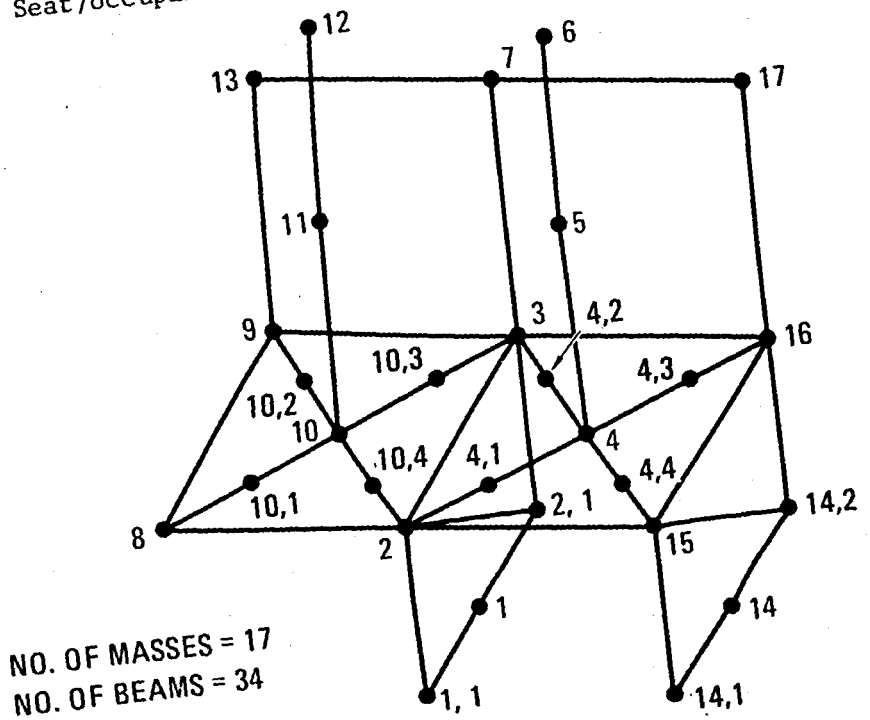

Figure 4-7. Two passenger seat/occupant model.

TABLE 4-1. - MODEL SIZE AND COSTS

	Airframe		Floor		Occupant/Seat		
	Total (2)	Fuselage	Single Row	Triple Row	Single	Double (1)	Triple
No. masses	26 – 41	8 – 23	7	21	7	17	13
No. beams	27 – 42	7 – 22	21	73	12	34	26
Integration interval time required (sec.)	.00002 – .00020		.00004 – .00008	.00004 – .00008	.00002 – .00004	.00002 – .00004	.00002 – .00004
Simulation time required	.5 – 1.5		.100 – .300	.100 – .300	.100 – .200	.100 – .200	.100 – .200
CPU sec/msec analysis	.6 – 5.25		1.2 – 2.4	1.2 – 7.2	0.8 – 1.6	1.35 – 2.7	1.1 – 2.2
Factor**	.30 – 7.85		.12 – .72	.36 – 2.16	.08 – .32	.135 – .54	.11 – .44

(1) Applicable to unsymmetrical model only

(2) Includes wing, landing gears, engine, occupant/seat masses (2 locations)

* Unsymmetrical models size increase ≈ 1.7 x symmetrical model

** (CPU sec/msec analyses) x simulation required time

TABLE 4-2. - RANGE OF MODEL REQUIREMENTS

	Symmetrical				Unsymmetrical			
	(1 Location)		(3 Location)		(1 Location)		(3 Location)	
	Masses	Beams	Masses	Beams	Masses	Beams	Masses	Beams
Airframe (1)(2)	18	19	18	19	26	37	36	27
Floor (1 row)	7	21	21	63	14	42	42	126
Seat (3 pax) (3)	11	25	33	75	22	50	66	150
Combined	36	65	72	157	62	119	134	303
Airframe (1)(2)	18	19	18	19	26	27	26	27
Floor (3 row)	21	73	63	216	42	146	124	438
Seat (3 pax) (3)	33	75	99	150	66	150	198	450
Combined	52	167	180	385	134	323	348	915

(1) Based on 8 mass fuselage.

(2) Some masses and beams are eliminated when model combined.

(3) Based on 1 seat per row each side of centerline.

model the minimum requirement is for 36 masses and 65 beams. For an unsymmetrical model the requirement could go as high as 348 masses and 915 beams.

The KRASH models applicable to this section of analysis are identified in Table 4-3 with regard to:

- Case Number
- Data Set
- A/P configuration
  - o Weight
  - o Type (narrow body (NB) or wide body (WB))
  - o Full airplane or stubwing
  - o Gear positions (retracted or extended)
  - o Lift
- Terrain
  - o Ground flexibility
  - o Slope
  - o Coefficient of friction
- A/P velocities
  - o Forward
  - o Vertical
  - o Side
- A/P attitude
  - o Roll
  - o Pitch
  - o Yaw
- Notation for allowance of beam failure in math model representation.

TABLE 4-3. - MATRIX OF ANALYSIS CONDITIONS, 6 AND 20-DEGREE SLOPE IMPACTS

Case No.	Data Set	Airplane Configuration					Terrain			Initial Conditions						Beam ⚠1 Rupture Allowed
		Weight Lb	Type	Full A/P Stub Wing	Gear Position	Lift	Ground Flexibility In/Lb	Coeff. Friction μ	Slope Degrees	Velocity Ft/Sec			Altitude, Degrees			
										Fwd	Vertical	Side	Roll	Pitch	Yaw	
NB-1	L1649.AEB1021	159,000	NB	Stub	Off	No	4.17×10^{-5}	1.0	6	172	18.0	0	0	0	0	No
NB-2	L1649.AEB1032	159,000	NB	Stub	Off	No	1.04×10^{-5}	1.0	6	172	18.0	0	0	0	0	No
NB-3	L1649G.AEB1032	159,000	NB	Stub	Off	No	Rigid	0.7	6	172	18.0	0	0	0	0	No
NB-4	L1649G.AEB1032X	159,000	NB	Stub	Off	No	Rigid	1.0	6	172	18.0	0	0	0	0	No
NB-5	L1649.AEB1029	159,000	NB	Stub	Off	No	4.17×10^{-5}	1.0	20	103	34.	0	0	0	0	Yes
NB-6	L1649.AEB1030	159,000	NB	Stub	Off	No	Rigid	0.5	20	103	34.	0	0	0	0	No
WB-1	WT328,AEB1023	328,000	WB	Stub	Off	No	1.04×10^{-5}	1.0	6	172	18.0	0	0	0	0	No
WB-2	WT432.AEB1023	432,000	WB	Stub	Off	No	1.04×10^{-5}	1.0	6	172	18.0	0	0	0	0	No
WB-3	WT328.AEB1023	328,000	WB	Stub	Off	No	Rigid	.7	6	172	18.0	0	0	0	0	No
WB-4	WT328.AEB1023	328,000	WB	Stub	Off	No	Rigid	.7	6	172	18.0	0	0	0	0	No
WB-5	WT328.AEB1023	328,000	WB	Stub	Off	No	4.17×10^{-5}	1.0	6	172	18.0	0	0	0	0	No
WB-6	WT432.AEB1023	432,000	WB	Stub	Off	No	4.17×10^{-5}	1.0	6	172	18.0	0	0	0	0	No

⚠1 Yes is only when failure load is included for cutoff. All Shears and Bending moments are monitored for comparison with airframe strength.

4.2 L1649 CRASH TEST ANALYSES

The L1649 crash test model is similar to that shown in Figure 4-2. The masses, stiffness and size have been modified to be consistent with the L1649 aircraft properties and test configuration. The weight of the simulated airplane is 159,000 pounds. Prior to the slope impacts the gears were deliberately collapsed and the wing fuel tanks were penetrated by trees. The left wing was severed inboard of the engines and the right wing was torn off outboard of the inboard engine. The model was modified to reflect changes in the configuration to match these initial conditions. These consisted of removal of all gears (mass and connection to structure), severing of wing outboard of masses 11 and 20 (Figure 4-2) and no lift. The analysis is performed using a symmetrical half model. The fact that the L1649 has four wing engines instead of two as shown in Figure 4-2 isn't of consequence in this particular analysis because of the assumption that tree penetration has resulted in wing rupture. While there is no mention in the test report, lift may have been deliberately suppressed to prevent lift-off, a procedure not uncommon in simulated crash test. The initial impact conditions used in the analyses are as follows:

- Six-degree slope
  forward velocity = 172 ft/sec
  ground flexibility: rigid, 1.04×10^{-5} in./lb and 4.16×10^{-5} in./lb flexibility
  ground coefficient of friction = .7 and 1.0

- Twenty-degree slope
  forward velocity = 110 ft/sec
  ground flexibility: rigid and 4.16×10^{-5} in/lb flexibility
  ground coefficient of friction = 0.5 and 1.0

The ground flexibilities equate to approximately 2 to 8 inches of ground deflection in the analytical model.

The external crushing characteristics representative of lower fuselage crushing were derived from the current widebody data which are available. The

crushing force levels were assumed to be in proportion to the airplane weight. The crushing distance was assumed to be in proportion to the depth of the structure below the passenger floor.

The terminology used throughout the analysis and with subsequent test data, with regard to the directions of force applied to the body, is as shown in Figure 4-8. The resulting inertia forces act in an opposite direction to the decelerative forces shown.

The analysis is performed considering variation in ground coefficient of friction, ground flexibility and fuselage failure. The analysis is performed for two levels of ground flexibility. While the test documentation does not define ground flexibility, it would appear from observations of test photographs and film that some flexibility should be included. Fuselage failure cutoff values were included for the impact onto the 20-degree slope, since the result of this test condition indicated two fuselage breaks. Figures 4-9 and 4-10 allow for a comparison of the longitudinal and vertical responses obtained analytically with the test data for the 6-degree slope impact. The test data are shown unfiltered and filtered at 20 and a 50 Hz cut-off frequency as noted in Section 3.

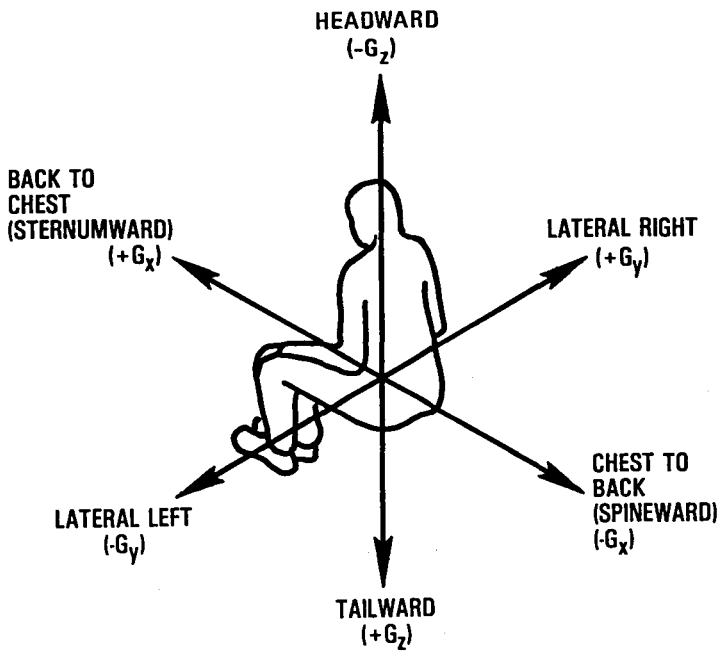

DIRECTION OF DECELERATIVE FORCE

VERTICAL

HEADWARD	–	EYEBALLS DOWN
TAILWARD	–	EYEBALLS UP

TRANSVERSE

LATERAL RIGHT	–	EYEBALLS LEFT
LATERAL LEFT	–	EYEBALLS RIGHT
BACK TO CHEST	–	EYEBALLS IN
CHEST TO BACK	–	EYEBALLS OUT

NOTE: THE DECELERATIVE FORCES APPLIED TO THE BODY ACT IN THE SAME DIRECTION AS THE ARROWS, THE RESULTING INERTIA FORCES ACT OPPOSITE.

Figure 4-8. - Decelerative forces on the body.

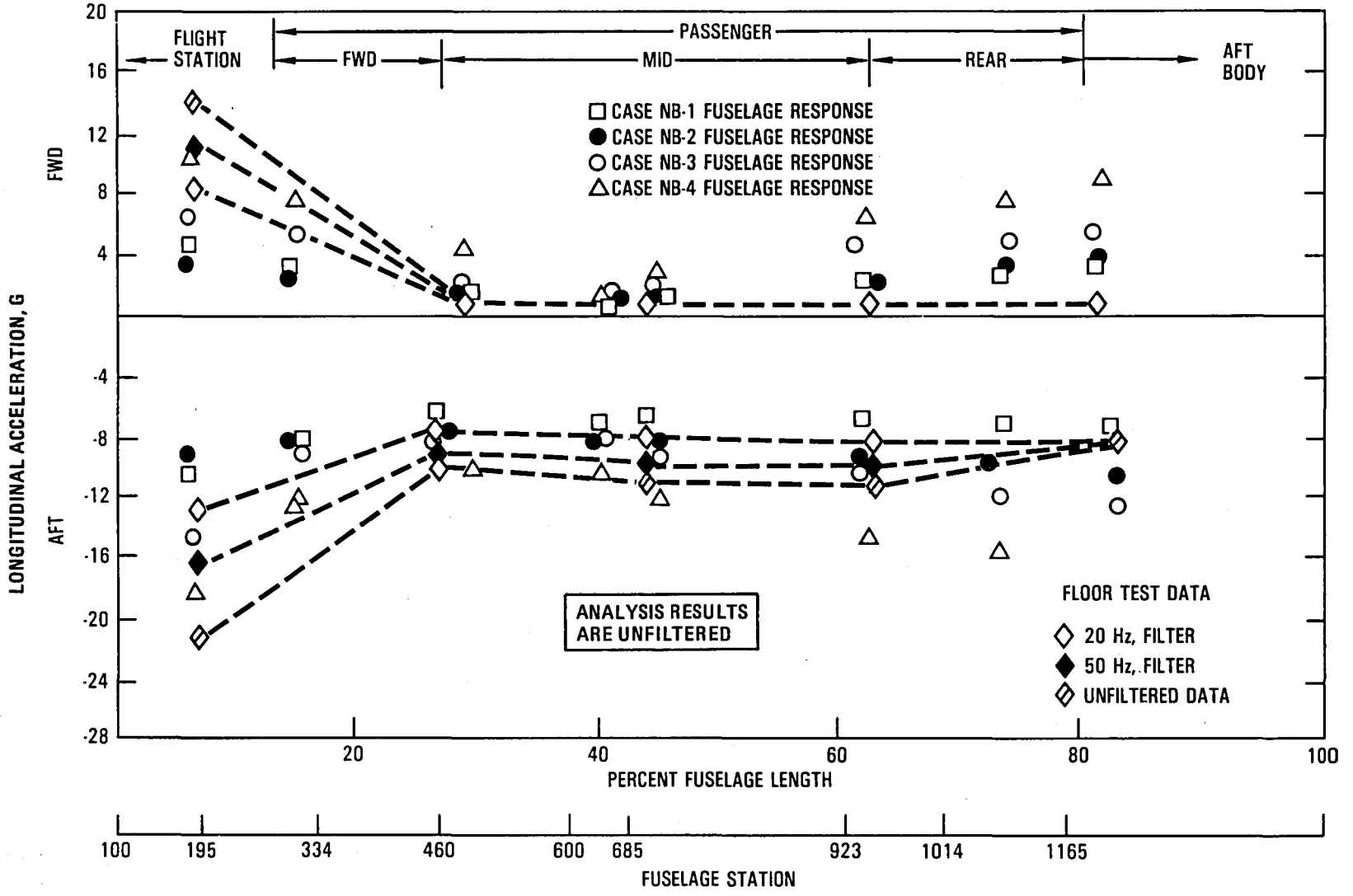

Figure 4-9. Longitudinal acceleration versus fuselage location, 6-degree slope impact, narrow-body airplane.

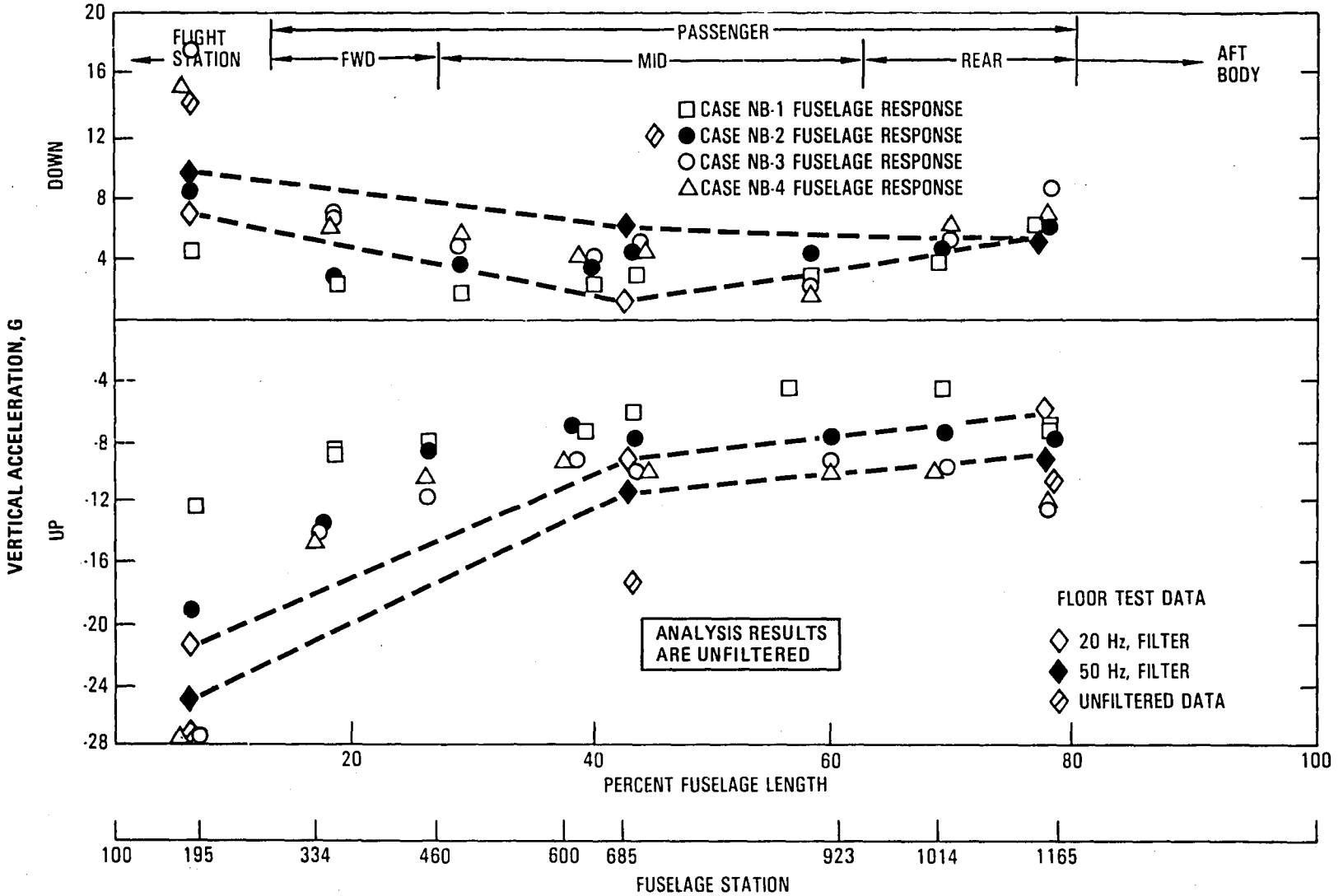

Figure 4-10. Vertical acceleration versus fuselage location, 6-degree slope impact, narrow-body airplane.

Transmissibility studies were also performed by exciting the floor models with longitudinal and vertical pulses through a range of pulse durations. The results showed peaks up to 1.10 times the excitation magnitude in both directions.

The results shown in Figures 4-9 and 4-10 indicate that the two conditions which most closely approximate the L1649 six-degree slope accelerations throughout the fuselage are conditions NB-2 and NB-3. In the longitudinal direction the analysis underestimates the test peak values at the extreme forward stations and overpredicts the test results at the extreme aft station. In the passenger region from FS 460 to 923 there is good agreement in the longitudinal direction regardless of which condition is used. In the vertical direction (Figure 4-9) the rigid ground condition NB-3 shows the agreement at FS 195 and FS 685 where reliable test data are available but overestimates the results at the extreme aft region (FS 1165). The flexible ground case (NB-2) tends to underestimate the vertical response in the forward region while showing good agreement from the mid to aft regions FS 685 to 1165. The addition of ground flexibility tends to soften the vertical response while the increase in ground friction coefficient causes an increase in longitudinal response. The NB-1 condition appears to be too soft particularly in the vertical direction. The rigid ground with μ=1.0 (case NB-4) results in too high a response particularly in the longitudinal direction. Table 4-4 summarizes the unfiltered results for the six-degree impact condition.

Figures 4-11 through 4-14 compare the longitudinal and vertical responses obtained analytically with the test data for the 20-degree slope impact. The test data are filtered as described earlier. The analysis is compared to the test data in two time frames. From the test data it can be seen that the peak loads in the front of the aircraft occur at initial impact with the 20-degree slope. In fact, break-up occurs at initial impact. The loads at the aft end of the fuselage occur approximately 80 to 100 milliseconds after the slope is first contacted by the aircraft. The comparison of the early time frame for this impact is presented in Figures 4-11 and 4-12. From these data it can be seen that the vertical accelerations are lower than reported in the test at the forward fuselage but in good agreement at the aft region with a trend that is consistent with the test data. From the test data (Figure 3-8) it can be seen

TABLE 4-4. L1649 6-DEGREE SLOPE IMPACT UNFILTERED RESPONSES

Region	Location	Direction		Case NB 1			Case NB 2			Case NB 3			Case NB-4		
				Peak g	@ time	(duration)	Peak g	@ time	(duration)	Peak g	@ time	(duration)	Peak g	@ time	(duration)
Flight Station	FS 177	Longitudinal	Aft	- 10.9	@ .150	(.050)	- 8.7	@ .300	(.080)	- 14.8	@ .080	(.040)	- 18.7	@ .090	(.040)
			Fwd	+ 4.4	@ .430	(.040)	+ 3.1	@ .410	(.030)	+ 6.4	@ .170	(.020)	+ 9.5	@ .180	(.030)
		Vertical	Up	- 12.1	@ .090	(.100)	- 18.7	@ .060	(.090)	- 28.3	@ .050	(.080)	- 27.6	@ .050	(.070)
			Down	+ 4.9	@ .330	(.100)	+ 8.9	@ .140	(.050)	+ 17.9	@ .31	(.080)	+ 75.1	@ .130	(.050)
	FS 334	Longitudinal	Aft	- 7.70	@ .150	(.050)	- 8.0	@ .310	(.100)	- 10.4	@ .080	(.040)	- 14.5	@ .080	(.050)
			Fwd	+ 3.3	@ .440	(.030)	+ 2.6	@ .410	(.030)	+ 5.2	@ .170	(.030)	+ 8.0	@ .170	(.020)
		Vertical	Up	- 9.3	@ .090	(.110)	- 13.6	@ .070	(.100)	- 15.1	@ .170	(.080)	- 15.0	@ .070	(.080)
			Down	+ 2.1	@ .480	(.060)	+ 3.3	@ .160	(.030)	+ 7.7	@ .180	(.040)	+ 7.1	@ .280	(.030)
Fwd	FS 460	Longitudinal	Aft	- 7.0	@ .110	(.120)	- 9.0	@ .080	(.110)	- 8.9	@ .080	(.100)	- 12.2	@ .080	(.080)
			Fwd	+ 1.9	@ .430	(.020)	+ 1.3	@ .410	(.030)	+ 2.0	@ .170	(.020)	+ 3.0	@ .140	(.020)
		Vertical	Up	- 7.8	@ .110	(.120)	- 9.3	@ .080	(.110)	- 11.8	@ .080	(.090)	- 11.4	@ .080	(.090)
			Down	+ 2.4	@ .430	(. 04)	+ 4.0	@ .410	(.040)	+ 6.3	@ .200	(.030)	+ 6.0	@ .280	(.030)
	FS 600	Longitudinal	Aft	- 7.6	@ .100	(.120)	- 9.2	@ .060	(.120)	- 8.7	@ .050	(.090)	- 12.2	@ .050	(.10)
			Fwd	+ 0.6	@ .450	(.020)	+ 0.9	@ .440	(.030)	+ 1.3	@ .200	(.02)	+ 1.4	@ .440	(.010)
		Vertical	Up	- 6.6	@ .110	(.120)	- 7.0	@ .090	(.120)	- 10.0	@ .320	(.060)	- 10.0	@ .330	(.050)
			Down	+ 2.7	@ .220	(.070)	+ 3.8	@ .210	(.080)	+ 4.5	@ .19	(.080)	+ 4.0	@ .190	(.070)
Mid	FS 685	Longitudinal	Aft	- 7.9	@ .100	(.120)	- 10.0	@ .070	(.120)	- 10.6	@ .05	(.100)	- 14.7	@ .050	(.080)
			Fwd	+ 1.0	@ .460	(.020)	+ 1.4	@ .440	(.030)	+ 2.4	@ .200	(.020)	+ 3.3	@ .200	(.020)
		Vertical	Up	- 5.9	@ .120	(.130)	- 8.7	@ .29	(.070)	- 10.7	@ .230	(.080)	- 11.0	@ .340	(.060)
			Down	+ 3.2	@ .220	(.060)	+ 4.8	@ .200	(.070)	+ 6.8	@ .19	(.050)	+ 6.3	@ .190	(.030)
	FS 923	Longitudinal	Aft	- 7.8	@ .110	(.120)	- 10.7	@ .070	(.100)	- 12.2	@ .060	(.060)	- 17.1	@ .060	(.060)
			Fwd	+ 2.4	@ .470	(.040)	+ 12.1	@ .200	(.030)	+ 6.0	@ .270	(.020)	+ 7.0	@ .210	(.030)
		Vertical	Up	- 4.1	@ .290	(.080)	- 9.6	@ .280	(.060)	- 9.7	@ .33	(.120)	- 11.4	@ .340	(.100)
			Down	+ 3.2	@ .500	(.050)	+ 5.1	@ .460	(.050)	+ 3.2	@ .490	(.030)	+ 2.5	@ .500	(.020)
Aft	FS 1015	Longitudinal	Aft	- 7.9	@ .110	(.120)	- 11.0	@ .070	(.100)	- 13.1	@ .060	(.060)	- 18.2	@ .060	(.060)
			Fwd	+ 3.3	@ .210	(.030)	+ 3.1	@ .490	(.030)	+ 5.2	@ .210	(.020)	+ 8.0	@ .210	(.020)
		Vertical	Up	- 5.0	@ .38	(.060)	- 9.8	@ .280	(.070)	- 18.7	@ .380	(.080)	- 10.9	@ .360	(.120)
			Down	+ 3.6	@ .500	(.050)	+ 6.4	@ .470	(.050)	+ 4.8	@ .510	(.080)	+ 5.6	@ .100	(.030)
Aft Body	FS 1165	Longitudinal	Aft	- 8.6	@ .120	(.160)	- 11.7	@ .070	(.100)	- 13.8	@ .060	(.060)	- 19.4	@ .060	(.050)
			Fwd	+ 3.8	@ .340	(.030)	+ 2.7	@ .200	(.030)	+ 6.0	@ .210	(.020)	+ 10.1	@ .140	(.030)
		Vertical	Up	- 8.3	@ .220	(.130)	- 7.7	@ .350	(.090)	- 14.3	@ .380	(.120)	- 1.3	@ .380	(.120)
			Down	+ 5.8	@ .130	(.120)	+ 6.3	@ .110	(.120)	+ 8.7	@ .100	(.100)	+ 6.3	@ .510	(.060)

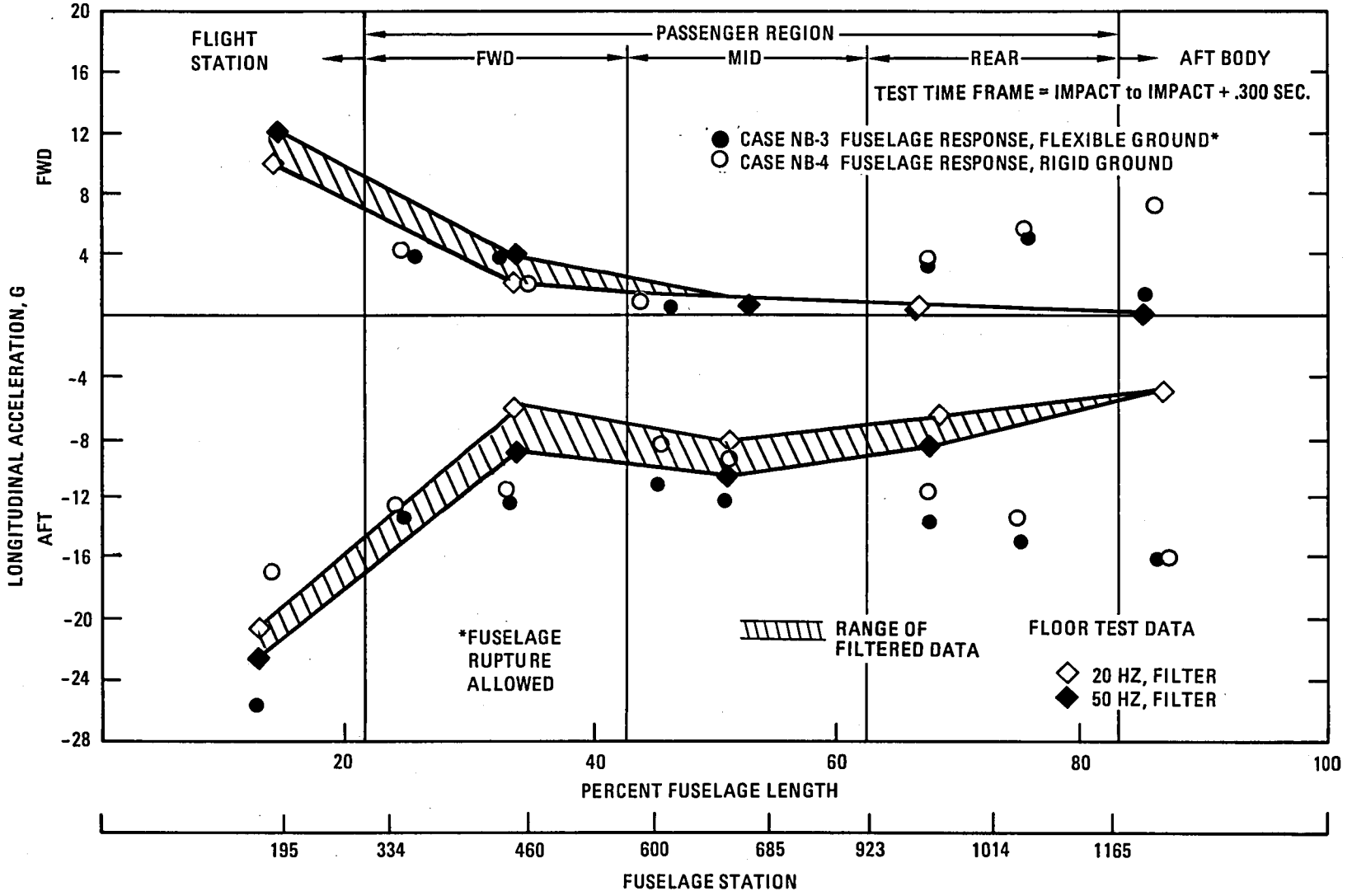

Figure 4-11. - Longitudinal acceleration versus fuselage location, 20 degree slope impact, narrow-body airplane.

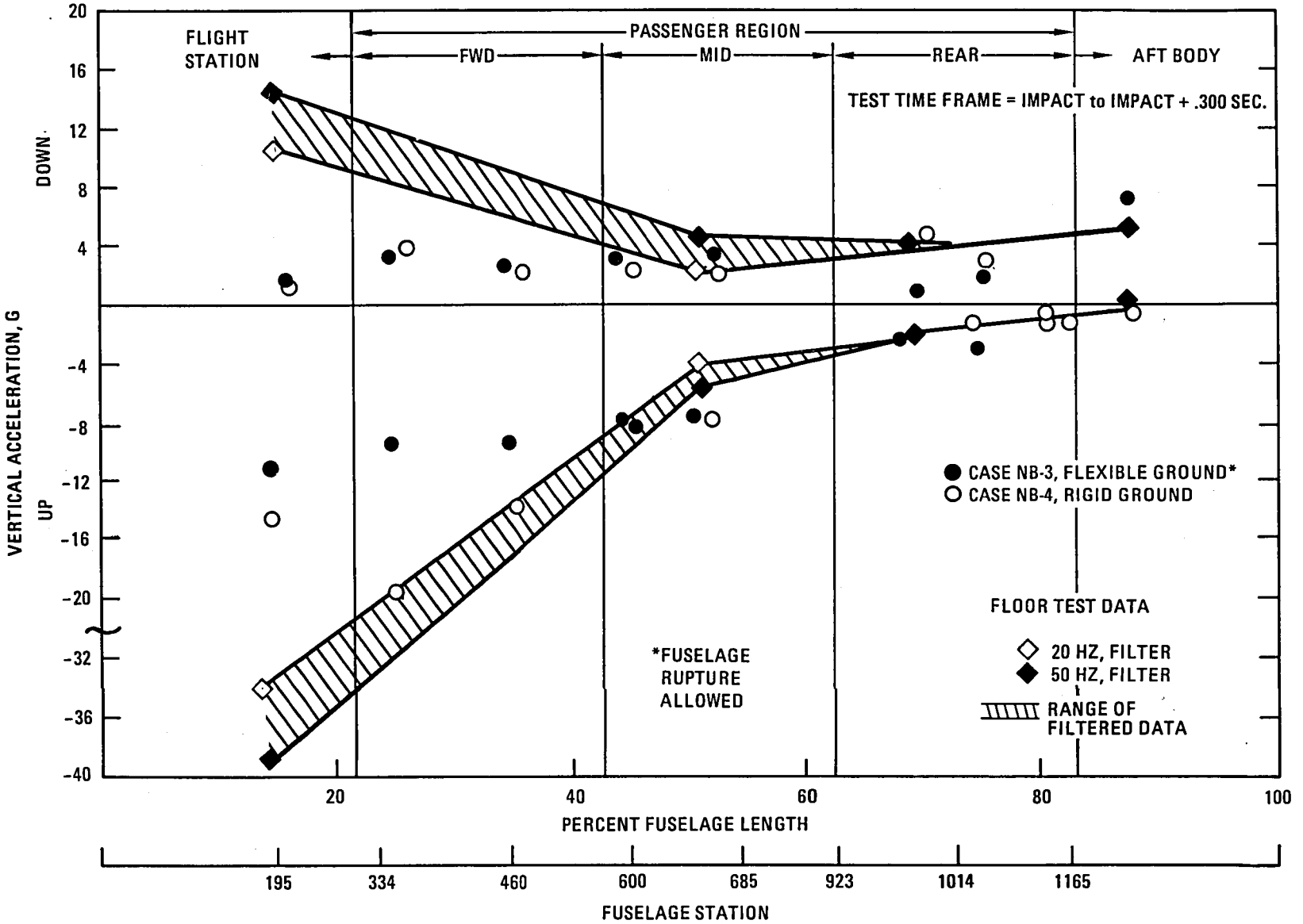

Figure 4-12. - Vertical acceleration versus fuselage location, 20 degree slope impact, narrow-body airplane.

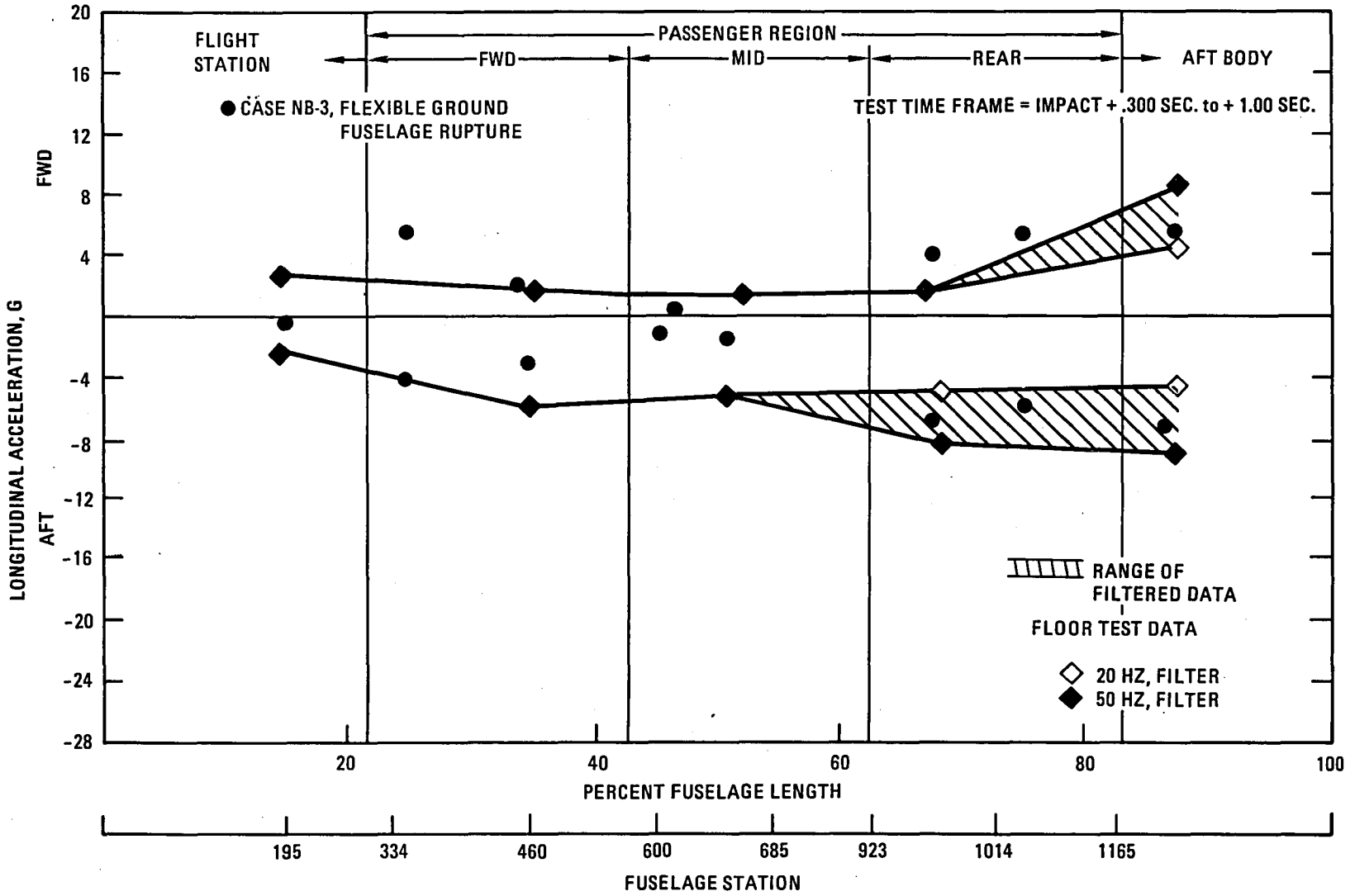

Figure 4-13. - Longitudinal acceleration versus fuselage location, 20 degree slope impact, narrow-body airplane.

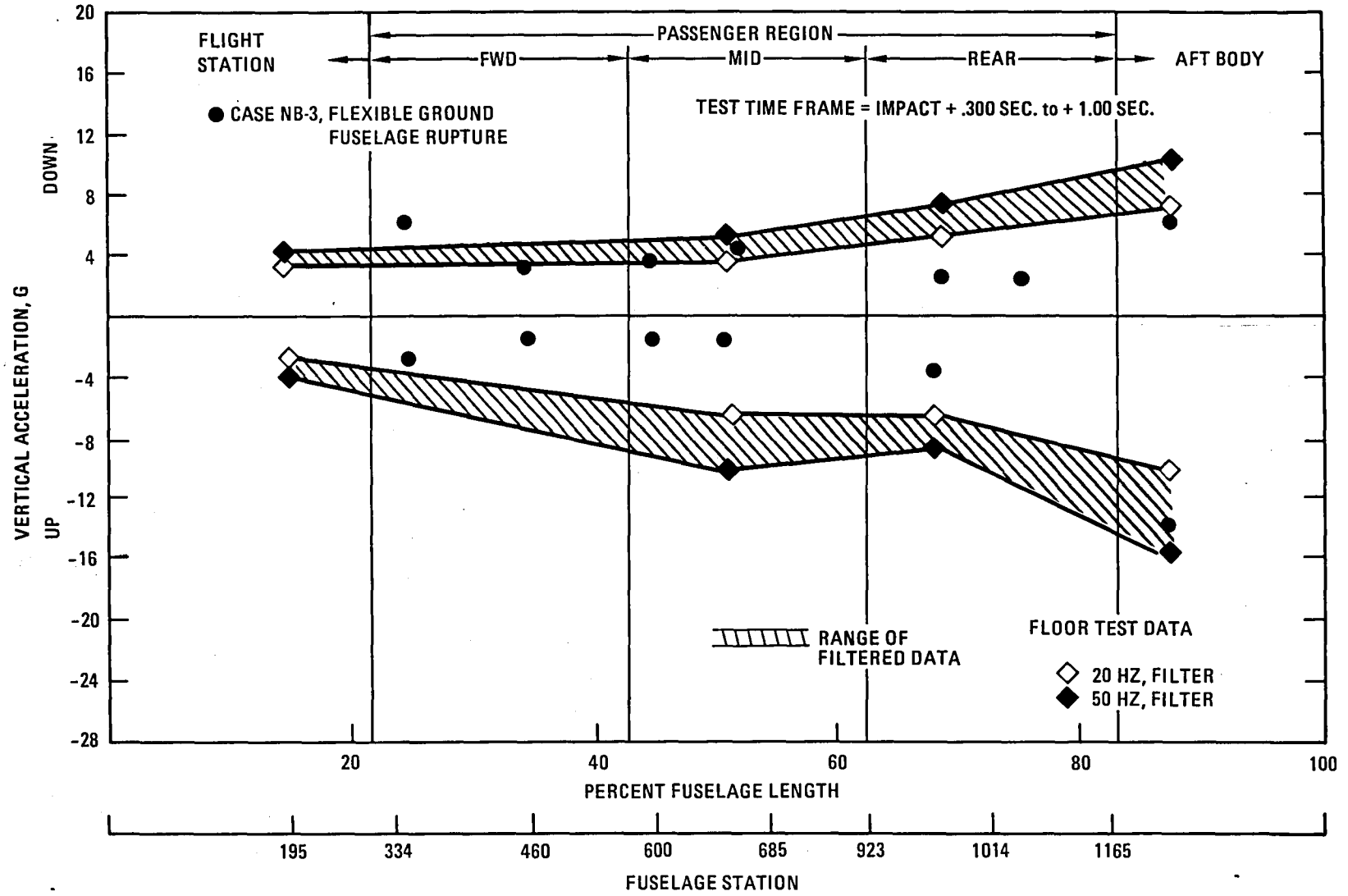

Figure 4-14. - Vertical acceleration versus fuselage location, 20 degree slope impact, narrow-body airplane.

that there is a spike (≥.010 seconds duration) occuring during the rupture of the fuselage. The analysis does not reproduce this spike. The test results, without the spike, would be closer to 15 g's trapezoidal for ~50 milliseconds, which would be close to the analysis results if a floor transmissibility factor were included. The longitudinal analyses results are consistent with the test results in the forward region, but higher in the aft region. In the analysis, the aft section ruptures at an earlier time than it should. If the aft region failure loads had occurred later in the analysis they would match better with the test data at failure (see Figures 4-11 and 4-13) of the tail section. From Figure 4-11 it can be observed that both the analysis and test are in reasonable agreement except for the accelerations associated with the fuselage break-up. Figure 4-14 shows the comparison of test and analysis results for the vertical acceleration toward the latter part of the 20 degree slope impact condition. As is the situation in the longitudinal direction, the analytical peak values in the aft fuselage region occur earlier than was indicated by the test results. Both Figures 4-11 and 4-12 show analytical results for the rigid surface impact (case NB-6 Table 4-3). The rigid surface appears to increase the vertical accelerations, which provides a closer approximation to the test results. The longitudinal results do not change significantly.

The results of the analyses indicate the sensitivity of the crash dynamics modeling to such parameters as ground effects (flexibility and coefficient of friction) as well as the representation of crushable structure. Additional model refinements could be attempted to try to match or tune the analysis results to the test results. However, while some improvement could be anticipated, it is doubtful that a total agreement would be achieved. Within the framework of reasonable assumptions, representations and utilization of available data, it is felt that the model has demonstrated all the significant response phenomena associated with the L-1649 full crash test. The six-degree slope impact, in particular, is important since it represents a condition prior to structure break-up, and, consequently, provides some insight into possible floor pulses.

4.3 COMPARISON OF WIDE-BODY AND NARROW-BODY ANALYSIS RESULTS

The analysis of the L-1649 narrow body airplane establishes a baseline KRASH model configuration for a particular crash condition. The baseline model can now be used to compare to other airplane configurations, for which current structural data are available and preliminary analysis was previously performed, (Reference 1). The crash condition in the wide-body airplane analysis are the same as those for the narrow-body:

- Six-degree slope impact
- Wing rupture
- Loss of aerodynamic lift
- Ground flexibility = Rigid and 1.04×10^{-5} lb/in
- Ground coefficient of friction = 1.0
- Forward velocity = 172 ft/sec.

The acceleration response results for two different aircraft weight, 328,000 lbs. landing and 432,000 lbs. takeoff, are provided in Figures 4-15 through 4-18 and Tables 4-5 and 4-6. Figure 4-19 shows the ratio of shear and bending loads to estimated ultimate values along the fuselage for both landing and takeoff weight analyses. An upper and lower bound ratio is presented. The lower bound values are obtained using KRASH internally calculated loads based on input data. The upper bound is based on the design limit data projected to ultimate values. The actual failure load (which is input by the user into KRASH) is most likely between the two. However, the actual values are not accurately known because tests to determine these values are not normally performed.

From the data presented in Figures 4-15, 4-16, and Table 4-5 which are based on rigid terrain, the longitudinal pulses are observed to be lower for the wide-body aircraft as compared to the narrow-body aircraft throughout the fuselage. In a comparable passenger region encompassing the region between .20 to .70 normalized fuselage length, the wide-body results show an amplitude decrease of

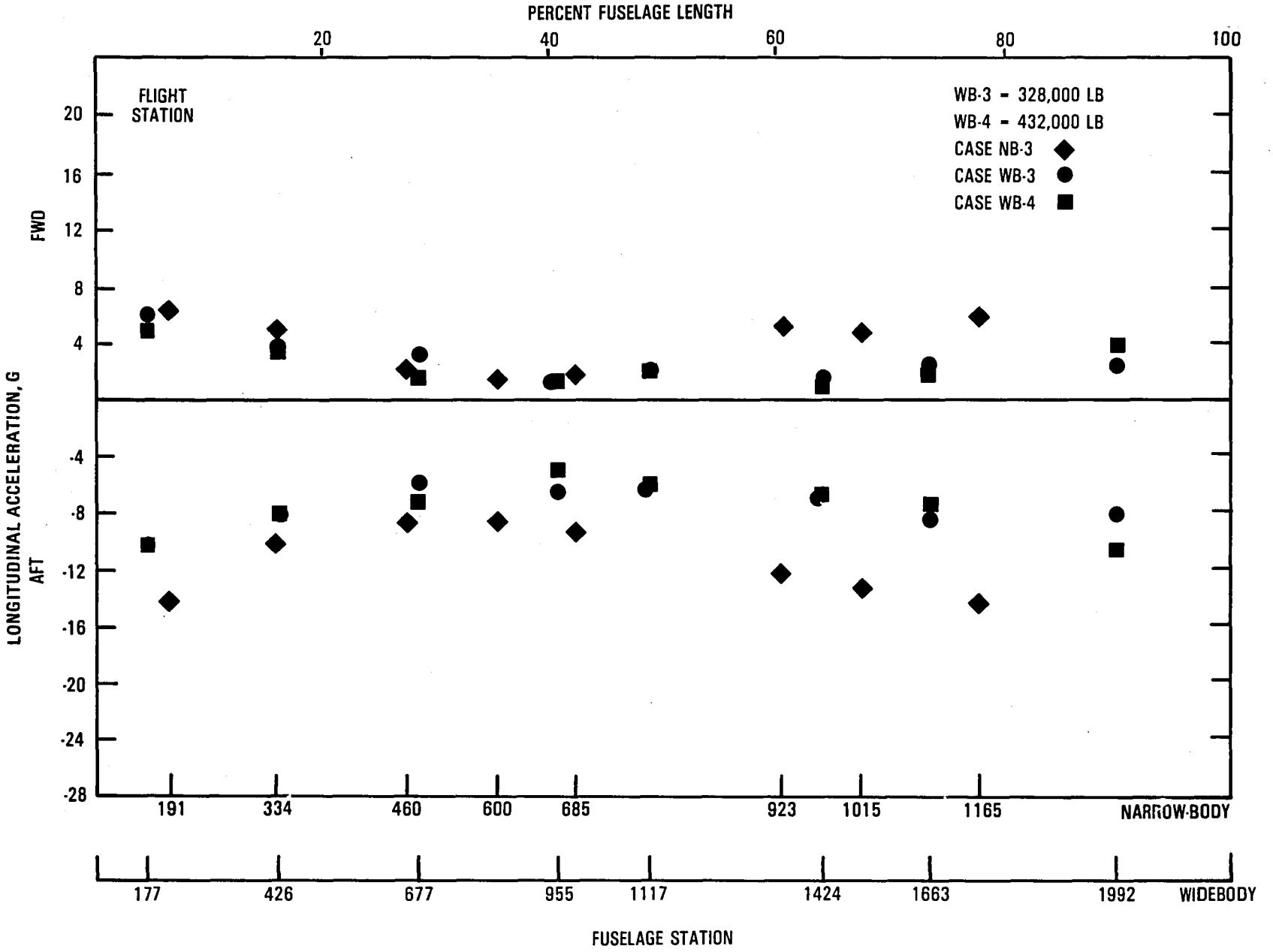

Figure 4-15. - Longitudinal acceleration versus fuselage location, 6 degrees slope impact, wide-body airplane, rigid ground.

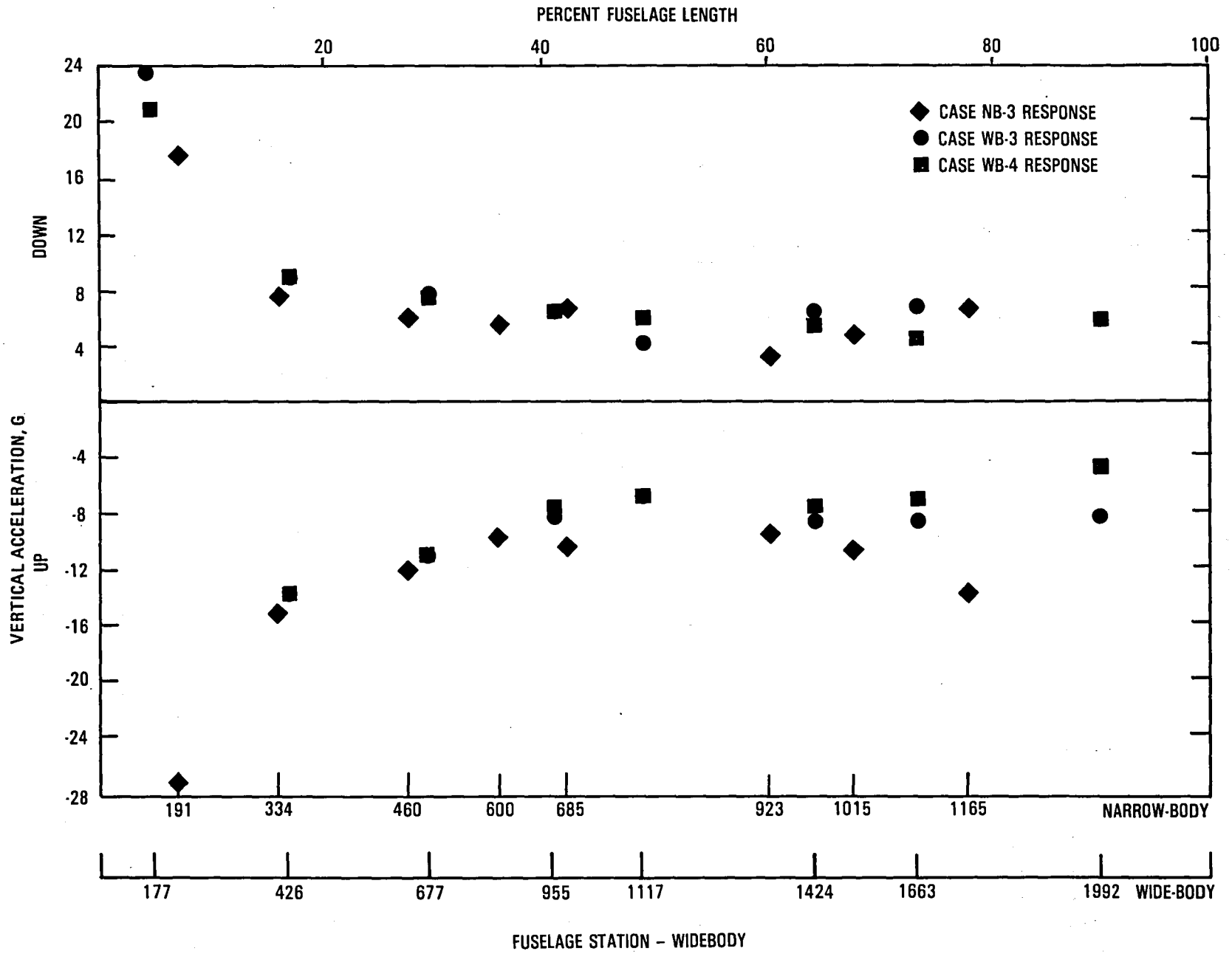

Figure 4-16. - Vertical acceleration versus fuselage location, 6 degrees slope impact, wide-body airplane, rigid ground.

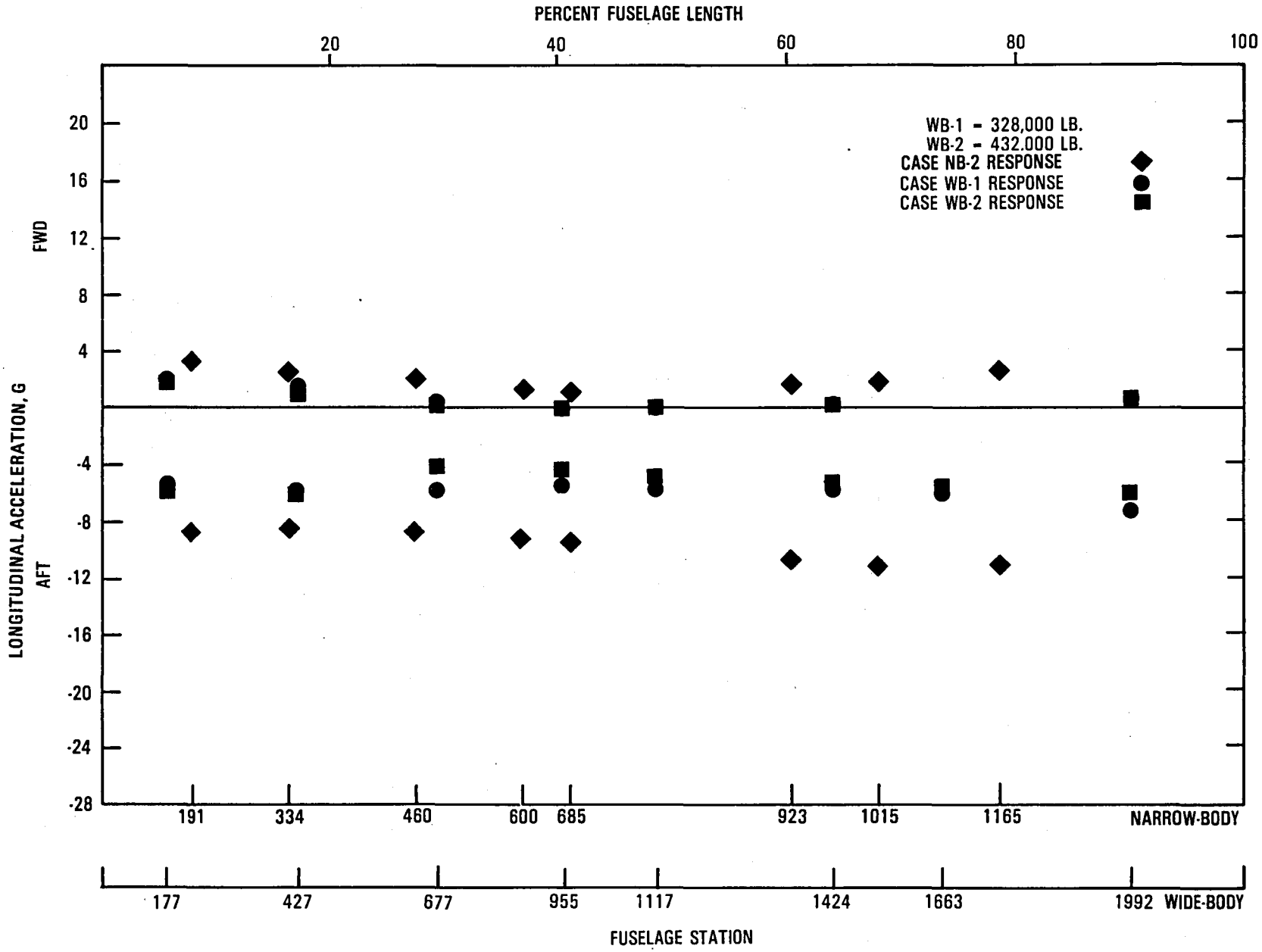

Figure 4-17. - Longitudinal acceleration versus fuselage location, 6 degrees slope impact, wide-body airplane, flexible ground.

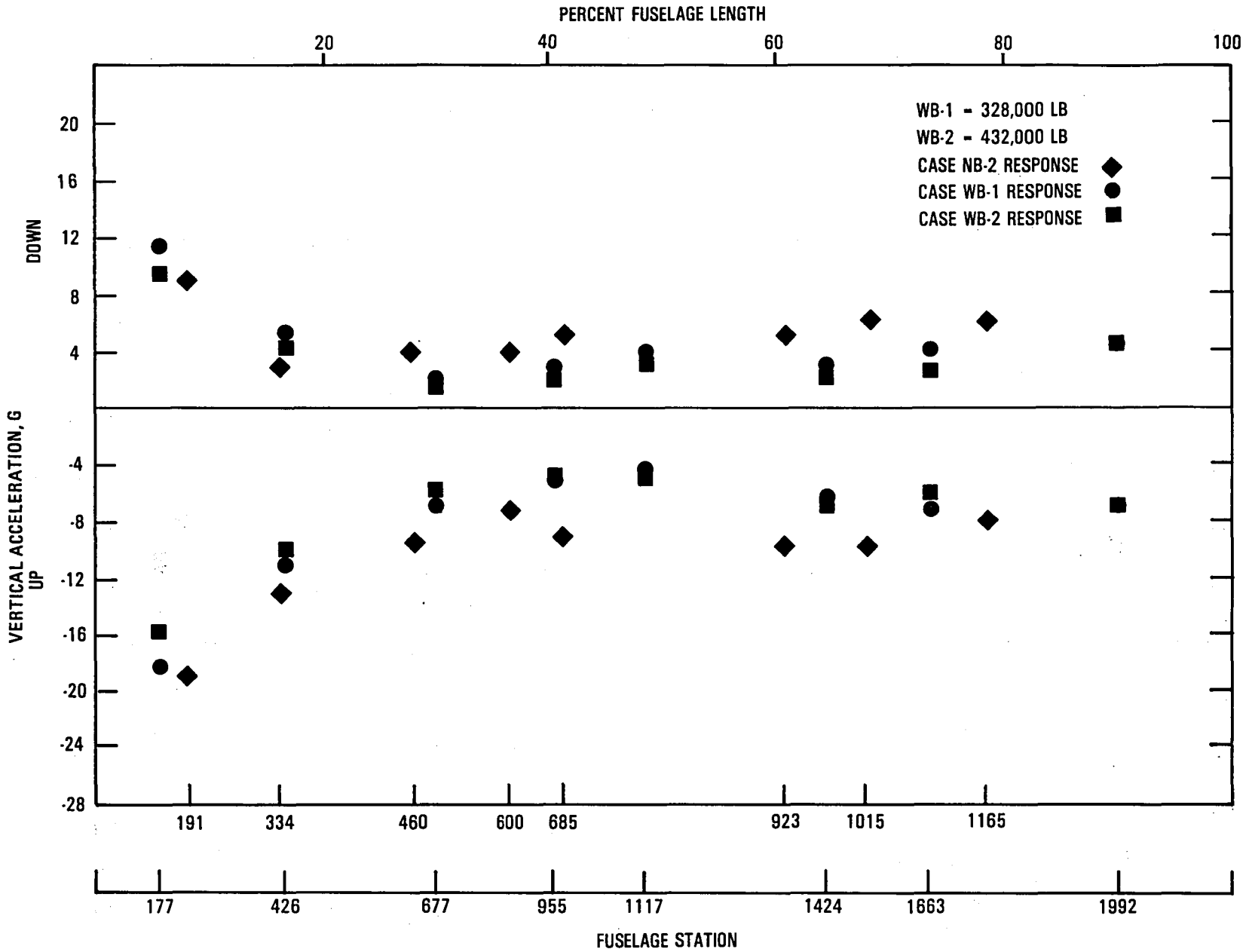

Figure 4-18. - Vertical acceleration versus fuselage location, 6 degrees slope impact, wide-body airplane, flexible ground.

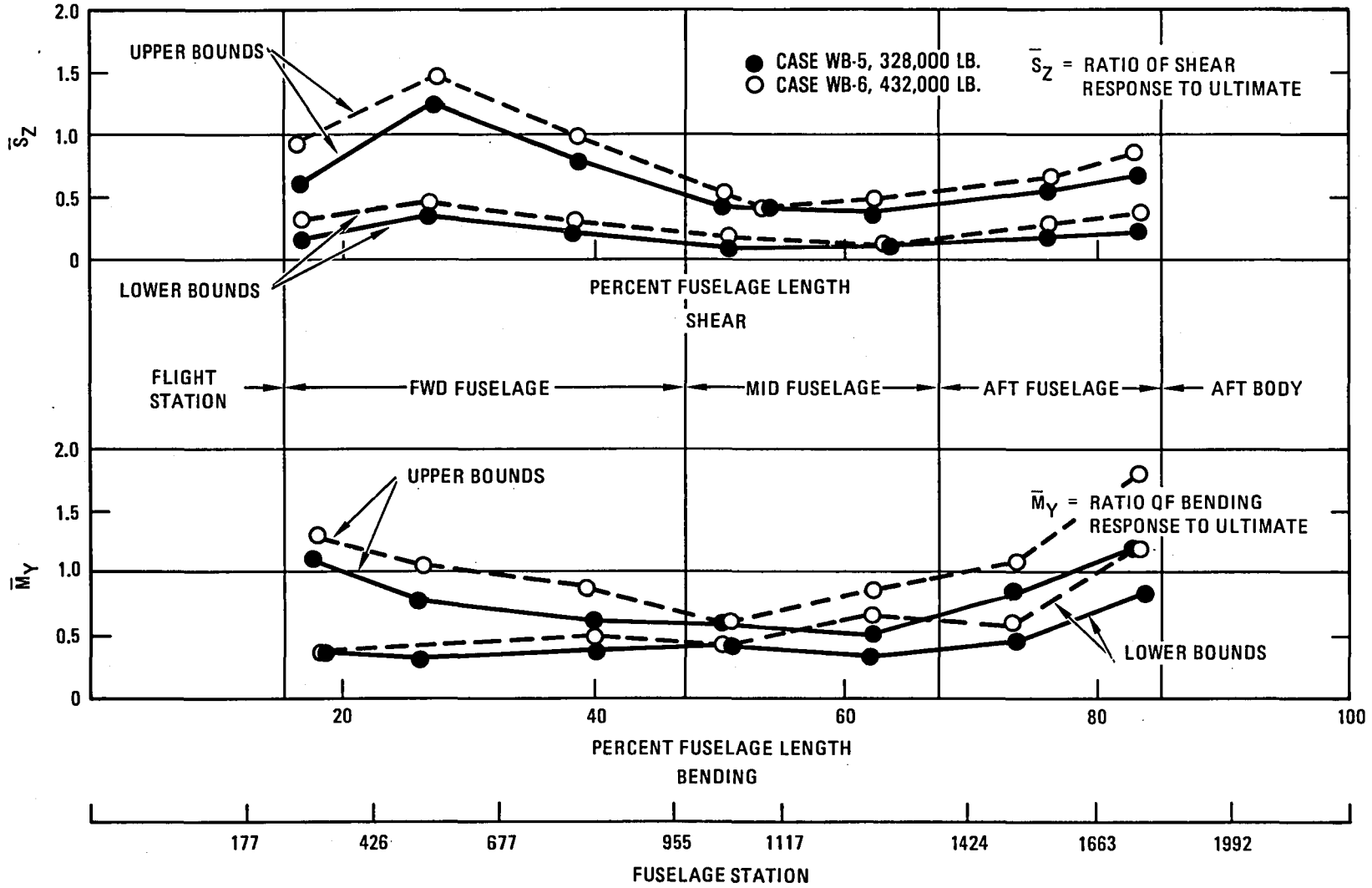

Figure 4-19. - Fuselage shear and bending loads, 6-degree slope, wide-body airplane.

TABLE 4-5. - SUMMARY OF NARROW-BODY AND WIDE-BODY ANALYTICALLY OBTAINED RESPONSES, 6-DEGREE SLOPE IMPACT, RIGID GROUND.

Region	Location ①/②	Direction		Case NB-2 Peak g @ time (duration)	Case WB-3 Peak g @ time (duration)	Case WB-4 Peak g @ time (duration)	Peak g @ time (duration)
Flight Station	FS 199/ 177	Longitudinal	Aft	- 14.8 @ .080 (.040)	- 10.2 @ .110 (.040)	- 10.5 @ .030 (.040)	
			Fwd	+ 6.4 @ .170 (.020)	+ 6.6 @ .130 (.020)	+ 5.2 @ .060 (.020)	
		Vertical	Up	- 28.3 @ .050 (.080)	- 33.8 @ .050 (.080)	- 30.3 @ .050 (.090)	
			Down	+ 17.9 @ .310 (.080)	+ 21.0 @ .120 (.060)	+ 24.3 @ .140 (.050)	
	FS 334/ 426	Longitudinal	Aft	- 10.4 @ .080 (.040)	- 8.0 @ .020 (.020)	- 8.1 @ .080 (.030)	
			Fwd	+ 5.2 @ .170 (.030)	+ 5.4 @ .140 (.020)	+ 3.3 @ .160 (.020)	
		Vertical	Up	- 15.1 @ .170 (.080)	- 15.8 @ .050 (.080)	- 14.0 @ .030 (.090)	
			Down	+ 7.7 @ .280 (.040)	+ 8.5 @ .380 (.100)	+ 9.2 @ .170 (.050)	
Fwd	FS 460/ 677	Longitudinal	Aft	- 8.9 @ .080 (.100)	- 5.8 @ .020 (.040)	- 6.7 @ .080 (.040–.100)	
			Fwd	+ 2.0 @ .170 (.020)	+ 3.7 @ .130 (.020)	+ 1.9 @ .160 (.010)	
		Vertical	Up	- 11.8 @ .080 (.090)	- 14.5* @ .030 (.090)	- 11.3 @ .080 (.040–.090)	
			Down	+ 6.3 @ .280 (.030)	+ 7.5 @ .46 (.050)	+ 7.8 @ .170 (.050)	
	FS 600/ 955	Longitudinal	Aft	- 8.7 @ .050 (.090)	- 7.1 @ .040 (.070)	- 5.3 @ .090 (.040–.100)	
			Fwd	+ 1.3 @ .200 (.02)	+ 1.7 @ .150 (.020)	+ 1.5 @ .130 (.020)	
		Vertical	Up	- 10.0 @ .370 (.060)	- 8.0 @ .040 (.090)	- 6.6 @ .040 (.05–.120)	
			Down	+ 4.5 @ .19 (.080)	+ 6.5 @ .270 (.080)	+ 6.1 @ .320 (.05–.09)	
Mid	FS 685/ 1117	Longitudinal	Aft	- 10.6 @ .050 (.100)	- 6.9 @ .050 (.080)	- 6.3 @ .050 (.07)	
			Fwd	+ 2.4 @ .200 (.020)	+ 1.7 @ .200 (.020)	+ 1.9 @ .180 (.02)	
		Vertical	Up	- 10.7 @ .230 (.080)	- 6.7* @ .050 (.060)	- 6.6 @ .410 (.060)	
			Down	+ 6.8 @ .190 (.050)	+ 5.4 @ .270 (.080)	+ 6.9 @ .320 (.050)	
	FS 923/ 1424	Longitudinal	Aft	- 12.2 @ .060 (.060)	- 7.5 @ .050 (.070)	- 6.8 @ .050 (.100)	
			Fwd	+ 6.0 @ .270 (.020)	+ 1.5 @ .110 (.010)	+ 0.8 @ .180 (.020)	
		Vertical	Up	- 9.7 @ .330 (.120)	- 11.4* @ .360 (.050)	- 6.7 @ .410 (.070)	
			Down	+ 3.2 @ .490 (.030)	+ 6.9 @ .230 (.060)	+ 5.8 @ .260 (.060)	
Aft	FS 1015/ 1663	Longitudinal	Aft	- 13.1 @ .060 (.060)	- 9.4 @ .060 (.060)	- 8.3 @ .060 (.070)	
			Fwd	+ 5.2 @ .210 (.020)	+ 2.7 @ .170 (.020)	+ 1.7 @ .310 (.020)	
		Vertical	Up	- 10.7 @ .380 (.080)	- 10.5* @ .360 (.040)	- 6.8 @ .380 (.060)	
			Down	+ 4.8 @ .510 (.080)	+ 6.8 @ .520 (.030)	+ 3.1 @ .120 (.050)	
Aft Body	FS 1165/ 1922F	Longitudinal	Aft	- 13.8 @ .060 (.060)	- 8.4 @ .060 (.060)	- 10.6 @ .060 (.060)	
			Fwd	+ 6.0 @ .210 (.120)	+ 2.3 @ .180 (.020)	+ 3.9 @ .160 (.020)	
		Vertical	Up	- 14.3 @ .380 (.120)	- 8.0 @ .370 (.040)	- 5.0 @ .350 (.07–.100)	
			Down	+ 8.7 @ .100 (.100)	+ 5.7 @ .53 (.020)	+ 6.0 @ .170 (.170)	

① Narrow-body
② Wide-body

* 50 Hz FILTERED DATA SHOWS -11.3, -5.1, -8.6 AND -8.0 "g" FOR MASS LOCATION FS677, 1117, 1663 & 1992, RESPECTIVELY.

TABLE 4-6. - COMPARISON OF NARROW-BODY AND WIDE-BODY ANALYTICALLY OBTAINED RESPONSES, 6-DEGREE SLOPE IMPACT, FLEXIBLE GROUND.

Region	Location ①/②	Direction		Case NB 2	Case WB-1	Case WB 2	
				Peak g @ time (duration)	Peak g @ time (duration)	Peak g @ time (duration)	Peak g @ time (duration)
Flight Station	FS 199/ 177	Longitudinal	Aft	- 8.7 @ .300 (.080)	- 5.2 @ .110 (.070)	- 5.8 @ .120 (.060)	
			Fwd	+ 3.1 @ .410 (.030)	+ 1.9 @ .180 (.010)	+ 2.0 @ .220 (.010)	
		Vertical	Up	- 18.7 @ .060 (.090)	- 18.1 @ .070 (.100)	- 15.4 @ .070 (.100)	
			Down	+ 8.9 @ .140 (.050)	+ 11.0 @ .150 (.090)	+ 8.7 @ .440 (.130)	
	FS 334/ 426	Longitudinal	Aft	- 8.0 @ .310 (.100)	- 5.8 @ .580 (.060)	- 5.0 @ .130 (.120)	
			Fwd	+ 2.6 @ .410 (.030)	+ 1.6 @ .320 (.010)	+ 1.0 @ .220 (.010)	
		Vertical	Up	- 13.6 @ .070 (.100)	- 11.3 @ .070 (.100)	- 10.3 @ .080 (.110)	
			Down	+ 3.3 @ .160 (.030)	+ 4.6 @ .170 (.080)	+ 3.7 @ .180 (.090)	
Fwd	FS 460/ 677	Longitudinal	Aft	- 9.0 @ .080 (.110)	- 5.5 @ .580 (.080)	- 4.1 @ .490 (.160)	
			Fwd	+ 1.3 @ .520 (.030)	+ 4.4 @ .060 (.100)	— — —	
		Vertical	Up	- 9.3 @ .080 (.110)	- 6.7 @ .080 (.110)	- 6.4 @ .100 (.140)	
			Down	+ 4.0 @ .410 (.040)	+ 2.0 @ .310 (.040)	+ 1.5 @ .340 (.050)	
	FS 600/ 955	Longitudinal	Aft	- 9.2 @ .060 (.120)	- 5.4 @ .570 (.080)	- 4.4 @ .090 (.160)	
			Fwd	+ 0.9 @ .440 (.030)	+ 5.1 @ .080 (.110)	— — —	
		Vertical	Up	- 7.0 @ .090 (.120)	- 4.9 @ .100 (.130)	- 4.9 @ .460 (.140)	
			Down	+ 3.8 @ .210 (.080)	+ 3.2 @ .280 (.080)	+ 2.3 @ .33 (.140)	
Mid	FS 685/ 1117	Longitudinal	Aft	- 10.0 @ .070 (.120)	- 5.3 @ .070 (.120)	- 4.6 @ .080 (.150)	
			Fwd	+ 1.4 @ .440 (.030)	— — —	— — —	
		Vertical	Up	- 8.7 @ .29 (.070)	- 4.2 @ .380 (.120)	- 4.8 @ .470 (.150)	
			Down	+ 4.8 @ .200 (.070)	+ 3.6 @ .290 (.090)	+ 2.8 @ .320 (.120)	
	FS 923/ 1424	Longitudinal	Aft	- 10.7 @ .070 (.100)	- 5.4 @ .080 (.120)	- 5.1 @ .080 (.160)	
			Fwd	+2.1 @ .200 (.030)	— — —	— — —	
		Vertical	Up	-9.6 @ .280 (.060)	- 6.4 @ .570 (.060)	- 6.7 @ .480 (.08–.14)	
			Down	+ 5.1 @ .460 (.050)	+ 2.8 @ .270 (.090)	+ 2.1 @ .320 (.080)	
Aft	FS 1015/ 1663	Longitudinal	Aft	- 11.0 @ .070 (.100)	- 5.8 @ .080 (.120)	- 5.5 @ .080 (.160)	
			Fwd	+ 3.1 @ .49 (.030)	— — —	— — —	
		Vertical	Up	- 9.80 @ .280 (.070)	- 6.8 @ .570 (.050)	- 5.8 @ .490 (.050)	
			Down	+ 6.4 @ .470 (.050)	+ 4.2 @ .450 (.050)	+ 1.5 @ .120 (.120)	
Aft Body	FS 1165/ 1922	Longitudinal	Aft	- 11.7 @ .070 (.100)	- 5.9 @ .080 (.100)	- 5.8 @ .090 (.120)	
			Fwd	+ 2.7 @ .200 (.030)	+ 7.5 @ .600 (.06)	— — —	
		Vertical	Up	- 7.7 @ .350 (.090)	- 7.0 @ .600 (.06)	- 7.2 @ .600 (.08+)	
			Down	+ 6.3 @ .110 (.120)	+ 4.7 @ .140 (.160)	+ 4.7 @ .160 (.200)	

① Narrow-body
② Wide-body

25 to 40 percent. In the vertical direction the responses are reasonably close except in the mid to aft fuselage region (.40 to .70 normalized fuselage length) where the widebody response is up to 20 percent less than the narrow-body response. The analysis results using the flexible ground show a similar trend as does the analysis with the rigid ground.

Figure 4-20 shows a forward fuselage cross-section for both a wide-body and narrow-body aircraft drawn to the same scale. At a forward fuselage station (FS 677) of the wide-body airplane the analysis indicates that an amplification factor of ≅1.25 in the vertical direction exists between the inboard seat floor location and airframe. The outboard seat location above the floor posts shows about the same response as the airframe. Since the narrow-body configuration seating arrangement results in occupants being closer to the floor posts the corresponding amplification factor at a comparable forward fuselage station is less than 1.1. Thus the peak floor vertical pulses could be nearly the same. The pulse durations for both the narrow and wide body analyses are reasonably close, in the range of 60 to 120 milliseconds.

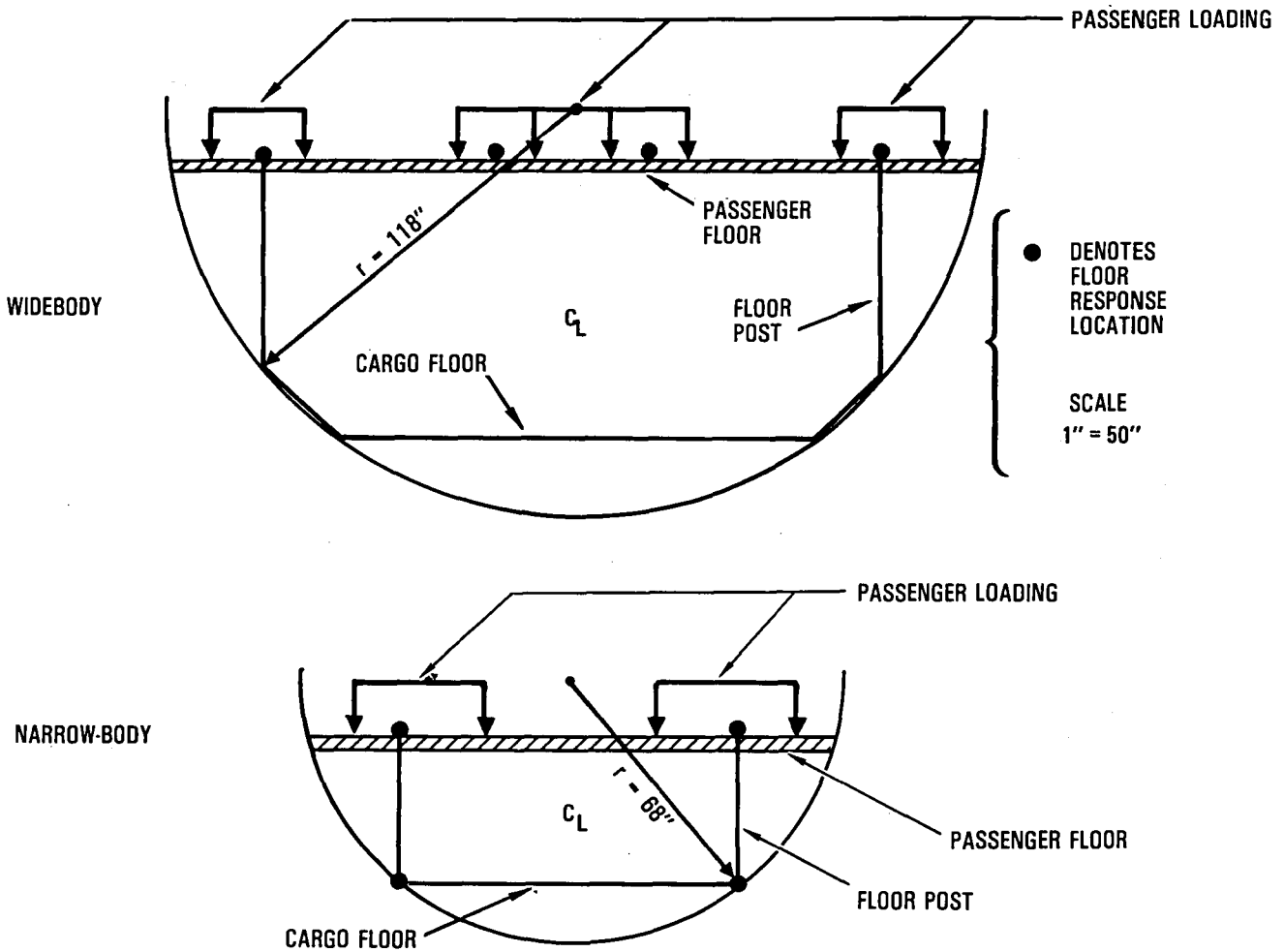

Figure 4-20. - Comparison of wide-body and narrow-body fuselage configurations.

5. WIDE-BODY CANDIDATE CRASH ANALYSIS

5.1 Candidate Crash Scenarios

The candidate crash scenarios formulated during the Reference 1 studies are described in Section 2. There are many mode of failures that can be associated with each of the scenarios. Figures 5-1, 5-2, and 5-3 illustrate the structure related events that can lead to occupant trauma hazards for each of the candidate crash scenarios. Some of the events which can lead to trauma form the basis for the wide-body analyses studies. Table 5-1 provides a matrix of conditions for which analyses are performed.

The ground-to-ground scenario analysis is performed for a range of forward velocities from 80 to 110 knots, for rigid and flexible terrain, and a rate of descent or Effective Normal Velocity (ENV) of from 6 to 18 ft/sec. For all overrun conditions aerodynamic lift is assumed to be available at time of impact, but will be ramped to zero in 1 second. Both take-off and landing weight configurations are analyzed. Only the collapsed gear condition is analyzed.

The hard landing ground impact scenario considers a landing weight configuration at a landing speed of 160 knots and an airplane pitch attitude of 0, 6 and 15 degrees nose-up. The impact surface is rigid and aerodynamic lift is available. The landing gears are extended in all cases. Two landing weights, but at a different airplane c.g. are considered.

The air-to-ground impact scenario runs are similar to the hard landing except that unsymmetrical conditions are introduced. No columnar, contour or frontal impacts are analyzed for the air-ground impacts.

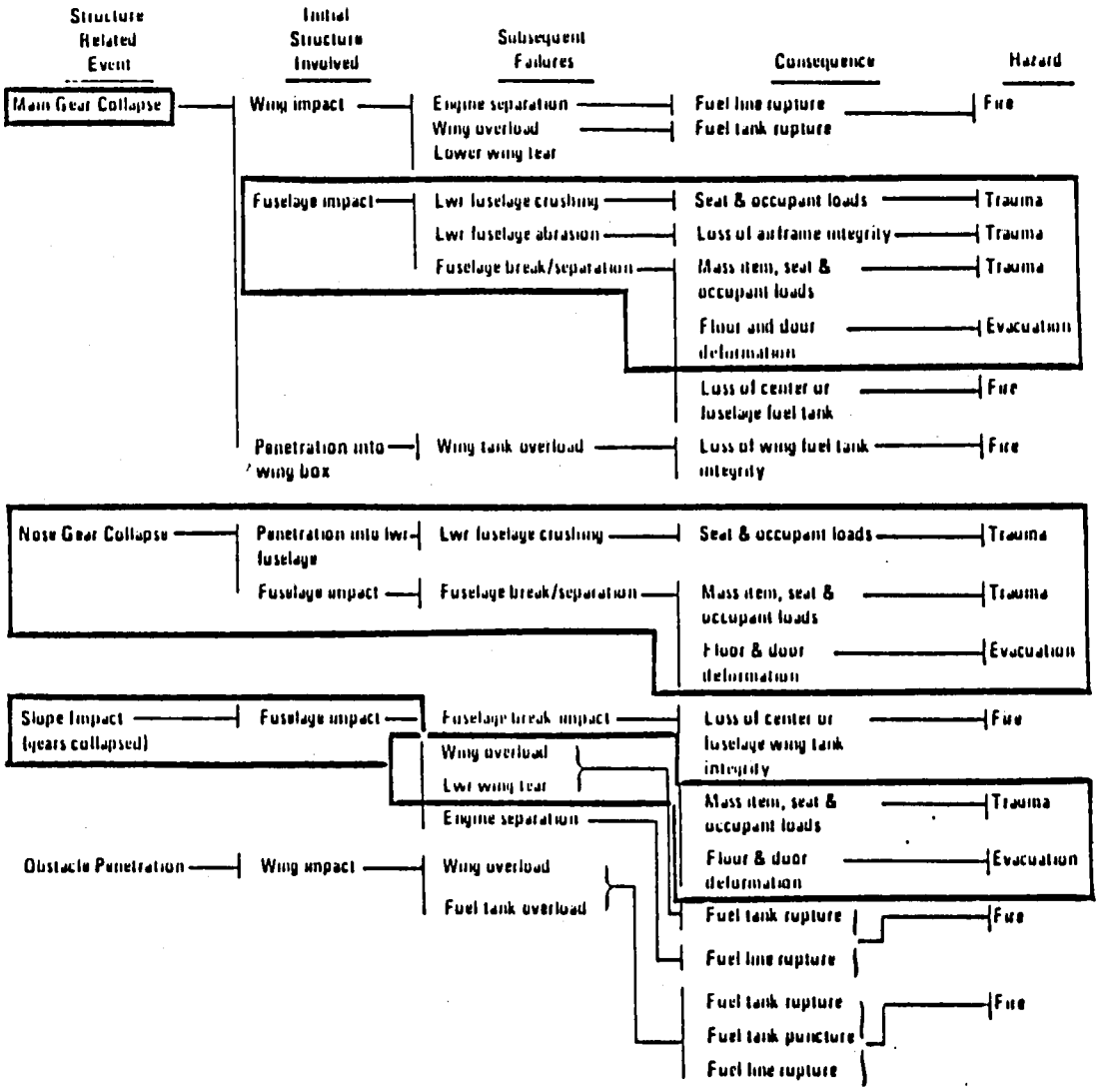

Figure 5-1. - Ground-to-ground, overrun crash scenario sequence.

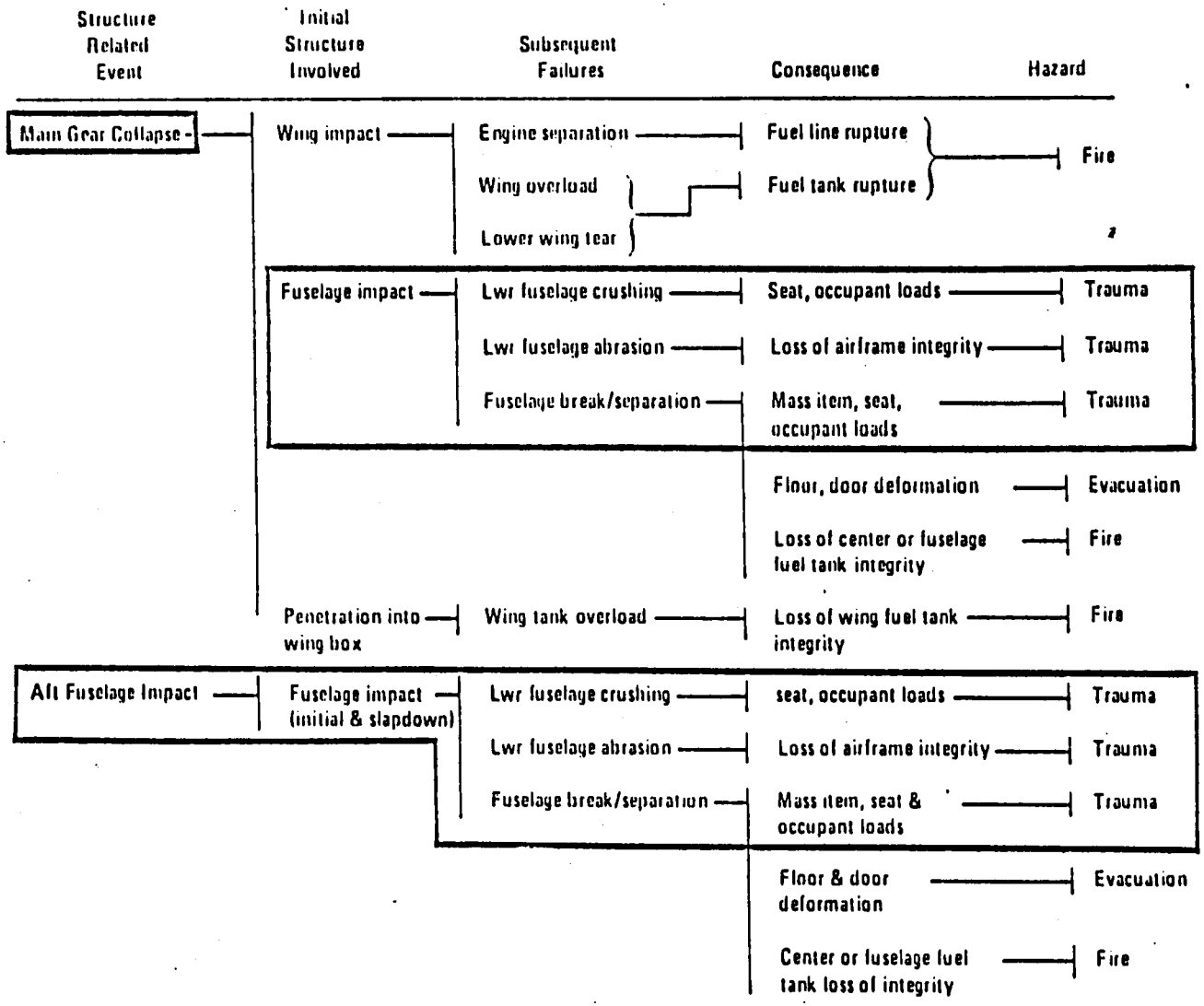

Figure 5-2. - Air-to-ground, hard landing crash scenario sequence.

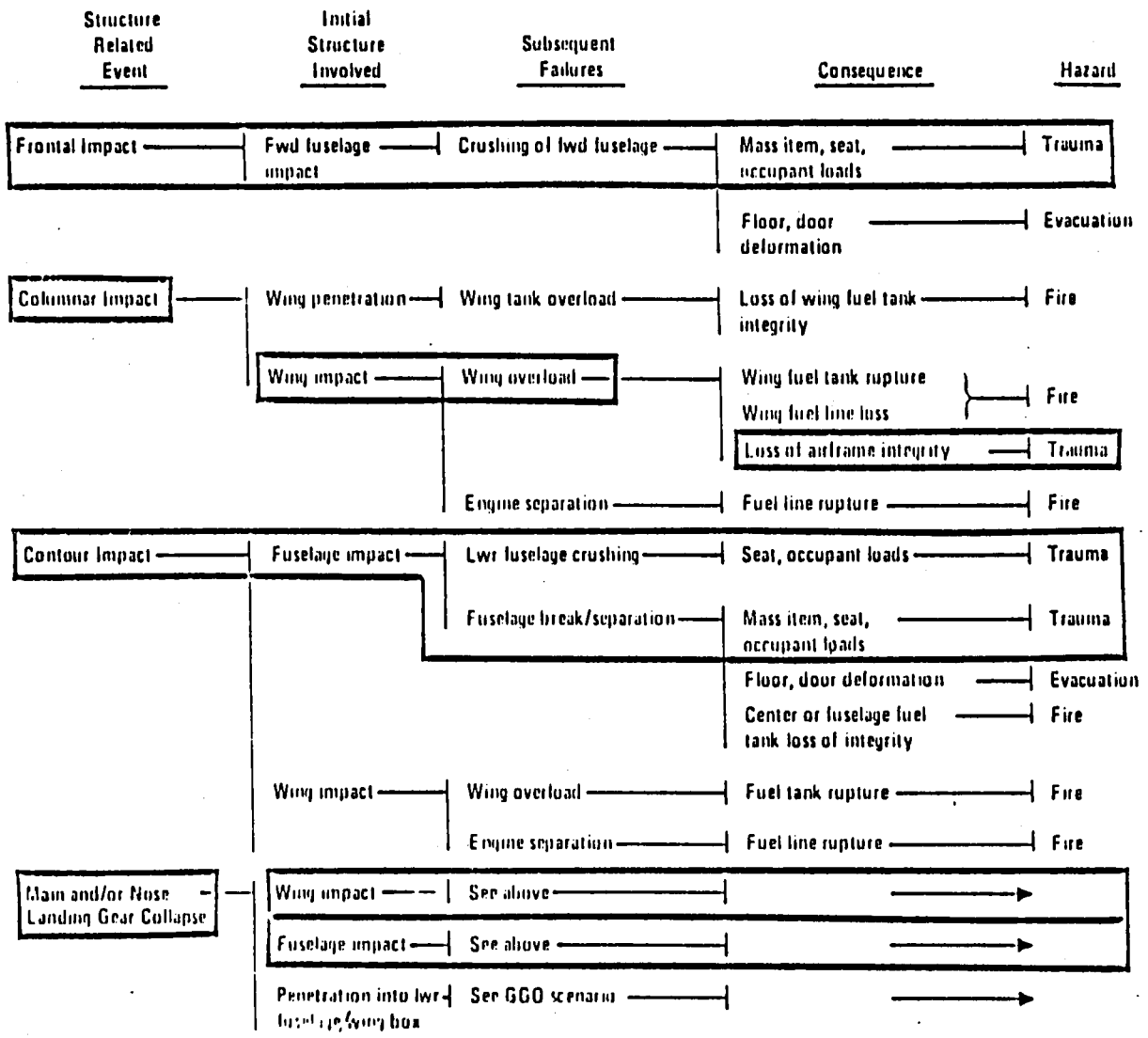

Figure 5-3. - Air-to-ground, impact crash scenario sequence.

TABLE 5-1. - MATRIX OF CANDIDATE CRASH SCENARIO CONDITIONS

Scenario	A - 358,000 Lb, 29% MAC									B - 328,000 Lb, 23% MAC									C - 432,000 Lb, 21% MAC								
	Ground	Slope	Fwd. Velocity (Kts)	Vertical Velocity (Ft/Sec)	Roll Angle, Deg	Pitch Angle, Deg	Yaw Angle, Deg	Gear Position	Lift	Ground	Slope	Fwd. Velocity (Kts)	Vertical Velocity (Ft/Sec)	Roll Angle, Deg	Pitch Angle, Deg	Yaw Angle, Deg	Gear Position	Lift	Ground	Slope	Fwd. Velocity (Kts)	Vertical Velocity (Ft/Sec)	Roll Angle, Deg	Pitch Angle, Deg	Yaw Angle, Deg	Gear Position	Lift
GGO-1										F	Yes	80	6				Off	Yes									
-2										R	Yes	80	6				Off	Yes	R	Yes	80	6				Off	Yes
3										F	Yes	110	18				Off	Yes									
4										R	Yes	110	18				Off	Yes	R	Yes	110	18				Off	Yes
5										F	Yes	80	6			30	Off	Yes									
6										R	Yes	80	6			30	Off	Yes									
AGHL-1	R	No	160	15		6		Ext	Yes	R	No	160	15		6		Ext	Yes									
-2	R	No	160	20		15		Ext	Yes	R	No	160	20		15		Ext	Yes									
-3	R	No	160	20		6		Ext	Yes																		
-4	R	No	160	20		0		Ext	Yes																		
-5	R	No	160	15		15		Ext	Yes																		
AGI-1	R	No	160	15		6	30	Ext	Yes																		
-2	R	No	160	20		6	30	Ext	Yes																		
-3	R	No	160	15	20	6	30	Ext	Yes	R	No	160	15	20	6	30	Ext	Yes									

F = Flexible ground
R = Rigid ground
Ext = Extended

5.2 Fuselage Structural Arrangement

The fuselage structural arrangement for the widebody airplane to be analyzed is shown in Figure 5-4. The fuselage is a conventional semi-monocoque structure of aluminum alloy material, and has a circular cross-section, 235 inches in diameter for the major portion of the length. All of this constant section plus the flight station and a small section where the fuselage begins to taper at the aft end form the fuselage pressure shell, which is designed for the pressure differential attained with an 8,000-foot cabin altitude at an airplane altitude of 42,000 feet. Cabin pressurization loads dictate the use of a skin thickness of 0.068 inches minimum in this constant-diameter section fuselage to ensure a satisfactory fatigue life.

The fuselage shell is assembled from large bonded panel assemblies - four of these being joined to make up a barrel section. Each of the quarter panels consists of skin, doublers, and titanium fail-safe straps, which are bonded together and reinforced with riveted stringers and splice plates.

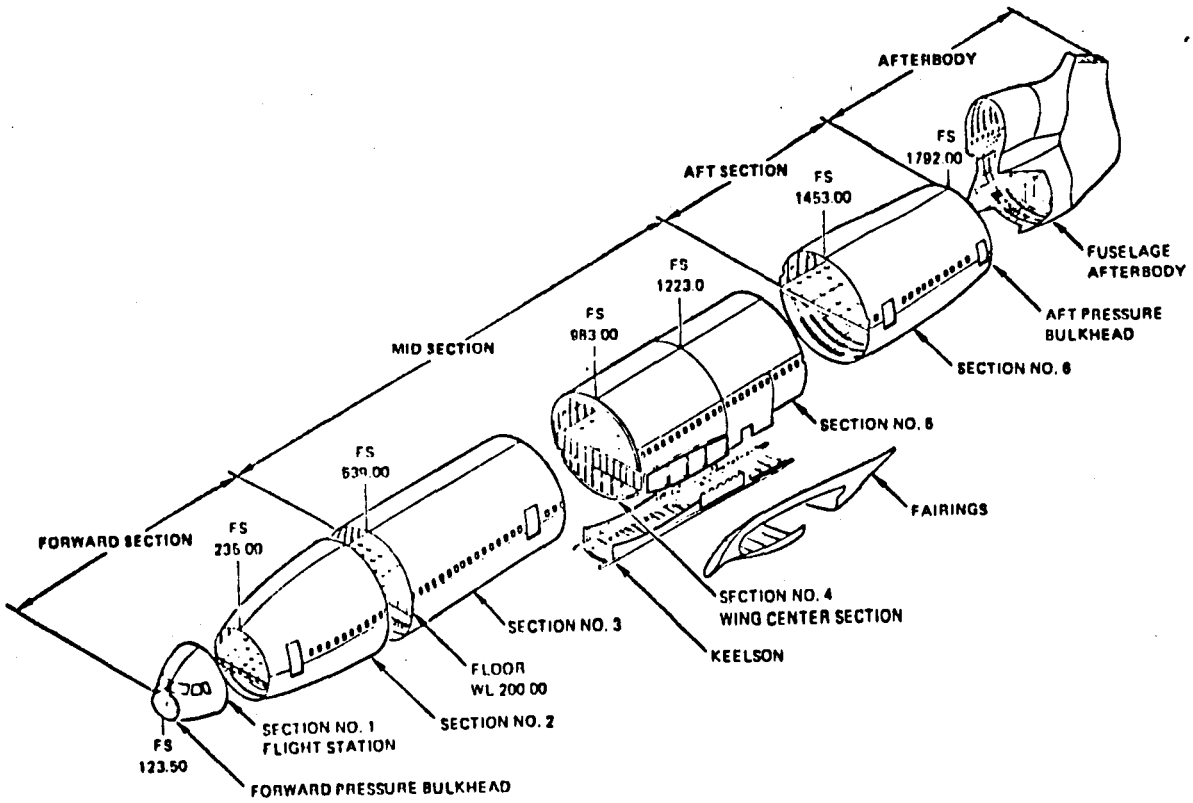

Figure 5-4. - Fuselage structural arrangement.

Clad 2024-T3 aluminum alloy is used predominantly for the light-forgings and extrusions. The frames are either 7075-T6 clad or 7178-T6 (bare or clad), depending on location. Heavier frames are used around all doors, and these are reinforced with doublers, intercostals, and fittings.

With the exception of the main frames and door members, the fuselage frames are three inches deep at the sides of the cabin. They widen to a depth of approximately six inches at the top of the fuselage and five inches at the bottom.

Each frame consists of two basic parts: a formed channel without cutouts for the stringers and an attaching clip angle which has the necessary cutouts. This two-piece fail-safe construction provides improved structural integrity since any cracks in the attaching clip angle cannot propagate to the frame proper.

The fuselage quarter panels are assembled into six barrel sections: section one (the flight station) and section two form the forward fuselage; the mid fuselage consists of barrel sections three, four and five; and section six forms the aft fuselage. The afterbody extends aft of section six and the aft pressure bulkhead.

Fuselage sections are joined through shear joints which are made by bringing the two fuselage barrels flush, then using short, overlapping stringers, riveted through the fuselage stringers to hold the barrels together. An aluminum alloy plate is also used outside or inside the fuselage, depending upon the location of the joint, for additional strength.

The fuselage floor line is located 19 inches below the centerline of the fuselage constant-section diameter. Transverse beams support the floor at each fuselage frame except in the areas of the wing box and main landing gear wheel wells. Over the wing center box section, the floor is supported by fore and aft intercostals attached to the upper surface of the wing box. Over the main landing gear wheel wells, the flooring and the pressure deck below the floor are supported by transverse beams that extend from side to side with intermediate support afforded by keelson shear beams. These lower keelson members bridge the main wheel wells and also carry the fore and aft loads in

this area of the fuselage. They continue fore and aft of the wheel well and are tied to the lower wing surface by shear webs. The pressure deck over the nose wheel well extends laterally to the sides of the fuselage, and is supported by transverse beams.

Figure 5-5 shows the forward section structure (Section 3) and is also applicable to fuselage Sections 2 and 6. The fuselage mid-section (Sections 5 and 6) is shown in Figure 5-6. The relationship of the Keelson structure to the wing center section is shown in Figure 5-7 and the Keelson structure itself is shown in Figure 5-8.

5.3 KRASH Model

The KRASH model (Figure 4-2) provides for crushing at several fuselage stations including:

- Flight Station (FS 177)
- Section 2(FS 426)
- Section 3 (FS 677, 955)
- Section 4 (FS 1117)
- Section 5 (FS 1424)
- Section 6 (FS 1663)
- Aft body (FS 1992).

Of particular concern in the determination of floor pulses is the variation in peak amplitude and duration that can exist throughout the fuselage. Two typical locations; one in Section 3 and one in Section 6, have been selected to demonstrate floor response variations. In addition to the airframe model (Figures 4-2 and 4-3), representations of floor structure design are also utilized in the analysis.

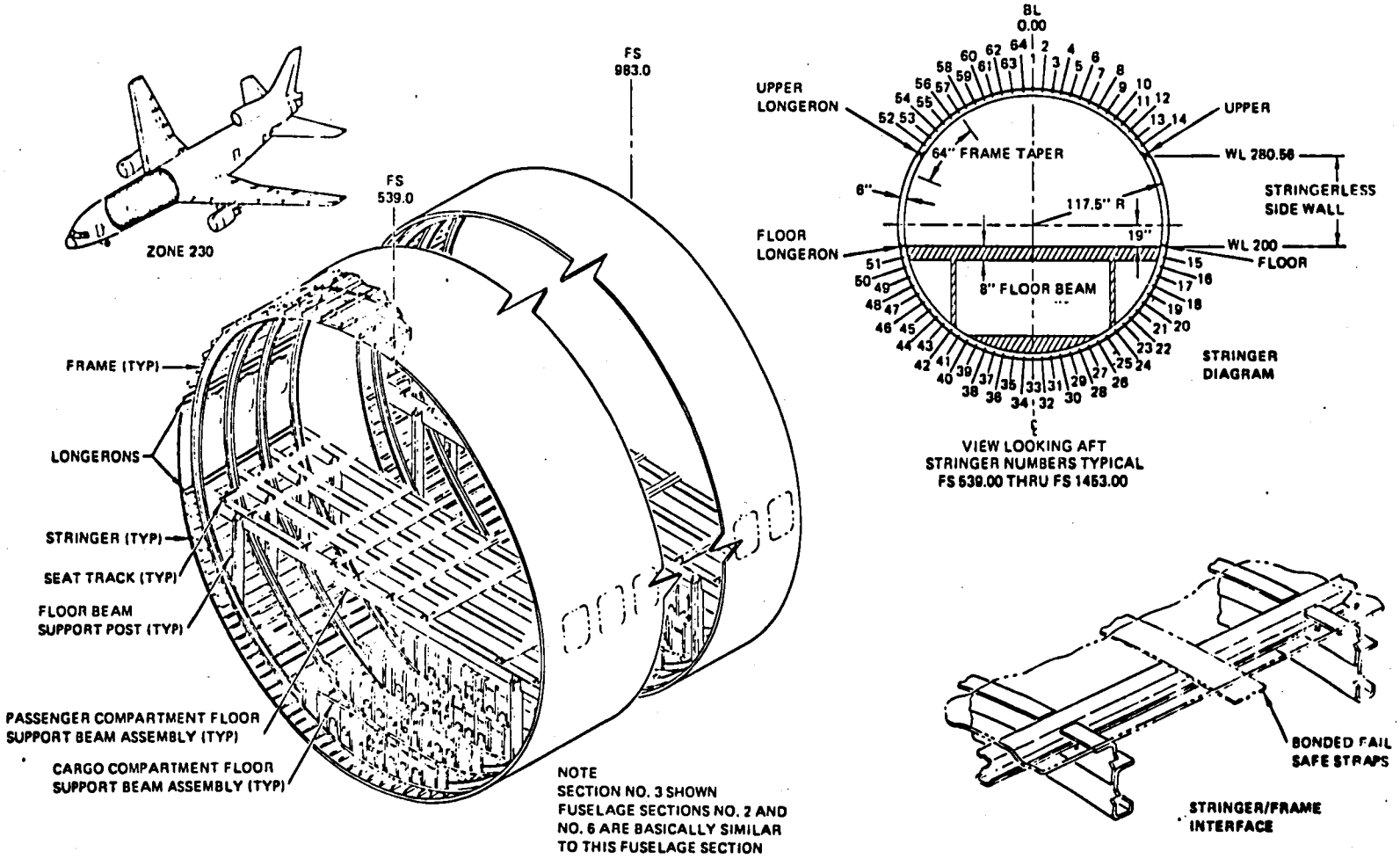

Figure 5-5. - Forward sections structure.

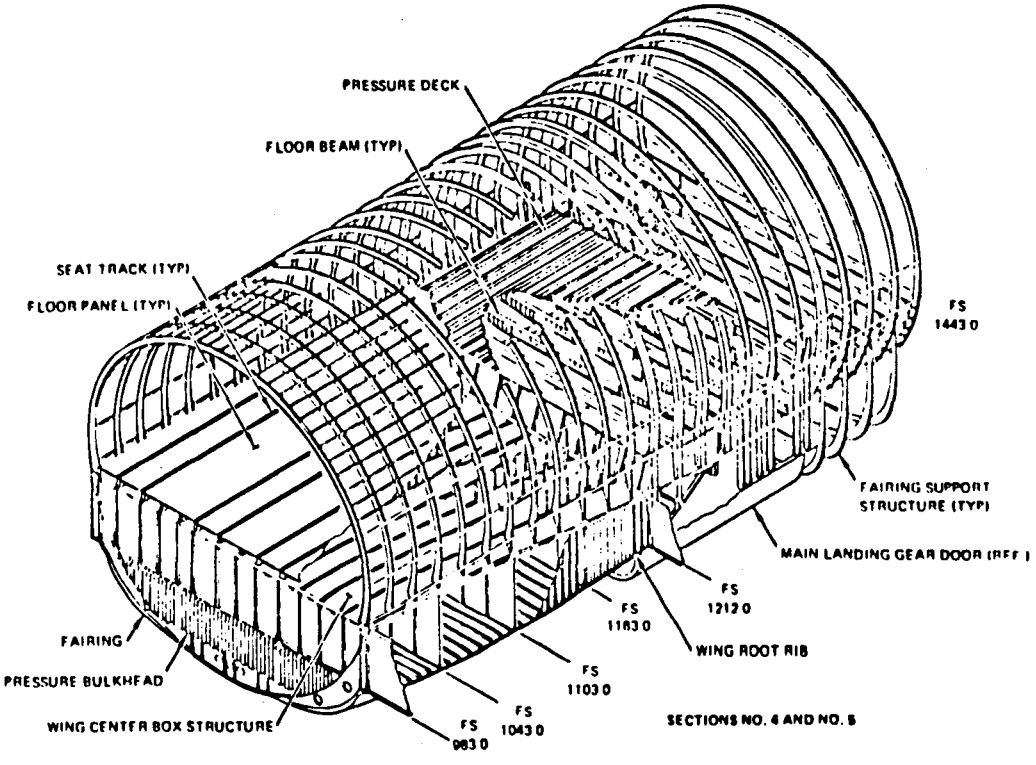

Figure 5-6. - Fuselage mid-section structure.

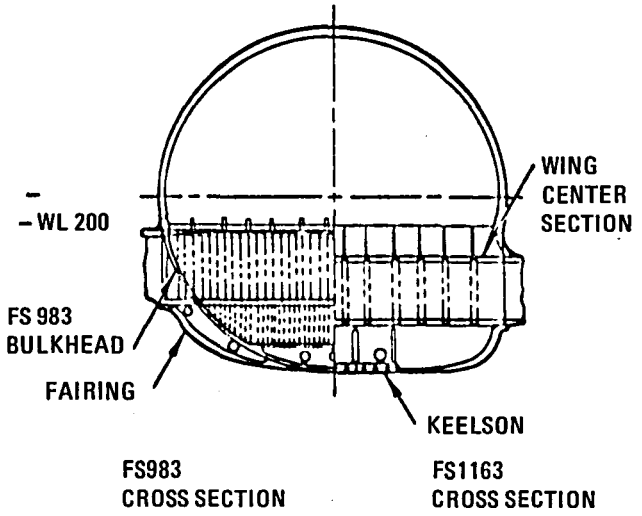

Figure 5-7. - Wing center section FS 983-1163.

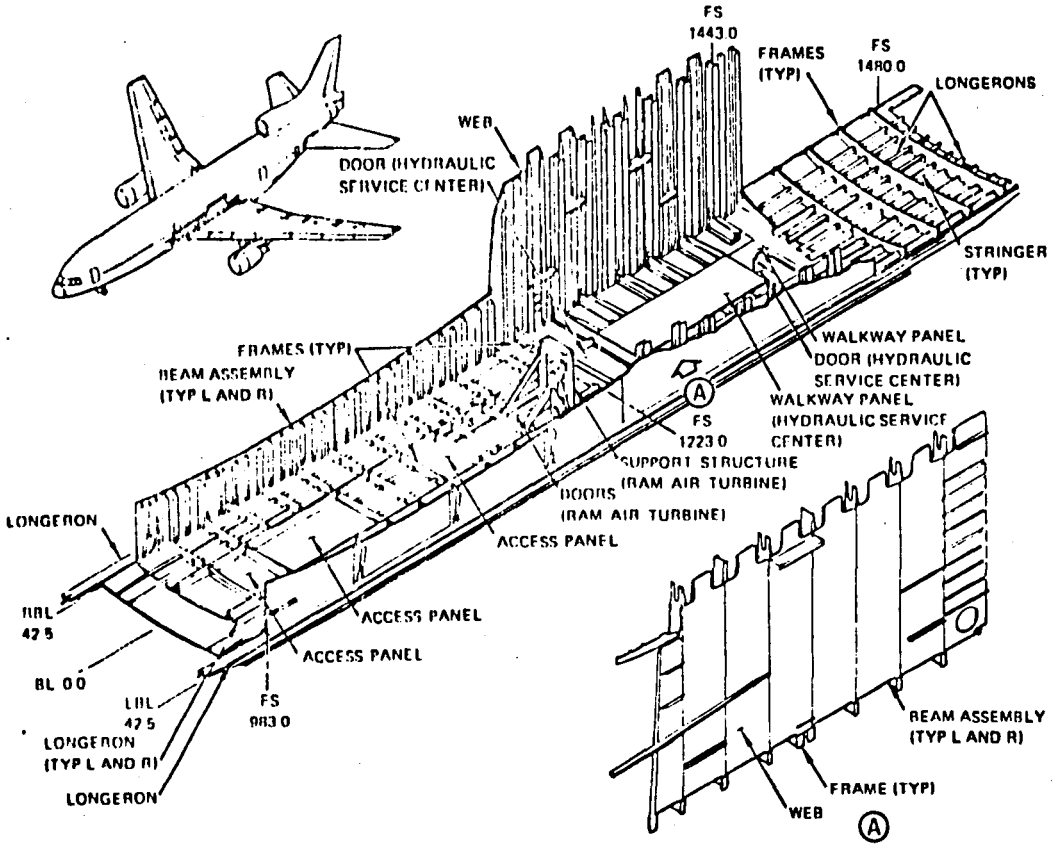

Figure 5-8. - Keelson structure.

5.4 Ground-to-Ground Overrun (GGO) Scenario

Table 5-2 shows a matrix of ground-to-ground overrun conditions in which the case number, data set identification, airplane configuration, terrain, and initial impact conditions are noted. Table 5-3 summarizes the results of the overrun analyses with regard to peak accelerations at a forward and an aft fuselage station location. The forward location (mass 3 in the model shown in Figure 4-1) is at F.S. 677 and the aft location (mass 6) is at F.S. 1424. These locations are representative of a forward cabin passenger station and mid-aft cabin passenger station. Included in Table 5-3 is a summary of masses which contact the ground and beam failures that occur during the run. The analyses are each run for 1 second slideout duration. Since this is an overrun condition it is assumed that Aerodynamic lift capability is available and that the airplane is intact as it leaves the runway, except that the main gears have collapsed. For purposes of analysis, the lift is assumed to ramp out in one second, as forward velocity decreases. Figure 5-9 can be used to identify mass and beam numbers referred to in Table 5-3 and subsequent summary tables. Some portions of representative time histories of unfiltered peak acceleration results are shown in Figures 5-10 through 5-12. Figures 5-13 and 5-14 show the distribution of peak loads throughout the passenger floor region for 6 ft/sec ENV* impacts (GGO-328 - 1 & 2). A comparison of fuselage shears and bending moments for these two cases is shown in Figure 5-15.

A comparison of results for landing (328,000 lb) and takeoff (432,000 lb) weight overruns indicate that for the conditions analyzed a decrease in peak accelerations may be expected as weight increases. This result is consistent with the mass and size relationships to be discussed in Section 6. Case numbers GGO-328-4 and GGO-432-4 show this comparison. These cases involve 18 ft/sec ENV impacts which, with wings attached and landing gears lost are extremely severe, as is noted by the potential failures of the wing both inboard and outboard of the engine. The wing loss potential creates a fuel spillage and post crash fire hazard as well. For the same symmetrical impact but at a substantially reduced (ENV) (6 ft/sec) and ground flexibility, case GGO-328-1, the acceleration levels are reduced to peak values of $-3.3G_X$, $+1.1G_X$, $-2.3G_Z$ and $+1.1G_Z$, without producing any structural failures. At an extremely

*ENV = Effective Normal Velocity

TABLE 5-2. - MATRIX OF ANALYSIS CONDITIONS, WIDE-BODY GROUND-TO-GROUND CANDIDATE CRASH SCENARIO

Case No.	Data Set	Airplane Configuration					Terrain			Initial Conditions						Beam Rupture Allowed
		Weight Lb	Type	Full A/P Stub Wing	Gear Position	Lift	Ground Flexibility In/Lb	Coeff. Friction μ	Slope Degrees	Velocity Ft/Sec			Altitude, Degrees			
										Fwd	Vertical	Side	Roll	Pitch	Yaw	
GGO-328-1	WT328.AEB1022	328,000	WB	Full A/P	Off	Yes	1.05×10^{-5}	1.0	2.54	135	6	0	0	0	0	No
GGO-328-2	WT328.AEB1022	328,000	WB	Full A/P	Off	Yes	Rigid	0.7	2.54	135	6	0	0	0	0	No
GGO-328-3	WT328.AEB1022	328,000	WB	Full A/P	Off	Yes	1.05×10^{-5}	0.7	6.0	172	18	0	0	0	0	No
GGO-328-4	WT328.AEB1022	328,000	WB	Full A/P	Off	Yes	Rigid	0.7	6.0	172	18	0	0	0	0	No
GGO-328-5	WT328.AEB1022	328,000	WB	Full A/P	Off	Yes	1.05×10^{-5}	0.7	2.54	135	6	0	0	0	30	No
GGO-328-6	WT328.AEB1022	328,000	WB	Full A/P	Off	Yes	Rigid	1.0	2.54	135	6	0	0	0	30	No
GGO-432-2	WT432.AEB1023	432,000	WB	Full A/P	Off	Yes	Rigid	0.7	6.0	172	18	0	0	0	0	No
GGO-432-4	WT432.AEB1023	432,000	WB	Full A/P	Off	Yes	Rigid	0.7	2.54	135	6	0	0	0	30	No

TABLE 5-3. - SUMMARY OF GROUND-TO-GROUND ANALYSIS RESULTS

CONDITION	PEAK ACCELERATIONS G'S / TIME / DURATION	POTENTIAL FAILURES BEAM / TIME / DOF	GROUND CONTACT MASS POINT
GGO-328-1	80KTS - 6 F/S - 0 ROLL - 0 PTCH - 0 YAW - NLG - SLP - 1E-5 GRD FLX		
MASS 3	L AFT -3.306 G'S@ .800 FOR .060		10
	FWD 1.143 G'S@ .420 FOR .035		2
	V UP -2.406 G'S@ .360 FOR .095		
	DWN 1.063 G'S@ .780 FOR .055		
MASS 6	L AFT -2.297 G'S@ .900 FOR .070		
	FWD 1.098 G'S@ .940 FOR .030		
	V UP -1.756 G'S@ .520 FOR .050		
	DWN 1.456 G'S@ .940 FOR .055		
GGO-328-2	80KTS - 06 F/S - 00 ROLL - 00 PTCH - 30 YAW - NLG - SLP - RIGID		
MASS 3	L AFT -8.112 G'S@ .160 FOR .027	11 @ .7156 IN 4	18
	FWD 4.446 G'S@ .480 FOR .030		2
			6
	V UP -9.983 G'S@ .170 FOR .065		7
	DWN 2.761 G'S@ .840 FOR .075		
MASS 6	L AFT -4.391 G'S@ .155 FOR .035		
	FWD 3.017 G'S@ .220 FOR .027		
	V UP -4.709 G'S@ .580 FOR .055		
	DWN 4.955 G'S@ .640 FOR .030		
GGO-328-3	110KTS - 18 F/S - 0 ROLL - 0 PTCH - 0 YAW - NLG - SLP - 1E-5 GRD FLX		
MASS 3	L AFT -11.42 G'S@ .220 FOR .017	9 @ .1590 IN 4	18
	FWD 5.64 G'S@ .210 FOR .010	10 @ .1724 IN 4	2
		11 @ .5102 IN 3	3
	V UP -12.90 G'S@ .150 FOR .040	12 @ .5978 IN 3	4
	DWN 6.27 G'S@ .370 FOR .035		5
			6
MASS 6	L AFT -12.12 G'S@ .250 FOR .015		7
	FWD 5.87 G'S@ .190 FOR .012		13
			14
	V UP - 8.00 G'S@ .370 FOR .050		15
	DWN 5.36 G'S@ .610 FOR .065		12
GGO-328-4	110KTS - 18 F/S - 00 ROLL - 00 PTCH - 00 YAW - NLG - SLP - RIGID		
MASS 3	L AFT -13.36 G'S@ .080 FOR .035	9 @ .1476 IN 4	18
	FWD 6.17 G'S@ .155 FOR .030	10 @ .1616 IN 4	2
		11 @ .5102 IN 3	3
	V UP -21.85 G'S@ .090 FOR .035		4
	DWN 10.73 G'S@ .160 FOR .015		5
			6
MASS 6	L AFT -9.012 G'S@ .240 FOR .015		13
	FWD 8.792 G'S@ .175 FOR .012		14
			12
	V UP -14.29 G'S@ .420 FOR .090		15
	DWN 7.72 G'S@ .590 FOR .070		

CONDITION	PEAK ACCELERATIONS G'S / TIME / DURATION	POTENTIAL FAILURES BEAM / TIME / DOF	GROUND CONTACT MASS POINT
GGO-328-5	80KTS - 6 F/S - 0 ROLL - 0 PTCH - 30 YAW - NLG - SLP - 1E-5 GRD FLX		
MASS 3	L AFT -3.102 G'S@ .640 FOR .055	15 @ .3884 IN 3	18
	FWD .595 G'S@ .420 FOR .010	10 @ .4050 IN 4	37
		33 @ .5650 IN 3	2
	S LFT -2.052 G'S@ .600 FOR .035		3
	RGT 4.009 G'S@ .640 FOR .055		4
			5
	V UP -3.440 G'S@ .360 FOR .120		6
	DWN 2.556 G'S@ .860 FOR .075		7
			10
MASS 6	L AFT -2.264 G'S@ .330 FOR .117		13
	FWD .626 G'S@ .400 FOR .010		
	S LFT - .555 G'S@ .700 FOR .030		
	RGT 1.426 G'S@ .500 FOR .055		
	V UP -2.805 G'S@ .660 FOR .090		
	DWN 1.759 G'S@ .960 FOR .070		
GGO-328-6	80KTS - 06 F/S - 00 ROLL - 00 PTCH - 30 YAW - NLG - SLP - RIGID		
MASS 3	L AFT -4.895 G'S@ .610 FOR .050	15 @ .5906 IN 3	18
	FWD 2.842 G'S@ .490 FOR .023	10 @ .6094 IN 4	37
		33 @ .7114 IN 3	2
	S LFT -7.981 G'S@ .380 FOR .040		3
	RGT 5.846 G'S@ .350 FOR .050		4
			7
	V UP -7.429 G'S@ .260 FOR .056		
	DWN 4.169 G'S@ .680 FOR .050		
MASS 6	L AFT -4.864 G'S@ .580 FOR .040		
	FWD 1.909 G'S@ .220 FOR .025		
	S LFT -2.865 G'S@ .470 FOR .045		
	RGT 5.344 G'S@ .350 FOR .050		
	V UP -7.759 G'S@ .590 FOR .040		
	DWN 3.161 G'S@ .710 FOR .030		
GGO-432-3	110KTS - 18 F/S - 0 ROLL - 0 PTCH - 0 YAW - NLG - SLP - 1E-5 GRD FLX		
MASS 3	L AFT - 9.34 G'S@ .210 FOR .035	15 @ .1420 IN 3	18
	FWD 4.95 G'S@ .475 FOR .035	10 @ .1642 IN 4	[illegible]
		11 @ .4294 IN 3	[illegible]
	V UP -13.59 G'S@ .155 FOR .070	12 @ .4604 IN 3	[illegible]
	DWN 7.25 G'S@ .295 FOR .045		
MASS 6	L AFT - 6.76 G'S@ .125 FOR .045		[illegible]
	FWD 1.13 G'S@ .360 FOR .035		13
			14
	V UP -17.04 G'S@ .280 FOR .075		15
	DWN 5.03 G'S@ .630 FOR .090		
GGO-432-4	110KTS - 18 F/S - 00 ROLL - 00 PTCH - 00 YAW - NLG - SLP - RIGID		
MASS 3	L AFT -15.23 G'S@ .225 FOR .030	9 @ .1492 IN 4	18
	FWD 8.77 G'S@ .490 FOR .035	10 @ .1636 IN 4	2
		11 @ .4220 IN 3	3
	V UP -17.95 G'S@ .135 FOR .045	12 @ .4604 IN 3	4
	DWN 7.05 G'S@ .195 FOR .020		5
			6
MASS 6	L AFT -10.39 G'S@ .165 FOR .027		7
	FWD 9.16 G'S@ .220 FOR .015		13
			14
	V UP -10.84 G'S@ .205 FOR .010		12
	DWN 5.24 G'S@ .680 FOR .095		15

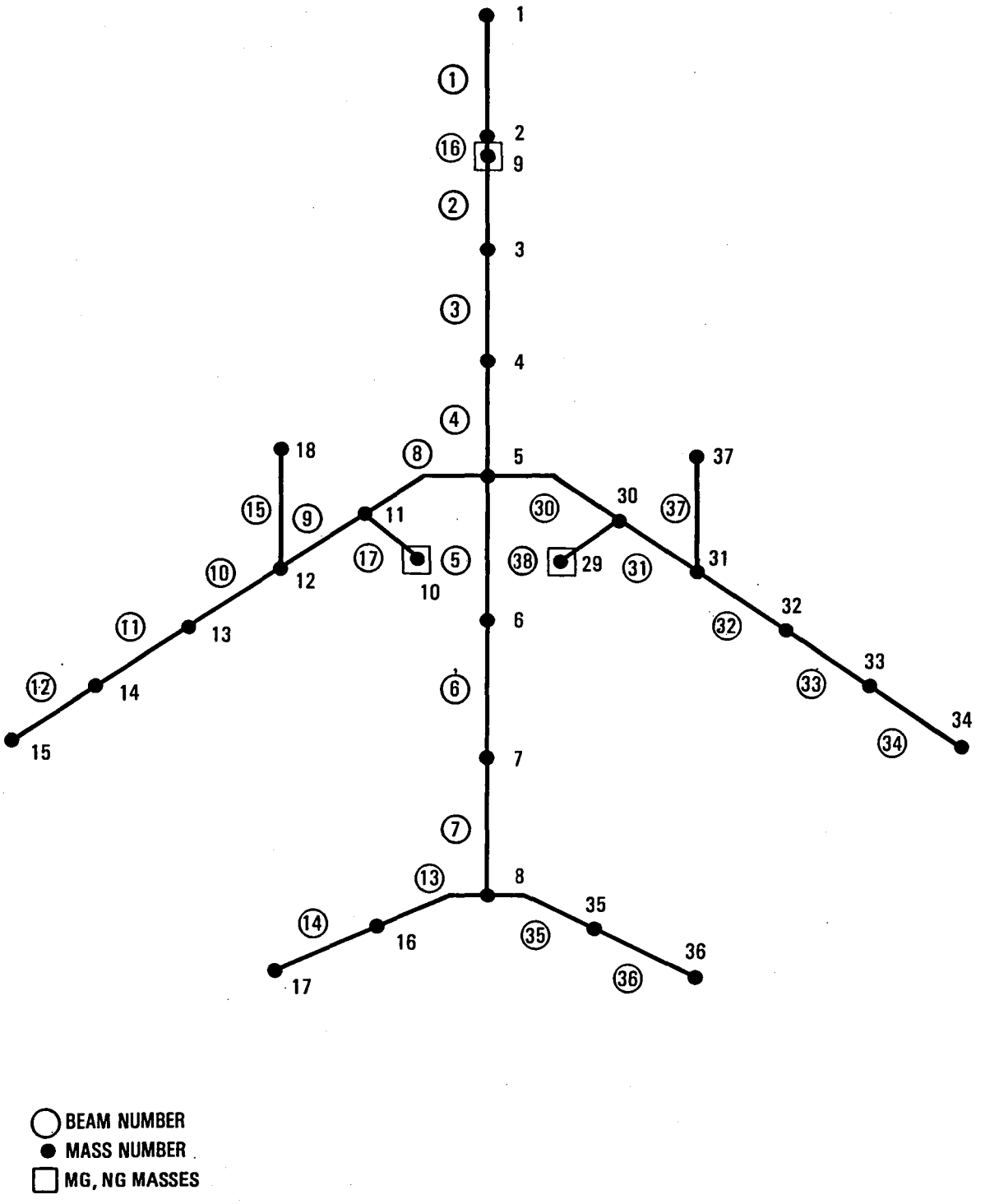

Figure 5-9. - KRASH model arrangement showing beam and mass identification.

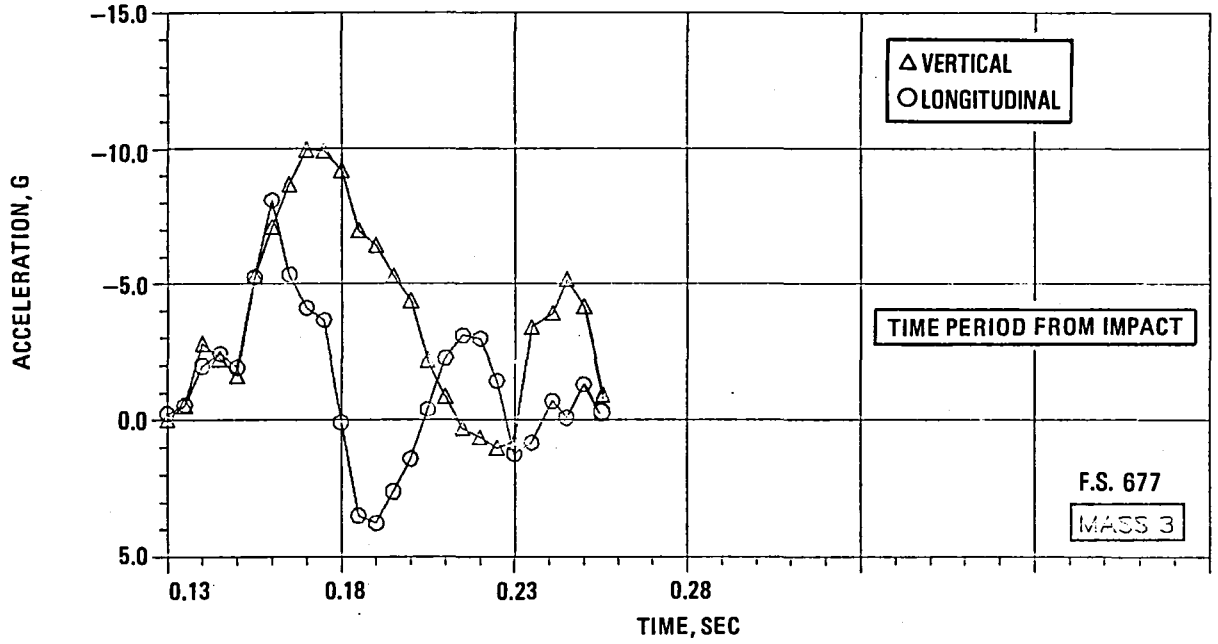

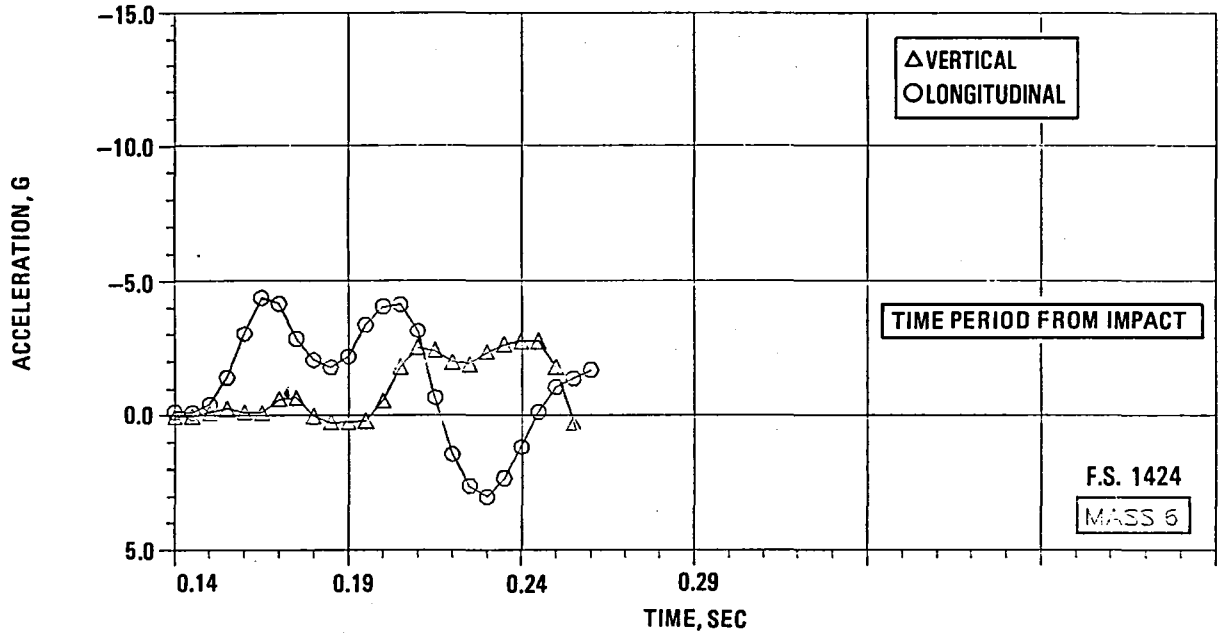

Figure 5-10. - Airframe responses, ground-to-ground overrun GGO-328-2.

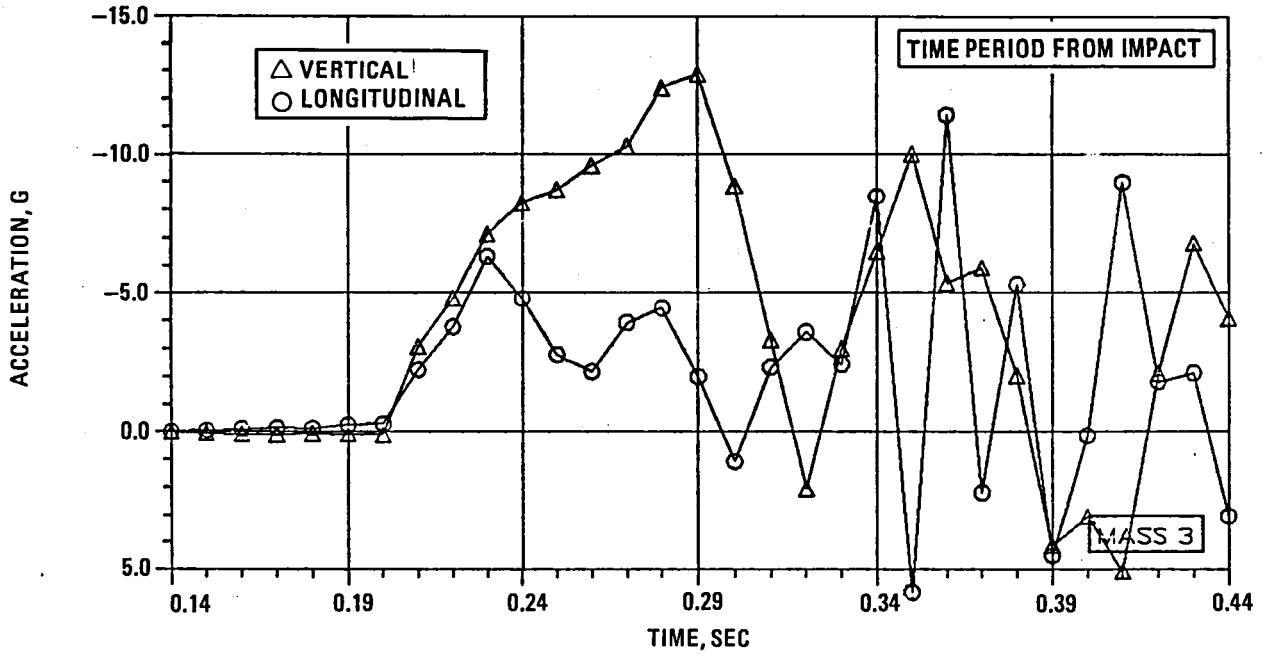

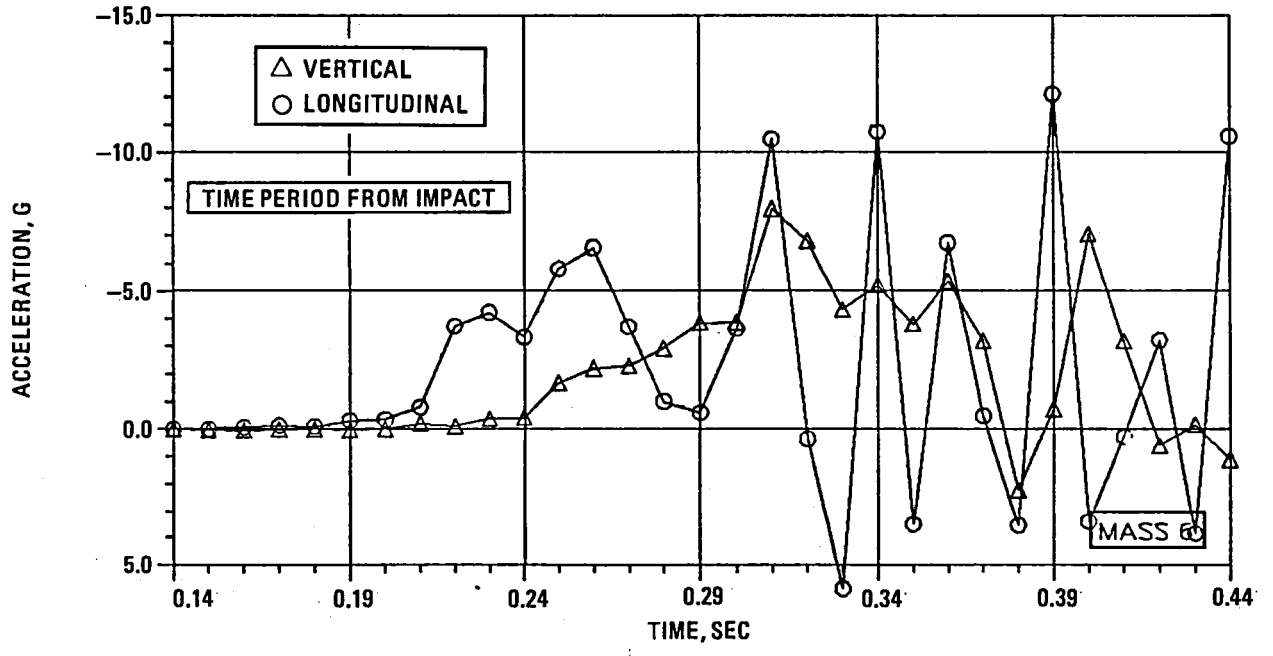

Figure 5-11. - Airframe responses, ground-to-ground overrun GGO-328-3.

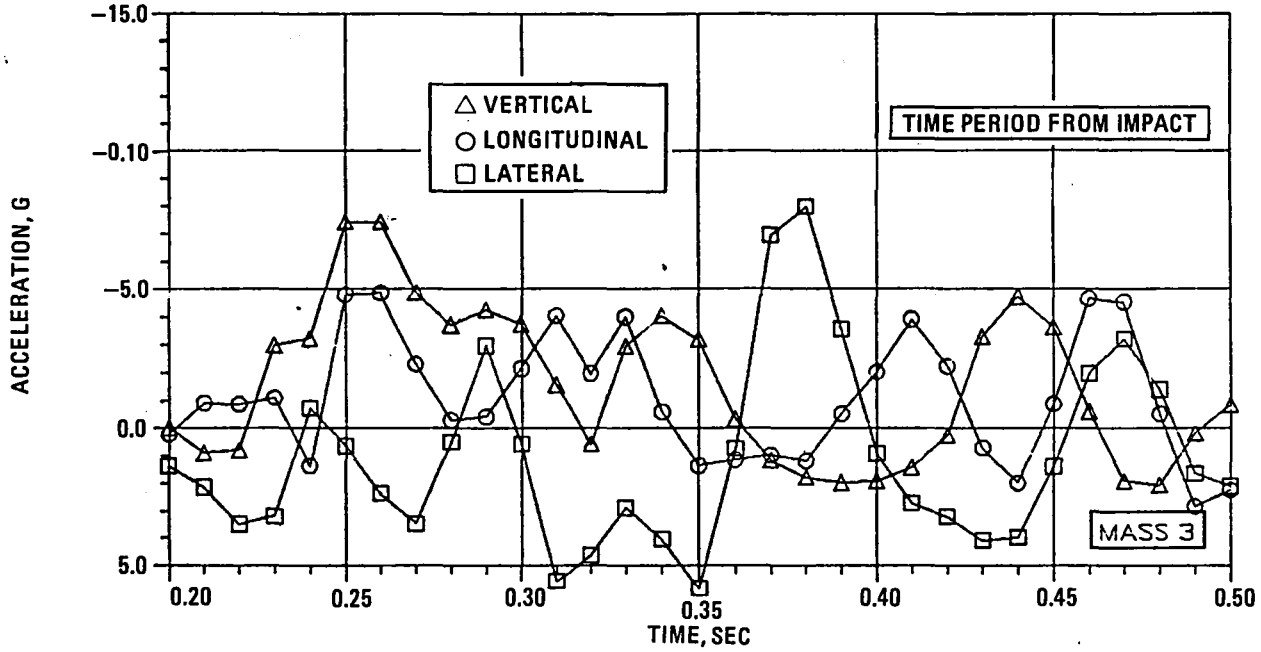

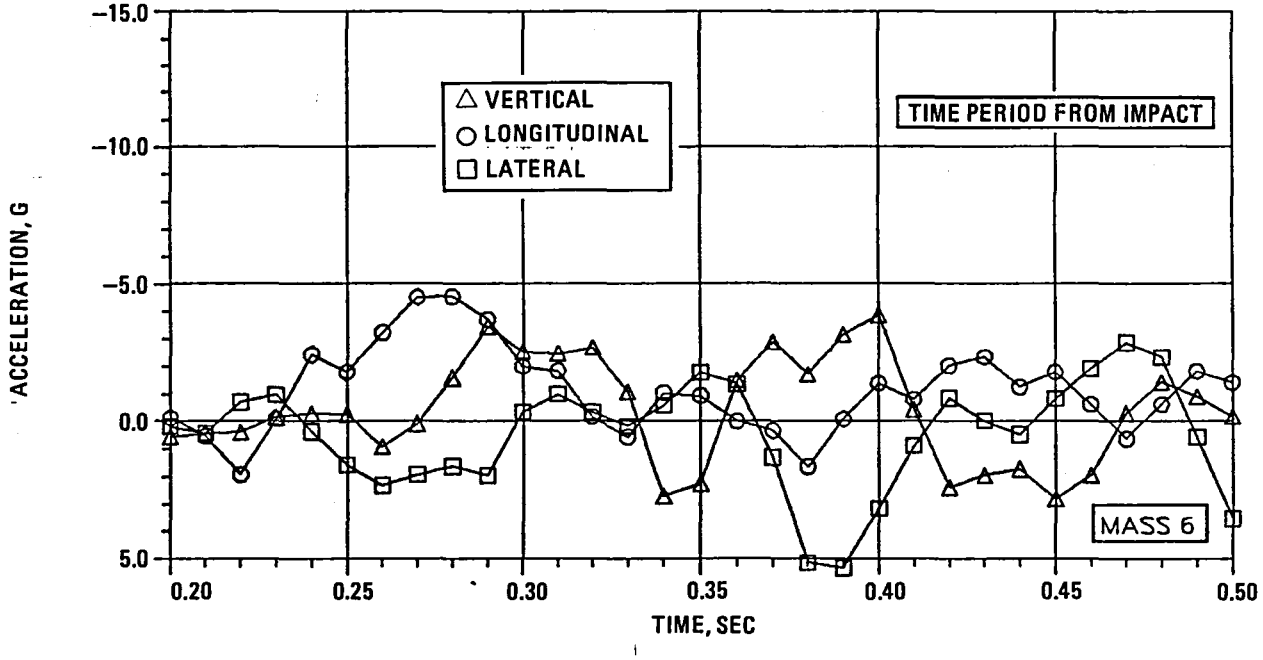

Figure 5-12. - Airframe responses, ground-to-ground overrun GGO-328-6.

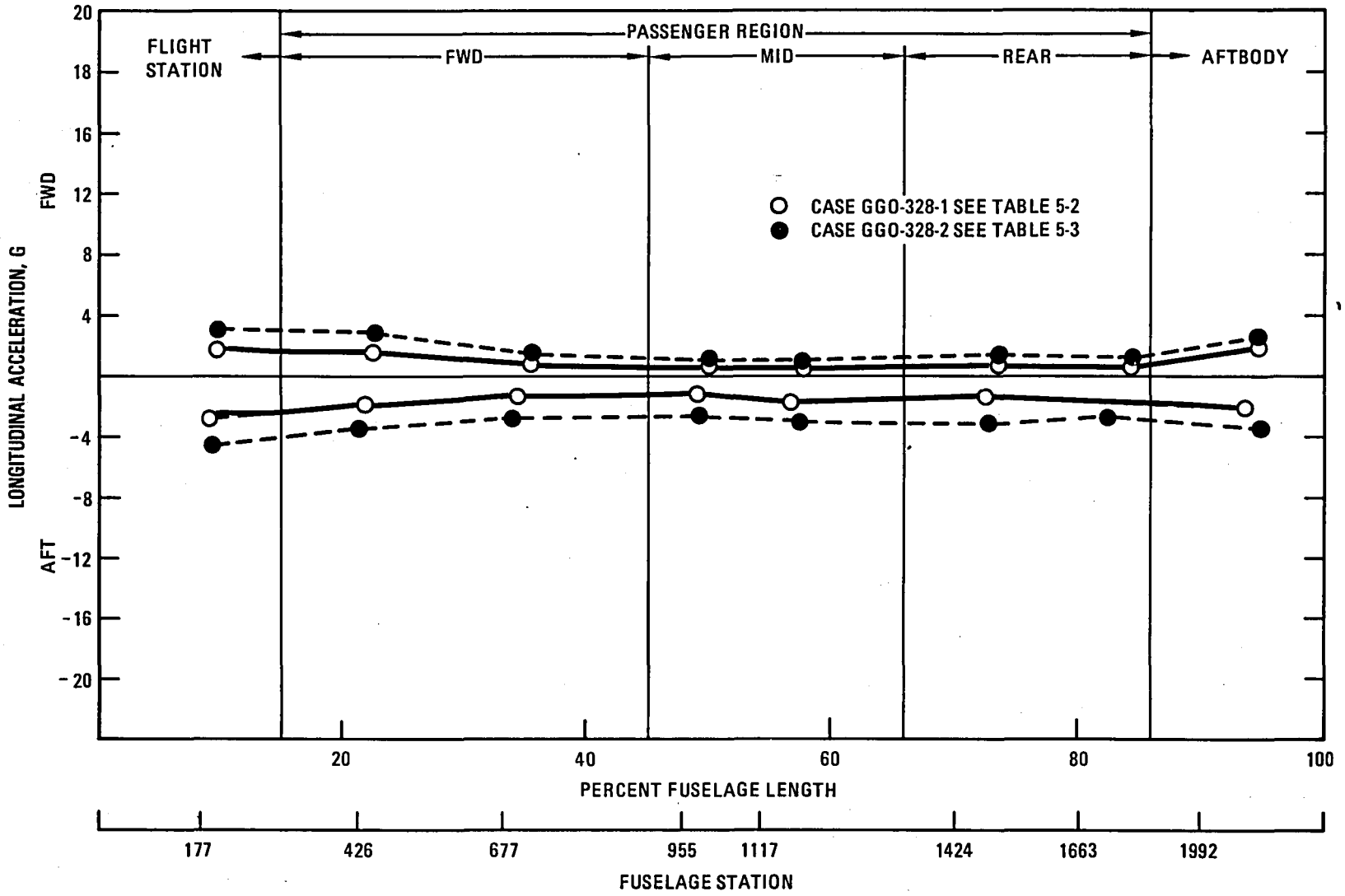

Figure 5-13. - Longitudinal acceleration versus fuselage location, overrun.

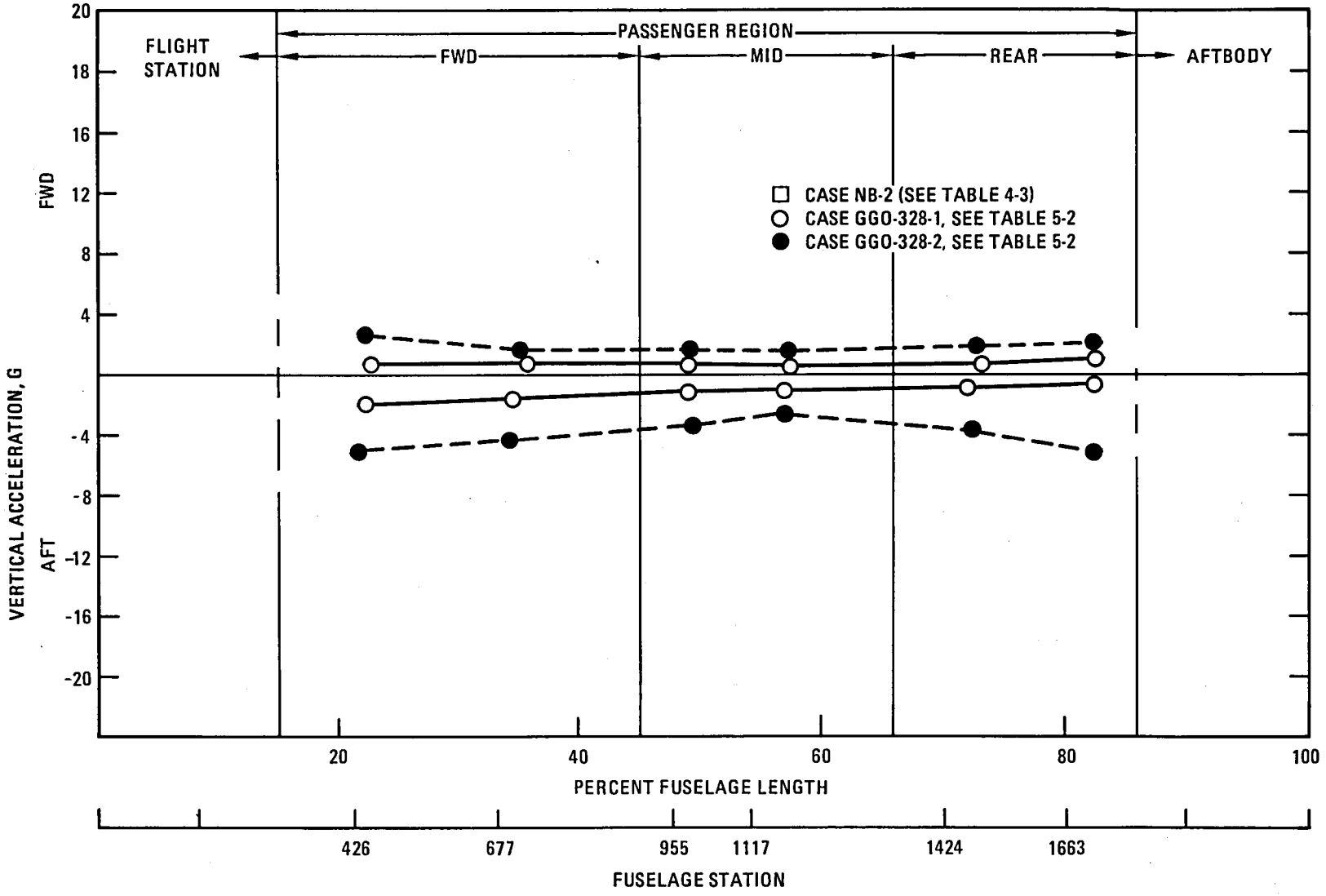

Figure 5-14. Vertical acceleration versus fuselage location, overrun

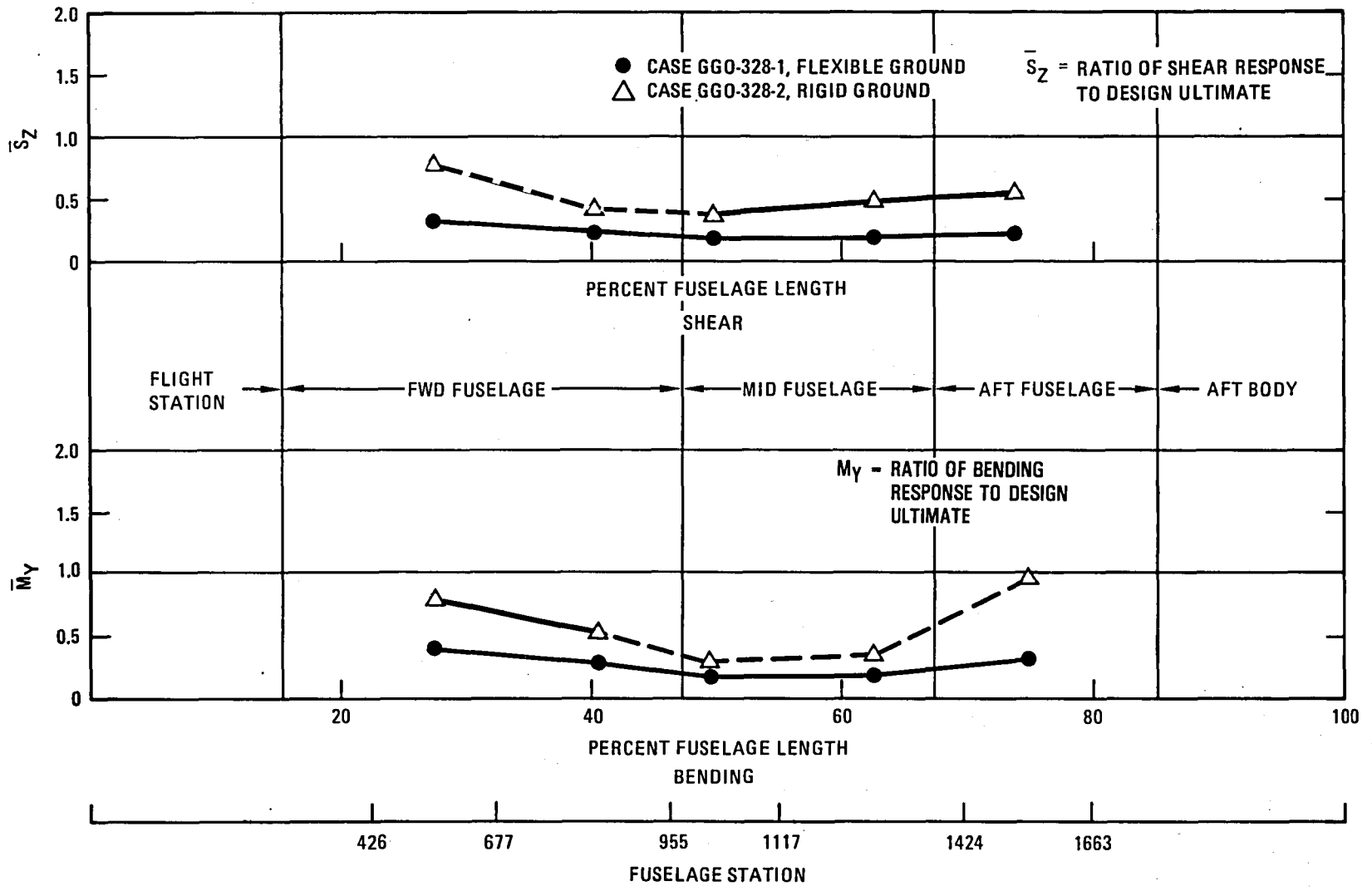

Figure 5-15. Fuselage shear and bending loads, overrun

severe 18 ft/sec ENV but with ground flexibility the peak accelerations are noted to be $-11.4G_X$, $+5.8G_X$, $-12.9G_Z$ and $+6.3G_Z$. These accelerations exist for extremely short periods of time (≤ 0.040 seconds) but substantial airframe damage can be anticipated at this severe impact condition.

The overrun condition with a 30 degree yaw shows a $5G_y$ (side) acceleration peak at the more aft passenger location (mass 6). The analysis also shows potential failure of the engine pylon and wing, outboard of the engines.

5.5 Air-to-Ground Hard Landing (AGHL) Scenario

As noted in Table 5-1 the hard landing conditions were run for a forward velocity of 160 knots, a nose-up attitude range of 0 to 15 degrees, and at 15 ft/sec and 20 ft/sec sink speeds. All hard landing analyses are performed for symmetrical impact onto a rigid surface. Aerodynamic lift is assumed to be present for this crash scenario condition. Table 5-4 identifies the hard landing conditions. Table 5-5 summarizes the results of the hard landing analyses for the same two passenger cabin region locations noted earlier. Portions of representative time histories of the peak responses are shown in Figure 5-16 through 5-20. Case numbers AGHL-328-1 and AGHL 358-1 represent symmetrical 6-degree, nose-up and 15 ft/sec sink speed conditions at different landing weights, the latter being the maximum design landing weight for the particular aircraft. Similarly AGHL 328-2 and AGHL 358-2 compare different landing weight results for a symmetrical 20 ft/sec sink speed and 15-degree noseup impact condition. In both comparisons the results show a consistent pattern of ground contact, main landing gear failure, and range of peak accelerations as well as time of occurrence. For the 6-degree nose-up impact with a 15 ft/sec sink speed the aircraft remains on the main landing gears after impact. Consequently, the results may be more representative of an initial impact. For the 15 degree-nose-up impact at 20 ft/sec sink speed, the aircraft main gears, aft fuselage, and engine contact the ground in that sequence. A potential overload failure of the wings outboard of the wing engines is indicated. The maximum peak accelerations obtained are approximately $\pm 7.5G_Z$ for these conditions, both of which are for short duration (0.030 seconds). The longitudinal acceleration levels are less than $\pm 2.3G_X$. With a low coefficient of ground friction ($\mu = .35$) and a long slideout, this condition is not

TABLE 5-4. - MATRIX OF ANALYSIS CONDITIONS, WIDE-BODY HARD LANDING CRASH SCENARIOS

Case No.	Data Set	Airplane Configuration					Terrain			Initial Conditions						Beam Rupture Allowed
		Weight Lb	Type	Full A/P Stub Wing	Gear Position	Lift	Ground Flexibility In/Lb	Coeff. Friction μ	Slope Degrees	Velocity Ft/Sec			Altitude, Degrees			
										Fwd	Vertical	Side	Roll	Pitch	Yaw	
AGHL-358-1	AEA 1005A	358,000	WB	Full A/P	Extended	Yes	Rigid	.35	Flat	270	15	0	0	6	0	Yes
AGHL-358-2	AEA 1006	358,000	WB	Full A/P	Extended	Yes	Rigid	.35	Flat	270	20	0	0	15	0	Yes
AGHL-358-3	AEA 1007	358,000	WB	Full A/P	Extended	Yes	Rigid	.35	Flat	270	20	0	0	6	0	Yes
AGHL-358-4	AEA 1008	358,000	WB	Full A/P	Extended	Yes	Rigid	.35	Flat	270	20	0	0	0	0	Yes
AGHL-358-5	AEA 1005T	358,000	WB	Full A/P	Extended	Yes	Rigid	.35	Flat	270	15	0	0	15	0	Yes
AGHL-328-1	AEA 1010	328,000	WB	Full A/P	Extended	Yes	Rigid	.35	Flat	270	15	0	0	6	0	Yes
AGHL-328-2	AEA 1011	328,000	WB	Full A/P	Extended	Yes	Rigid	.35	Flat	270	20	0	0	15	0	Yes

TABLE 5-5. - SUMMARY OF AIR-TO-GROUND HARD LANDINGS ANALYSIS RESULTS

CONDITION	PEAK ACCELERATIONS G'S / TIME / DURATION	POTENTIAL FAILURES BEAM / TIME / DOF	GROUND CONTACT MASS POINT
AGHL-358-1	160KTS - 15 F/S - 00 ROLL - 06 PTCH - 00 YAW - LG - 0 SLP - RIGID		
MASS 3	L AFT - .998 G'S@ .270 FOR .155		10
	FWD .245 G'S@ .590 FOR .055		
	V UP -3.002 G'S@ .320 FOR .090		
	DWN 1.290 G'S@ .790 FOR .055		
MASS 6	L AFT -1.032 G'S@ .280 FOR .155		
	FWD .228 G'S@ .840 FOR .070		
	V UP -3.445 G'S@ .320 FOR .220		
	DWN 1.023 G'S@ .630 FOR .055		
AGHL-358-2	160KTS - 20 F/S - 00 ROLL - 15 PTCH - 00 YAW - LG - 0 SLP - RIGID		
MASS 3	L AFT -2.203 G'S@ .980 FOR .055	11 @ .2882 IN 3	10
	FWD 1.276 G'S@ .940 FOR .050		8
			7
	V UP -5.017 G'S@ .200 FOR .070		17
	DWN 2.209 G'S@ .980 FOR .030		
MASS 6	L AFT -1.268 G'S@ .320 FOR .060		
	FWD .703 G'S@ .700 FOR .050		
	V UP -6.656 G'S@ .155 FOR .095		
	DWN 3.668 G'S@ .320 FOR .065		
AGHL-358-3	160KTS - 20 F/S - 00 ROLL - 06 PTCH - 00 YAW - LG - 0 SLP - RIGID		
MASS 3	L AFT -1.825 G'S@ .840 FOR .035	17 @ .2084 IN 1	10
	FWD 1.098 G'S@ .310 FOR .010	16 @ .8200 IN 3	7
			9
	V UP -7.481 G'S@ .820 FOR .095		18
	DWN 3.190 G'S@ .310 FOR .045		6
MASS 6	L AFT -3.697 G'S@ .710 FOR .010		
	FWD 1.286 G'S@ .720 FOR .010		
	V UP -2.219 G'S@ .760 FOR .090		
	DWN 4.885 G'S@ .220 FOR .050		
AGHL-358-4	160KTS - 20 F/S - 00 ROLL - 00 PTCH - 00 YAW - LG - 0 SLP - RIGID		
MASS 3	L AFT -3.494 G'S@ .920 FOR .040	16 @ .1126 IN 3	10
	FWD 3.149 G'S@ .740 FOR .050	17 @ .2220 IN 1	9
		10 @ .2500 IN 4	18
	V UP -5.290 G'S@1.000 FOR .020		2
	DWN 4.372 G'S@ .980 FOR .020		3
MASS 6	L AFT -5.199 G'S@ .880 FOR .035		
	FWD 5.070 G'S@1.000 FOR .040		
	V UP -8.655 G'S@1.000 FOR .095		
	DWN 4.492 G'S@ .240 FOR .030		
AGHL-358-5	160KTS - 15 F/S - 00 ROLL - 15 PTCH - 00 YAW - LG - 0 SLP - RIGID		
MASS 3	L AFT -1.023 G'S@ .300 FOR .060		10
	FWD .457 G'S@ .540 FOR .040		8
			7
	V UP -2.629 G'S@ .240 FOR .095		17
	DWN .803 G'S@ .860 FOR .080		
MASS 6	L AFT - .930 G'S@ .260 FOR .045		
	FWD .247 G'S@ .520 FOR .040		
	V UP -4.285 G'S@ .180 FOR .135		
	DWN 1.093 G'S@ .340 FOR .065		
AGHL-328-1	160KTS - 15 F/S - 00 ROLL - 06 PTCH - 00 YAW - LG - 0 SLP - RIGID		
MASS 3	L AFT -1.088 G'S@ .280 FOR .155		10
	FWD .296 G'S@ .840 FOR .045		
	V UP -2.262 G'S@ .320 FOR .165		
	DWN .872 G'S@ .900 FOR .130		
MASS 6	L AFT -1.064 G'S@ .280 FOR .160		
	FWD .342 G'S@ .860 FOR .095		
	V UP -3.064 G'S@ .300 FOR .240		
	DWN .890 G'S@1.000 FOR .060		
AGHL-328-2	160KTS - 20 F/S - 00 ROLL - 15 PTCH - 00 YAW - LG - 0 SLP - RIGID		
MASS 3	L AFT -2.323 G'S@ .320 FOR .060	11 @ .2718 IN 3	10
	FWD 1.004 G'S@ .900 FOR .040		8
			7
	V UP -3.892 G'S@ .360 FOR .065		17
	DWN 2.308 G'S@ .880 FOR .075		
MASS 6	L AFT -1.463 G'S@ .980 FOR .050		
	FWD 1.440 G'S@ .940 FOR .060		
	V UP -5.911 G'S@ .140 FOR .170		
	DWN 3.231 G'S@ .800 FOR .090		

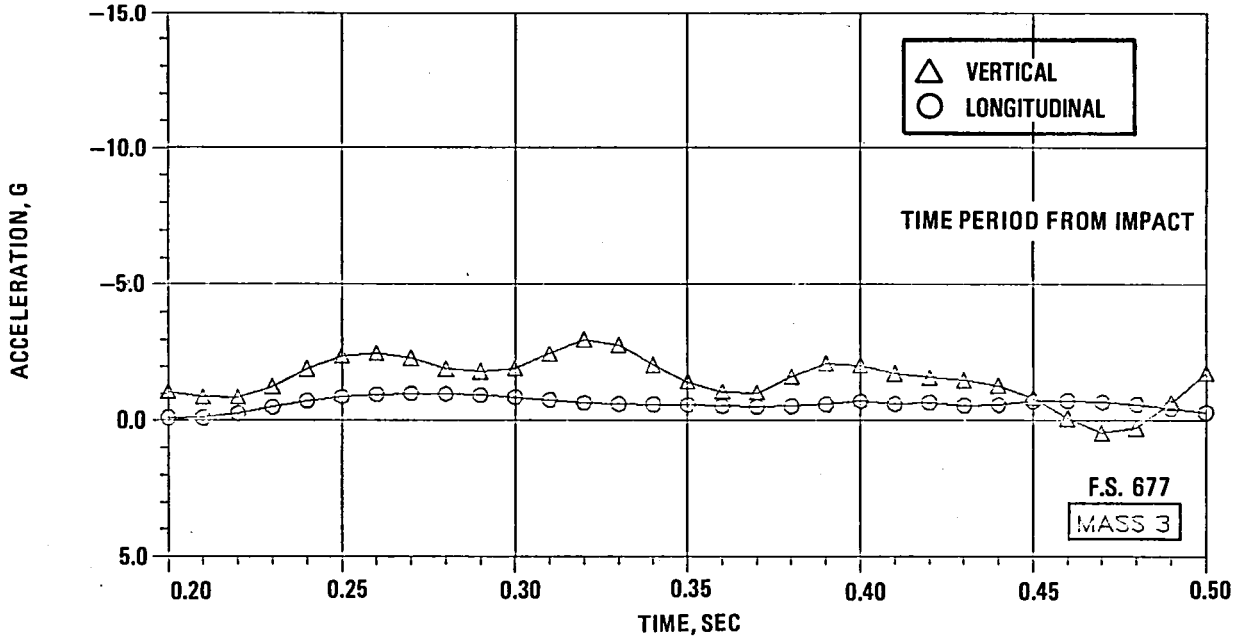

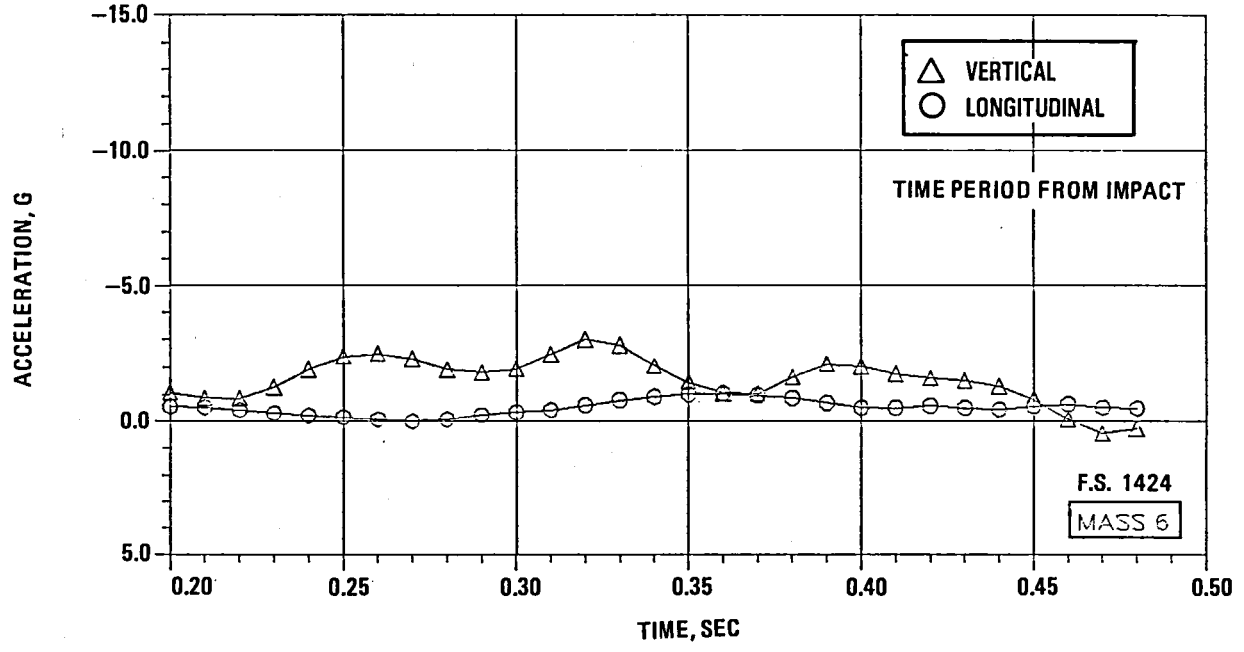

Figure 5-16. - Airframe responses, air-to-ground hard landings, AGHL-358-1.

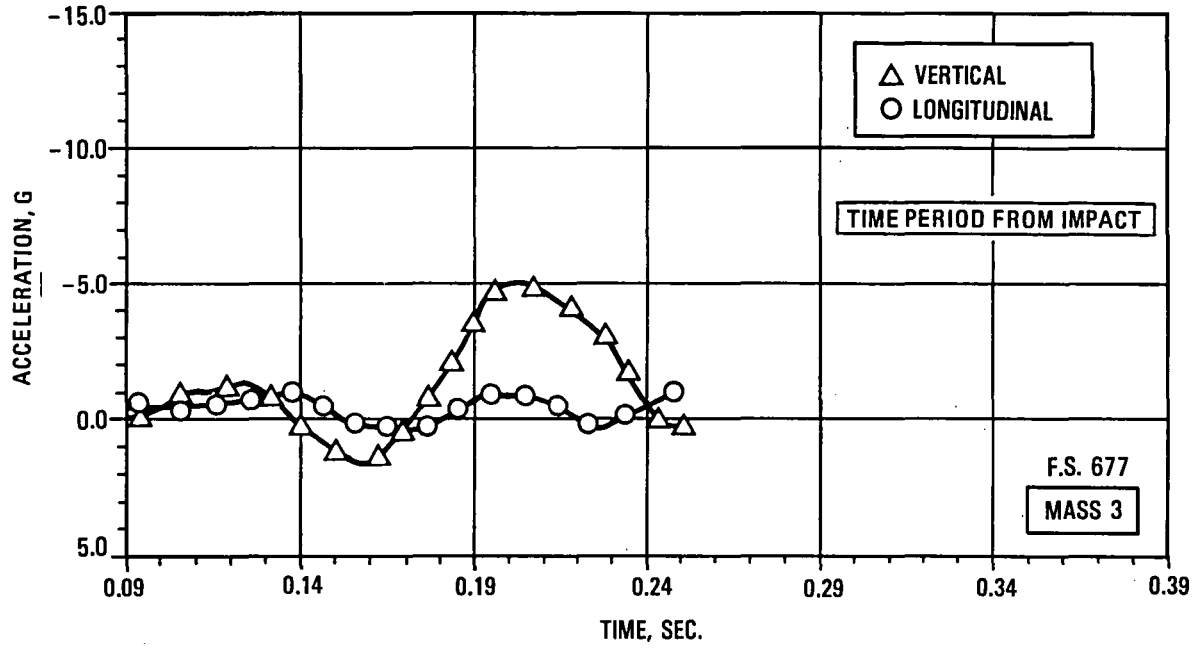

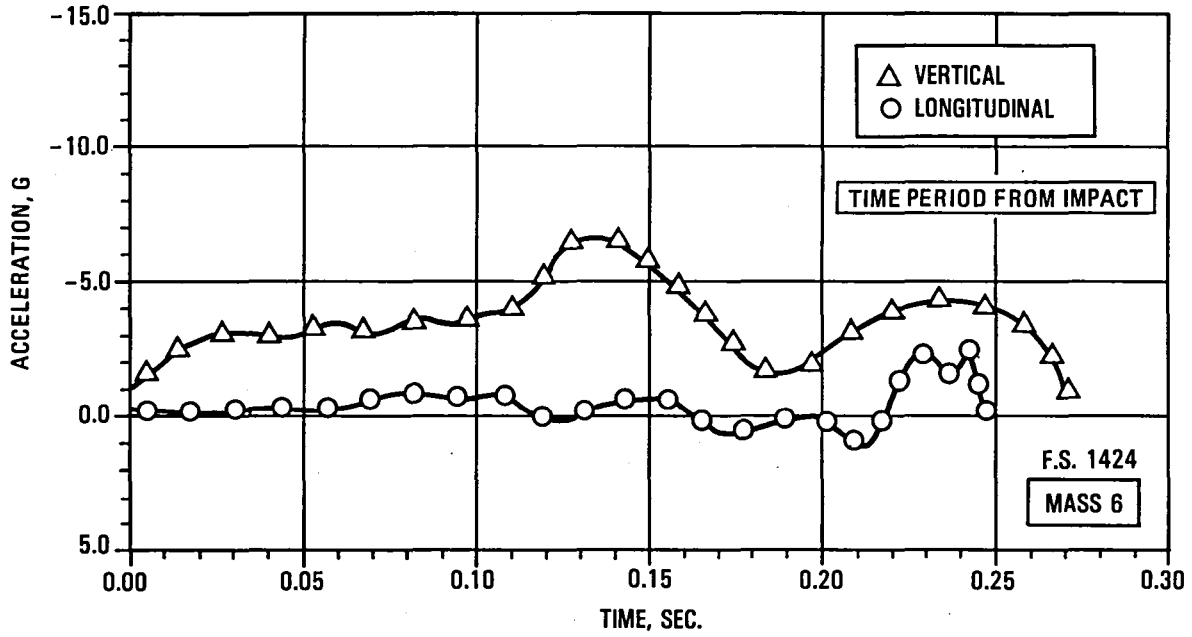

Figure 5-17. - Airframe responses, air-to-ground hard landings, AGHL-358-2.

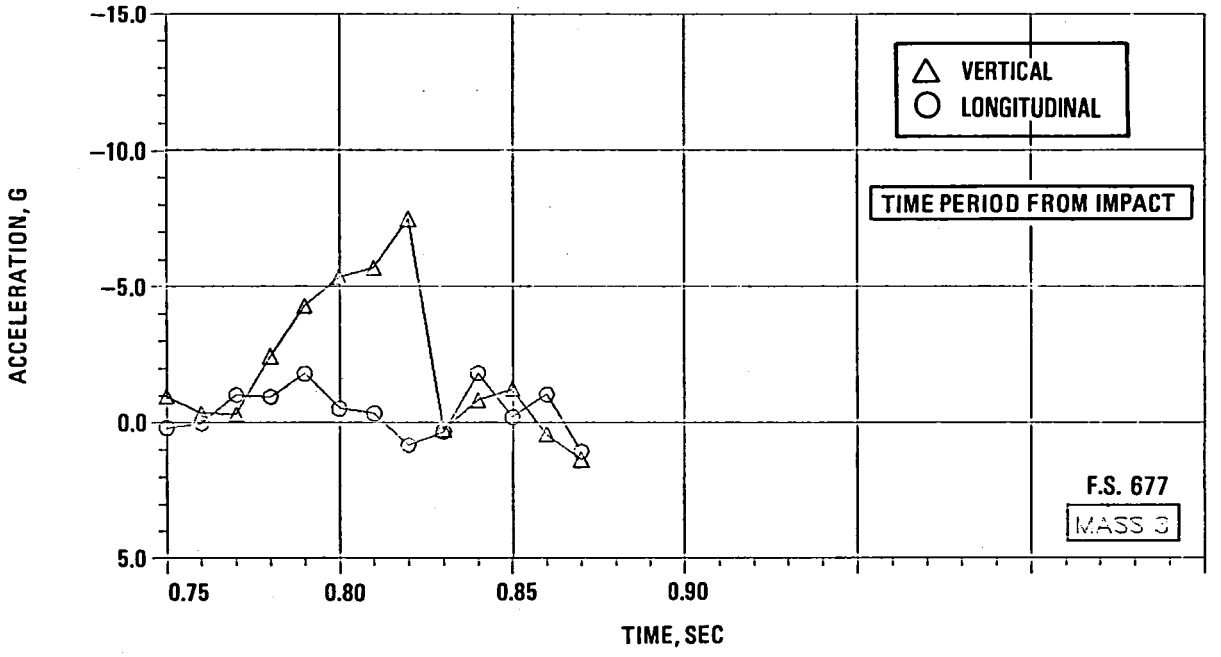

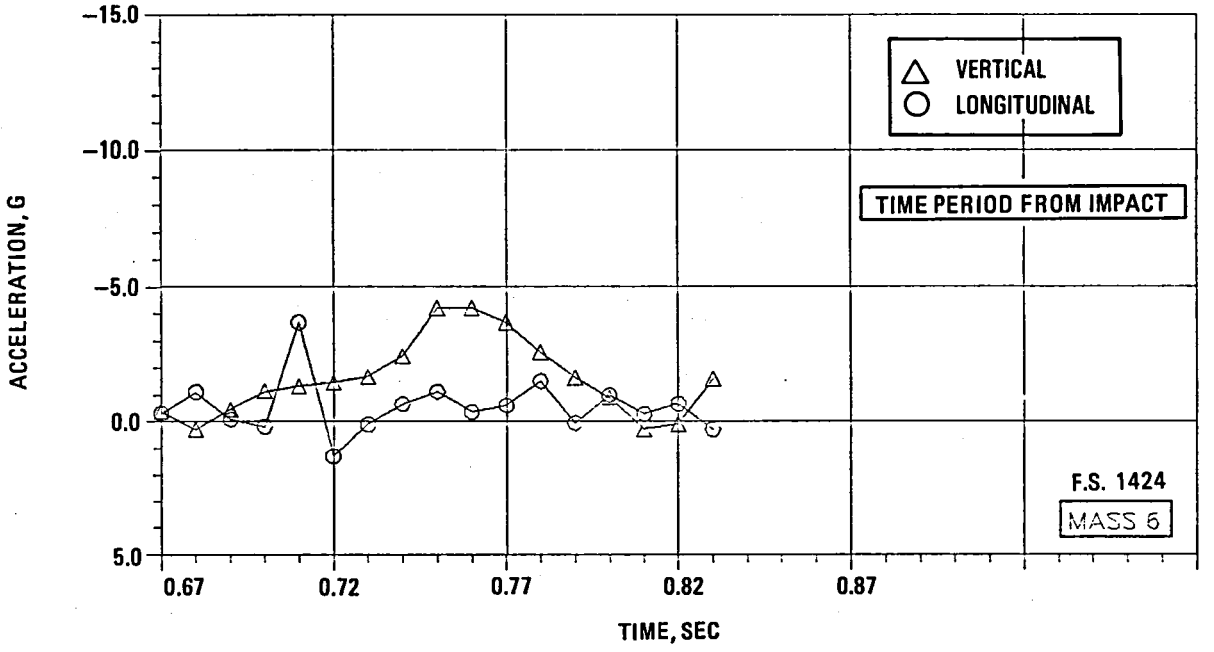

Figure 5-18. - Airframe responses, air-to-ground hard landings, AGHL 358-3.

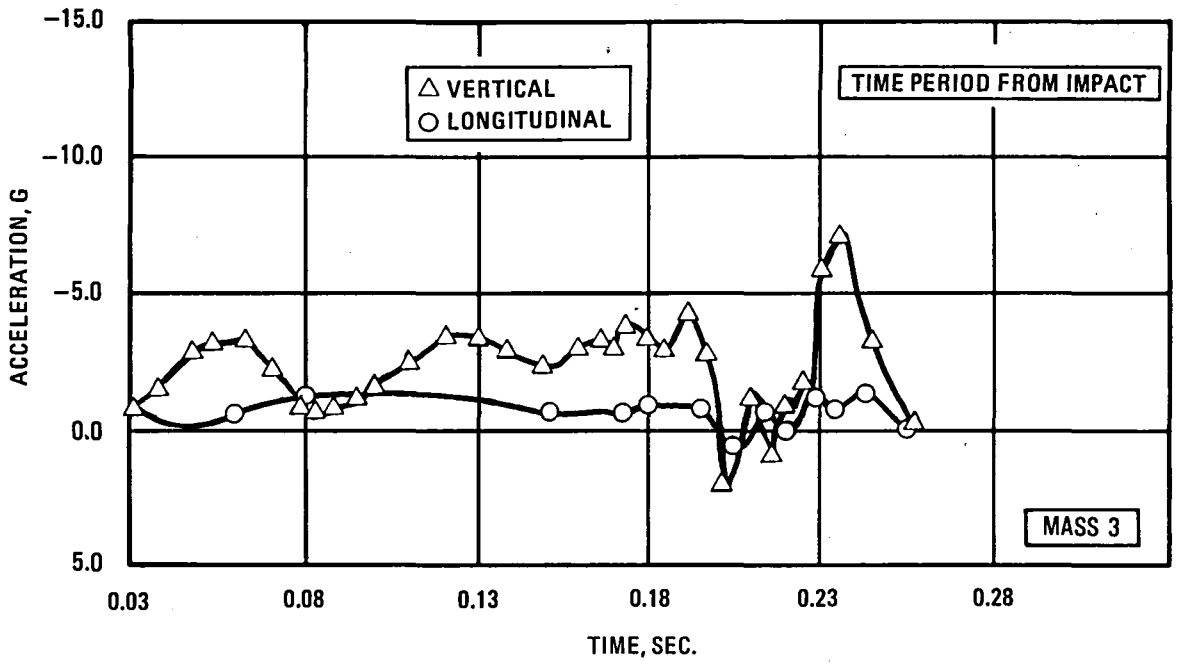

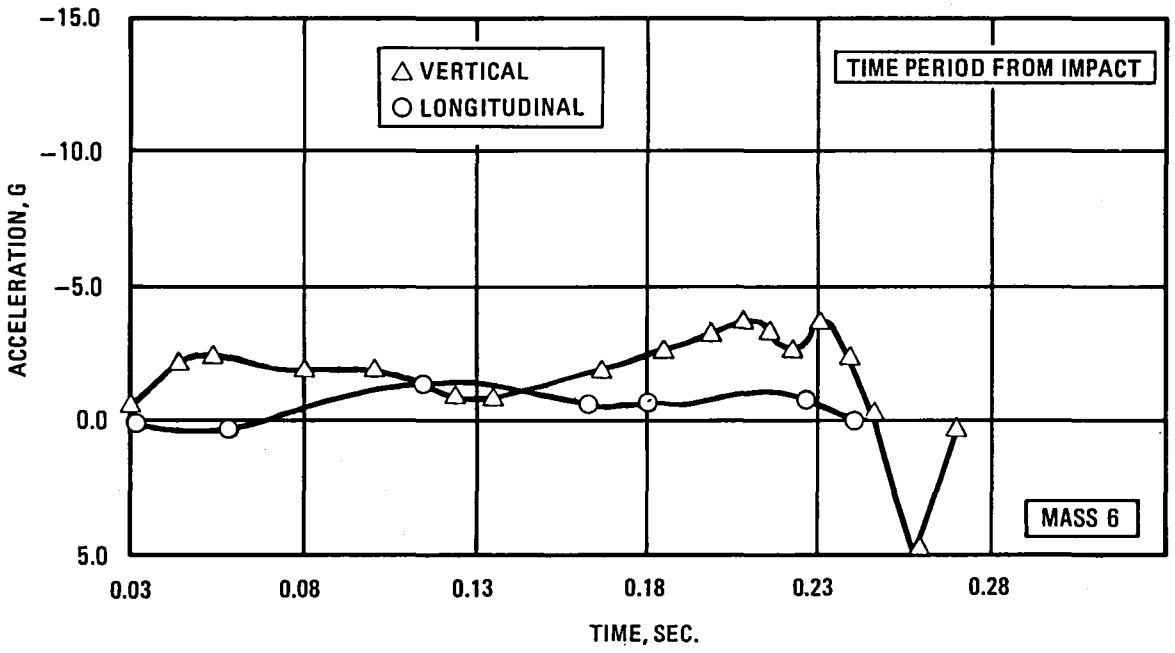

Figure 5-19. - Airframe responses, air-to-ground hard landings, AGHL 358-4.

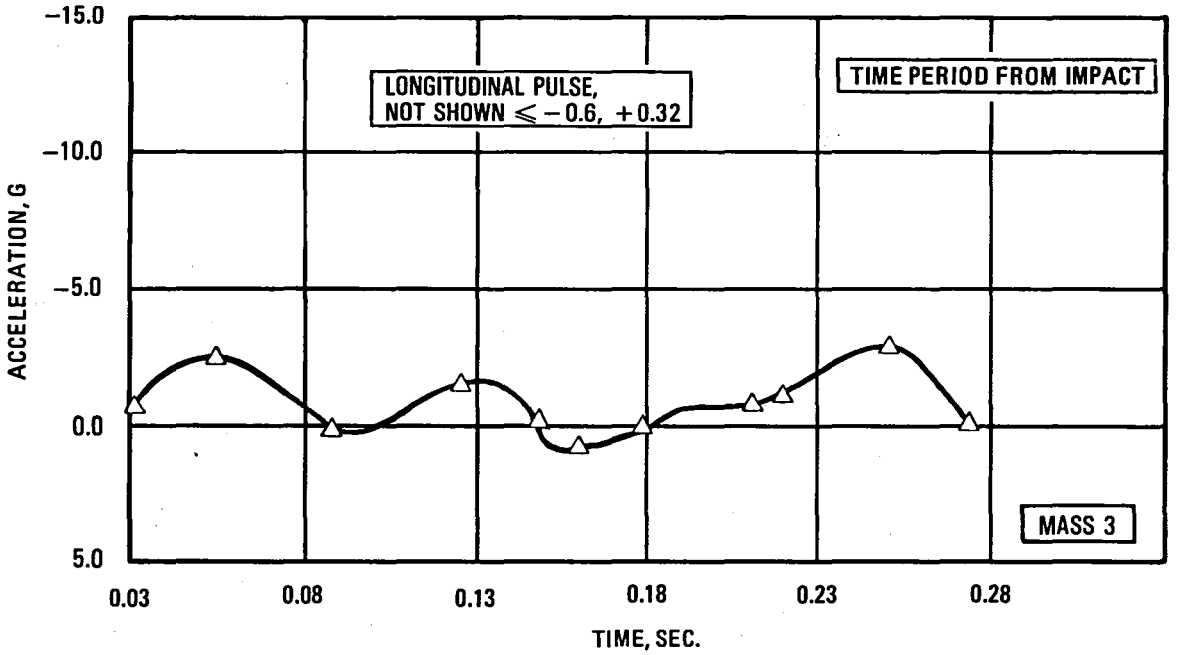

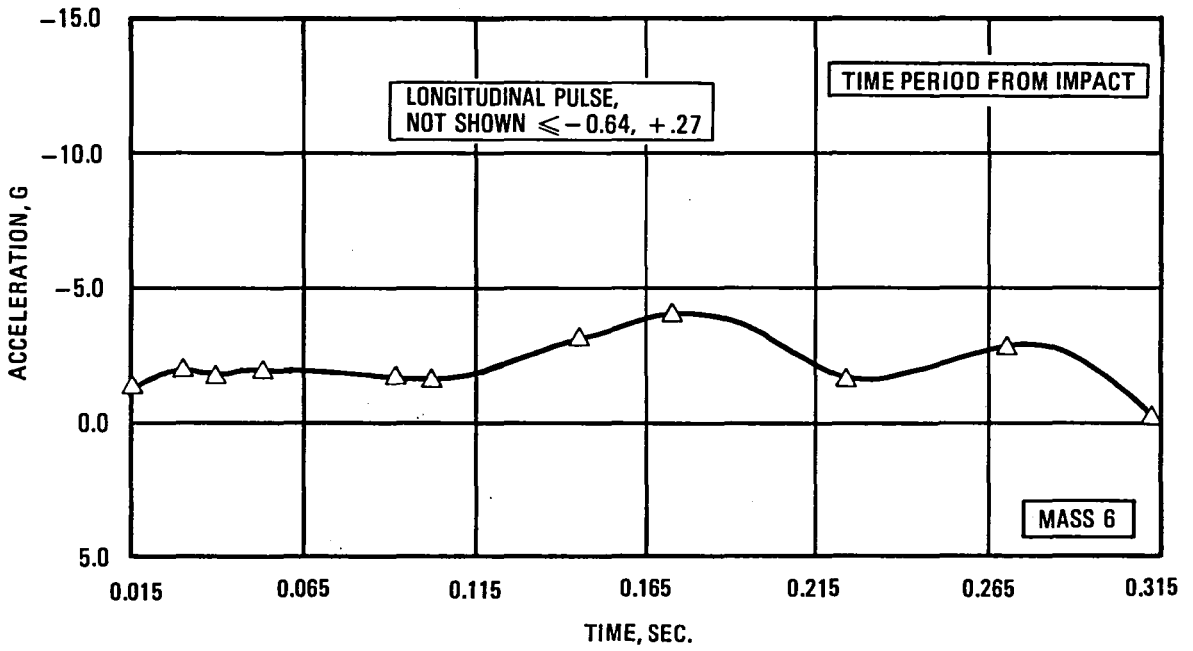

Figure 5-20. - Airframe response, air-to-ground hard landings, AGHL 358-5.

anticipated to produce high longitudinal acceleration. The 20 ft/sec impact conditions can be expected to produce landing gear and/or airframe structural failures.

Cases AGHL-358-2, -3, and -4 compare a 20 ft/sec hard landing for three different nose-up pitch attitudes; 15-degrees, 6-degrees, and 0-degrees. The passenger compartment responses are shown in Figure 5-21 and 5-22 for the longitudinal and vertical directions, respectively. All three airplane attitudes at the 20 ft/sec impact speed show a potential for fuselage failure due to shear and/or bending at stations which would approximate the locations of the wing leading and trailing edges. The potential for failure would appear to increase at the extreme forward and aft locations, such as aft of the cockpit and forward of the pressure bulkhead. As noted in the Reference 1 accident data, these locations are vulnerable to break-up under extreme impact conditions. KRASH results show that for the 15-degree impact condition the horizontal stabilizer and the fuselage at stations 1636 and 1992, contacts the ground after the first hitting on the main gears. Failure of the wing outboard of the engines is possible. For the 6-degree impact the contact sequence is main gears, fuselage station 1663, nose gear, engines and fuselage station 1424 with main and nose gear failures occurring. For the zero-degree impact condition the sequence of ground contact is main gear, nose gear, engine and fuselage at stations 426 and 677. Failure occurs for the main and nose gears and wing, outboard of the engine. The sequence of ground contact and potential failure regions are very much dependent on the pitch attitude and velocity at impact. During this 15 ft/sec impact the loads do not reach ultimate except possibly aft of station 1117. For the 20 ft/sec impact the airplane main landing gear contacts the ground initially, followed by the fuselage (FS 1663), nose gear, engine and fuselage again (FS 1424 and 1663). However, during all the 20 ft/sec, 6-degree nose-up impacts the shear loads in the forward section and most bending loads could result in fuselage rupture. The KRASH model used for these runs provides for landing gear and wing failures, but fuselage peak loads are only monitored and compared to strength envelopes.

Both the main and nose gear show the occurrence of failure at the 20 ft/sec (0 and 6-degree nose) sink speed. These results are consistent with previous

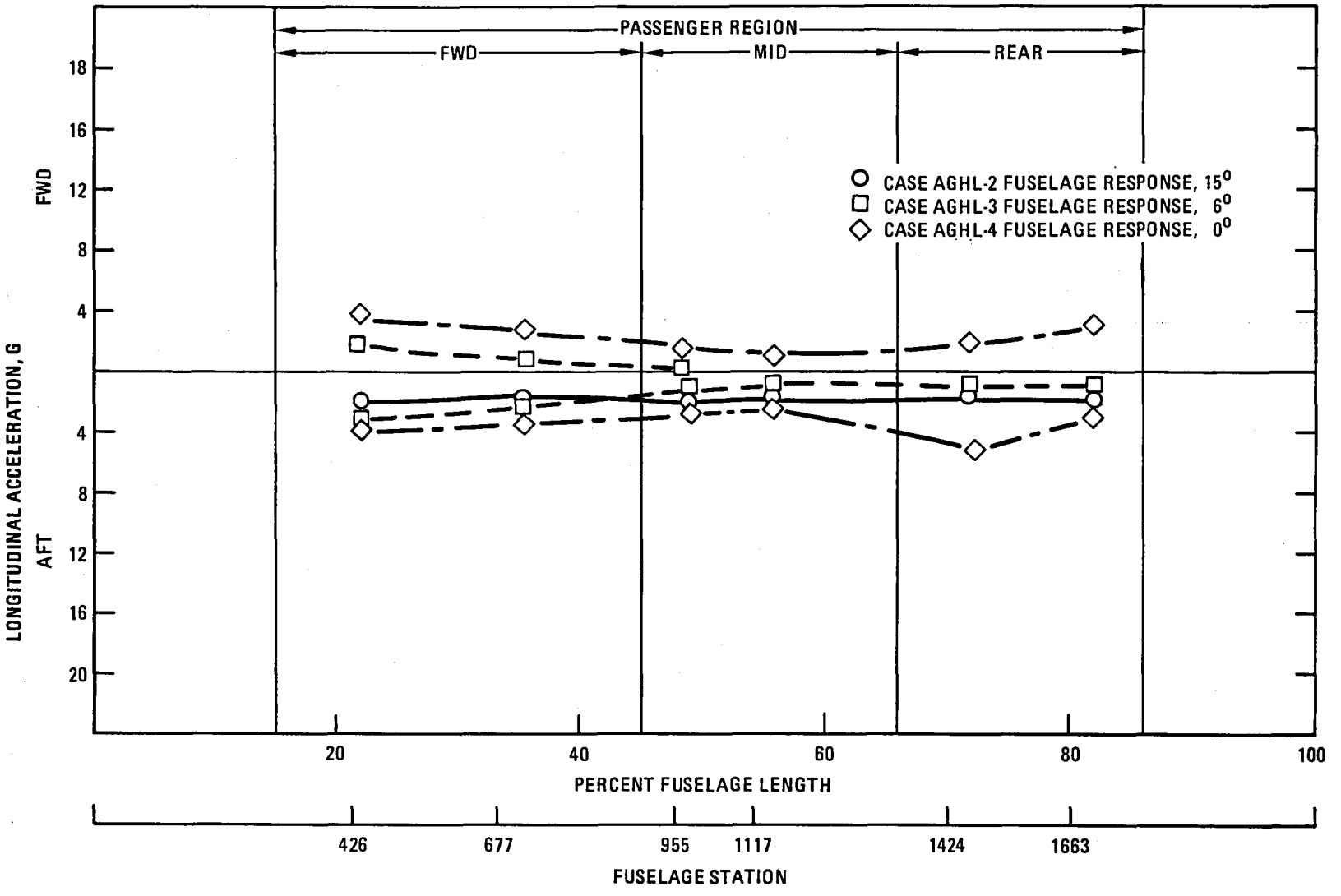

Figure 5-21. - Longitudinal acceleration versus fuselage location, 20 ft/sec hard landing, 0-degree, 6-degree, 15-degree pitch.

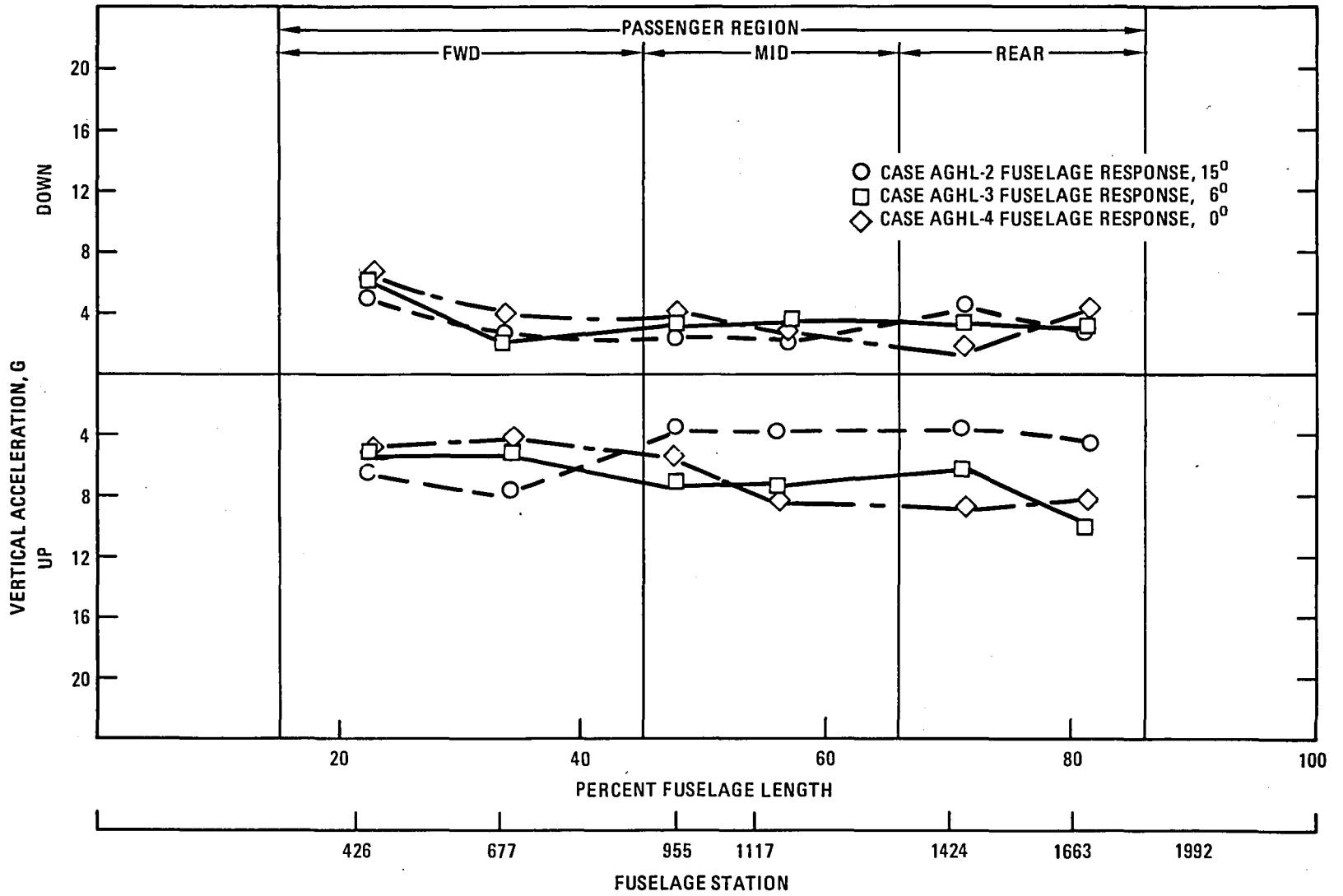

Figure 5-22. - Vertical acceleration versus fuselage location, 20 ft/sec hard landing, 0-degree, 6-degree, 15-degree pitch.

study (Reference 1) results where it was noted that for a symmetrical impact (Roll angle -0 degrees), the main landing gear would not fail for sink speed up to 17.5 ft/sec. Figure 5-23, obtained from reference 1, shows that failure mode of the main gear depends on the roll angle. Furthermore, as the roll angle increases the sink speed will decrease for gear failure to occur.

5.6 Air-to-Ground Impact (AGI) Scenario

Table 5-6 identifies the air-to-ground impact conditions. From the data provided in Table 5-1 it can be noted that these cases are the same as the hard landing except for the introduction of roll and yaw. Table 5-7 summarizes the results of these analyses for the forward and aft passenger regions. Portions of an applicable acceleration response history are shown in Figure 5-24. The peak side acceleration for the 15 ft/sec impact with both roll (20 degrees) and yaw (30 degrees) reaches $\pm 2.4\ G_y$. During this condition the aircraft outboard wing contacts the ground initially, followed by the MLG, wing engines and wing inboard of the tip. Potential failures occur at the wing outboard tip, inboard of the tip and for the MLG. The sequence of events

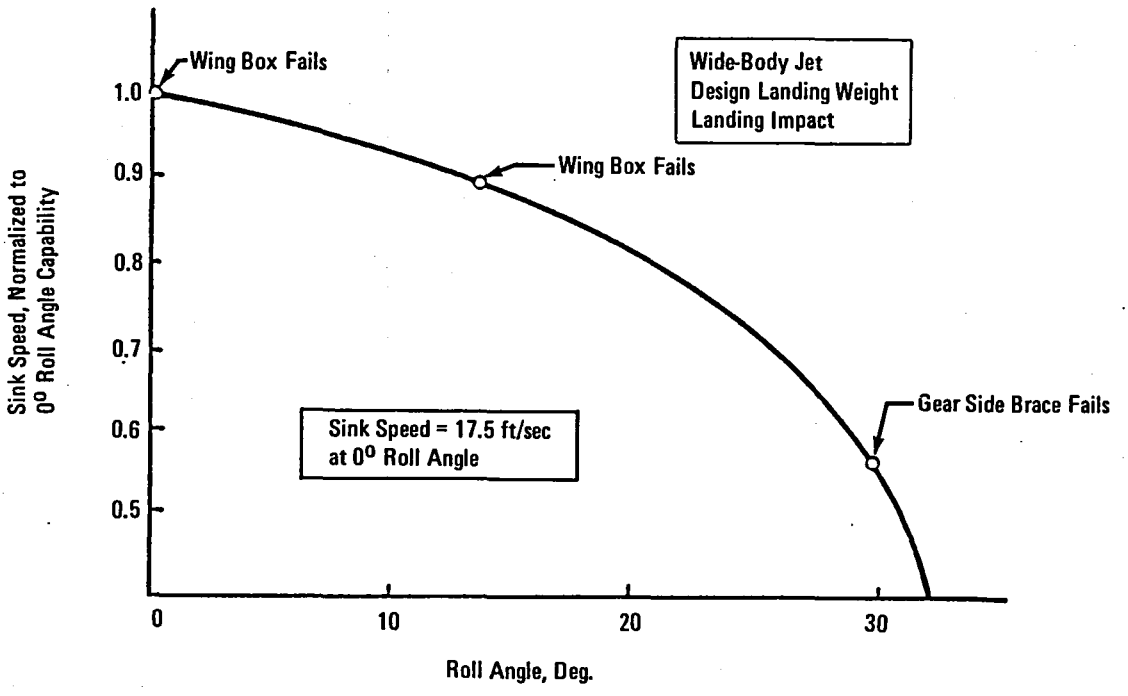

Figure 5-23. - Envelope of sink speed versus roll angle. (Reference 1.)

TABLE 5-6. - MATRIX OF ANALYSIS CONDITIONS, WIDE-BODY AIR-TO-GROUND IMPACT CRASH SCENARIOS

Case No.	Data Set	Airplane Configuration					Terrain			Initial Conditions						Rupture Allowed
		Weight Lb	Type	Full A/P Stub Wing	Gear Position	Lift	Ground Flexibility In/Lb	Coeff. Friction μ	Slope Degrees	Velocity Ft/Sec			Altitude, Degrees			
										Fwd	Vertical	Side	Roll	Pitch	Yaw	
AGI-358-1	AEA 1005A	358,000	WB	Full/AP	Extended	Yes	Rigid	.35	Flat	270	15	0	0	6	30	Yes
AGI-358-2	AEA 1006	358,000	WB	Full/AP	Extended	Yes	Rigid	.35	Flat	270	20	0	0	6	30	Yes
AGI-358-3	AEA 1007	358,000	WB	Full/AP	Extended	Yes	Rigid	.35	Flat	270	15	0	20	6	30	Yes
AGI-328-3	AEA 1008	328,000	WB	Full A/P	Extended	Yes	Rigid	.35	Flat	270	15	0	20	6	30	Yes

TABLE 5-7. - SUMMARY OF AIR-TO-GROUND IMPACT ANALYSIS RESULTS

CONDITION	PEAK ACCELERATIONS G'S / TIME / DURATION	POTENTIAL FAILURES BEAM / TIME / DOF	GROUND CONTACT MASS POINT
AGI -358-1 160KTS - 15 F/S - 00 ROLL - 06 PTCH - 30 YAW - LG - 0 SLP - RIGID			
MASS 3 L AFT	-1.016 G'S@ .420 FOR .130		10
FWD	.314 G'S@ .640 FOR .080		29
S LFT	- .790 G'S@ .580 FOR .075		
RGT	1.117 G'S@ .340 FOR .155		
V UP	-2.983 G'S@ .260 FOR .170		
DWN	.929 G'S@ .880 FOR .090		
MASS 6 L AFT	-1.024 G'S@ .420 FOR .160		
FWD	.344 G'S@ .660 FOR .070		
S LFT	- .919 G'S@ .920 FOR .095		
RGT	1.103 G'S@ .320 FOR .150		
V UP	-3.145 G'S@ .300 FOR .210		
DWN	.483 G'S@ .580 FOR .045		
AGI -358-2 160KTS - 20 F/S - 00 ROLL - 06 PTCH - 30 YAW - LG - 0 SLP - RIGID			
MASS 3 L AFT	-1.374 G'S@ .720 FOR .075	17 @ .1896 IN 1	10
FWD	.792 G'S@ .360 FOR .040	38 @ .1938 IN 1	29
		33 @ .7994 IN 5	7
S LFT	-5.023 G'S@1.000 FOR .050	11 @ .8152 IN 5	18
RGT	2.878 G'S@ .940 FOR .040	10 @ .8792 IN 4	37
		16 @ .8984 IN 2	6
V UP	-4.225 G'S@ .260 FOR .035		9
DWN	4.336 G'S@ .300 FOR .045		
MASS 6 L AFT	-1.147 G'S@ .720 FOR .100		
FWD	1.201 G'S@ .780 FOR .025		
S LFT	-1.635 G'S@ .940 FOR .060		
RGT	2.211 G'S@ .900 FOR .040		
V UP	-7.665 G'S@ .640 FOR .090		
DWN	4.565 G'S@ .200 FOR .075		
AGI -358-3 160KTS - 15 F/S - 20 ROLL - 06 PTCH - 30 YAW - LG - 0 SLP - RIGID			
MASS 3 L AFT	-1.279 G'S@ .640 FOR .055	34 @ .3048 IN 3	34
FWD	.980 G'S@ .620 FOR .040	33 @ .3220 IN 3	29
		38 @ .5320 IN 1	37
S LFT	-1.157 G'S@ .740 FOR .035		10
RGT	1.967 G'S@ .580 FOR .030		
V UP	-2.772 G'S@ .660 FOR .030		
DWN	2.118 G'S@ .700 FOR .035		
MASS 6 L AFT	-1.586 G'S@ .660 FOR .085		
FWD	.538 G'S@ .680 FOR .020		
S LFT	- .341 G'S@ .960 FOR .045		
RGT	2.400 G'S@ .540 FOR .040		
V UP	-1.995 G'S@ .360 FOR .065		
DWN	5.356 G'S@ .540 FOR .040		
AGI -328-3 160KTS - 15 F/S - 20 ROLL - 06 PTCH - 30 YAW - LG - 0 SLP - RIGID			
MASS 3 L AFT	-1.514 G'S@ .660 FOR .075	34 @ .3098 IN 3	34
FWD	.495 G'S@ .620 FOR .017	33 @ .3256 IN 3	29
		38 @ .5640 IN 1	37
S LFT	-2.452 G'S@ .620 FOR .040		33
RGT	1.277 G'S@ .600 FOR .040		
V UP	-3.386 G'S@ .680 FOR .030		
DWN	3.788 G'S@ .580 FOR .035		
MASS 6 L AFT	-1.007 G'S@ .620 FOR .045		
FWD	.358 G'S@ .700 FOR .020		
S LFT	-1.003 G'S@ .640 FOR .020		
RGT	1.147 G'S@ .660 FOR .040		
V UP	-2.628 G'S@ .540 FOR .080		
DWN	1.106 G'S@ .640 FOR .035		

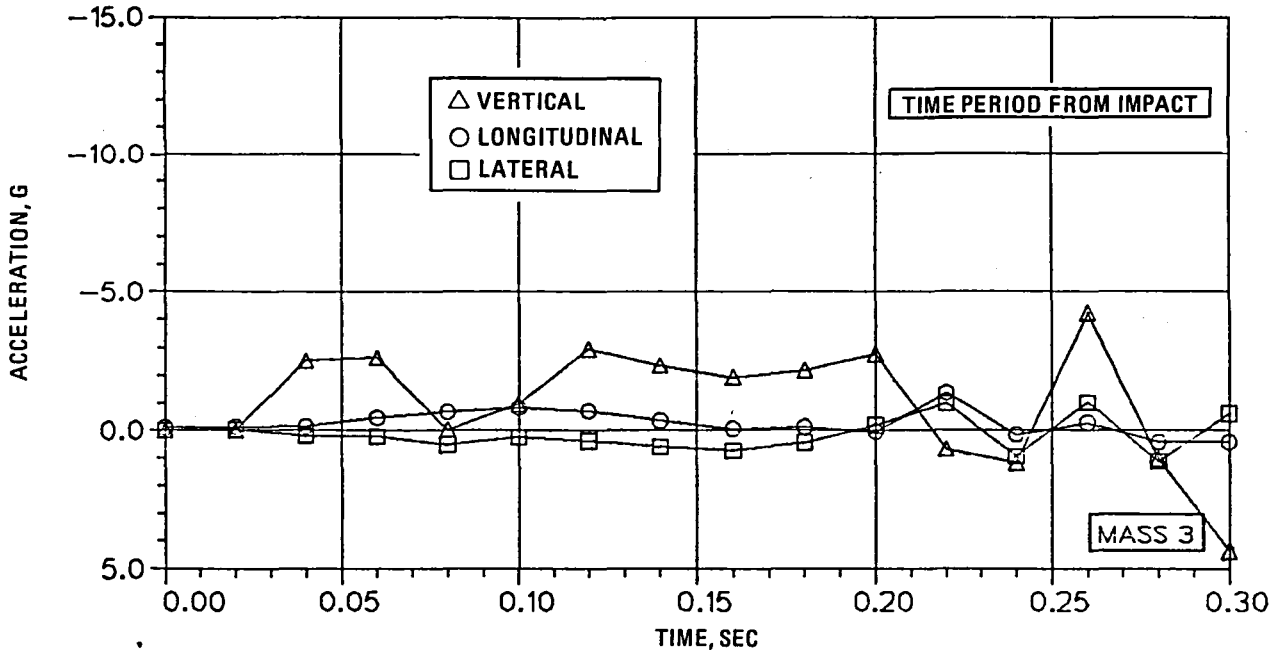

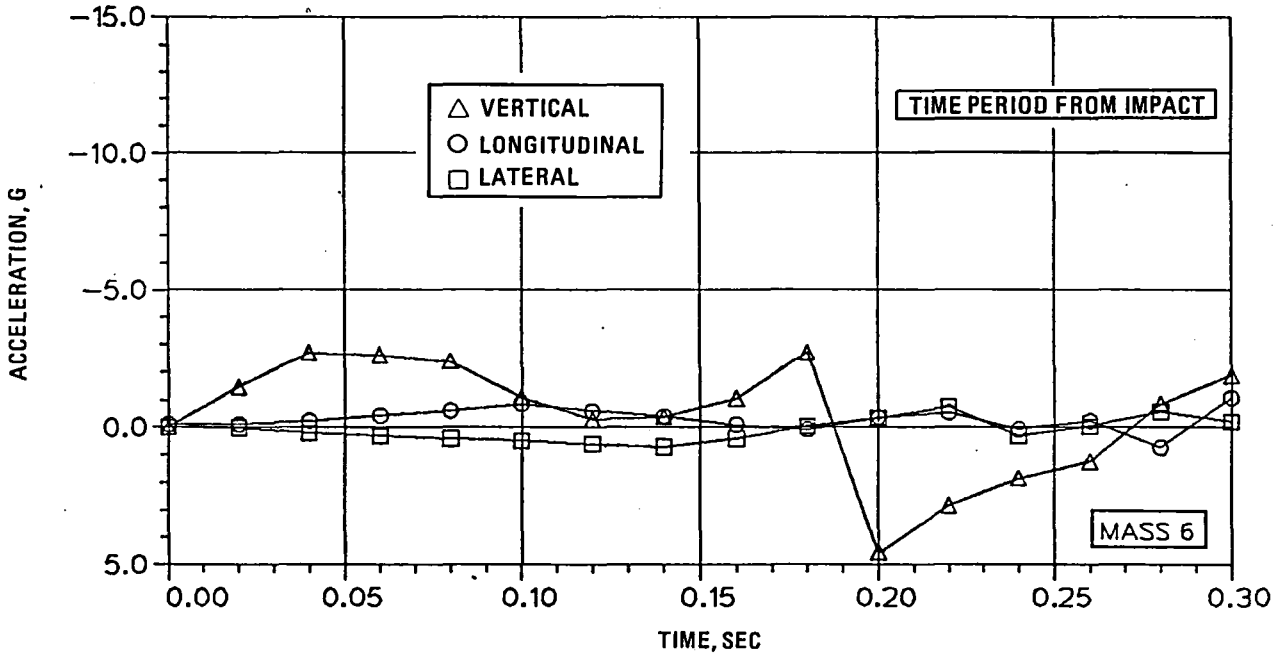

Figure 5-24. - Airframe responses, air-to-ground inpact AGI-358-2.

and peak responses are generally the same for both the 328000 lb and 358000 lb airplane configurations analyzed. For the 20 ft/sec impact with 30 degree yaw, a $\pm 5G_y$ side load is experienced at the forward location (mass 3). For this higher sink speed case the aircraft sequence of ground contact is main landing gears, aft fuselage, wing engines, fuselage again and nosegear. Several potential failures are noted, including; main gears, wings outboard of engine and nose gear. The yaw condition results in considerably more potential failures than does the symmetrical hard landing.

SECTION 6

MASS AND SIZE SCALING TRENDS

Figure 6-1, obtained from Reference 1, shows the range of weight class and classifications of transport aircraft. Some typical aircraft within each of these classifications are shown in Table 6-1. From the data shown in Table 6-1, it can be seen that even within a class of aircraft there can be a significant variation in operating weight, size, loading configuration and engine mounting configuration. In general, it can be assumed that mass and size are related in the sense that the longer wider aircraft are designed for the purpose of carrying a higher payload, coupled possibly with a longer route structure which also means higher fuel capacity. However, there is a limiting scale effect as can be seen when comparing different aircraft cross-sections. The height within the passenger cabin regions can only be reduced to a point. Another factor which makes scaling on size or mass difficult is the location of engines which can influence the crash dynamic behavior of aircraft. The currently available test data are from the L-1649 test in which the wing fuel tanks ruptured and the wing was severed due to pole and barrier impacts. Earlier in section 4 the wide-body analyses were performed for what is referred to as a stub wing configuration due to the loss of wing structure. This configuration allows for an assessment of fuselage, floor and occupant response on the basis of changes in basic airframe structure such as fuselage diameter and length, floor design, seating arrangements, and underfloor crushing characteristics. Accordingly the mass, size scaling trends are based on the same impact condition as described in Section 4.2 which are:

- Six-degree slope
- Forward velocity 172 ft/sec.

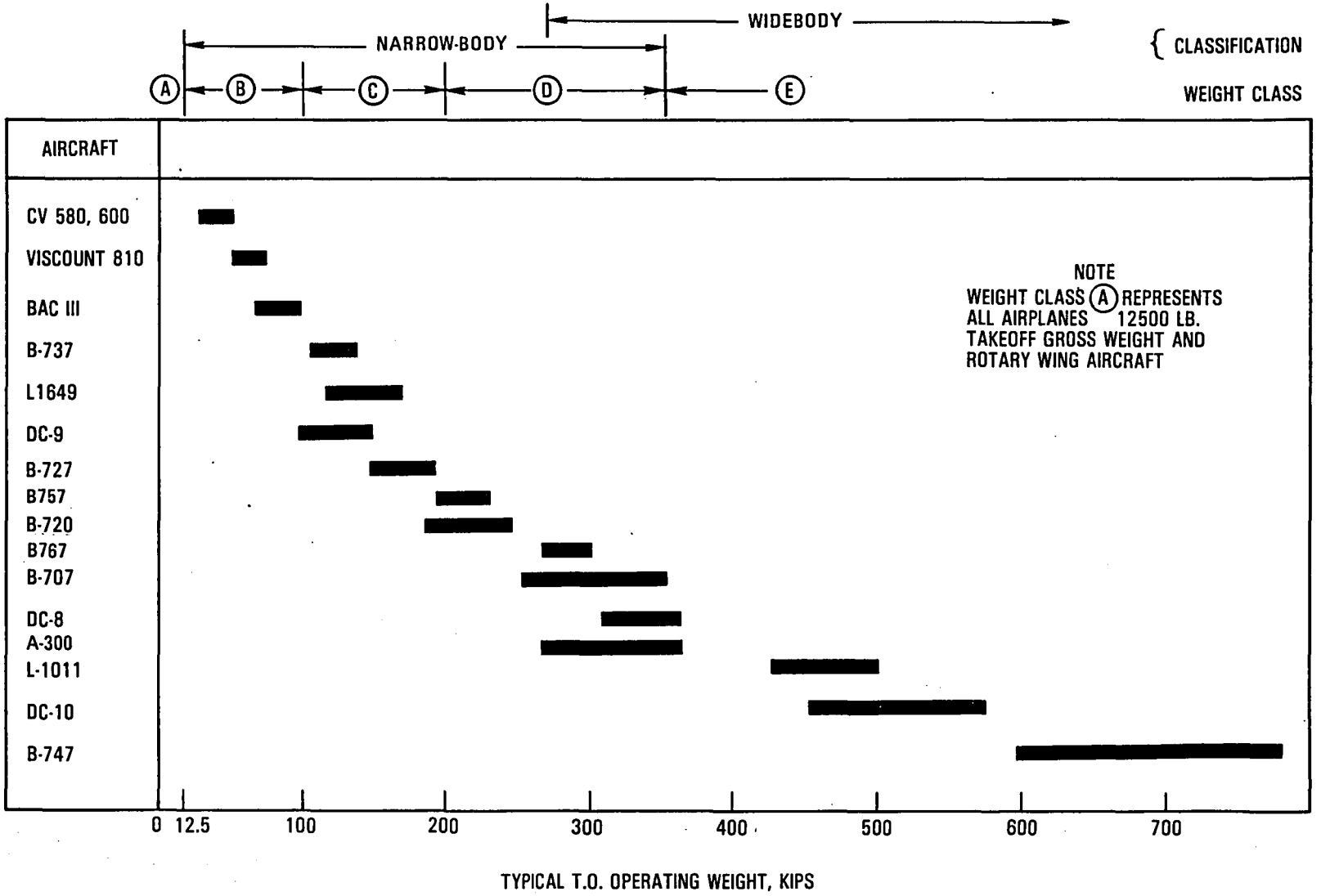

Figure 6-1. - Transport airplane vs takeoff G.W.

TABLE 6-1. - AIRPLANE SIZE AND WEIGHT CHARACTERISTICS

Class or Category	Aircraft	Weight x 10^3, Lb.				No. Passengers	Approximate Size, Ft.					
		Empty Operating	Zero Fuel	Max. Ldg	Max. T.O.		Fuselage Dia.	Overall Length	Wing Span	Cabin Height	Below PAX Floor	Engine Configuration
B	CV440, 600	31	–	44	57	-56	10	75 – 79	91 – 105	–	3	2
	Viscount-800	41	54	58	73	-67	11	85	94	–	3	4W
	BAC 111	46	71	69	105	-80	11	93	88	–	3	2F
C	L-1649	85	116	123	156	-92	12	116	150	7	4	4W
	B737	65	95	105	125	-115	12	100	93	7	5	2W
	DC-9	50	87	82	147	-90	12	119	93	7	4	2F
	B-727	88	140	142	191	-89	14	133	108	7	5	3F
D	B-720	110	156	175	235	-116	14	137	131	7	7	4W
	B-707	125	230	190	366	-219	14	152	146	7	7	4W
	DC-8	124	180	207	350	-179	14	151	143	7	7	4W
	B757	131	184	198	220	-220	14	155	124	7	7	2W
	B767**	180	248	270	300	-255	16	159	156	8	8	2W
	A300**	195	275	293	363	-345	18	176	147	8	9	2W
E	L-1011**	240	320	358	500	256 – 400*	20	180	155	8	9	2W, 1F
	DC-10**	236	368	363	565	270 – 390*	20	180	155	8	9	2W, 1F
	B-747**	350	525	465	785	385 – 500*	22	231	196	8	10	4W

W = Wing
*All Tourist Configuration

F = Fuselage
**Wide-body aircraft

- Rigid ground
- Ground coefficient of friction = .70

The premises for the trend analysis are as follows:

- The underside crushing spring length is related to the below passenger floor distance.
- The fuselage underside crushing force is related to the aircraft fuselage weight.
- The fuselage beam properties are obtained from aircraft section properties. Where unavailable they are related to the fuselage cross-section properties as follows:

$$\text{Area} = K_1 \pi r^2 \left[1 - \left(1 - \frac{t}{r}\right)^2\right]$$

$$\text{Inertia} = K_2 \frac{\pi}{4} r^4 \left[1 - \left(1 - \frac{t}{r}\right)^4\right]$$

where:

r = radius of shell section

t = thickness of shell section

K_1, K_2 = factors determined from available data

The term (t/r) can be thought of as an effective skin thickness ratio and is obtained from available information. It is different for the axial and bending terms. K_1 and K_2 can be developed from known data for different aircraft configurations.

- The fuselage weight properties are obtained from aircraft section-properties. The fuselage stations are located in proportion to the total length. Where unavailable, mass inertia properties are allocated in proportion to aircraft weight distribution.
- Two floor designs are used. One representative of a wide-body aircraft and another representative of a narrowbody aircraft.
- The same general two-passenger seat arrangement is used for all analysis and it is assumed that each seat is fully loaded with 176 lb. occupants.

The airframe, floor and seat models, described earlier in Section 4, are analyzed in sequence with each preceding model accounting for mass interaction; i.e., occupant with floor or floor and occupant with airframe. The aircraft model representations used are described below:

Representation	Weight Lb X 10^3	Fuselage Dia., In.	Overall Fuselage Length, In.	Maximum Underfloor Distance, In.
B Type	80	130	1020	40
C Type	159	140	1367	50
* D Type	175 – 220	170	1566	78
* D Type	245 – 320	170	1746	78
E Type	328 – 432	220	2127	100

*Analysis to be performed in conjunction with B720 crash test program

The results of the trend analysis are shown in Figure 6-2. The unfiltered and 50 Hz filtered peak accelerations in the longitudinal aft and vertical up directions, averaged over four fuselage locations, (masses 3, 4, 5, and 6) which represent approximately the region from the forward to aft passenger regions, are plotted. The trend indicated is a reduction in acceleration level as the aircraft size and mass increase. Normalized to L-1649 filtered data the variation in the vertical direction appears to be ±20 percent. Normalized to L-1649 filtered data the variation in the longitudinal direction appears to be +15 percent to -30 percent for the gross weight range from 80K to 432K. The results are sensitive to the assumptions regarding model property relationships, particularly in the representation of the lower fuselage crushing and the ground representation. Figures 6-3 through 6-6 show the response obtained analytically for the "C" class aircraft throughout the occupant occupied floor region. The pulse shape varies in magnitude, shape, and time of peak occurrence. While differing in magnitude and duration slightly, the pulse variation throughout the floor region is similar to the aircraft in the other categories.

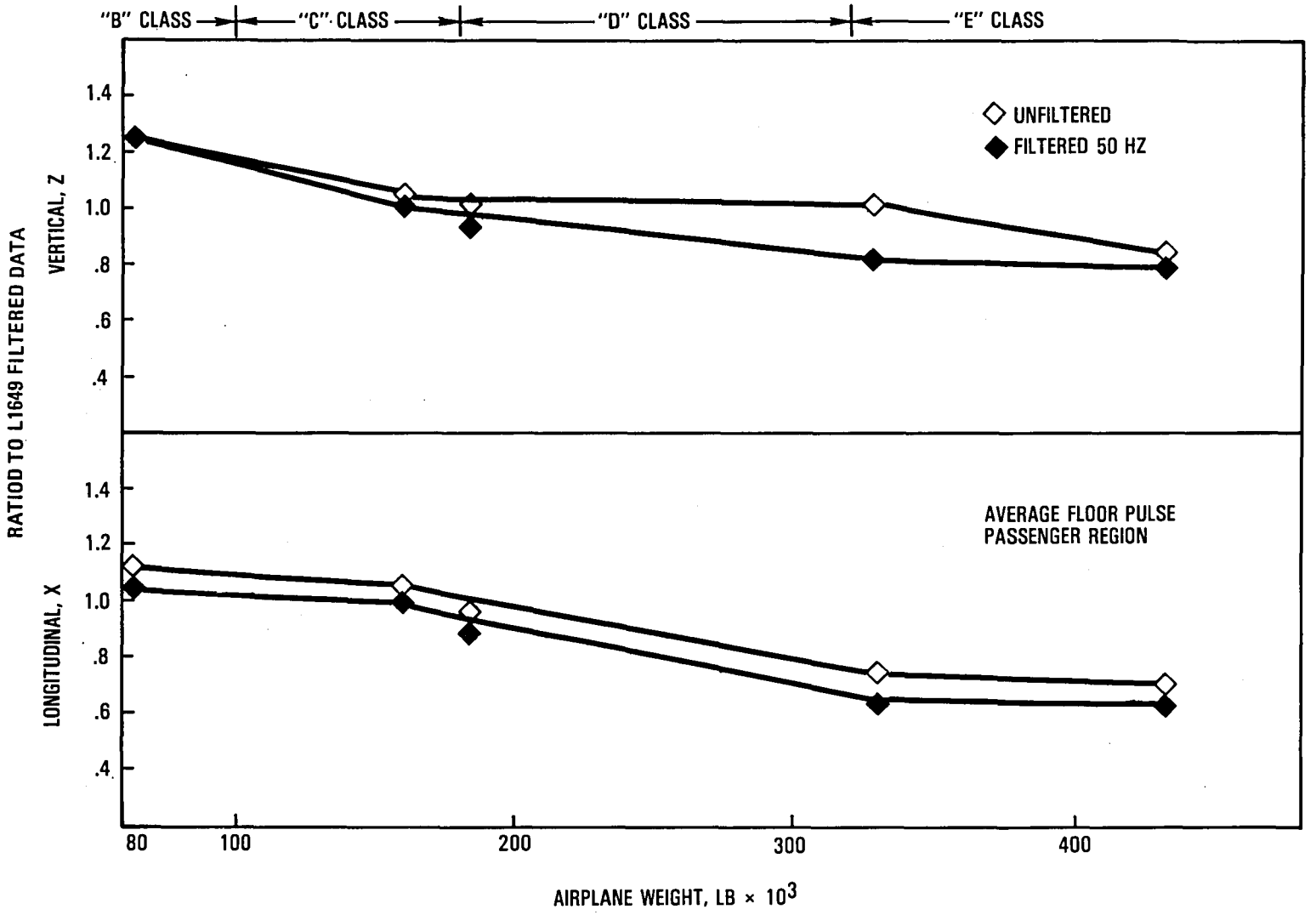

Figure 6-2. - Peak acceleration versus airplane size and weight

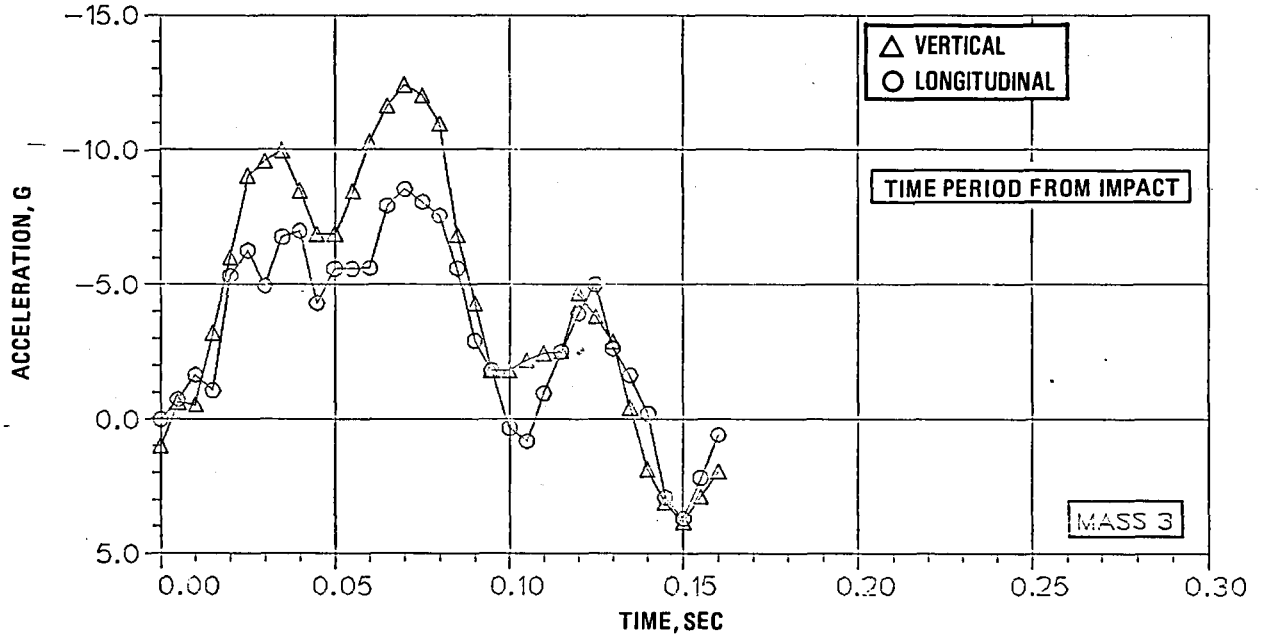

Figure 6-3. - Airframe response, stub wing configuration F.S. 460

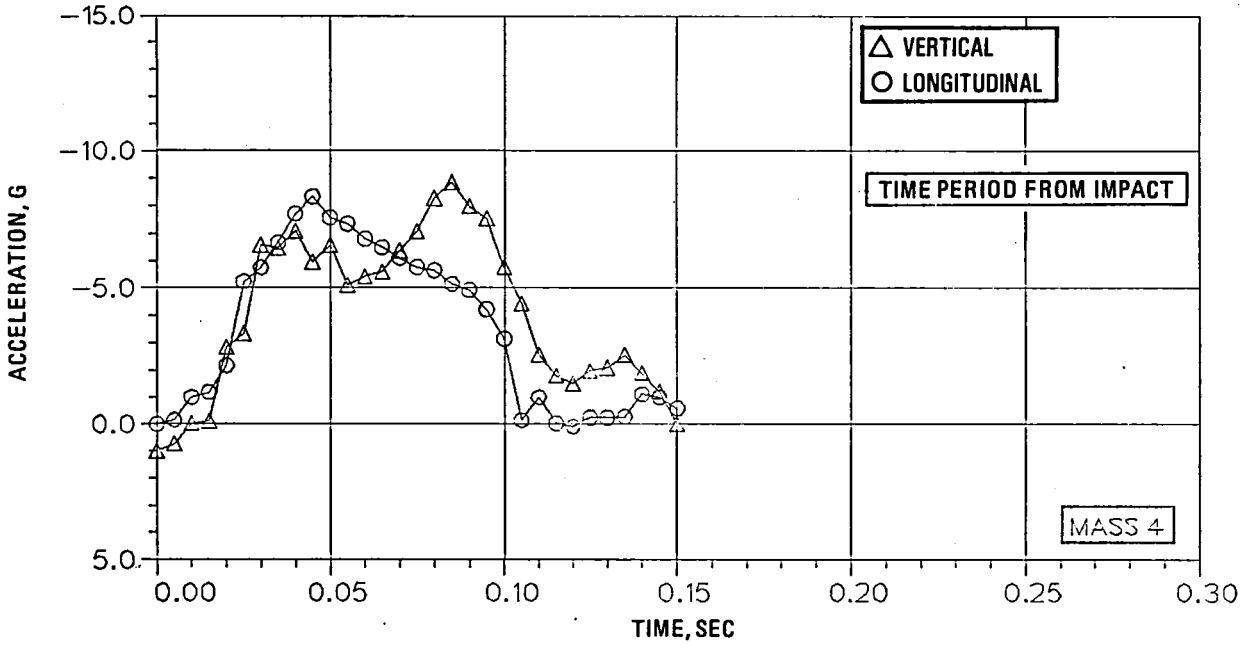

Figure 6-4. - Airframe response, stub wing configuration, F.S. 600

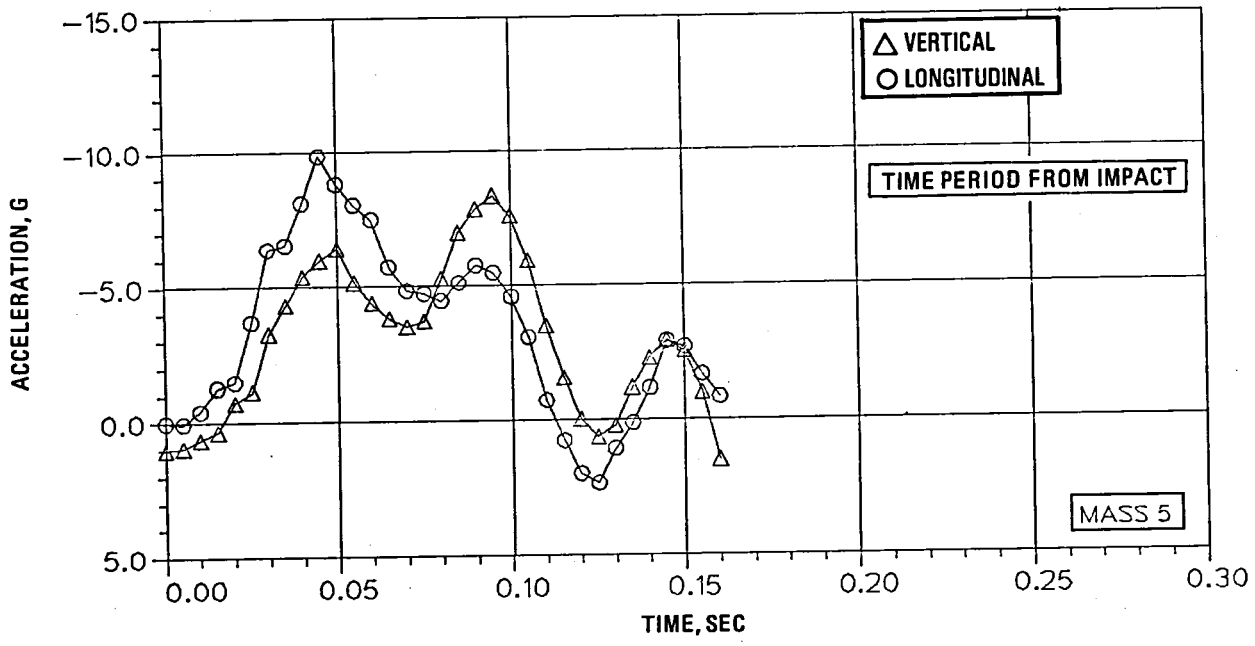

Figure 6-5. - Airframe response, stub wing configuration, F.S. 685

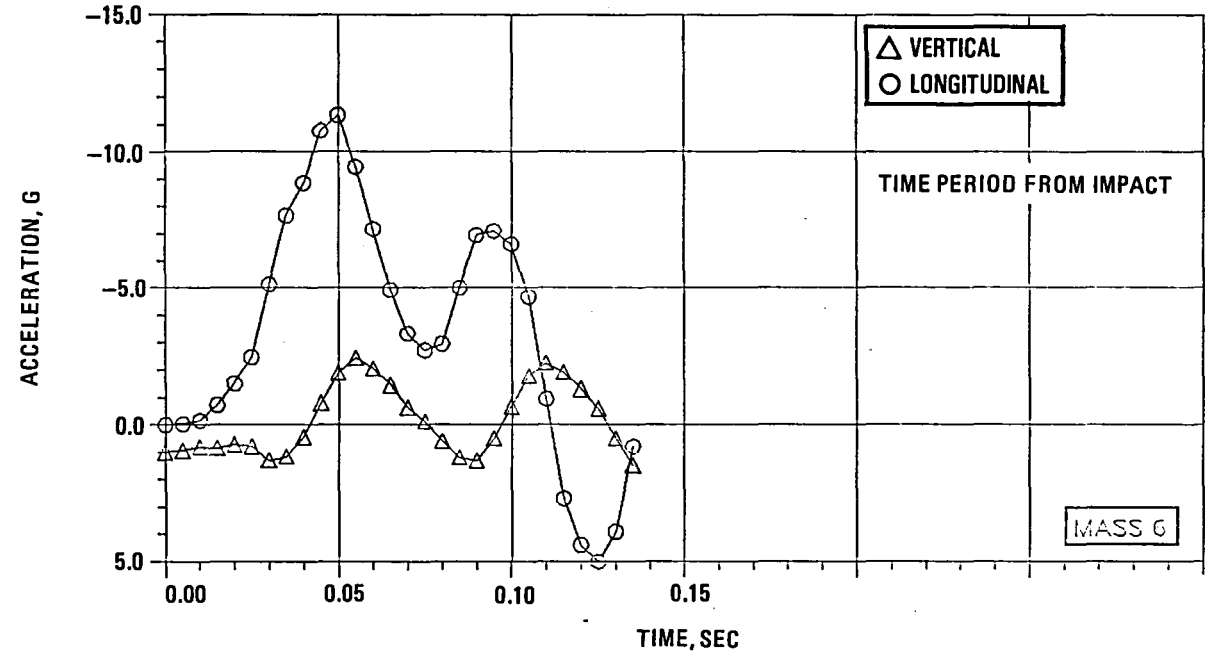

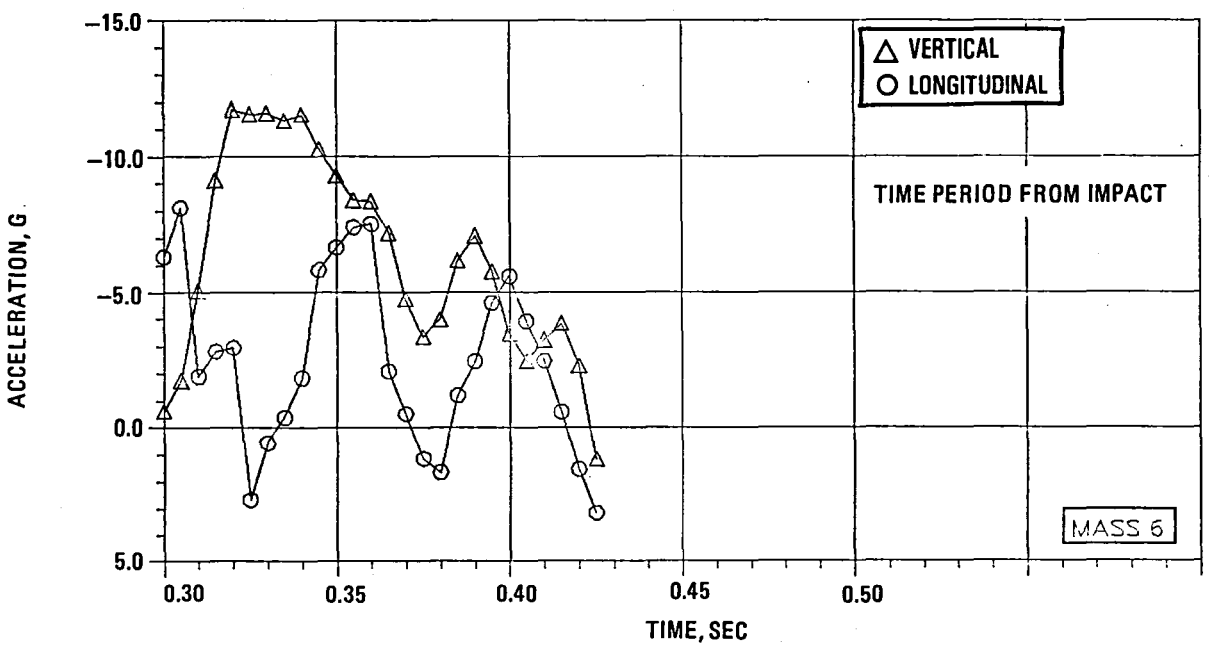

Figure 6-6. - Airframe response, stub wing configuration, F.S. 923

SECTION 7

TRANSPORT SEAT TEST PERFORMANCE

7.1 FAA CAMI Test/Seat Configuration Description

The FAA Civil Aeromedical Institute (CAMI) recently completed a series of static and dynamic tests for several transport aircraft seat configurations. The test program, described in Reference 10, is an attempt to expand the available data base and is designed to obtain information regarding seat performance for different conditions/configurations. No attempt is made to relate the seat performance to the crash environment. The planned test conditions are described in Figure 7-1. The seat configurations are described in Table 7-1. The dynamic pulse, in all cases, is a trapezoidal shaped acceleration-time history with a relatively short (30 millisecond) onset time to generate a response approaching that of the acceleration step function, and is one which can be easily generated in the laboratory. As long as the pulse duration is sufficiently long, so that the maximum response and/or failure of the seat-restraint-occupant system (SROS) occurs during the pulse, the objective of the test will be achieved. A summary of the seat configuration test combinations is shown in Table 7-2.

7.2 Evaluation of Test Results

The evaluation of the test results is presented with regard to:

- Dynamic versus static inputs
- Deformed versus underformed floor
- Unidirectional versus multidirectional loading

Test Conditions	Static	Dynamic	Loading			Deformed Floor	Aft Seated Passengers	Comments
			Fwd	Down	Side			
1	X		X					Static test, forward loading
2	X		X			X		One track rolled 10 degrees, one track pitched to 10 degrees US Army Crash Survival Design Guide
3		X	X					Dynamic evaluation of Test 1
4		X	X				X	Same as Test 3 with Aft Seated Passengers
5		X	X			X		Dynamic evaluation of Test 2
6		X	X			X	X	
7	X		X		X			Yawed 30 degrees
8		X	X		X			Dynamic Evaluation of Test 7
9		X	X		X	X		Same as Test 8, includes deformed floor
10		X	X	X	X			Ratio of 9:4.5:1.5 in forward, downward, and sideward directions

Figure 7-1. - FAA-CAMI planned test conditions.

To assess the results, the following tests were compared:

- No. 1 vs No. 3 (static versus dynamic forward loading)
- No. 1 vs No. 2 (static, undeformed versus deformed floor)
- No. 3 vs No. 5 (dynamic, undeformed versus deformed floor)
- No. 3 vs No. 8 (dynamic, forward vs 30 degree yaw)
- No. 3 vs No. 10 (dynamic, forward vs 9:4.5:1.5)
- No. 8 vs No. 9 (dynamic, 30 degree yaw, undeformed versus deformed floor)

To assist in the overall evaluation, tables were established to compare loads and failure modes. In addition, a summary comparison of equivalent acceleration levels, failures and ratio of loads is presented.

TABLE 7-1. - FAA-CAMI TEST SEAT CONFIGURATIONS

Seat No.	Configuration Name	No. Passengers 2	No. Passengers 3	Description
1	Hardman 9750-103735-8	X		From wide-bodied aircraft. The aisle side assembly is splayed out toward the aisle (30^0). Seat uses rectangular torque tube as primary structural member, with legs and seat belt/seat back brackets bolted to tube. Seat pan formed by the tube and light sheet metal extensions fore-aft riveted to tubes. Lightning holes in torque tube.
2	Hardman 9750-103735-023	X		Similar to No. 1 except both legs vertical.
3	Hardman 9750-106160-12	X		Appears the same as No. 2.
4	Hardman 9750-106160-8		X	Similar in construction to No. 2 and No. 3 except no lightening holes in torque tube.
5	Hardman 9750-10500-3/4	X		Similar in construction to No. 4 but with provisions for storage of oxygen generators in seat backs.
6	Hardman 9500-102307		X	Coach seat. Primary structure is a rectangular torque tube. Seat pans are formed aluminum sheet metal, hinged at the aft support bracket. Legs attached differently than Nos. 1-5.
7	Hardman 9300-101433	X		First class seat with service console between seats. Primary structure is peripheral frame with formed, and extruded aluminum elements. Seat legs and seat back/seat belt fittings attached to frame. Seat pan formed of perforated aluminum sheet suspended between front and rear.
8	TECO TE1003-2-401	X		Unique modular construction. Primary structural element is circular aluminum torque tube. Seat legs, arm rests and seat bucket assemblies are clamped (clamshell clamps) to tube to prevent rotation about the tube by a square leg which fits in the keyway in the clamshell clamp. Legs are aluminum forging of inverted "V" design with I-beam cross-section. Seat bucket molded from foam filled fiberglass epoxy composite and carried structure for lapbelt attachment seat bucket attached to torque tube by clamp which incorporates an energy absorber. The absorber is an oversized hook designed to separate a slot in a ductile steel plate as the seat bucket rotated about the torque tube.
9	UOP816		X	Primary structure is welded steel frame.
10	Weber 804002-615	X		First class seat using an internally reinforced full width sheet metal box as the primary structure with legs, back and seat cushion suspended from the box.

TABLE 7-2. - SUMMARY OF FAA-CAMI SEAT CONFIGURATION/TEST CONDITION COMBINATIONS

Test Condition	Seat Configuration Tested								
	1	2/3	4	5	6	7	8	9	10
1	L81010	L81011	L81008	L81005 L81006	L81001	L81003	(b)	L81009	L81007
2	(a)	(a)	L81012	(c)	L81002	L81004	(b)	L81013	L81015
3	A81049 A81050	A81046 A81047 A81048	A81056 A81057 A81058	A81060 A81061	A81008 A81009 A81010	A81012 A81014 A81015	A81068 A81069	A81052 A81053	A81063 A81064
4	(a)	(a)	A81073 A81074	(a)	A81020 A81021 A81022 A81023	A81017 A81018 A81019	(a)	(a)	(a)
5	A81051	(a)	A81059	(c)	(c)	A81016	A81072	A81054 A81055	A81065 A81066 A81067
6		Not Performed							
7									
8	(a)	A81041 A81042	A81075	A81039	A81025 A81026	A81027	A81028 A81029 A81030	A81076	A81034 A81035 A81036
9	(a)	(a)	A81080	(c)	(c)	(c)	A81031 A81032	A81077	A81037 A81038
10	(a)	(a)	A81081 A81083 A81084	A81092 A81093	A81088	A81089 A81090	A81096	A81085 A81086	A81094 A81096

(a) Not tested

(b) Not tested, body block too big for seat

(c) Failed during floor static deformation

(d) L series is static test, A series is dynamic test

The equivalent G_x of the occupant is obtained as follows:

(a) dynamic

$$\left[\frac{F_X \text{ Reaction Load} - \text{Seat Weight} \times G_x \text{ (input)}}{\text{Occupant Weights*}}\right]$$

(b) static

$$\left[\frac{\text{Block force}}{\text{Occupant Weights*}}\right]$$

The equivalent G_x values are used for comparative purposes only.

7.2.1 Static Versus Dynamic (Test 1 vs Test 3)

The FAA-CAMI data comparing dynamic vs static tests is shown in Tables 7-3 and 7-4 for eight FAA-CAMI seat configuration tests. The results indicate that an average dynamic amplification factor of 1.72 per 1G of loading exists, as determined by dividing the equivalent G_x of the occupant by the dynamic G_x input. A value of 1.69 is reported in Reference 10.

The average equivalent static G_x, based on body block force is 16.3. Correspondingly, the average equivalent dynamic G_x is 17.3. The ratio of the dynamic to static results for these two equivalences from Table 7-4 is approximately 1.08. The average ratio for reaction loads and seat belt loads is between 1.02 and 1.20. The implication of a ratio greater than 1.0 is that the seat failed at dynamic loads that were higher than for the corresponding static test. However, this suggests that a 9G trapezoidal pulse (nearly step) is expected to be more severe than a 9G static load. From a simple single seat/occupant KRASH model one would expect a dynamic amplification factor of 1.7 to 1.85 for a 0.030 second onset of a pulse, which is pretty much in agreement with the 1.69 to 1.72 test values noted earlier. Figure 7-2 shows a comparison of KRASH results for the single seat/occupant model subjected to step, trapezoid and triangular pulses. Interpreting the analysis results in light of the test results would indicate that a 9G dynamic step should produce a more severe loading condition than the static case.

*Occupant Weight = 165 lb., individual seat weight = 25 lb.

TABLE 7-3. - SUMMARY OF LOADS, TEST CONDITIONS 1 AND 3, STATIC VERSUS DYNAMIC $-G_x$

SEAT CONFIG.	$-G_x$ ACCELERATION, G's		SEAT BELT LOADS (LB) × 10^2		(a)(b) LEG REACTION NET LOADS × 10^2				(a)(b) FWD. LEG REACTION LOADS × 10^2				(a)(b) REAR LEGS REACTION LOADS × 10^2			
	TEST 1 (d)	TEST 3 (d)	TEST 1	TEST 3	TEST 1		TEST 3		TEST 1		TEST 3		TEST 1		TEST 3	
					F_x	F_z	F_x	F_z	F_x	F_z	F_x	F_z	F_x	F_z	F_x	F_z
1	- (18.5)	9 (16.8)	61	76	-57	-17	-60	-11	-6	41	-12	48	-51	-58	-48	-59
2/3	- (20.9)	12 (20.3)	69	92	-67	-17	-73	-15	-7	48	-13	52	-60	-65	-60	-67
4(c)	- (17.2)	9 (13.0)	85	64	-79	-17	-71	-16	-9	58	-11	62	-70	-75	-60	-78
5	- (17.3)	9 (15.9)	57	43	-54	-14	-57	-23	-9	40	-10	35	-45	-54	-47	-58
6(c)	- (13.5)	12 (18.0)	67	112	-67	-12	-98	-28	-12	65	-14	83	-55	-77	-84	-111
7	- (19.4)	12 (22.7)	64	87	-63	-14	-81	-14	-11	74	-13	73	-52	-88	-68	-87
8				NO STATIC TEST												
9(c)	- (12.7)	9 (13.6)	63	62	-66	-2	-74	-13	-16	91	-12	58	-50	-93	-62	-71
10	- (10.9)	9 (18.8)	36	52	-37	-40	-62	-14	-10	50	-12	53	-27	-54	-50	-67

(a) $-F_x$ = FWD. REACTION LOAD

(b) $+F_z$ = UP REACTION LOAD

(c) THREE OCCUPANT SEATS, ALL OTHERS TWO OCCUPANT SEATS

(d) EQUIVALENT - G_x

TABLE 7-4. - COMPARISON OF TEST RESULTS, TEST CONDITIONS 1 AND 3, STATIC VERSUS DYNAMIC $-G_x$

PARAMETER			SEAT CONFIGURATION									
			1	2/3	4	5	6	7	8	9	10	AVG
EQUIVALENT G_x ACCELERATION LEVEL	EQUIVALENT ACCELERATION LEVEL, G	<10										
		10 - 12									1	
		12 - 14			3		1			1,3		
		14 - 16				3						
		16 - 18	3		1	1						
		18 - 20	1				3	1			3	
		>20		1,3				3				
FAILURES	SEAT PAN		1	1	1	1						
	LAP BELT		1	1,3	1	1	3	3				
	REAR LEG ATTACHMENT			3	3	1,3	1	1,3		1,3	1,3	
	FRONT LEG ATTACHMENT		3				1					
	TRACK											
RATIO OF: TEST CONDITION 3 / TEST CONDITION 1	EQUIVALENT G_x		.92	.97	.76	.92	1.33	1.17		1.07	1.56	1.09
	VERTICAL REACTION, F_z (REAR)		1.02	1.03	1.04	1.07	1.26	1.		.76	1.24	1.05
	VERTICAL REACTION, F_z (FORWARD)		1.17	1.08	1.07	.88	1.28	1.		.64	1.06	1.02
	LONGITUDINAL REACTION F_x (SUM OF FWD. & REAR)		1.05	1.09	0.9	1.06	1.46	1.28		1.12	1.67	1.20
	BELT LOADS		1.25	1.33	.75	.75	1.67	1.36		.98	1.44	1.19
	AVERAGE OF RATIOS		1.08	1.10	.90	.94	1.4	1.16		.91	1.40	

PULSE CONDITION	PULSE *	FWD SEAT LEG **	REAR SEAT LEG **	G_X TORSO / $G_X(=9)$	TORSO FOR 9 G_X EXCITATION	EQUIVALENT STATIC G_X TO PRODUCE 9 G_X TORSO RESPONSE
STEP	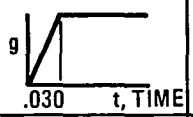	1.79	1.85	1.70	15.3	5.3
TRAPEZOID		1.68	1.41	1.60	14.4	5.6
TRIANGULAR		1.39	1.13	1.33	12.0	6.8
TRIANGULAR	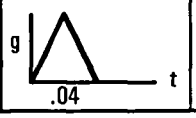	.78	.62	.77	7.0	11.6

* 9G PEAK FOR ALL CONDITIONS, TIME IN SECONDS
** RATIO OF DYNAMIC LOAD TO STATIC BODY BLOCK FOR FORE-AFT DIRECTION REACTION LOAD, BASED ON ANALYSIS

Figure 7-2. - Comparison of KRASH results for different dynamic pulses.

The FAA-CAMI test results do not substantiate a need for dynamic tests in lieu of static tests for the following reasons.

- Failure modes experienced in the static tests for seat configurations 1, 2/3, 4 and 5 all of which are basically the same type (except for the seat pan), one different than the failure modes noted in the dynamic test results. However, it is very likely that the body block design for this type of seat can lead to this type of failure and not the indicative of dynamic vs static effects. In subsequent seat configuration tests 7, 9 and 10, the static and dynamic test failures are similar.

- Failures are predominantly tension type and occur at attachments to the seat or at the base. Tension type failures are not as sensitive to the rate of loading as are compression failures. This would indicate that static tests could account for the seat failure modes experienced in a dynamic test, provided the body block is representative of occupant motion loading.

- The scatter in the data indicates that the results are very sensitive to design construction and possibly load variations. For example, for similar seat configurations 1 through 5, the variations in the ratios of dynamic to static factors are:

  - Equivalent G_x, .76 to .97
  - Vertical reaction, .88 to 1.17
  - Longitudinal reaction, .90 to 1.09
  - Belt loads, .75 to 1.33

- There is no noticeable crunching of structure in either the static or dynamic tests. To some extent the test setup precludes this phenomenon. The test is designed to restrain the seat movement after a failure occurs, and the lack of interaction of fore and aft seat rows prevents additional deformation being experienced.

7.2.2 Deformed Versus Undeformed Floors (Test 1 vs Test 2 and Test 3 vs Test 5

The FAA-CAMI data, comparing deformed floor versus undeformed floor tests, are shown in Tables 7-5 and 7-6 for static tests and 7-7 and 7-8 for dynamic tests. In 3 of the 14 tests the seats failed during application of floor static deformation prior to testing. Five seats (Nos. 4, 6, 7, 9, and 10) were tested statically. In general, the seats with a deformed floor failed at comparable longitudinal reactions and equivalent G_x values, except for seat configuration No. 7. The failure locations are similar with perhaps some track failures noted on the deformed floor condition not experienced with an undeformed floor. Six of the seats were tested dynamically. Three of the seats with deformed floors (Nos. 1, 4 and 7) failed at substantially lower loads (reaction, belt and/or equivalent G_x) than the seats tested with an undeformed floor. The other three seats (Nos. 8, 9, and 10) exhibited equal, or greater, loads at failure with the deformed floor versus the undeformed floor. The failure location and types appeared to be similar regardless of the floor deformation state.

While the tests may indicate that deformation of floors can influence results for some seat configurations, there is a need to determine realistically what degree of floor deformation the crash environment will induce.

TABLE 7-5. - SUMMARY OF LOADS, TEST CONDITIONS 1 AND 2, STATIC UNDEFORMED VERSUS DEFORMED FLOOR

SEAT CONFIG.	$-G_x$ ACCELERATION, G's		SEAT BELT LOADS (LB) × 10^2		(a)(b) LEG REACTION NET LOADS × 10^2				(a)(b) FWD. LEG REACTION LOADS × 10^2				(a)(b) REAR LEGS REACTION LOADS × 10^2			
	TEST 1 (d)	TEST 2 (d)	TEST 1	TEST 2	TEST 1		TEST 2		TEST 1		TEST 2		TEST 1		TEST 2	
					F_x	F_z	F_x	F_z	F_x	F_z	F_x	F_z	F_x	F_z	F_x	F_z
1							NO DEFORMED									
2/3							FLOOR TESTS									
4(c)	- (17.2)	- (18.8)	85	93	-79	-17	-86	-36	-9	+58	-8	46	-70	-75	-78	-82
5				SEAT FAILED DURING FLOOR DEFORMATION												
6(c)	(13.5)	(15.6)	67	78	-67	-12	-82	-25	-12	65	-11	67	-55	-77	-71	-92
7	(19.4)	(10.3)	64	34	-63	-14	-35	-8	-11	74	-4	44	-52	-88	-31	-52
8							NO TEST									
9(c)	- (12.7)	- (13.3)	63	66	-66	-2	-65	-10	-16	91	-21	89	-50	-93	-44	-99
10	(10.9)	(10.9)	36	36	-37	-4	-33	4	-10	50	-7	52	-27	-54	-26	-48

(a) - F_x - FWD. REACTION LOAD

(b) + F_z - UP REACTION LOAD

(c) THREE OCCUPANT SEATS, ALL OTHERS TWO OCCUPANT SEATS

(d) EQUIVALENT - G_x

TABLE 7-6. - COMPARISON OF TEST RESULTS, TEST CONDITIONS 1 AND 2, STATIC UNDEFORMED VERSUS DEFORMED FLOOR

PARAMETER			SEAT CONFIGURATION									
			1	2/3	4	5	6	7	8	9	10	AVG
EQUIVALENT G_x ACCELERATION LEVEL	EQUIVALENT ACCELERATION LEVEL, G	<10										
		10 - 12						2			1,2	
		12 - 14					1			1,2		
		14 - 16					2					
		16 - 18			1							
		18 - 20			2			1				
		>20										
FAILURES	SEAT PAN				1							
	LAP BELT				1							
	REAR LEG ATTACHMENT						1	1,2		1	1,2	
	FRONT LEG ATTACHMENT						1,2				2	
	TRACK				2					2		
RATIO OF: TEST CONDITION 2 / TEST CONDITION 1	EQUIVALENT G_x				1.09		1.2	.55		1.	.89	.95
	VERTICAL REACTION, F_z (REAR)				1.09		1.19	.59		1.05	.89	.96
	VERTICAL REACTION, F_z (FORWARD)				.79		1.03	.59		.98	1.04	.88
	LONGITUDINAL REACTION F_x (SUM OF FWD. & REAR)				1.09		1.22	.56		1.	.89	.95
	BELT LOADS				1.05		1.16	.53		1.05	1.	.96
	AVERAGE OF RATIOS				1.02		1.16	.56		1.02	.95	

TABLE 7-7. - SUMMARY OF LOADS, TEST CONDITIONS 3 AND 5, DYNAMIC $-G_x$, UNDEFORMED VERSUS DEFORMED FLOOR

SEAT CONFIG.	$-G_x$ ACCELERATION, G's		SEAT BELT LOADS (LB) × 10^2		(a)(b) LEG REACTION NET LOADS × 10^2				(a)(b) FWD. LEG REACTION LOADS × 10^2				(a)(b) REAR LEGS REACTION LOADS × 10^2			
	TEST 3 (d)	TEST 5 (d)	TEST 3	TEST 5	TEST 3		TEST 5		TEST 3		TEST 5		TEST 3		TEST 5	
					F_x	F_z	F_x	F_z	F_x	F_z	F_x	F_z	F_x	F_z	F_x	F_z
1	8 (16.9)	6 (10.9)	76	48	-60	-11	-39	-21	-12	48	-6	-25	-48	-59	-33	-46
2/3							NO TEST									
4(c)	9 (13.0)	6 (10.2)	64	34	-71	-16	-55	-24	-11	62	-13	34	-60	-78	-42	-59
5					FAILED DURING											
6(c)					SEAT DEFORMATION											
7	12 (22.7)	7 (15.3)	87	42	-81	-14	-56	-22	-13	73	-9	53	-68	-87	-47	-75
8	6 (12.1)	6 (11.5)	44	36	-43	-19	-41	- 9	- 6	33	-10	50	-37	-47	-31	-59
9(c)	9 (13.6)	9 (13.2)	62	76	-74	-13	-72	-37	-12	58	-21	46	-62	-71	-51	-83
10	9 (17.4)	12 (18.5)	52	67	-62	-14	-67	-20	-12	53	-13	45	-50	-67	-54	-65

(a) $-F_x$ = FWD. REACTION LOAD

(b) $+F_z$ = UP REACTION LOAD

(c) THREE OCCUPANT SEATS, ALL OTHERS TWO OCCUPANT SEATS

(d) EQUIVALENT - G_x

TABLE 7-8. - COMPARISON OF TEST RESULTS, TEST CONDITIONS 3 AND 5, DYNAMIC $-G_x$, UNDEFORMED VERSUS DEFORMED FLOOR

PARAMETER			SEAT CONFIGURATION									
			1	2/3	4	5	6	7	8	9	10	AVG
EQUIVALENT G_x ACCELERATION LEVEL	EQUIVALENT ACCELERATION LEVEL, G	<10										
		10 - 12	5		5				5			
		12 - 14			3				3	3,5		
		14 - 16						5				
		16 - 18	3								3	
		18 - 20									5	
		>20						3				
FAILURES	SEAT PAN											
	LAP BELT							3				
	REAR LEG ATTACHMENT				3,5			3,5	3,5	3,5	3,5	
	FRONT LEG ATTACHMENT		3,5									
	TRACK											
RATIO OF: TEST CONDITION 5 / TEST CONDITION 3	EQUIVALENT G_x		.65		.78			.67	.95	.97	1.06	.85
	VERTICAL REACTION, F_z (REAR)		.78		.76			.86	1.25	1.17	.97	.91
	VERTICAL REACTION, F_z (FORWARD)		.52		.56			.73	1.78	.79	.85	.69
	LONGITUDINAL REACTION F_x (SUM OF FWD. & REAR)		.65		.77			.69	.95	.97	1.08	.69
	BELT LOADS		.63		.53			.48	.82	1.2	1.29	.83
	AVERAGE OF RATIOS		.65		.74			.68	1.0	1.03	1.05	

7.2.3 Unidirectional Versus Multidirectional Loading (Test 3 vs Test 8 and Test 10)

The comparison of data from the FAA-CAMI tests with regard to directional loading effects is shown in Tables 7-9 and 7-10 for forward versus 30-degree yaw (combined forward and side) and Tables 7-11 and 7-12 for forward versus combined forward, up and side loading. Eight seat configurations (all except No. 1) were tested for comparison between forward-only versus forward with 30-degree yaw. For all the seat configurations the loads at which failure occurs are less for the yaw condition than forward-only condition, in addition, the failure mode for the yaw condition is associated with the attachment to the track as opposed to a fitting failure. The significant decrease in load capability with a 30-degree yaw loading indicates an area of concern. The crash scenario analyses should be related to the requirements for testing with combined yaw and longitudinal forces.

For the comparison between the forward only versus the combined forward, up and side load the results are more mixed. The equivalent G_x value and reaction loads vary substantially for each seat configuration. Some show increases in reaction loads while others show a decrease for the combined loading.

Of interest is that three seat configurations (Nos. 6, 9, and 10), in both tests 8 and 10, failed at the track, while seat configurations 4, 5 and 7 exhibited tension failures at the frame or base attachment for side or combined loading, just as in the forward direction only loading condition.

7.2.4 Undeformed Versus Deformed Floor for Yaw Condition (Test 8 vs Test 9)

The comparison of data from the FAA-CAMI tests, with regard to the effect of floor deformation for a yawed condition is shown in Tables 7-13 and 7-14. Four seat configurations were tested. The data from seat configuration No. 8 are omitted since in both tests it was tested at two acceleration levels with fix-up between tests which introduces some confusion with regard to the results. The results for the other three configurations (Nos. 4, 9 and 10) that were tested, indicate that track failures occur due to the yaw. Deformation of the floor does not appear to provide any further degradation. Thus it appears that the yawing loads are more critical than floor deformation.

TABLE 7-9. - SUMMARY OF LOADS, TEST CONDITIONS 3 AND 8, DYNAMIC, $-G_x$ VERSUS 30° YAW

SEAT CONFIG.	$-G_x$ ACCELERATION, G's		SEAT BELT LOADS (LB) × 10^2		(a)(b) LEG REACTION NET LOADS × 10^2				(a)(b) FWD. LEG REACTION LOADS × 10^2				(a)(b) REAR LEGS REACTION LOADS × 10^2			
	TEST 3 (d)	TEST 8 (d)	TEST 3	TEST 8	TEST 3		TEST 8		TEST 3		TEST 8		TEST 3		TEST 8	
					F_x	F_z	F_x	F_z	F_x	F_z	F_x	F_z	F_x	F_z	F_x	F_z
1								NO	TEST							
2/3	12 (20.3)	7.8 (14.3)	92	40	-73	-15	-51	-12	-13	52	-12	40	-60	-67	-39	-52
4(c)	9 (13.0)	5.2 (9.9)	64	46	-71	-16	-53	-22	-11	62	-10	34	-60	-78	-43	-56
5	9 (15.9)	5.2 (9.2)	43	27	-57	-23	-33	+4	-10	35	-7	32	-47	-58	-26	-28
6(c)	12 (18.0)	6.2 (12.8)	112	68	-98	-28	-68	-25	-14	83	-10	54	-84	-111	-58	-79
7	12 (22.7)	6 (11.8)	87	27	-81	-14	-42	+3	-13	73	-12	50	-68	-87	-30	-47
8	9 (11.7)	5.2 (9.8)	44	25	-43	-3	-35	-18	-8	22	-6	33	-35	-25	-33	-47
9(c)	9 (13.6)	5.2 (9.7)	62	44	-74	-13	-52	-13	-12	58	-13	43	-62	-71	-39	-56
10	9 (17.4)	7.8 (17.0)	52	48	-62	-14	-60	-23	-12	53	-12	48	-50	-67	-48	-71

(a) $-F_x$ = FWD. REACTION LOAD

(b) $+F_z$ = UP REACTION LOAD

(c) THREE OCCUPANT SEATS, ALL OTHERS TWO OCCUPANT SEATS

(d) BASED ON ΣF_x REACTION LOADS

TABLE 7-10. - COMPARISON OF TEST RESULTS, TEST CONDITIONS 3 AND 8, DYNAMIC, $-G_x$ VERSUS 30° YAW

PARAMETER			SEAT CONFIGURATION									
			1	2/3	4	5	6	7	8	9	10	AVG
EQUIVALENT G_x ACCELERATION LEVEL	EQUIVALENT ACCELERATION LEVEL, G	< 10			8	8			8	8		
		10 - 12						8	3			
		12 - 14			3		8			3		
		14 - 16		8		3						
		16 - 18									3,8	
		18 - 20					3					
		> 20		3				3				
FAILURES	SEAT PAN											
	LAP BELT			3			3	3				
	REAR LEG ATTACHMENT			3	3,8	3,8		3,8	3,8	3	3	
	FRONT LEG ATTACHMENT											
	TRACK			8			8			8	8	
RATIO OF: TEST CONDITION 8 / TEST CONDITION 3	EQUIVALENT G_x			.70	.76	.58	.71	.52	.84	.71	.98	.72
	VERTICAL REACTION, F_z (REAR)			.78	.72	.48	.71	.54		.79	1.06	.73
	VERTICAL REACTION, F_z (FORWARD)			.77	.55	.91	.65	.68		.74	.90	.74
	LONGITUDINAL REACTION F_x (SUM OF FWD. & REAR)			.70	.75	.58	.69	.52	.81	.70	.97	.71
	BELT LOADS			.43	.72	.63	.61	.31	.56	.71	.92	.61
	AVERAGE OF RATIOS			.67	.70	.64	.72	.51		.73	.96	

TABLE 7-11. - SUMMARY OF LOADS, TEST CONDITIONS 3 AND 10, DYNAMIC, $-G_x$ VERSUS COMBINED 9:4.5:1.5

SEAT CONFIG.	$-G_x$ ACCELERATION, G's		SEAT BELT LOADS (LB) × 10^2		(a)(b) LEG REACTION NET LOADS × 10^2				(a)(b) FWD. LEG REACTION LOADS × 10^2				(a)(b) REAR LEGS REACTION LOADS × 10^2			
	TEST 3 (d)	TEST 10 (d)	TEST 3	TEST 10	TEST 3		TEST 10		TEST 3		TEST 10		TEST 3		TEST 10	
					F_x	F_z	F_x	F_z	F_x	F_z	F_x	F_z	F_x	F_z	F_x	F_z
1							NOT									
2/3							TESTED									
4(c)	9 (13.0)	9.6 (14.7)	64	36	-71	-16	-80	-5	-11	62	-12	71	-60	-78	-68	-76
5	12 (15.5)	9 (10.2)	43	27	-57	-23	-38	-2	-10	35	-5	35	-47	-58	-33	-57
6(c)	12 (18.0)	10.6 (15.8)	112	92	-98	-28	-86	-4	-14	83	-16	80	-84	-111	-70	-84
7	9 (23.2)	10.6 (15.4)	87	41	-81	-14	-56	+6	-13	73	-11	61	-68	-87	-45	-56
8	9 (11.7)	5.3 (12.8)	44	27	-43	-3	-45	-5	-8	22	-6	33	-35	-25	-39	-38
9(c)	9 (13.6)	9.6 (14.5)	62	40	-74	-13	-79	-1	-12	58	-13	70	-62	-71	-66	-71
10	9 (17.4)	10.6 (19.9)	52	46	-62	-14	-71	+1	-12	53	-19	73	-50	-67	-52	-72

(a) $-F_x$ = FWD. REACTION LOAD

(b) $+F_z$ = UP REACTION LOAD

(c) THREE OCCUPANT SEATS, ALL OTHERS TWO OCCUPANT SEATS

(d) EQUIVALENT - G_x

TABLE 7-12. - COMPARISON OF TEST RESULTS, TEST CONDITIONS 3 AND 10, DYNAMIC, $-G_x$ VERSUS COMBINED 9:4.5:1.5

PARAMETER			SEAT CONFIGURATION									
			1	2/3	4	5	6	7	8	9	10	AVG
EQUIVALENT G_x ACCELERATION LEVEL	EQUIVALENT ACCELERATION LEVEL, G	<10										
		10 - 12				10			3			
		12 - 14			3				10	3		
		14 - 16			10	3	10	10		10		
		16 - 18									3	
		18 - 20					3				10	
		>20						3				
FAILURES	SEAT PAN								10(b)			
	LAP BELT						3	3				
	REAR LEG ATTACHMENT				3,10	3,10		3,10	3	3	3,10	
	FRONT LEG ATTACHMENT											
	TRACK						10			10		
RATIO OF: TEST CONDITION 10 / TEST CONDITION 3	EQUIVALENT G_x				1.13	.66	.88	.66	1.09	1.07	1.14	0.95
	VERTICAL REACTION, F_z (REAR)				.99	.64	.76	.64		1.	1.07	.85
	VERTICAL REACTION, F_z (FORWARD)				1.15	1.	.98	.85		1.21	1.38	1.1
	LONGITUDINAL REACTION F_x (SUM OF FWD. & REAR)				1.12	.67	.88	.69	1.04	1.07	1.15	.95
	BELT LOADS				.56	.63	.82	.47	.61	.65	.88	.66
	AVERAGE OF RATIOS				.99	.75	.86	.66		1.00	1.12	

TABLE 7-13. - SUMMARY OF LOADS, TEST CONDITIONS 8 AND 9, DYNAMIC 30° YAW, UNDEFORMED VERSUS DEFORMED FLOOR

SEAT CONFIG.	$-G_x$ ACCELERATION, G's		SEAT BELT LOADS (LB) × 10^2		(a)(b) LEG REACTION NET LOADS × 10^2				(a)(b) FWD. LEG REACTION LOADS × 10^2				(a)(b) REAR LEGS REACTION LOADS × 10^2			
	TEST 8 (d)	TEST 9 (d)	TEST 8	TEST 9	TEST 8		TEST 9		TEST 8		TEST 9		TEST 8		TEST 9	
					F_x	F_z	F_x	F_z	F_x	F_z	F_x	F_z	F_x	F_z	F_x	F_z
1							NOT		TESTED							
2/3							NOT		TESTED							
4(c)	5.2 (9.9)	6.1 (10.8)	46	29	-53	-22	-54	-16	-10	-34	-12	41	-43	-56	-42	-57
5				FAILED DURING STATIC FLOOR DEFORMATION												
6(c)							NOT		TESTED							
7				FAILED DURING STATIC DEFORMATION												
8	8.7 (12.9)	7.8 (9.4)	28	44	-47	-8	-35	-17	-6	+33	9	39	-41	-58	-44	-56
9(c)	5.2 (9.7)	5.2 (8.7)	44	24	-52	-13	-47	-17	-13	43	-21	30	-39	-56	-26	-47
10	7.8 (14.6)	8.7 (18.4)	48	42	-52	-13	-65	-39	-12	48	-13	37	-48	-71	-52	-76

(a) $-F_x$ = FWD. REACTION LOAD

(b) $+F_z$ = UP REACTION LOAD

(c) THREE OCCUPANT SEATS, ALL OTHERS TWO OCCUPANT SEATS

(d) BASED ON ΣF_x REACTION LOADS

TABLE 7-14. - COMPARISON OF TEST RESULTS, TEST CONDITIONS 8 AND 9, DYNAMIC 30° YAW, UNDEFORMED VERSUS DEFORMED FLOOR

PARAMETER			SEAT CONFIGURATION									
			1	2/3	4	5	6	7	8	9	10	AVG
EQUIVALENT G_x ACCELERATION LEVEL	EQUIVALENT ACCELERATION LEVEL, G	<10			8				9	8,9		
		10 - 12			9							
		12 - 14							8			
		14 - 16									8	
		16 - 18										
		18 - 20									9	
		>20										
FAILURES	SEAT PAN											
	LAP BELT											
	REAR LEG ATTACHMENT				8				8			
	FRONT LEG ATTACHMENT											
	TRACK				9					8,9	8,9	
RATIO OF: TEST CONDITION 9 / TEST CONDITION 8	EQUIVALENT G_x				1.10				.73	.90	1.26	1.00
	VERTICAL REACTION, F_z (REAR)				1.				1.	.84	1.07	.97
	VERTICAL REACTION, F_z (FORWARD)				1.2				1.18	.7	.77	.96
	LONGITUDINAL REACTION F_x (SUM OF FWD. & REAR)				1.				.9	.9	1.25	1.03
	BELT LOADS				.69				.5	.55	.88	.66
	AVERAGE OF RATIOS				1.01				.92	.78	1.05	

However, it must be recognized that this evaluation is based on only three test comparisons.

7.3 Seat Test Versus Analysis Results

KRASH transport seat models for two passenger and three passenger occupancy are shown in Section 4. The analytical model is a general representation in that it is not tailored after any particular seat configuration tested by FAA-CAMI. The model represents a seat with stiff and straight legs, 20 inch wide by 17 inch deep frame connected by beam members. Diagonal tension members are used to represent the seat pan. The interaction between occupant and seat during a forward loading condition is represented by unidirectional compression-only members. Torso rotation is resisted by a torsional spring at the pelvic location.

To help assess seat-occupant performance in a crash environment, the KRASH two occupant seat model (Figure 4-7) was used to compare with available $-6G_x$ test data (Test No. A81063). The results for seat reaction and seat belt loads are shown in Figure 7-3. The analysis tends to show consistently lower values (19% to 49%) for the vertical loads and consistently higher values (1.5% to 15.5%) for the longitudinal loads. The analytically obtained seat belt peak load is approximately 12.5% lower than the corresponding test value. The time history of load responses is shown in Figures 7-4, 7-5 and 7-6. A comparison of analysis and test occupant responses is shown in Figure 7-7 for the pelvis and chest. Figure 7-8 shows occupant motion versus time for the analysis. Cursory film analysis has been performed which shows the analysis in agreement with the test up to .200 second of time. The data shown in Figures 7-3 through 7-7 is for the time period <.250 second. Since additional model validation is required, comprehensive film analysis and comparisons of occupant responses should be included. Also the effects of parameter changes i.e. torsional pelvic resistance, and occupant-seat interface stiffness should be fully evaluated. Thus the analytical results should be considered preliminary and used for comparative studies only.

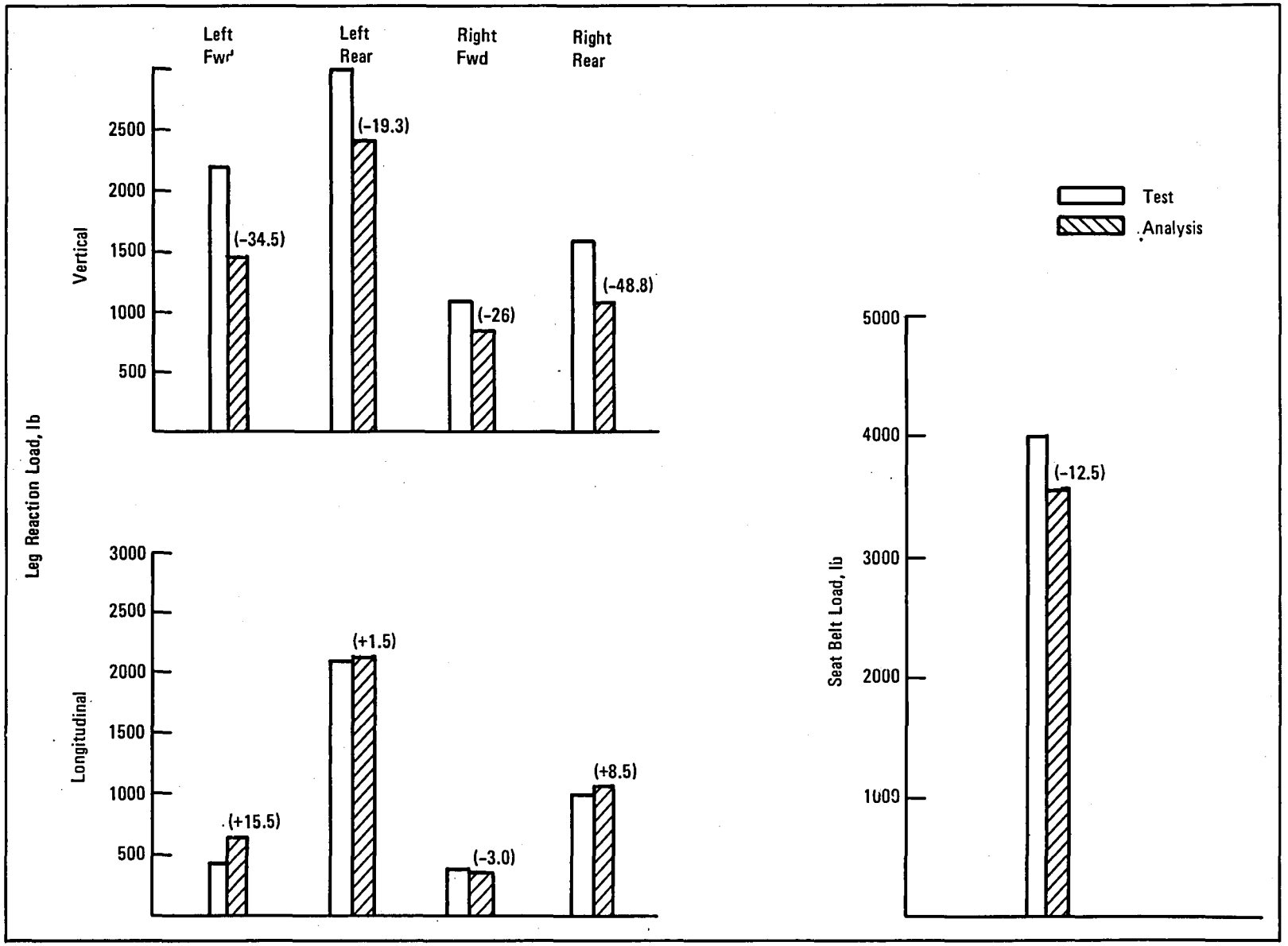

Figure 7-3. Comparison of Seat-Occupant Test and Analysis Results, $-6G_x$ Step Pulse

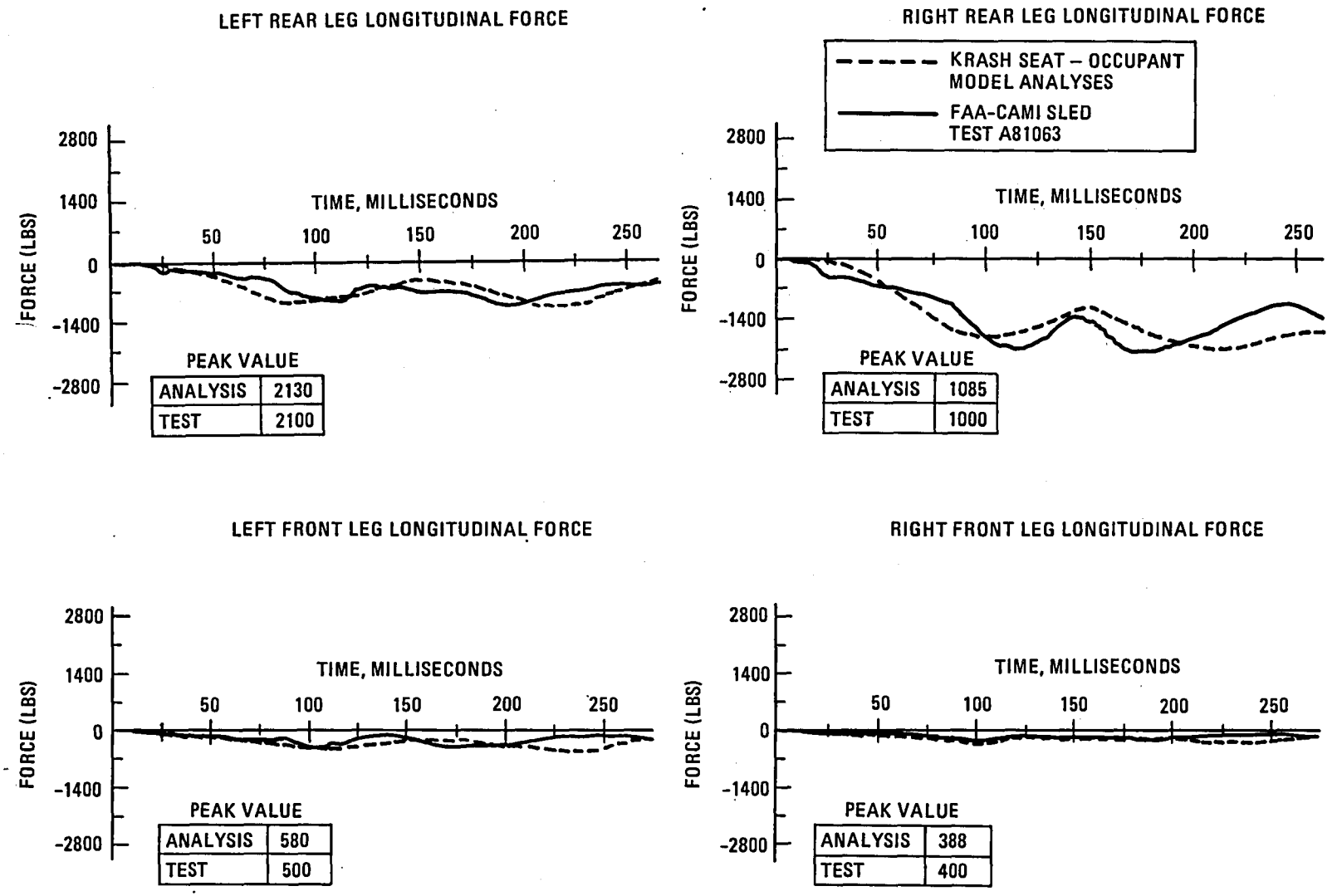

Figure 7-4. Comparison of Test and Analysis Longitudinal Reaction Forces, $-6G_x$ Ramped (.030) Step Pulse

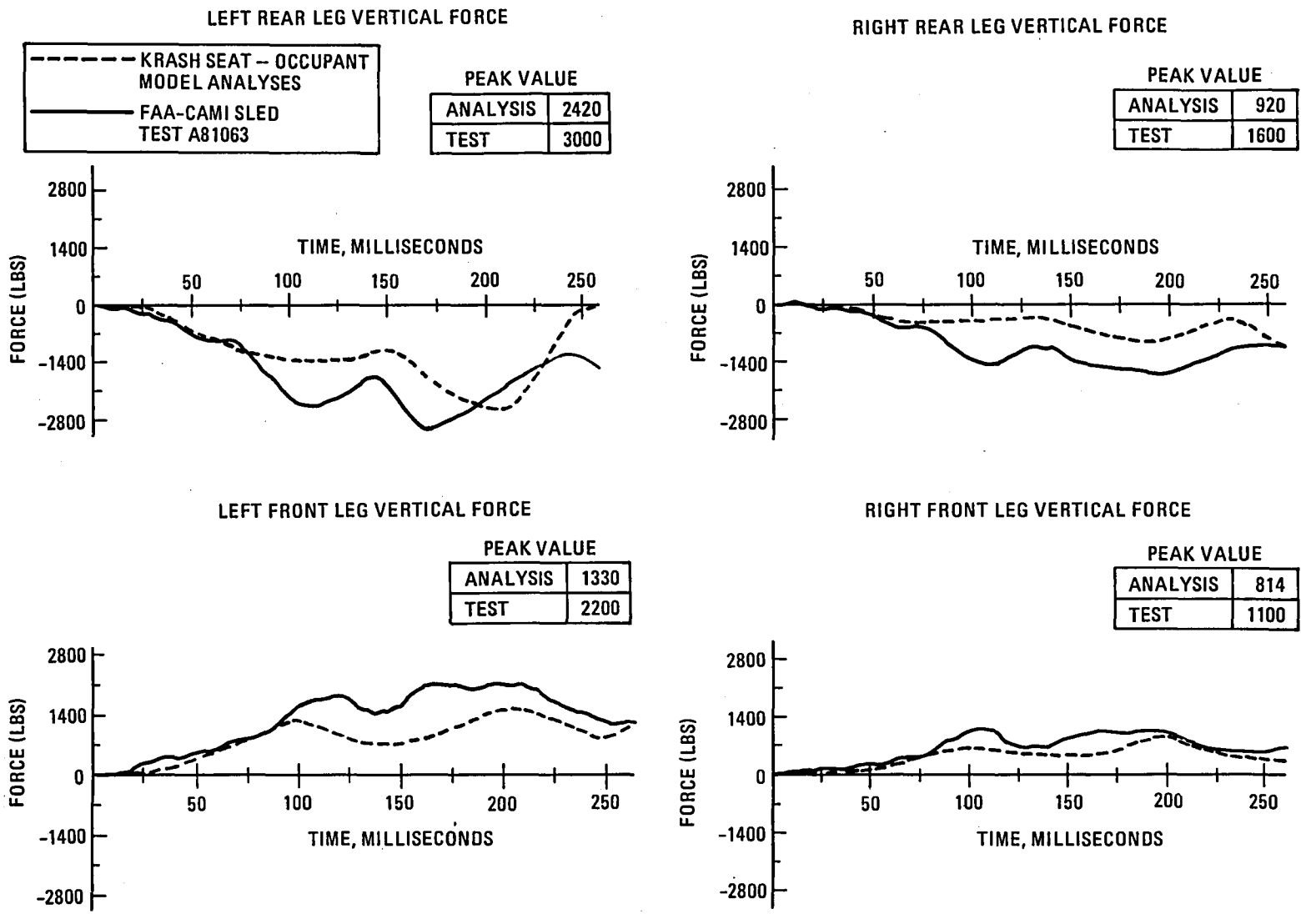

Figure 7-5. Comparison of Test and Analysis Vertical Reaction Forces, $-6G_x$ Ramped (.030) Step Pulse

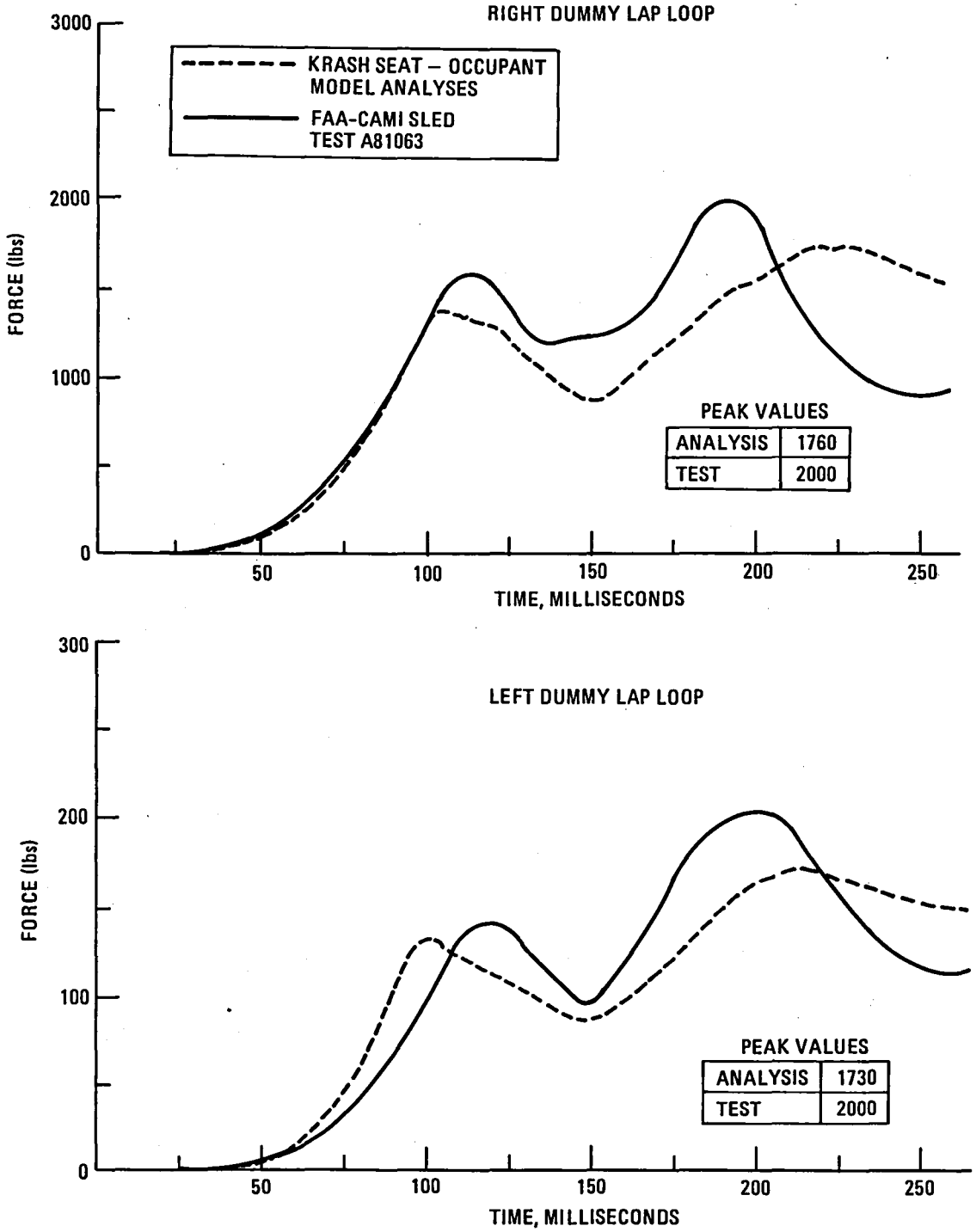

Figure 7-6. Comparison of Test and Analysis Lap Belt Loop loads $-6G_x$ Ramped (.030) Step Pulse

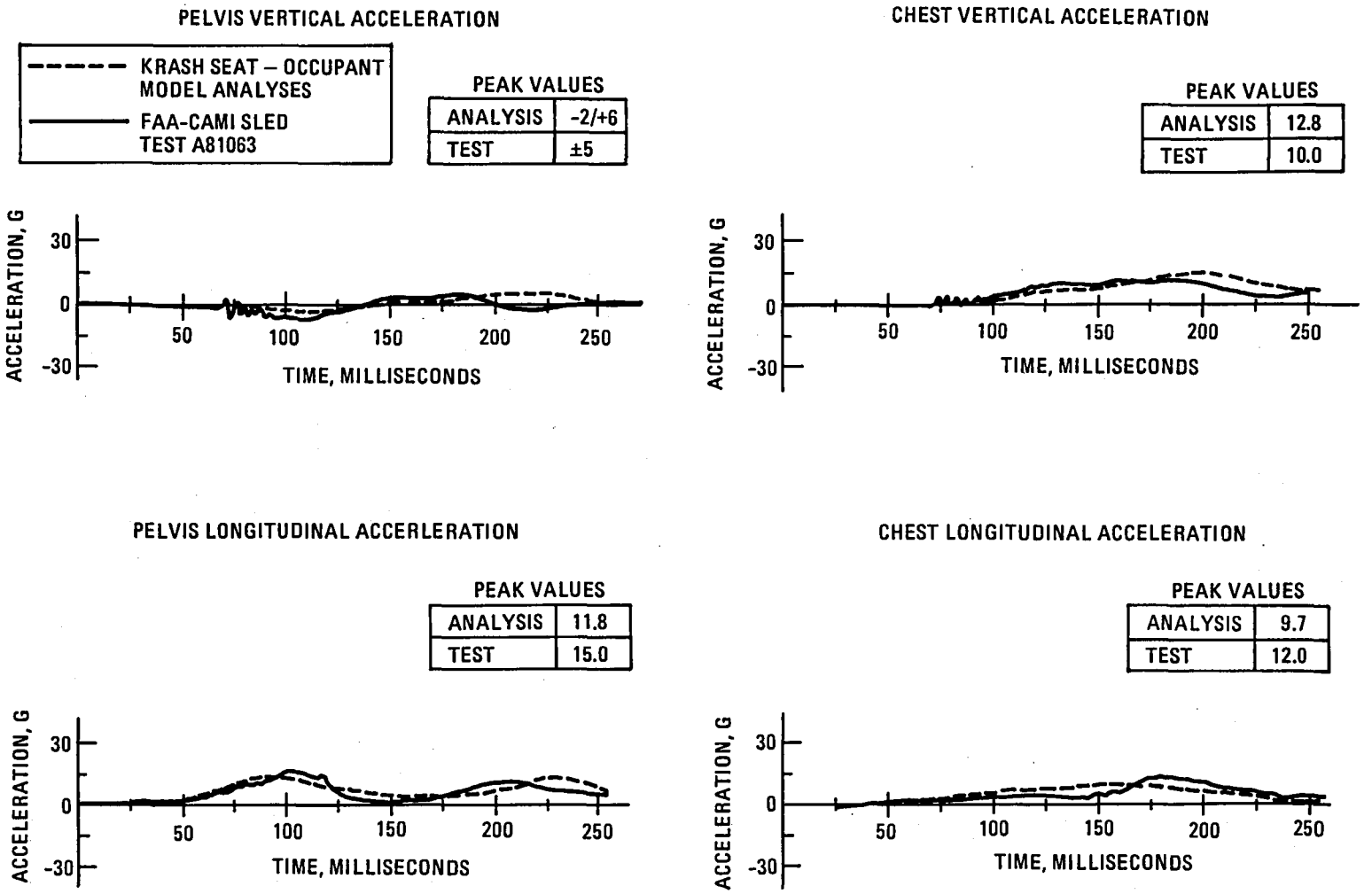

Figure 7-7. Comparison Test and Analysis Pelvis and Chest Accelerations, $-6G_x$ Ramped (.030) Step Pulse

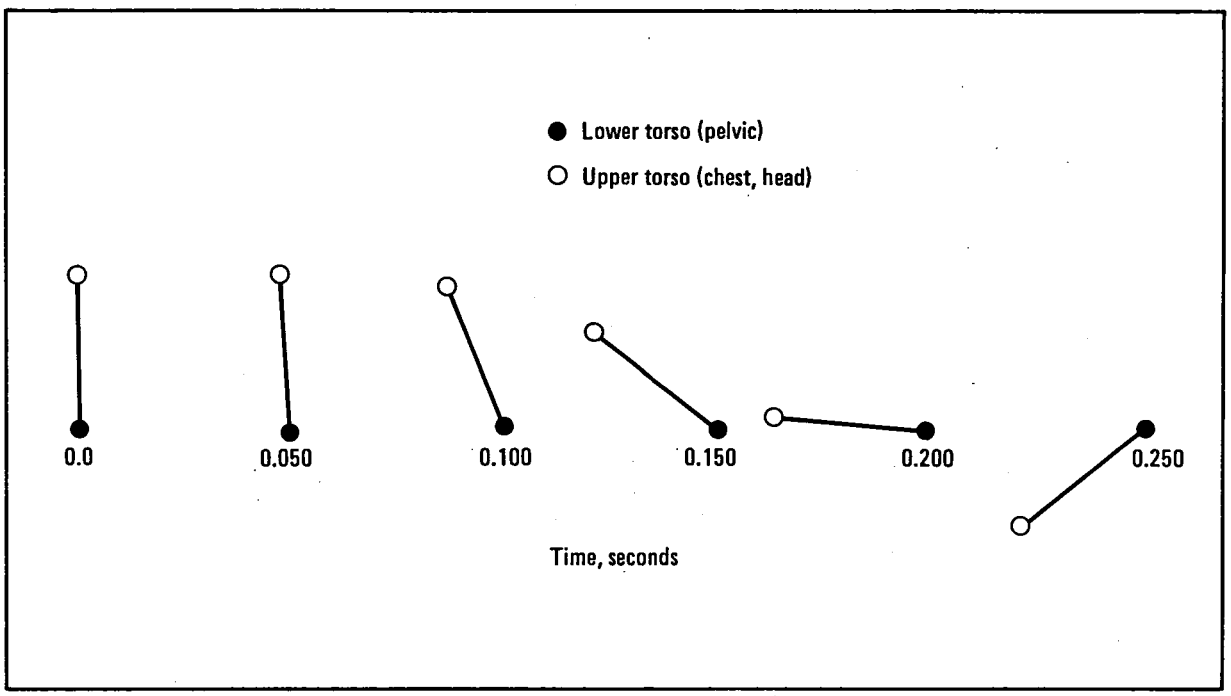

Figure 7-8. Occupant Motion History, Analysis of $-6G_x$ Step Pulse

SECTION 8

SEAT-OCCUPANT PERFORMANCE IN A CRASH ENVIRONMENT

The FAA-CMI transport seat test results are discussed in Section 7. The tests provide data with regard to failure levels as related to a series of loading conditions (see Table 7-1). The FAA-CAMI tests, however, do not address seat-occupant behavior in an anticipated crash environment. Thus, using the KRASH seat-occupant model, analyses were performed to obtain seat reaction loads for various floor pulses. The unfiltered longitudinal floor pulses used in the trend analyses (stub wing slope impact) are shown in Figure 8-1, for the "B," "C," and "E" class aircraft. Figures 8-2 and 8-3 show the wide-body ground-to-ground overrun analyses floor pulses. The pulses at floor locations near fuselage mass 3 (FS 460) and mass 6 (FS 925) are used in the analysis. Figure 8-4 is the longitudinal pulse measured at FS 925 for the L-1649 six-degree slope impact test. Also shown in Figure 8-4 is an overly conservative envelope of that pulse. From the measured longitudinal pulse for the L-1649 test shown in Figure 8-4, the ΔV is $\approx$16 fps for the unfiltered data. This ΔV is slightly higher than the analytical pulse obtained from the class "C" airplane analysis (15 fps) (Figure 8-1). The average FAA-CAMI longitudinal pulse for two-occupant seats is superimposed on all the pulses shown in Figures 8-1 through 8-4. Figure 8-5 shows the relationship between the rear leg combined F_x, F_z tension loads and seat belt loop loads and the peak G value of an equivalent .030 second ramped step pulse. The analysis showed agreement within the range of -12.5% to +15.5% with test data for these two parameters. The solid line in Figure 8-5 represents analytically obtained response loads as a function of input acceleration for a .030 second ramped step pulse and a two-occupant seat KRASH model. The associated test step values at $-6G_x$ and $-10\ G_x$ amplitude are shown on Figure 8-5. Using the KRASH seat-occupant model and analytically or L-1649 test determined floor pulses, rear leg tension and seat belt loads were then obtained. Horizontal lines (dashed) from these values on the ordinate scale

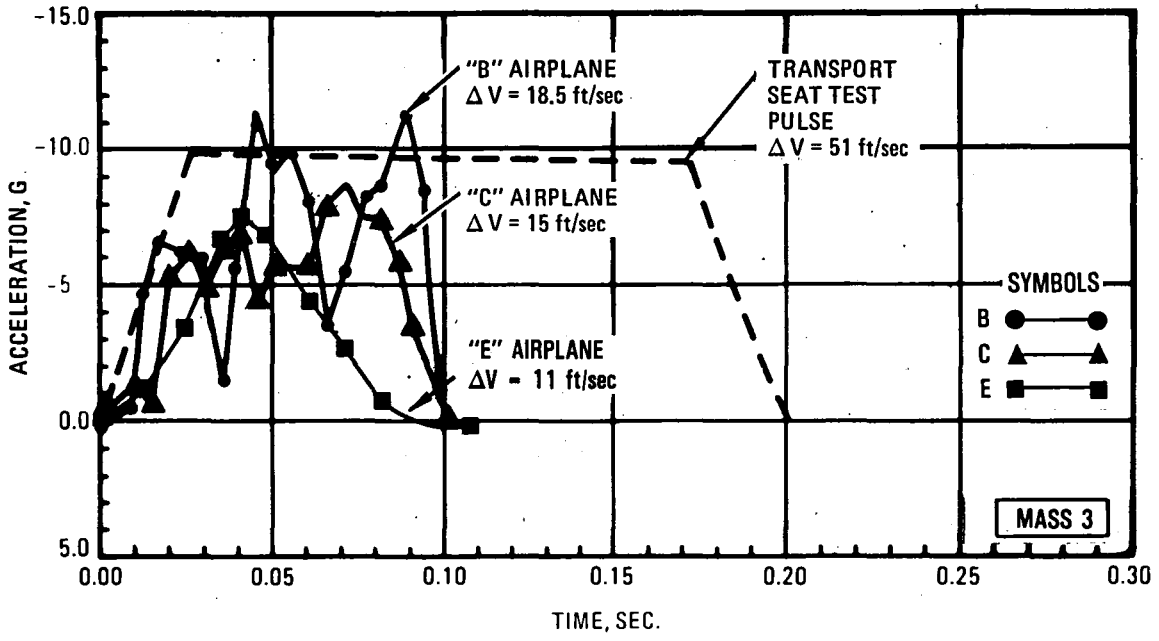

Figure 8-1. Longitudinal Pulses, Classes "B," "C" and "E" Stub Wing Configurations, 6-Degree Slope Impact

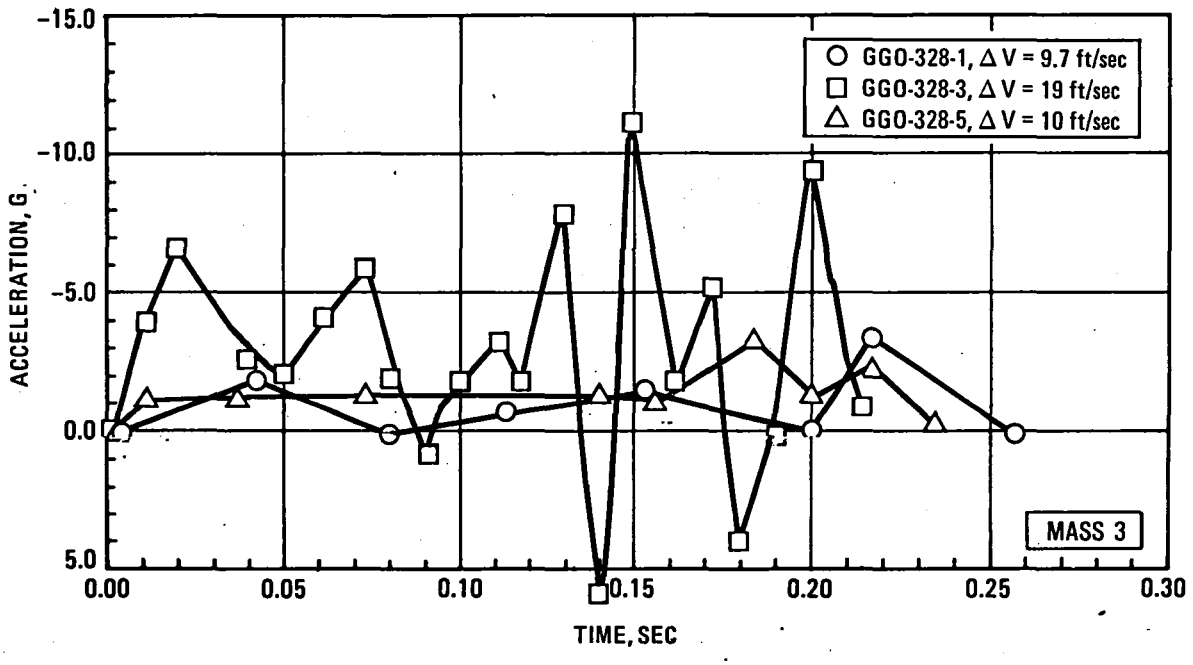

Figure 8-2. Longitudinal Pulses, Ground-to-Ground Overruns, GGO-328-1, -3, 5, Flexible Ground

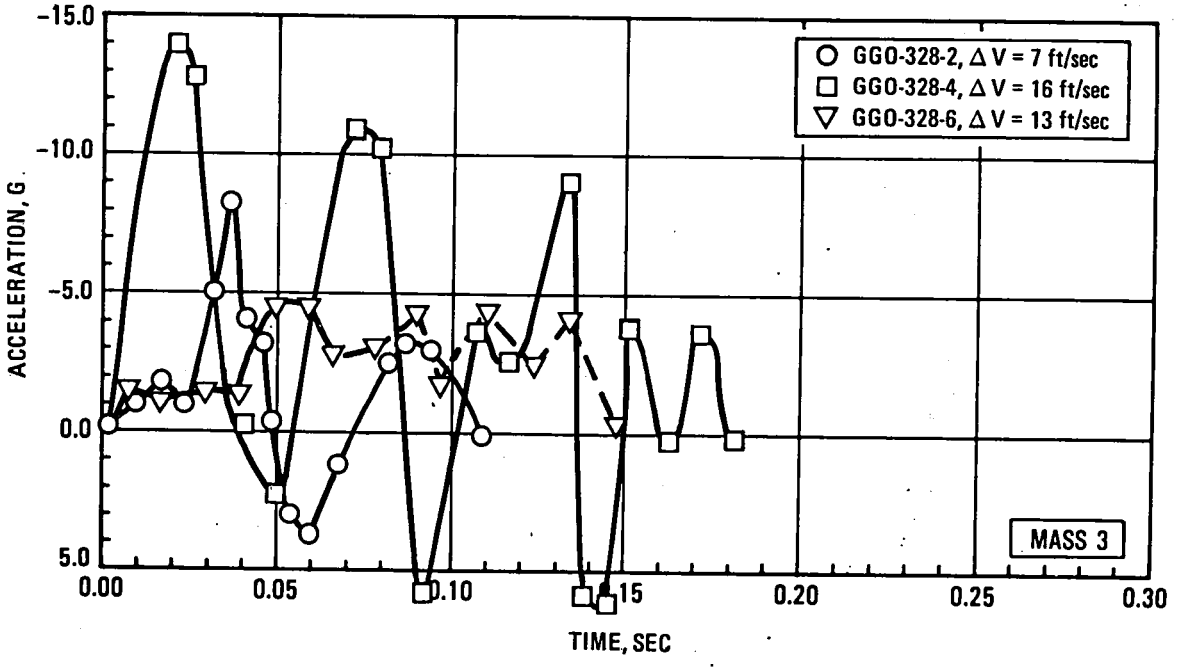

Figure 8-3. Longitudinal Pulses, Ground-to-Ground Overruns GGO-328-2, -4, -6, Rigid Ground

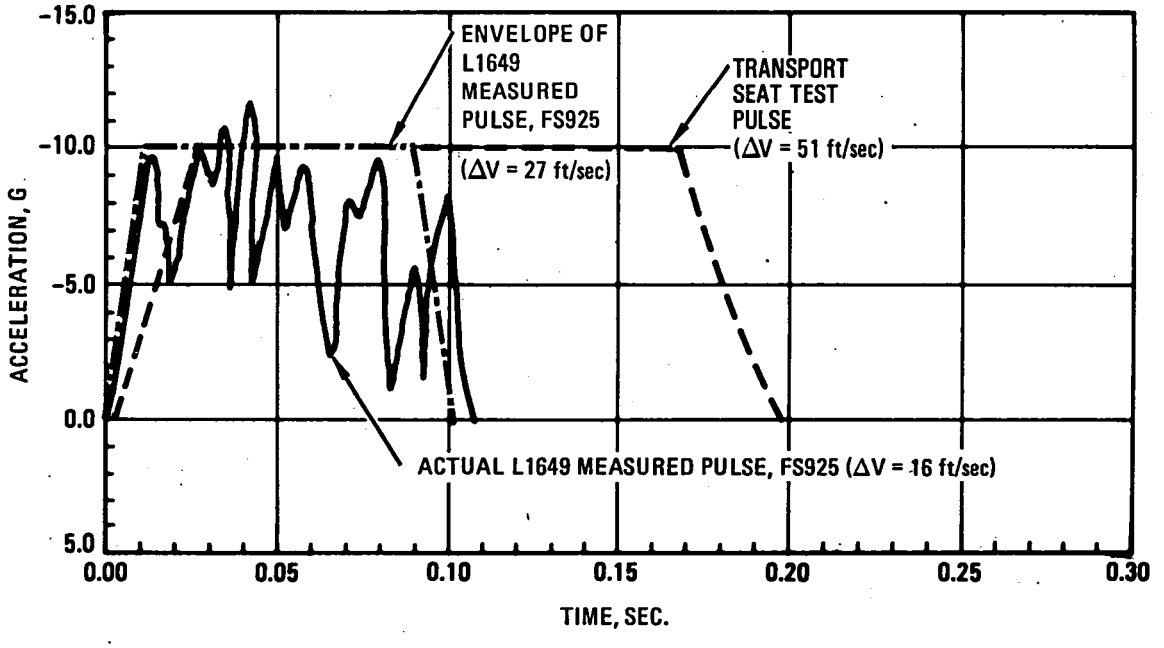

Figure 8-4. Longitudinal Pulse, L1649 6-Degree Slope Impact Test, FS 925

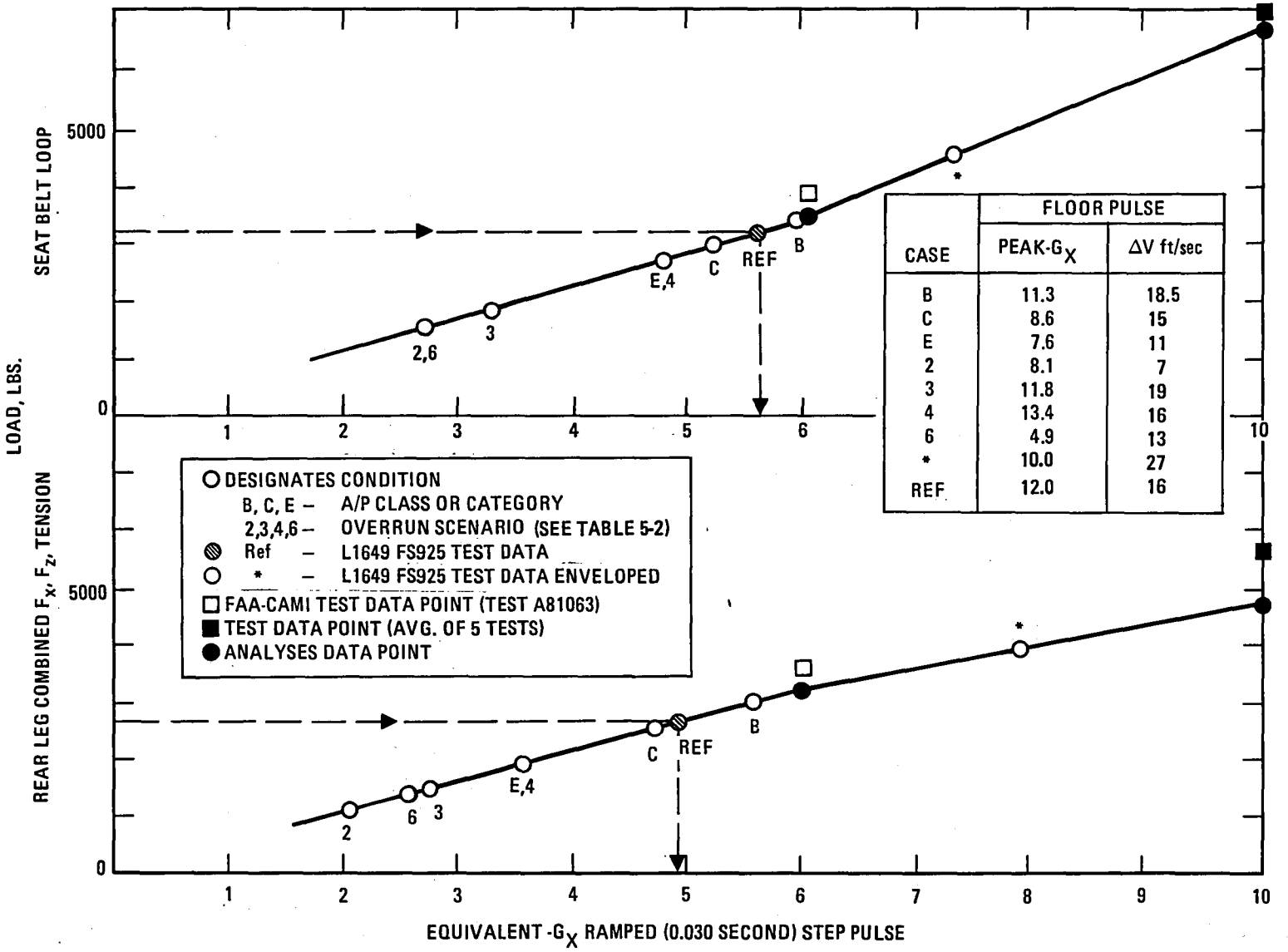

CASE	FLOOR PULSE PEAK-G_X	FLOOR PULSE ΔV ft/sec
B	11.3	18.5
C	8.6	15
E	7.6	11
2	8.1	7
3	11.8	19
4	13.4	16
6	4.9	13
*	10.0	27
REF	12.0	16

Figure 8-5. Equivalent $-G_x$ Ramped Step Input for Analytically Obtained Ground Overrun Pulses

are drawn until they intersect their respective solid lines. At this point dashed vertical lines are drawn which intersects the abscissa. The value at the abscissa is the equivalent $-G_x$ input needed from a .030 ramped step pulse to produce the respective loads obtained analytically from the time-history floor pulse study. Included in the plotted data are analyses results for several ground overrun conditions, impacts onto a six-degree slope for stub wing configurations of three different category aircraft, a reference L-1649 test measured pulse, and the reference L-1649 pulse conservatively enveloped. For each of these unfiltered floor pulses a peak $-G_x$ and ΔV are noted on Figure 8-5. The wide-body aircraft analysis floor pulses tend to be equivalent to a $\leq -4.8\ G_x$ step pulse while the narrow body analysis results as depicted by Category "B" and "C" are closer to $\leq -6G_x$. The actual L1649 measured pulse at FS 925 shows an equivalent step pulse of $\approx -5.7G_x$. The interpretation of Figure 8-4 plots is that the analytically produced floor pulse for the "C" category aircraft yields seat leg and belt loop loads equivalent to the L1649 test pulse, despite differences in peak G's. Enveloping the L-1649 pulse as shown in Figure 8-4 produces an extremely conservative result. The comparison of conditions "B" and "C" appears to be consistent with the trend results provided in Figure 6-2. Based on a dynamic amplification factor of 1.7 alluded to in Section 7 in comparing static and dynamic test results it can be deduced that the equivalent static results might be between $-8.2\ G_x$ and $-10.2\ G_x$ for configurations "C" and "B", respectively.

The analyses of the vertical and combined vertical/horizontal acceleration impacts are more difficult to evaluate since the recent tests did not include any vertical-only impacts and the combined 9:4.5:1.5 test included side loads which may have contributed significantly to the failure. To evaluate the effect of vertical impacts on seat-occupant performance, a single occupant seat KRASH model was utilized. The analysis is for comparative purposes only since two-occupant seats can be expected to respond unsymmetrically and with different magnitude reaction loads. Without a calibration with test data for vertical loading only, quantification of analyses results could be misleading. The analyses are heavily dependent on the representation

of the stiffness, as well as the occupant mass concentration. For the analytical results presented, the occupant mass was located longitudinally halfway between the seat center and rear legs. As the mass moves forward toward the center of the seat, the compressive load is more uniformly reacted by the front and rear legs. Changes in occupant-seat stiffness could affect transmissibility factors, depending on the relative duration of pulse and the occupant-seat system response.

The hard landing conditions are primarily vertical-only impacts, and thus, represent rational conditions to compare to idealized vertical-only pulses. Table 8-1 shows the 5 hard landing analyses from which results are used. The cases represent a spectrum of acceleration values and pulse shapes. Only a segment of each pulse which is considered most severe is presented. Figures 8-6 through 8-10 show the pulses used. For reference purposes an analytically developed floor pulse for the L-1649 six-degree slope impact at the airplace CG, as well as unfiltered test data at FS 685 are presented in Figure 8-11. Figure 8-12 presents the results of the more severe floor pulses obtained from the hard landing analyses in relation to equivalent .030 second - ramped step $-G_z$ (headward deceleration) pulses based on both the total maximum compressive reaction loads and Dynamic Response Index (DRI) for vertical-only loading. The same procedure as described for Figure 8-5 is

TABLE 8-1. PEAK $-G_z$ ACCELERATION AND PULSE VELOCITIES FOR HARD LANDING CASES ANALYZED

	AGHL358-									
	-1		-2		-3		-4		-5	
	(1)	(2)	(1)	(2)	(1)	(2)	(1)	(2)	(1)	(2)
$-G_z$ Peak	3.5	3.0	6.6	5.0	4.2	2.6	4.1	7.2	4.3	2.9
ΔV_1 ft/sec (3)	20.3	17.8	30.0	11.1	13.8	11.1	15.4	21.5	20.6	8.1

(1) Mass 6, FS 1424

(2) Mass 3, FS 677

(3) Velocity associated with pulse analyzed

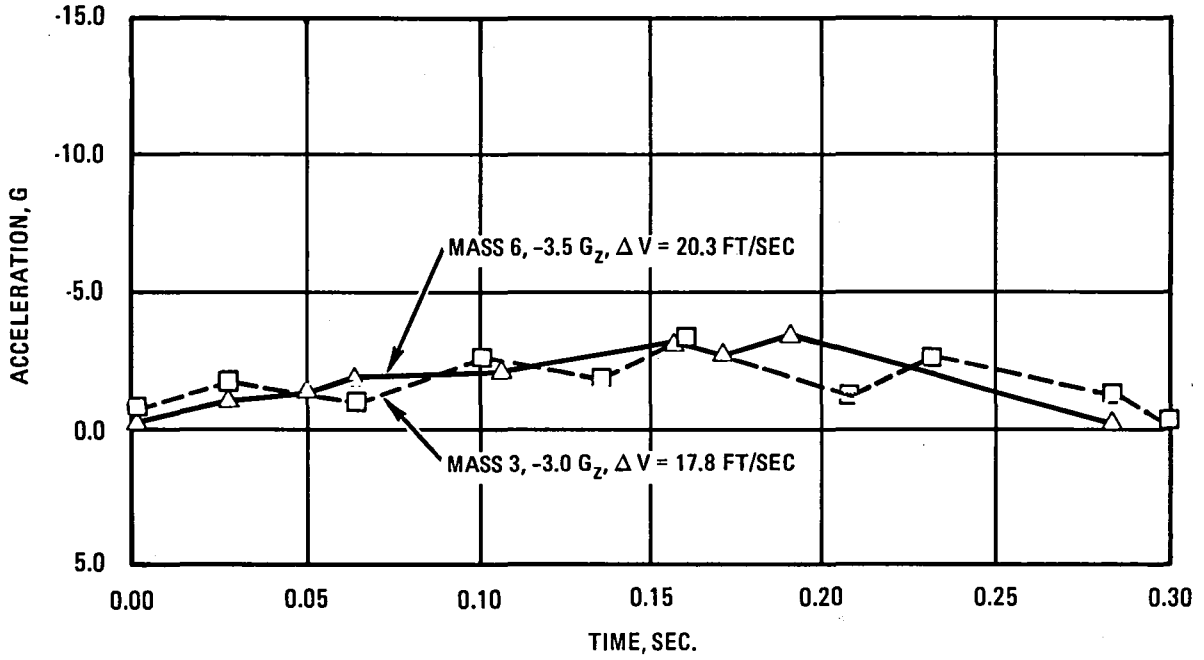

Figure 8-6. Floor Vertical Pulses, AGHL-358-1

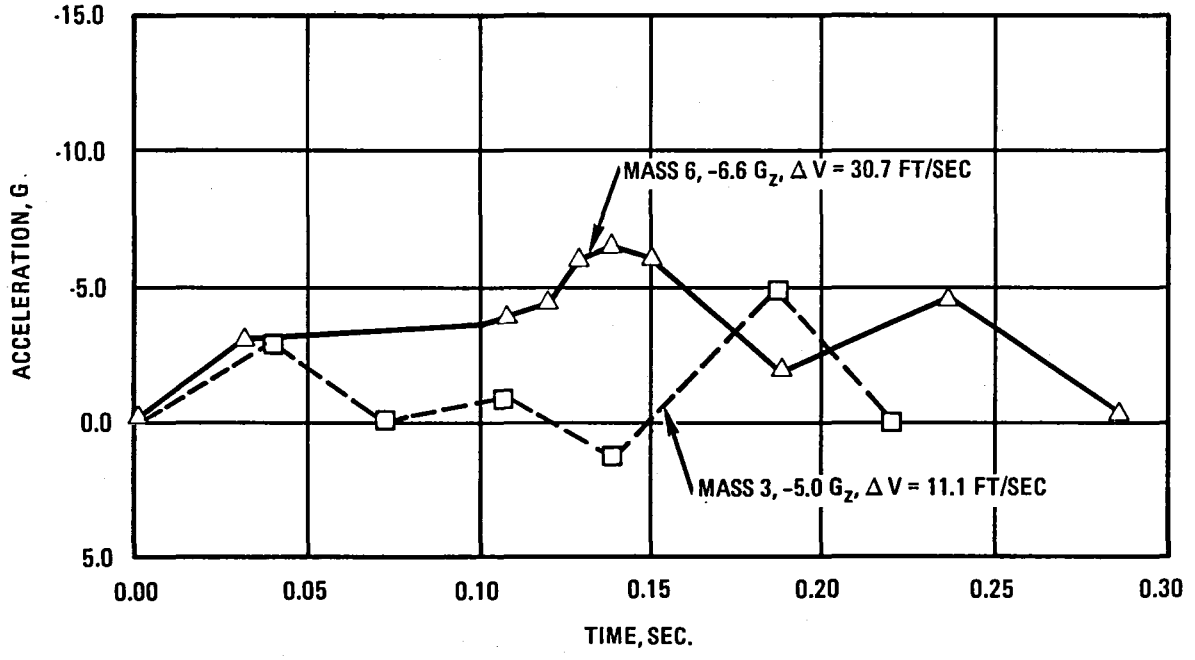

Figure 8-7. Floor Vertical Pulses, AGHL 358-2

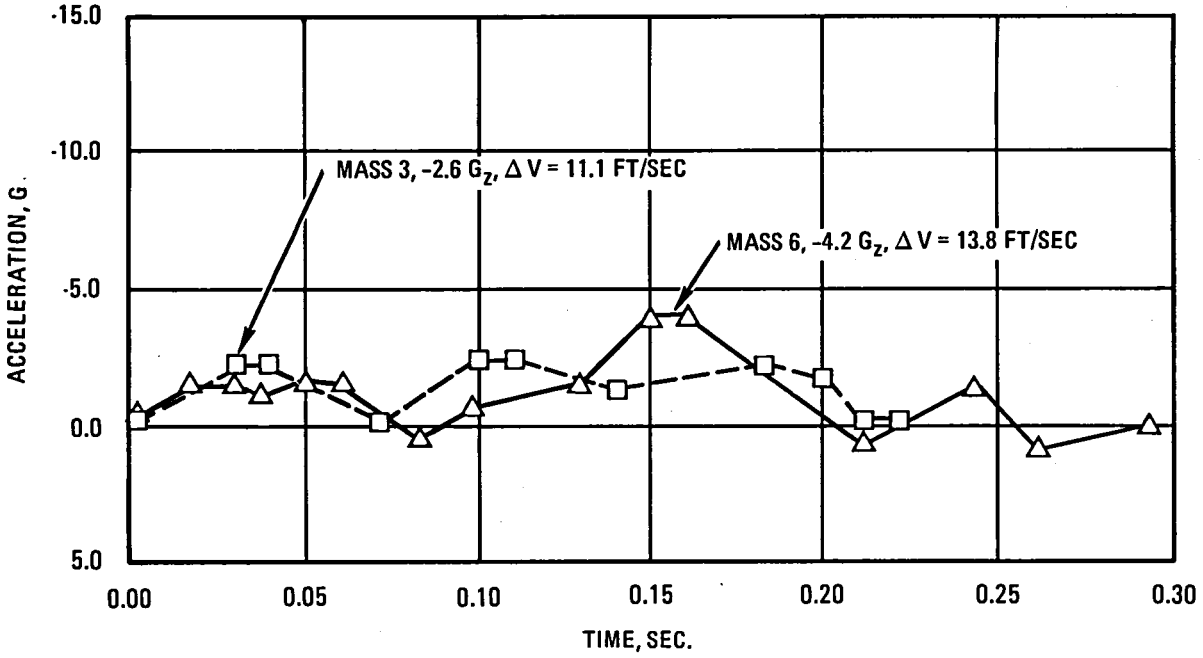

Figure 8-8. Floor Vertical Pulses, AGHL 358-3

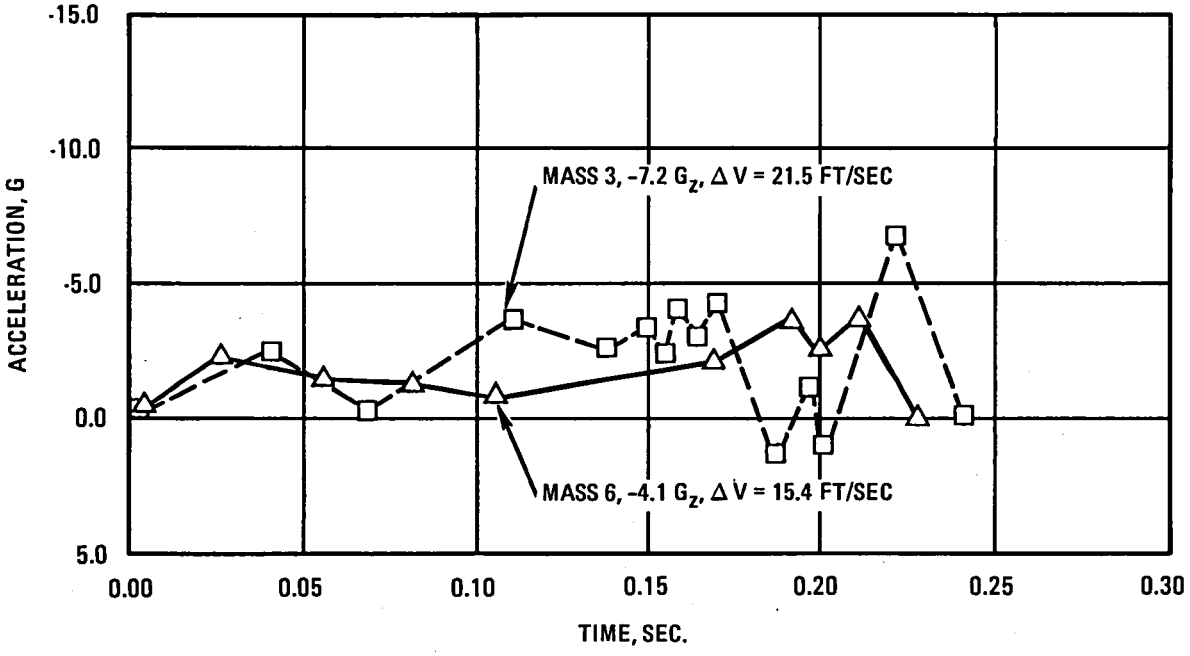

Figure 8-9. Floor Vertical Pulses, AGHL 358-4

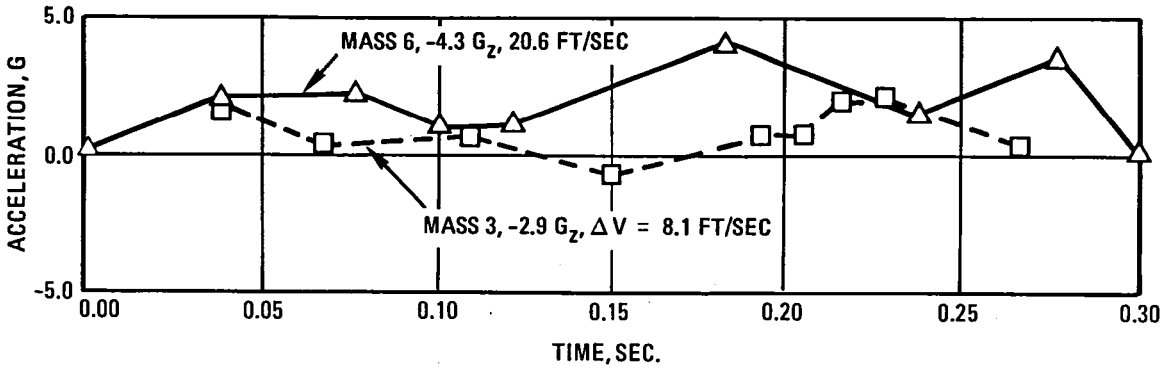

Figure 8-10. Floor Vertical Pulses, AGHL 358-5

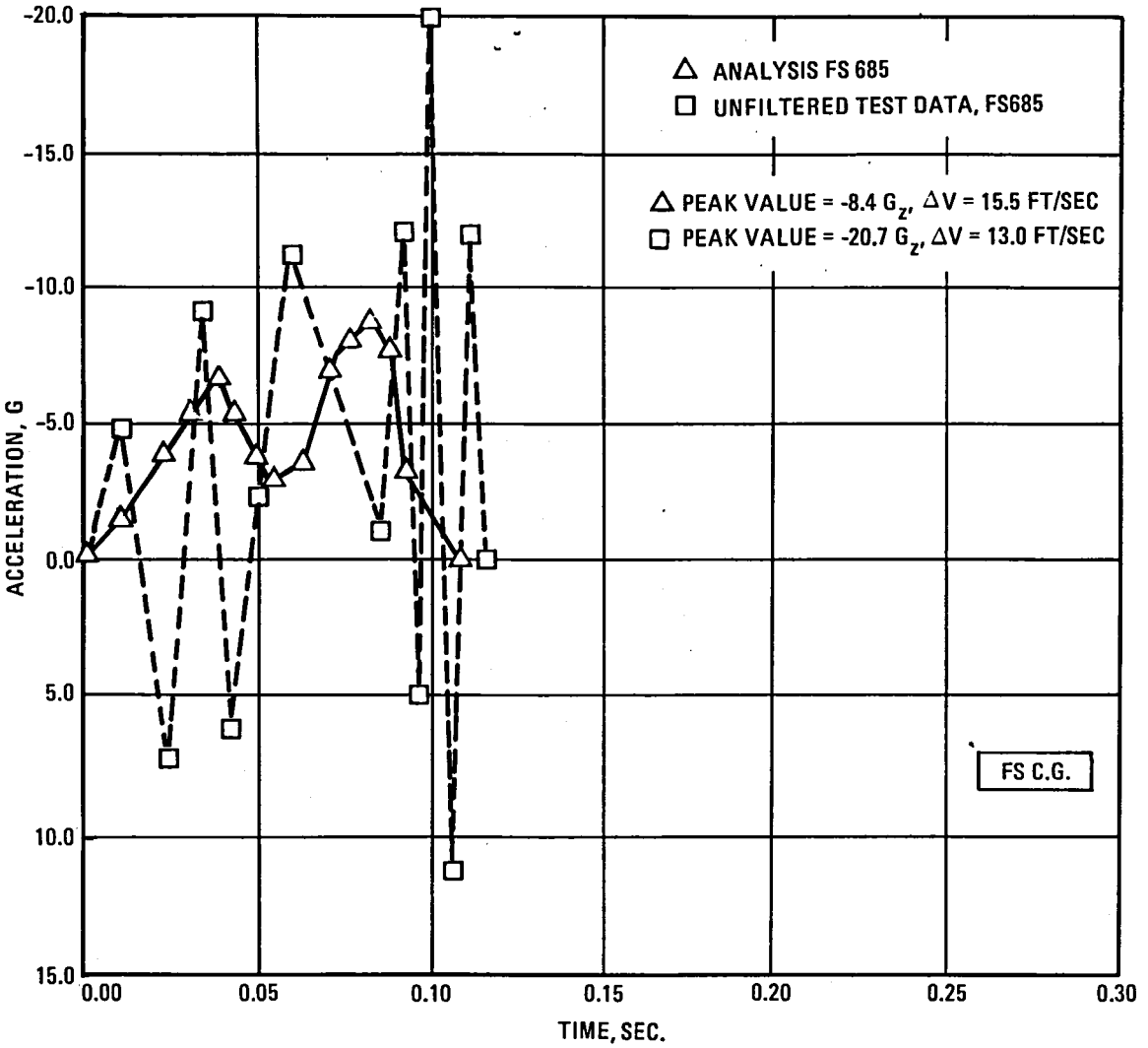

Figure 8-11. Floor Vertical Pulse, L1649 Stub Wing

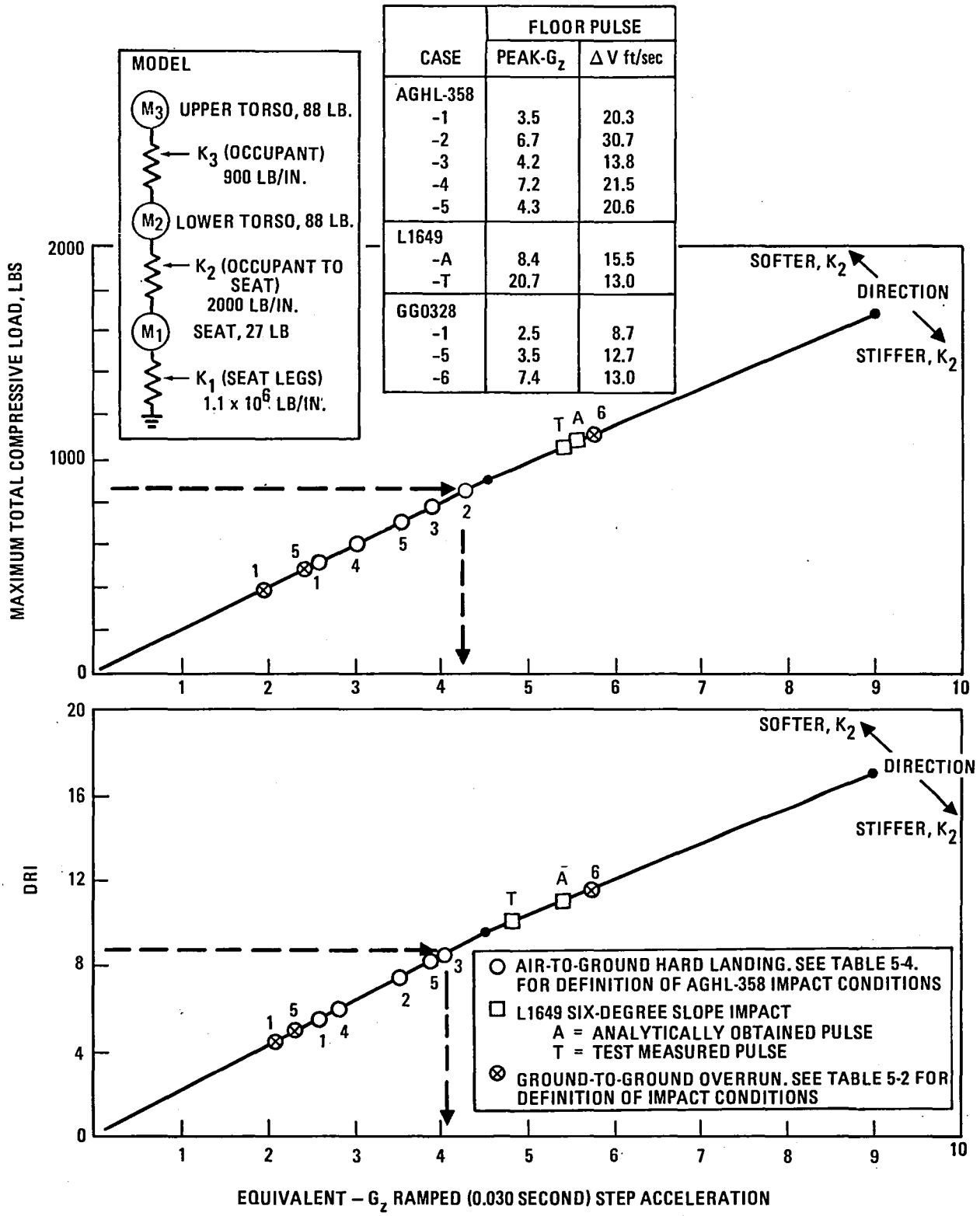

CASE	FLOOR PULSE PEAK-G_z	FLOOR PULSE ΔV ft/sec
AGHL-358		
-1	3.5	20.3
-2	6.7	30.7
-3	4.2	13.8
-4	7.2	21.5
-5	4.3	20.6
L1649		
-A	8.4	15.5
-T	20.7	13.0
GG0328		
-1	2.5	8.7
-5	3.5	12.7
-6	7.4	13.0

Figure 8-12. Equivalent $-G_z$ Ramped Step Input for Analytically Obtained Hard Landing Pulses

applicable for the interpretation of Figure 8-12 data. The results shown in Figure 8-12 indicate that an equivalent ramped step acceleration of -4.2 G_z would cover the spectrum of cases analyzed for a single occupant seat, provided the effective vertical stiffness (seat pan and frame) between the occupant and seat is 2000 lbs/in. For the measured test pulse the equivalent step pulse is -4.8 G_z, despite the peak magnitude reaching -20.7 G_z. The analytically obtained pulse (Figure 8-11), while lower in amplitude, is more broad band than the transient test pulse, and thus results in a higher DRI. Several overrun analyses results are included in Figure 8-12. These cases represent conditions for which the structural integrity of the fuselage is more likely to be preserved during the crash scenario. The vertical pulses for these overrun cases are shown in Figure 8-13. For cases GGO-328-1 and -5 the analysis results indicate an equivalent $-G_z$ of ≤ 3 exists and no fuselage loads in excess of the respective allowables. However, for the GGO-328-6 case the equivalent step is approximately -5.6 G_z and the fuselage bending moments obtained via analysis exceed their allowables at fuselage stations forward of FS 677. It is anticipated that two-occupant seats or unsymmetrically loaded three-occupant seats would respond differently than the configuration analyzed. However, until these analytical results are calibrated with test data the extension of the analyses to two and three occupant seats would be only an academic exercise. Futhermore, it must be recognized that in reality there is a longitudinal component which could alter the seat reaction load magnitude and distribution. This factor has not been taken into account in the single-occupant seat analysis for vertical only loading floor pulses.

Figures 8-14 and 8-15 illustrate sample plots of the fuselage shear loads and bending moments in the passenger region (FS 426 to FS 1663) for the overrun and hard landing analyses, respectively, normalized to the ultimate allowable loads. Since actual failure loads are not available, a region has been arbitrarily designated in which fuselage deformation could be anticipated. The data points at the high end of the deformation regime indicate a high potential for fuselage break-up. The data points within the deformation region can be interpreted as marginal performance with regard to structural integrity. The data points below the deformation region would be indicative of satisfactory fuselage performance in that the fuselage would be

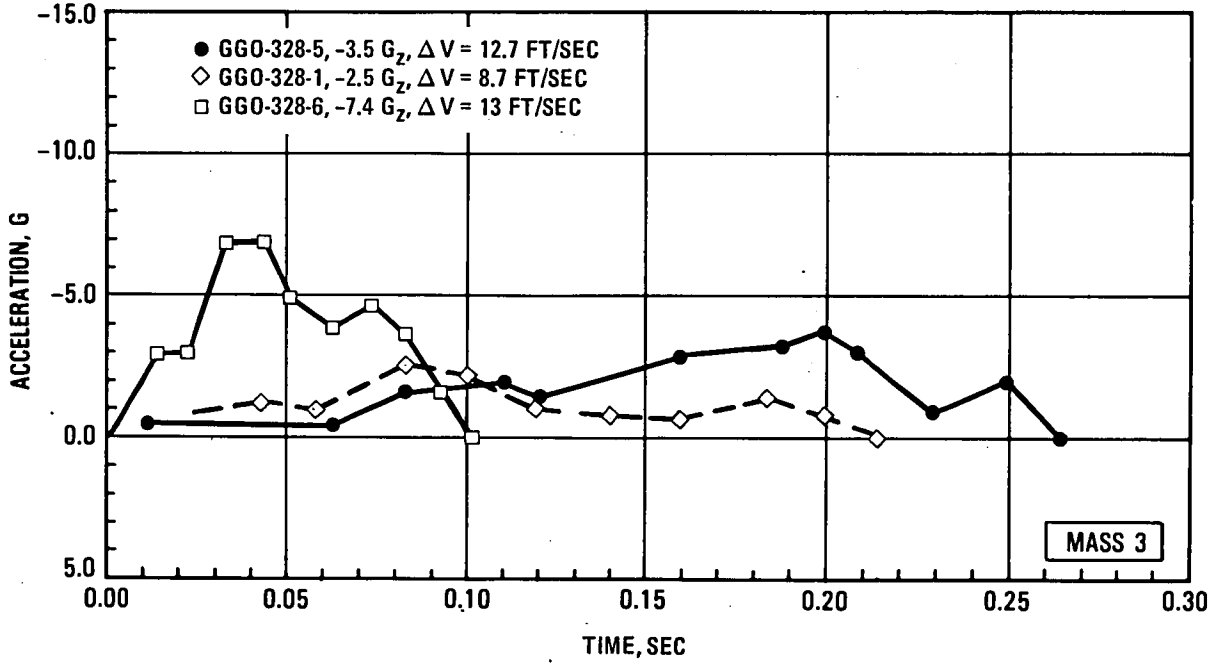

Figure 8-13. Floor Vertical Pulse, Ground-to-Ground Overruns GGO-328-1, -5 and -6

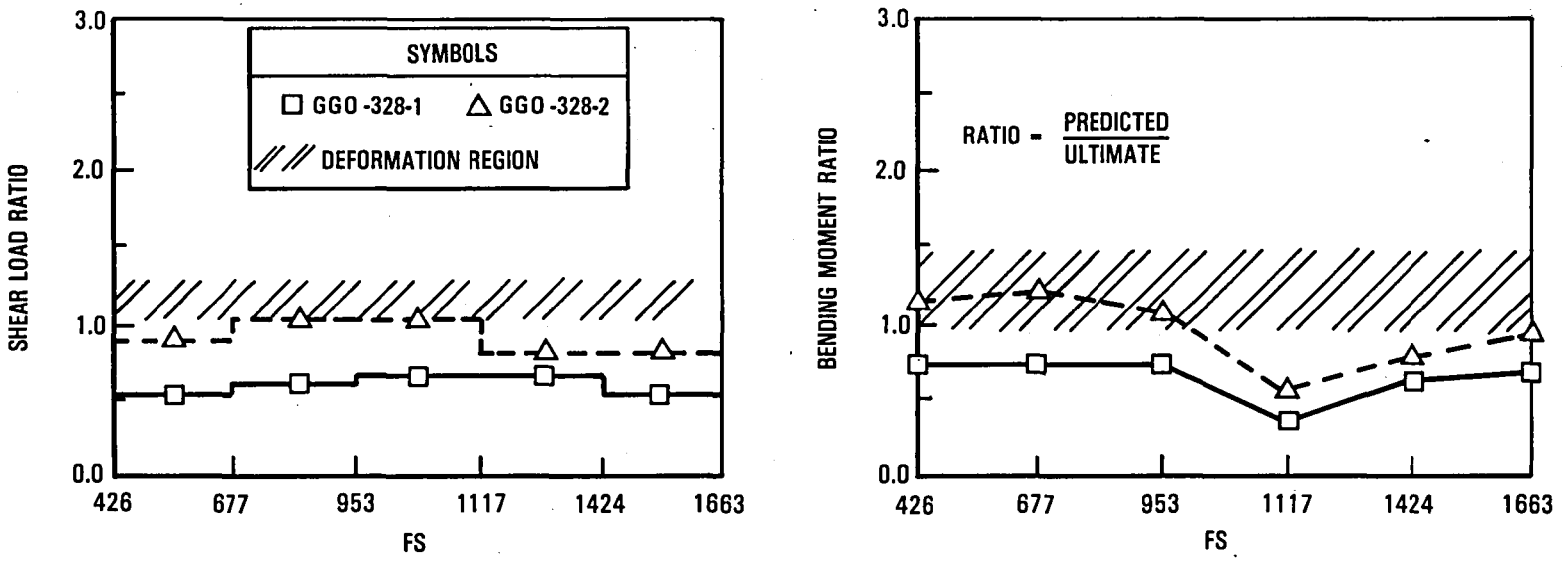

Figure 8-14. Fuselage Shear and Bending Moment Versus Allowable as a Function of Passenger Region, Ground to Ground Overruns

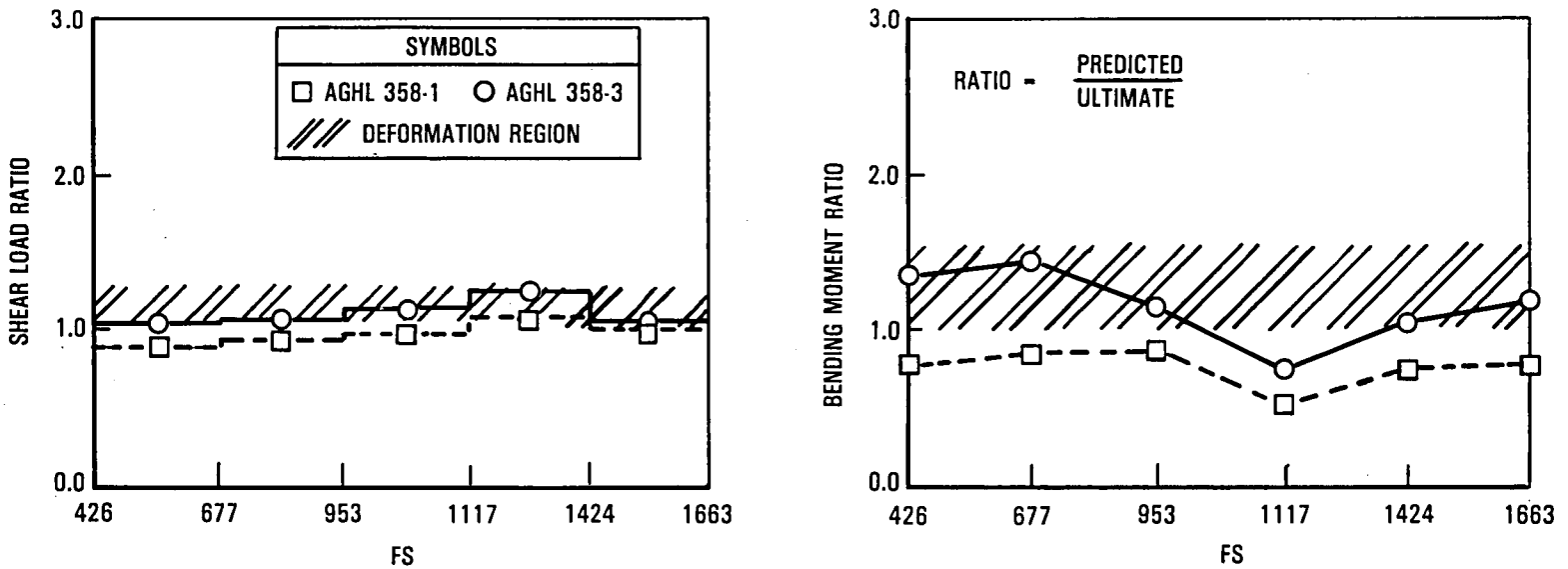

Figure 8-15. Fuselage Shear and Bending Moment Versus Allowable as a Function of Passenger Region, Air-To-Ground Hard Landings

expected to maintain its structural integrity. From the data shown in Figure 8-14, the shear and moment responses from overrun conditions GGO-328-1, which represent an impact into a slope with flexible ground and an ENV ≈6 ft/sec, are well below the deformation region. However, a similiar impact onto a rigid surface (GGO-328-2) results in shears and bending moments which potentially result in fuselage deformation. For higher effective normal velocity impacts the resultant loads increase, along with more likelihood of fuselage breakup. From the data shown in Figure 8-15, the analyses for the hard landing condition at the 15 ft/sec sink speed (AGHL-358-1), indicate that the fuselage loads may not be severe enough to result in deformation. However, at the 20 ft/sec sink speed impact (AGHL-3), the analyses results show substantially increased fuselage shear and bending such that fuselage break-up could occur. The two conditions illustrated in Figure 8-15 are for a 6° nose-up attitude impact. Similar comparative results exist for a more severe 15° nose-up attitude.

SECTION 9

SUMMARY OF RESULTS

9.1 Overall Program

The overall program is diagrammed in Figure 1-5. The various tasks which led to the conclusions and recommendations in the subsequent section are:

- Evaluation of existing floor pulse test data
- Analysis of narrow-body airplane and wide-body airplane response for six-degree slope impact
- Analysis of wide-body airplane response to candidate crash scenarios
- Trend analysis of airplane mass and size effects
- Evaluation of current transport seat test performance
- Evaluation of occupant-seat response to candidate crash scenario conditions

The objectives of the program with regard to a) an assessment of transport seat test performance and b) a definition of the crash environment produced floor pulses for a range of transport aircraft were accomplished with the use of available test and airplane data combined with the hybrid analysis techniques associated with program KRASH. Figure 9-1 shows the relationship of the available data for input and the methodology employed to meet the objectives as well as the overall results and recommendations.

9.2 Existing Floor Pulse Data

The existing floor pulse data are limited. The L-1649 slope-impact test, performed nearly two decades ago, represents the basis for available floor pulses. The longitudinal direction pulses shown in Figure 4-5 are reasonably well defined . Within the passenger floor region an approximate triangular

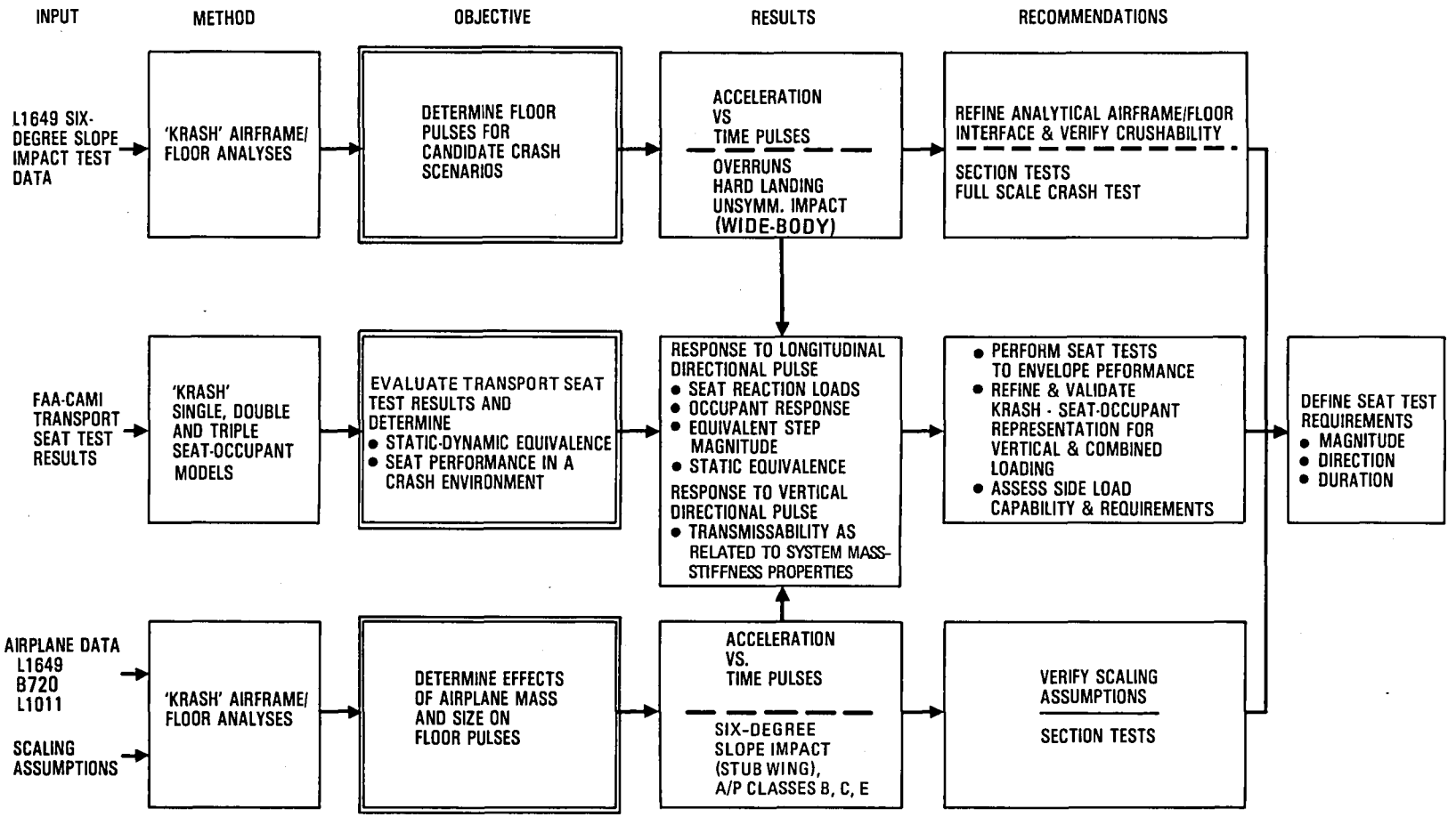

Figure 9-1. Overall Program Summary

pulse between -8 G_X and -10 G_X peak and with .07 to .100 seconds duration appears likely. In the vertical direction, the passenger region floor pulses, shown in Figure 3-6, appear oscillatory and are more difficult to define. At best they can be characterized as -5 G_Z to -13 G_Z peak, triangular with a duration of .02 to .04 seconds. Figures 9-2 and 9-3 show the floor pulse data obtained from the L-1649 tests both unfiltered and KRASH low-pass (20 Hz and 50 Hz) filtered in the longitudinal and vertical directions, respectively.

9.3 Analysis of L-1649 Six Degree Slope Impact

Both narrow-body and wide-body airplane analyses have been performed. The analyses are first performed in an attempt to compare with the available L-1649 test data. Prior to impact with first a six-degree slope and, subsequently, with a 20-degree slope, the model representation of the test article is deliberately damaged to, a) remove landing gears and, b) simulate wing tank rupture due to columnar type penetration. The analyses show that an exact match of acceleration peak levels, acceleration distribution and failure modes simultaneously, is difficult. However, within a range of assumed configuration and ground representations, the acceleration levels, particularly in the passenger region, are reasonably close to the test data (Figure 4-9 and 4-10). For comparable impact conditions the analyses show wide-body aircraft to have potentially lower longitudinal and vertical responses (Figures 4-16 and 4-17) than those of a narrow-body aircraft.

The determination of floor pulses, particularly for the slope overrun condition is sensitive to the assumed values of ground flexibility, ground coefficient of friction and fuselage underside crushing. These parameters were altered for the L-1649 model and the six-degree slope impact condition. The results are plotted in Figure 9-4. One can observe from Figure 9-4 that the higher longitudinal accelerations occur for the rigid ground μ=.7 condition and the lower accelerations for the rigid ground μ=.5 condition. The higher vertical accelerations are associated with the rigid ground conditions and the lower accelerations with the flexible ground and greater crush representations. Taking all representations into account the variation in longitudinal accelerations at a mid fuselage station (FS 700) is ≈9 ±2g.

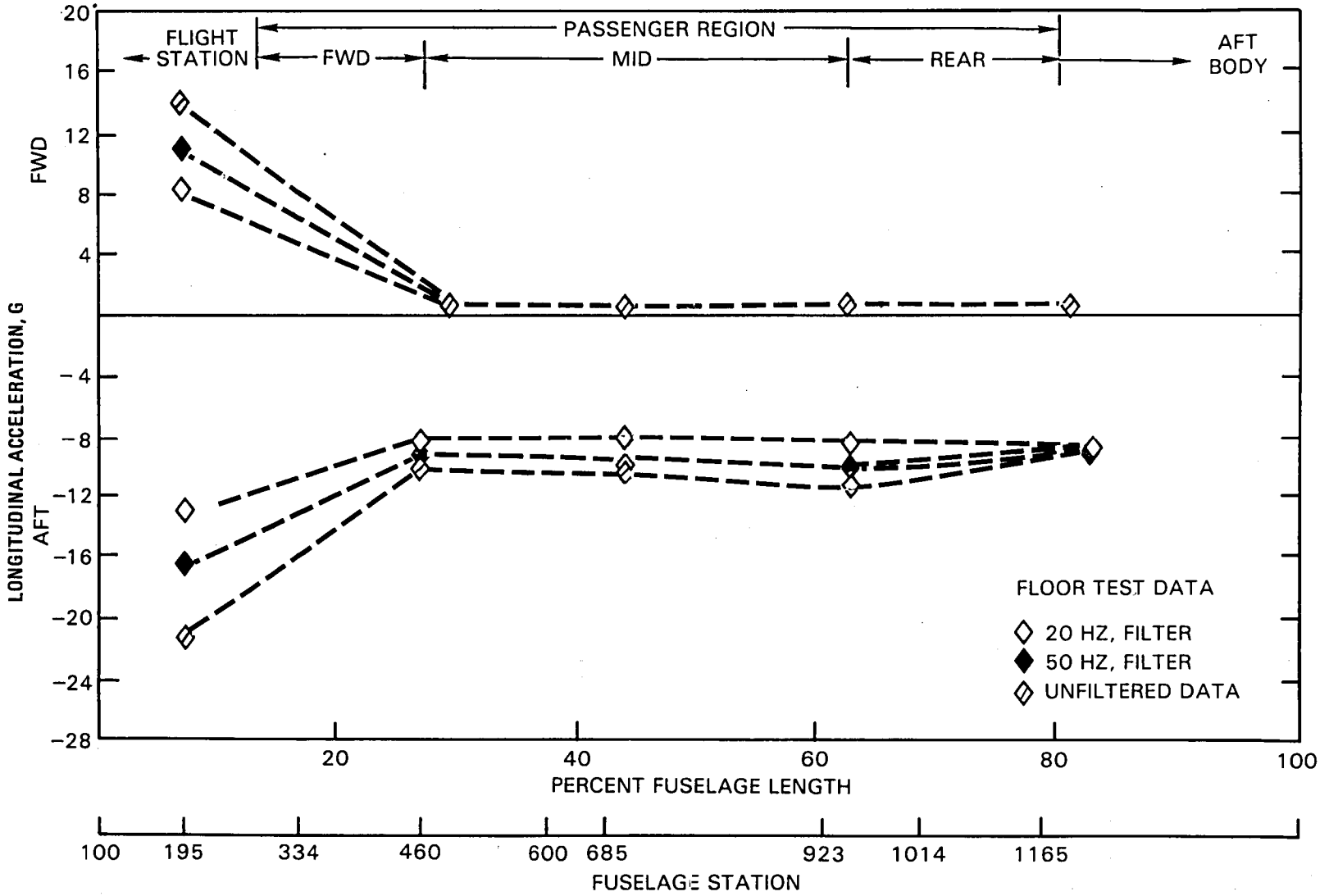

Figure 9-2. L1649 Unfiltered and Filtered Floor Pulse Test Data, Longitudinal Direction

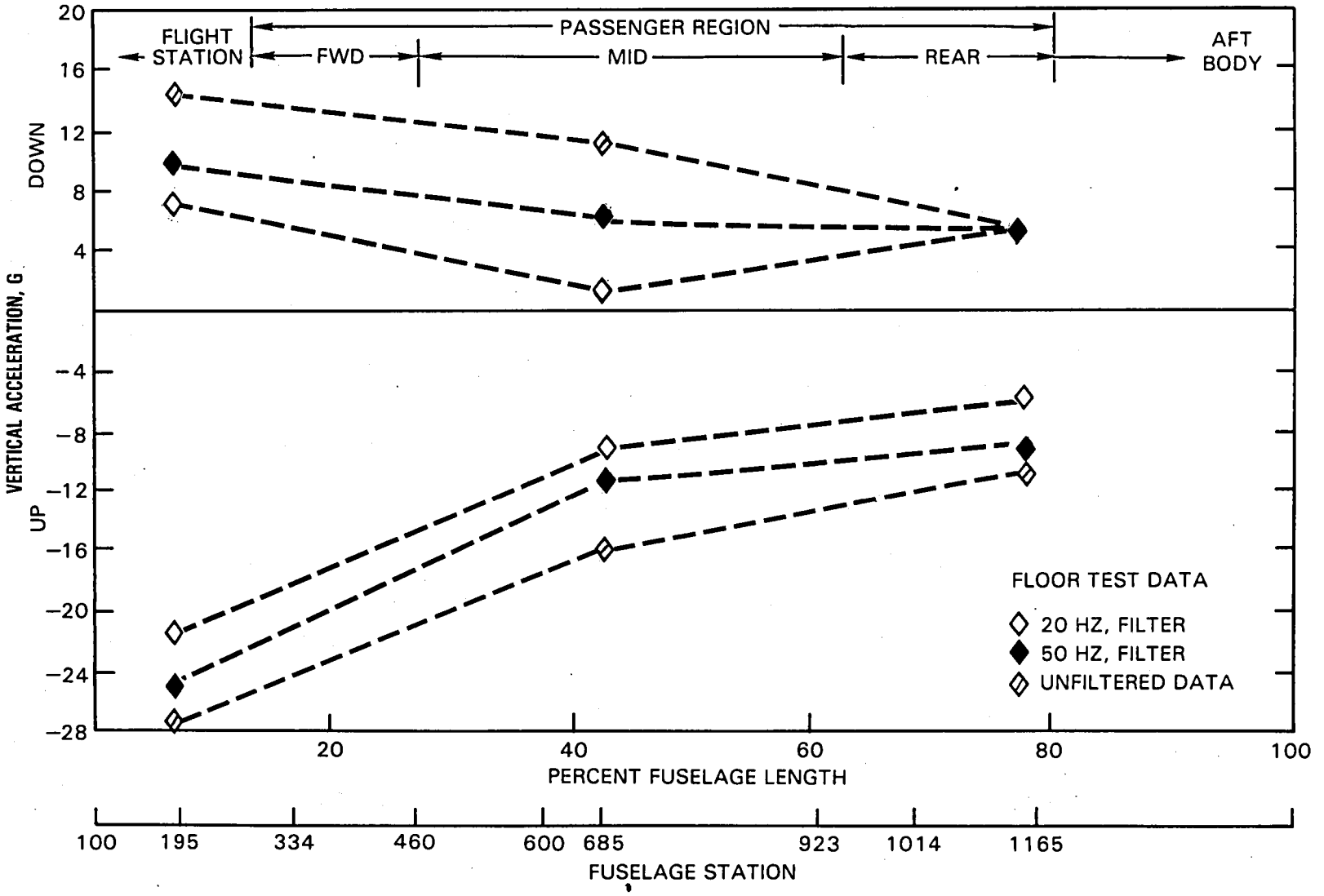

Figure 9-3. L1649 Floor Pulse Unfiltered and Filtered Test Data, Vertical Direction

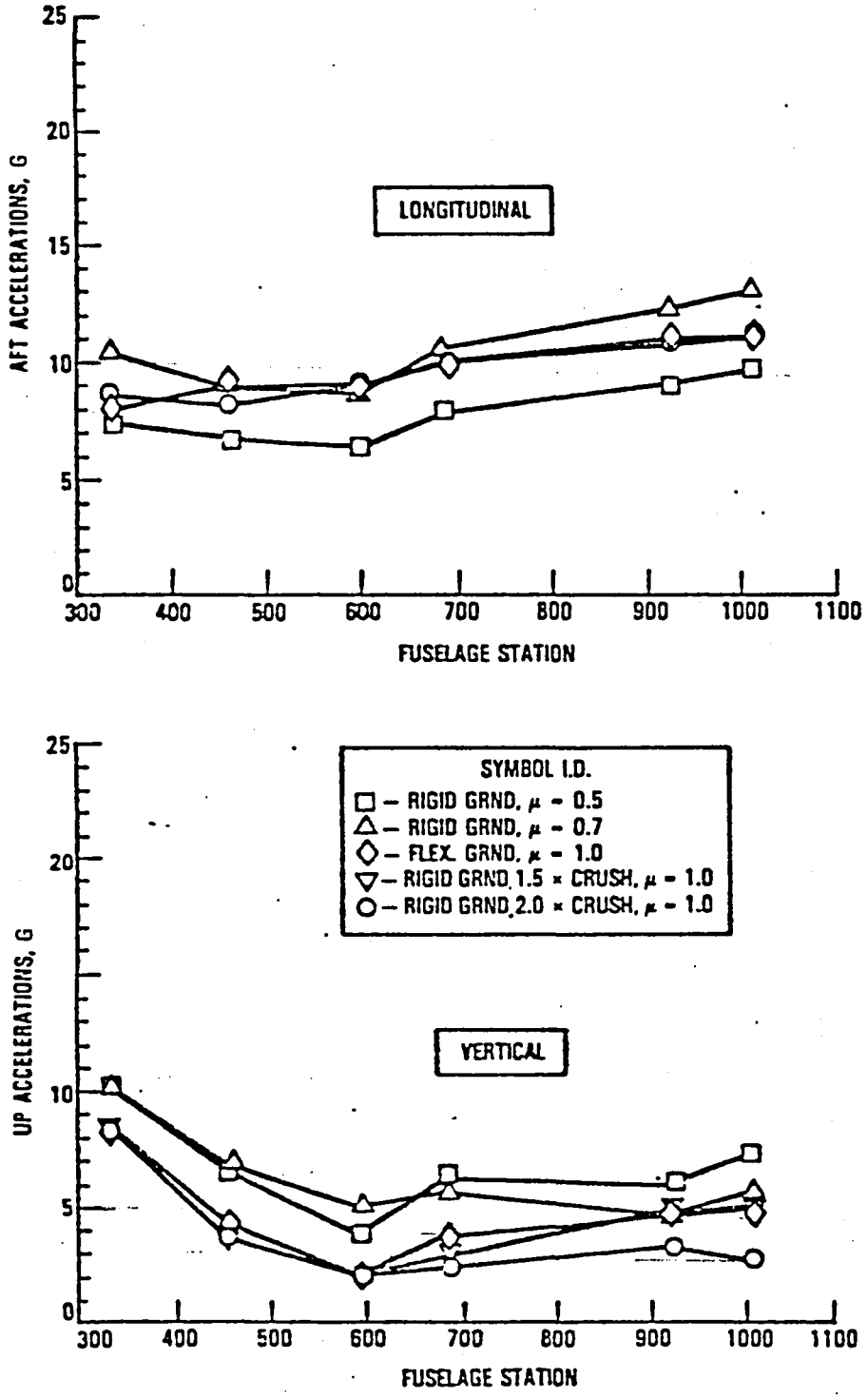

Figure 9-4. Comparison of Unfiltered Passenger Floor Peak Accelerations As A Function of Ground and Crushing Representations

The variation in vertical acceleration at the same fuselage station is ≈5 ±2g. When considering the flexible ground and increased crush representations only the variation in accelerations is more like < 10 percent in the longitudinal direction and < 25 percent in the vertical direction. Ground flexibility has the effect of providing additional fuselage underside crushing. The range of ±10 to ±25 percent is realistically the quantitative assessment that can be expected from a crash analysis.

9.4 Wide-body Airplane Candidate Crash Scenario Analysis

The candidate crash scenarios, depicted in Table 5-1, are analyzed to obtain peak acceleration (longitudinal and vertical) floor pulses. The results are summarized in Tables 5-3, 5-5, and 5-7. Figures 9-5, 9-6, and 9-7 show the peak simultaneous longitudinal-vertical, longitudinal-lateral and vertical-lateral responses at two floor locations for the ground-to-ground symmetrical overruns, the air-to-ground symmetrical hard landings and the unsymmetrical impacts, respectively.

The ground-to-ground overrun accelerations are shown in Figure 9-5. The peak dynamic longitudinal pulses associated with slope impacts can be as high as -13.4 G_X. However, as was shown in Section 8 (Figure 8-5), the effective step pulse is more like -4.8 G_X and with an equivalent static $\leq$-9 G_X. This scenario condition produces combined vertical-longitudinal pulses which should be considered in evaluating seat performance.

From Figure 9-6 it can be noted that the loading direction is primarily vertical with maximum peak upward accelerations in the range of -3.5 G_Z to -7.5 G_Z. The downward acceleration pulses are generally of short duration ($\leq$ .060). The peak longitudinal (dynamic) pulses are relatively small in magnitude with all but one response less than -3.7 G_X.

The results for the yaw condition for both air-to-ground and ground-to-ground crash scenarios are shown in Figure 9-7. The peak side loads produced in the air-to-ground analyses are generally $\leq$ 5 G_y, although an 8 G_y peak for < .040 seconds is noted. The corresponding vertical and longitudinal accelerations are comparable to their respective values produced in the symmetrical impacts

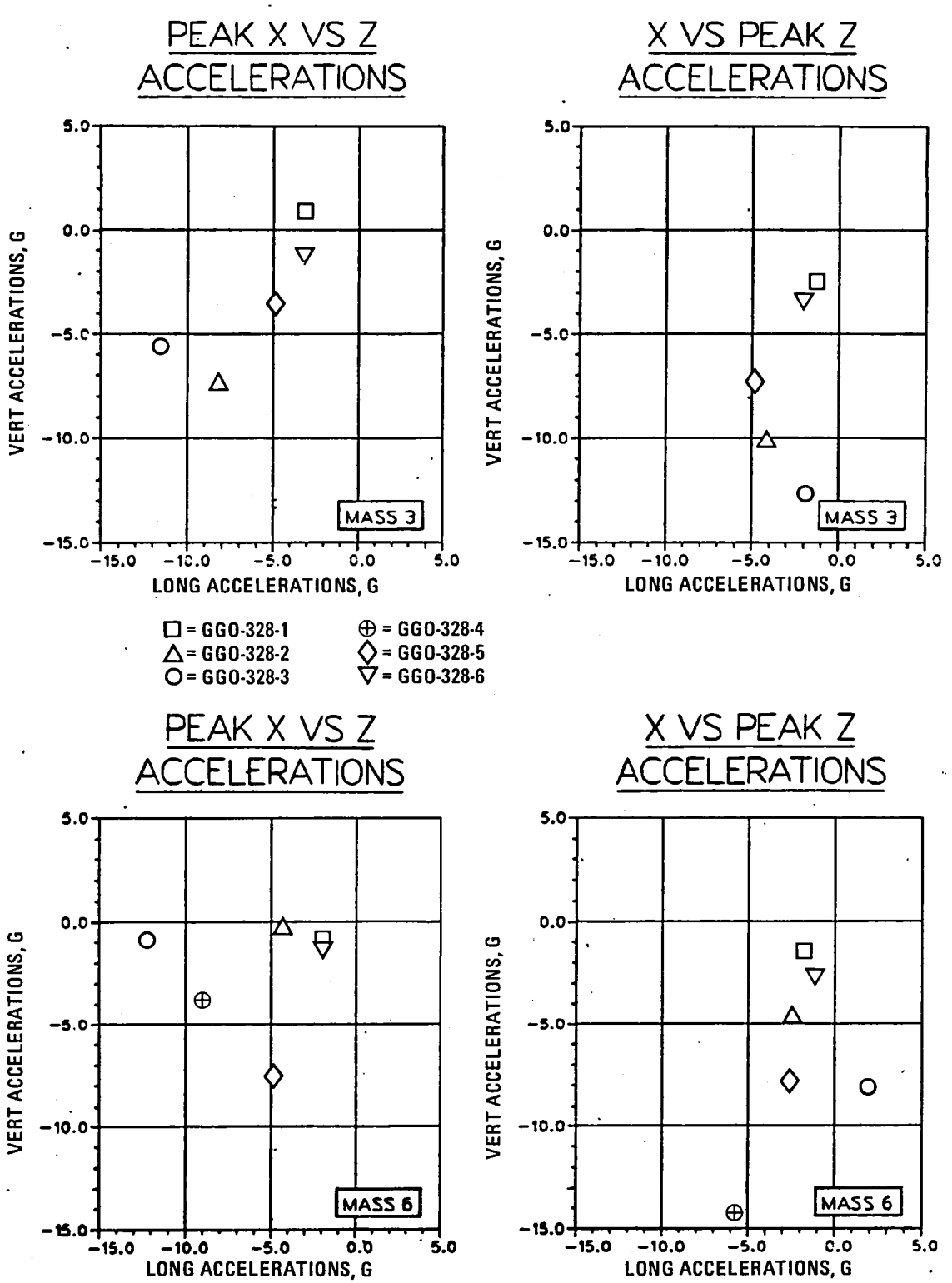

Figure 9-5. Simultaneous Accelerations, Ground-To-Ground Symmetrical Overruns

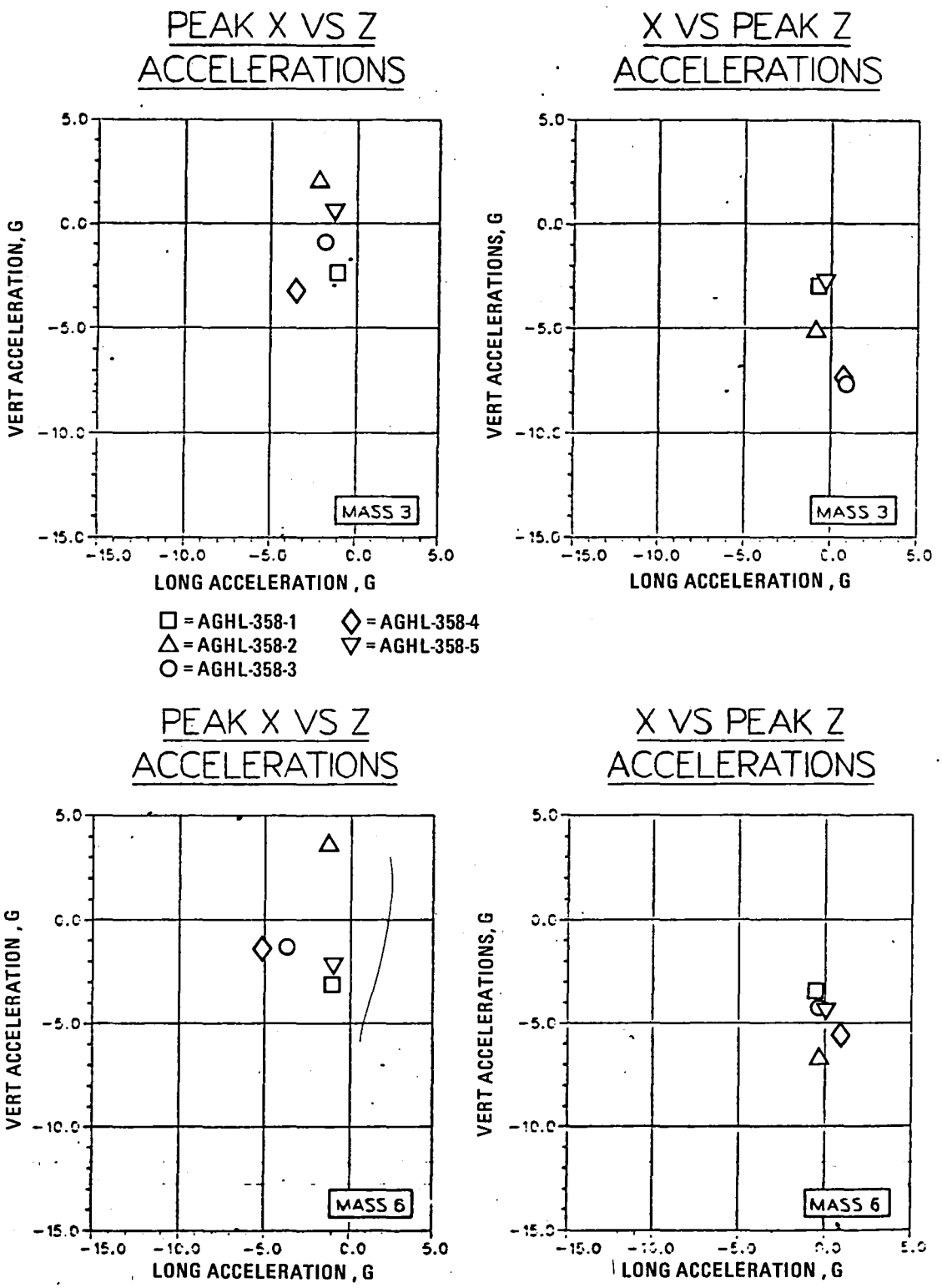

Figure 9-6. Simultaneous Accelerations, Air-To-Ground Symmetrical Hard Landings

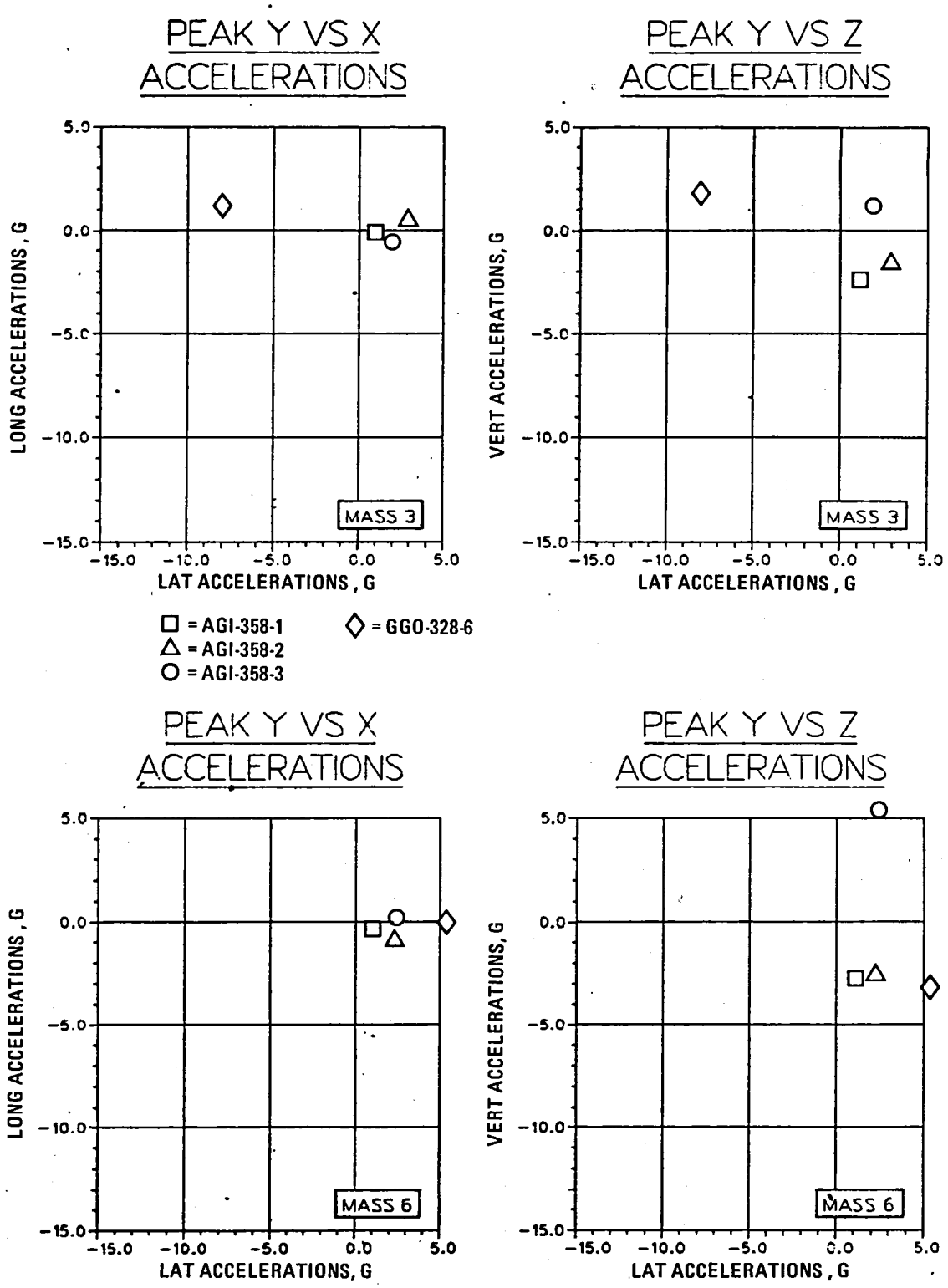

Figure 9-7. Simultaneous Accelerations, Unsymmetrical Impact Conditions

The time durations associated with the magnitudes, provided in Figure 9-5 through 9-7, are not shown. However, the response of both the seat and occupant can be affected not only by the peak acceleration but also by the relative durations of the seat-occupant system natural period and floor panel pulse. The consequence of the various candidate scenario pulses on seat and occupant performances is evaluated in Section 8.

9.5 Mass-Size Scaling Trends

Mass-size scaling trend analyses are described in section 6. The analyses are performed for only one crash condition; the simulated L-1649 six-degree slope impact. The assumptions for the trend analysis relate

- Crushing distance to available distance below floor
- Crushing force to aircraft weight
- Fuselage stiffness properties to aircraft cross-sectional properties
- Floor properties to aircraft type

The analyses based on these premises show a decrease in response as the size and weight of aircraft increase (see Figure 6-2). The trend insofar as aircraft, size and mass indicates potentially higher requirements for smaller narrow-body versus larger wide-body aircraft. As a rule one would inherently expect the larger aircraft design to reflect higher loads capability due to increased weight, (via sizing of members), since all current aircraft must meet the same load factor requirements. However, larger aircraft contain more crushable structure which overcompensates for impacts which occur at about the same sink speed. Or, looking at it another way, one can visualize that for the same sink speed the larger aircraft have the advantage of more crushable structure.

9.6 Transport Seat Test Evaluation

The FAA-CAMI seat test results are evaluated in Section 7. Acceleration (.030 second ramped step) pulse relationships for the longitudinal-only, the combined longitudinal lateral and the combined longitudinal-vertical-lateral

dynamic tests with unwarped floors are shown in Figure 9-8, 9-9 and 9-10, respectively. The results of the seat performances in the FAA-CAMI test series indicate that

- Body blocks for some seat configurations do not properly load the seat and improvements in the design are needed. A potential improved design used by the Navy is shown in Figure 9-11.

- Dynamic and static equivalence for longitudinal-only loading appear to exist, notwithstanding differences due to static body block versus anthropomorphic dummy loading. Failure modes for this type of loading are generally rear-leg tension at the attachment of the fitting.

- Since no vertical-only or predominantly vertical loading tests were performed, it cannot be ascertained what static equivalence to a dynamic condition for this type of loading may exist.

- The failure mode for the yawed condition is primarily a track failure which is different than the compression-tension type failures that can be expected from vertical or longitudinal loading conditions.

- While floor deformation could degrade seat performance, it

  (a) Appears to be less influential than side loading

  (b) Remains to be quantified in the crash environment

In conjunction with the seat test evaluation program, KRASH was used to model two and three-occupant seats for comparison with available test data. The analyses results duplicate the trends in the tests with regard to seat reactions and occupant responses.

9.7 Seat/Occupant Performance

The candidate crash scenario response pulses obtained via analyses and summarized in Section 7 were input into a KRASH seat-occupant representation. The load reactions and occupant responses are compared with results obtained from the use of the same analytical seat-occupant model with an idealized .030 second ramped pulse input, for a range of peak accelerations up to 9 g's.

The results of the ground-to-ground overrun analyses for longitudinal ($-G_x$) loading conditions; i.e., rear leg tension and seat belt loads, are plotted as a function of equivalent $-G_x$ ramped step input in Figure 8-5. From the data in Figure 8-5, following the procedure described in Section 8, it appears that an equivalent $-4.8\ G_x$ ramped step pulse could exist for the

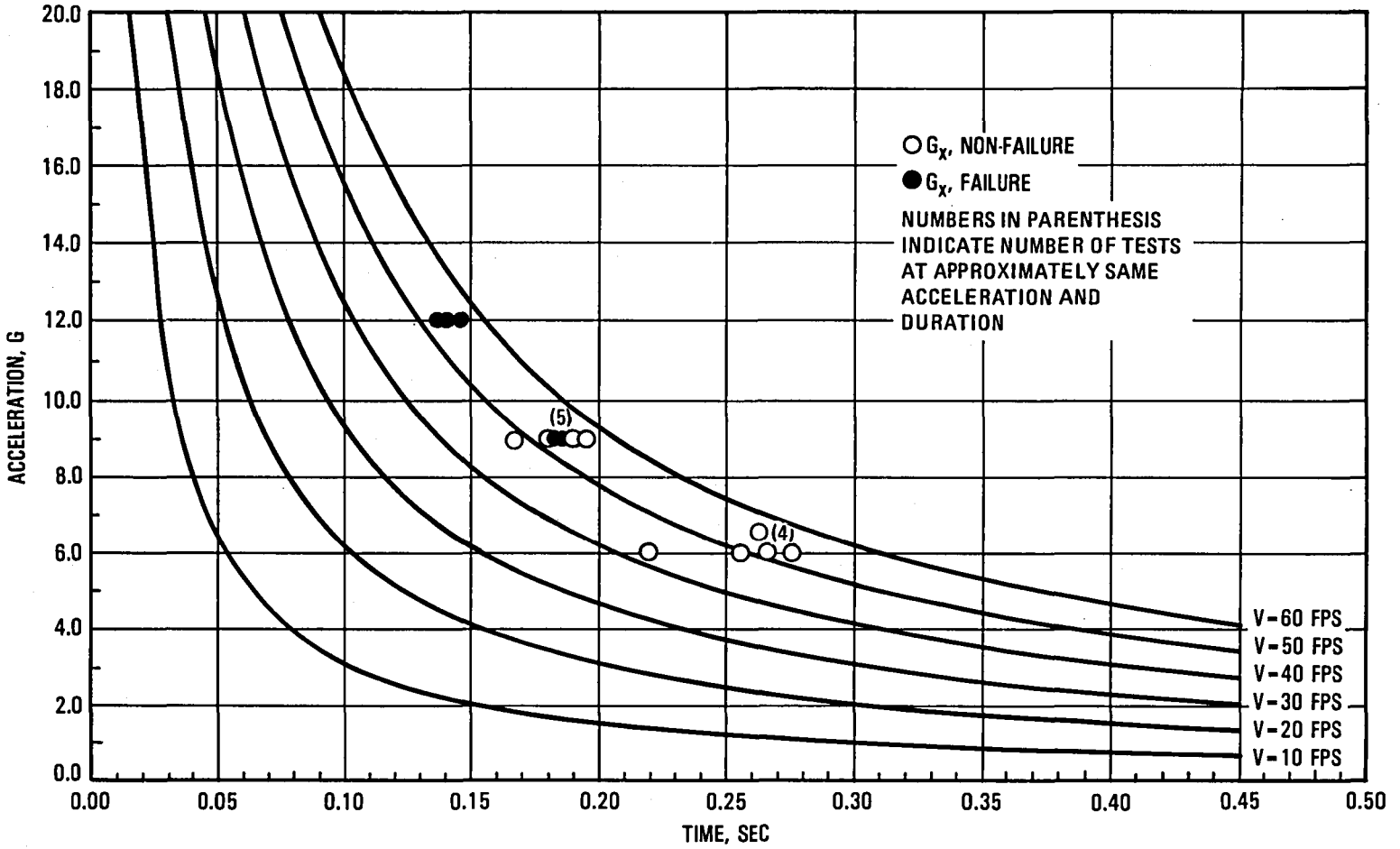

Figure 9-8. Acceleration Versus Time Duration, Longitudinal $-G_x$ Loading (Test No. 3) Condition

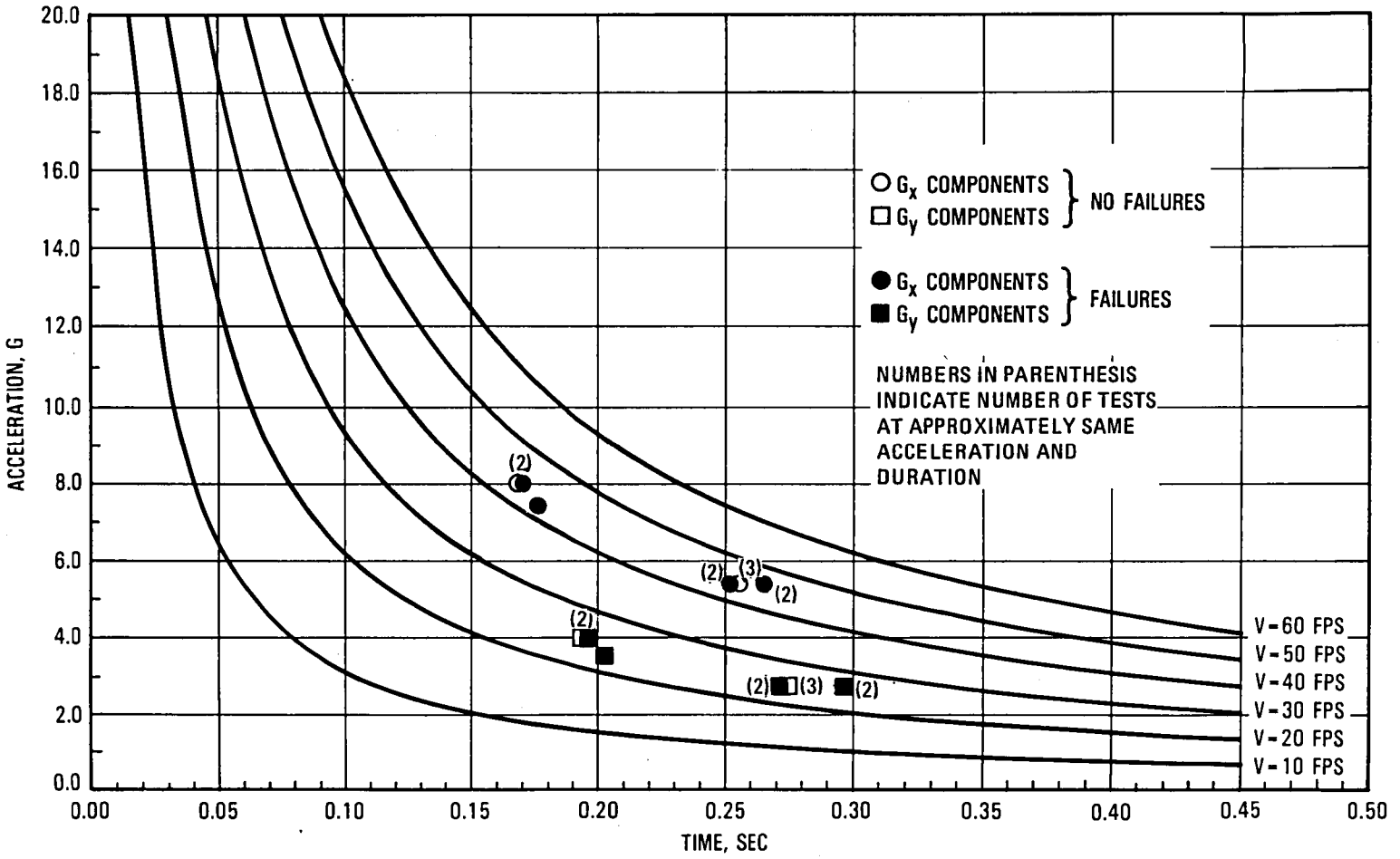

Figure 9-9. Acceleration Versus Time Duration, 30 Degree Yaw (Test 8) Condition

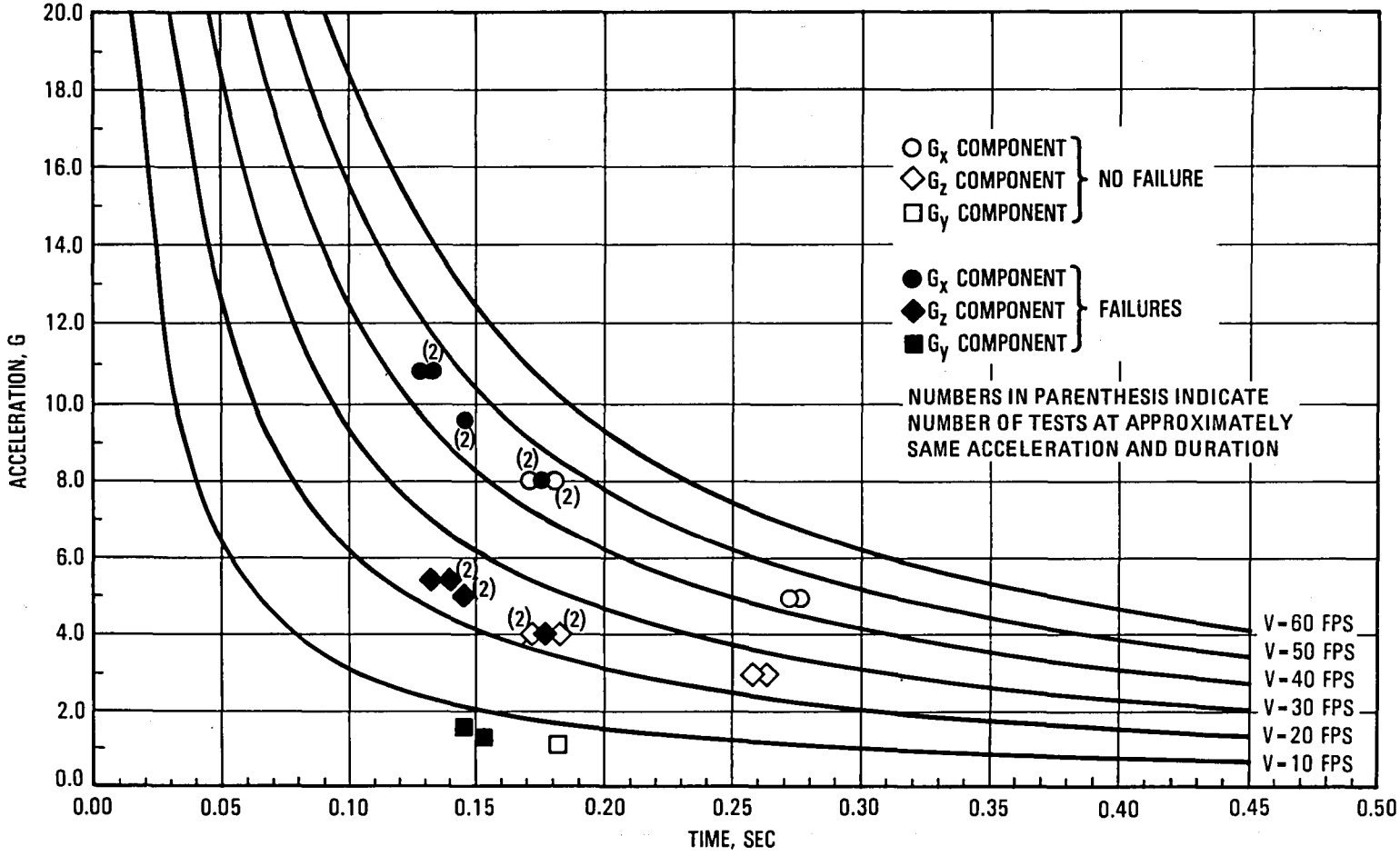

Figure 9-10. Acceleration Versus Time Duration, 9:4.5:1.5 Loading (Test No. 10) Condition

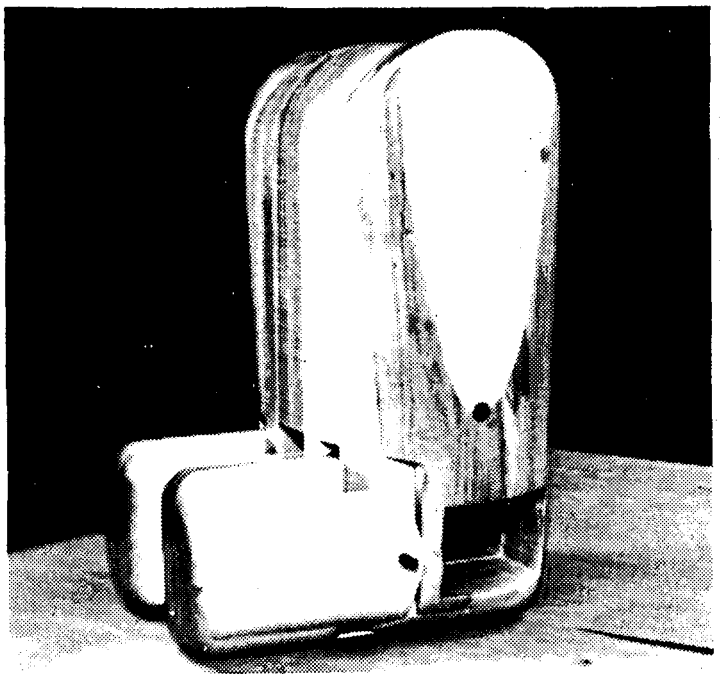

Figure 9-11. Potential Improved Body Block Design

most severe overrun condition analyzed. Based on a 1.7 static to dynamic amplification factor discussed in Section 7, the corresponding static value is -8.2 G_x. The results of these analyses indicate that the current 9G static seat forward-only loading requirement is adequate. There is little evidence that floor sternumward loads (aft inertia) are significant in the crash environment. A nominal seat 3G static aft load requirement appears more than adequate.

The air-to-ground hard landing analyses show higher vertical than longitudinal acceleration responses. However, until analytical models are calibrated with experimental data, it will be difficult to quantify equivalences. Analyses to determine equivalent $-G_z$ ramped step input values for vertical only loading are described in Section 8. The results of analyses for hard landing conditions are shown in Figure 8-12. Based on a simple one occupant-seat analysis with an occupant-to-seat vertical stiffness of 2000 lbs/in equivalent step accelerations of approximately -4.3 G_z might exists for hard landing conditions. Using the L1649 test measured pulse and the same single occupant seat model, the equivalent step pulse is between -4.8 G_z and -5.3 G_z (Figure 8-12). Based on the analyses of the overrun conditions the equivalent $-G_z$ step value would be less using

the same analytical model and approach. The analysis shows higher equivalent step pulses; i.e. -5.6 G_z for condition GGO-328-G. However this condition is accompanied by some indication of marginally high fuselage shear and bending moments in the passenger region and thus the potential for fuselage deformation and/or breakup. Higher floor pulses are developed for conditions GGO-328-3, and -4, but as noted in Figure 8-13, the shear and bending moments are high enough to result in fuselage breakup, a condition which could invalidate the use of these as realistic floor pulses.

The transmissability of the floor pulse to the occupant is very dependent on the pulse shape and system frequency. Figures 9-12 and 9-13 illustrate this for a simple system. For the same ratio of t_ℓ/T the dynamic response factor differs for the two pulses shown. Thus, to quantify seat-occupant performance it is necessary to define both floor pulses and seat-occupant stiffness/mass properties. Pure vertical loading can be expected to produce leg compression loads. If the 1.7 amplification factor for longitudinal-only loading is applicable, the seat performance for vertical loads produces inertia loads approximately in the range of 7.0g to 9.0g down and 3.5g to 4.5g up, statically, with corresponding dynamic step pulses of ≈4.0g to 5.0g and 2.0g to 2.5g, respectively. This direction of loading is extremely sensitive to the crushable structure between the passenger floor and lower fuselage impact point, as well as the stiffness of the seat pan. Additional passenger seat tests for this direction of loading could determine the appropriate amplification factor to be used. The analyses results for vertical direction floor pulses for hard landing and overrun conditions may be further altered if the effect of combined longitudinal-vertical loading is taken into account. The symmetrical overrun analyses results show a need for evaluating combined longitudinal-vertical loading effects on seat-occupant performance. The unsymmetrical impact condition analyses results show the need to evaluate the effects of lateral loads. As noted earlier the loading in the lateral direction results in different failure modes than those associated with pure longitudinal loading. Track related failures are associated with a lateral loading condition. Transient Peak values of ≤5g lateral are noted in the analyses which may be equivalent to something in the order of 3g static.

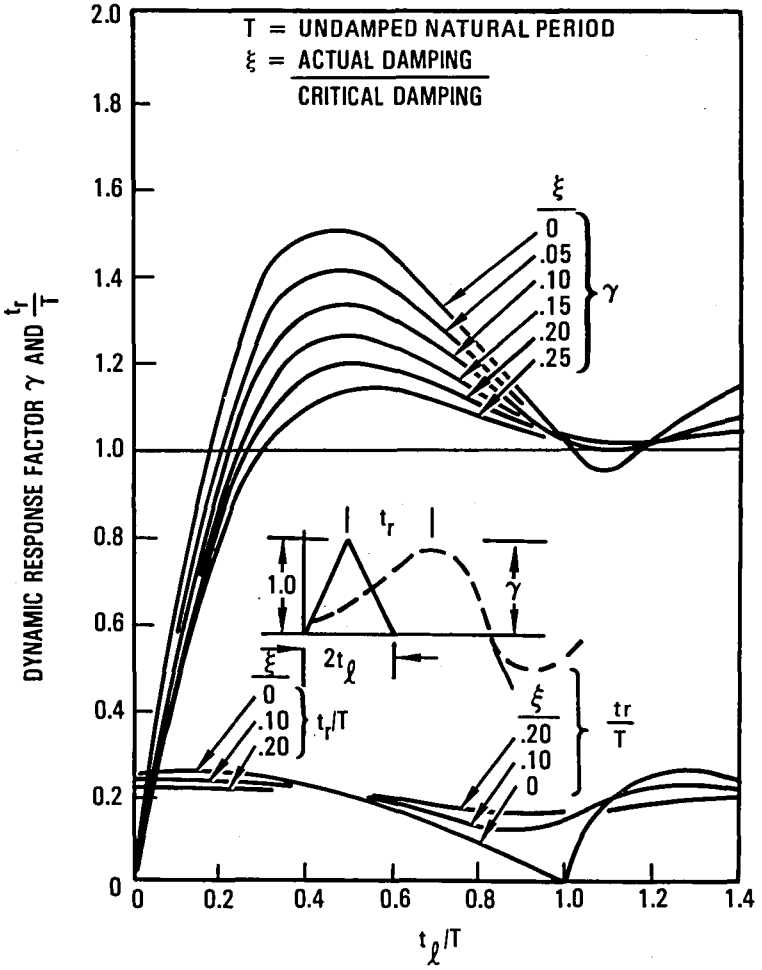

Figure 9-12. Dynamic Response Factor Curves for Triangular Pulse

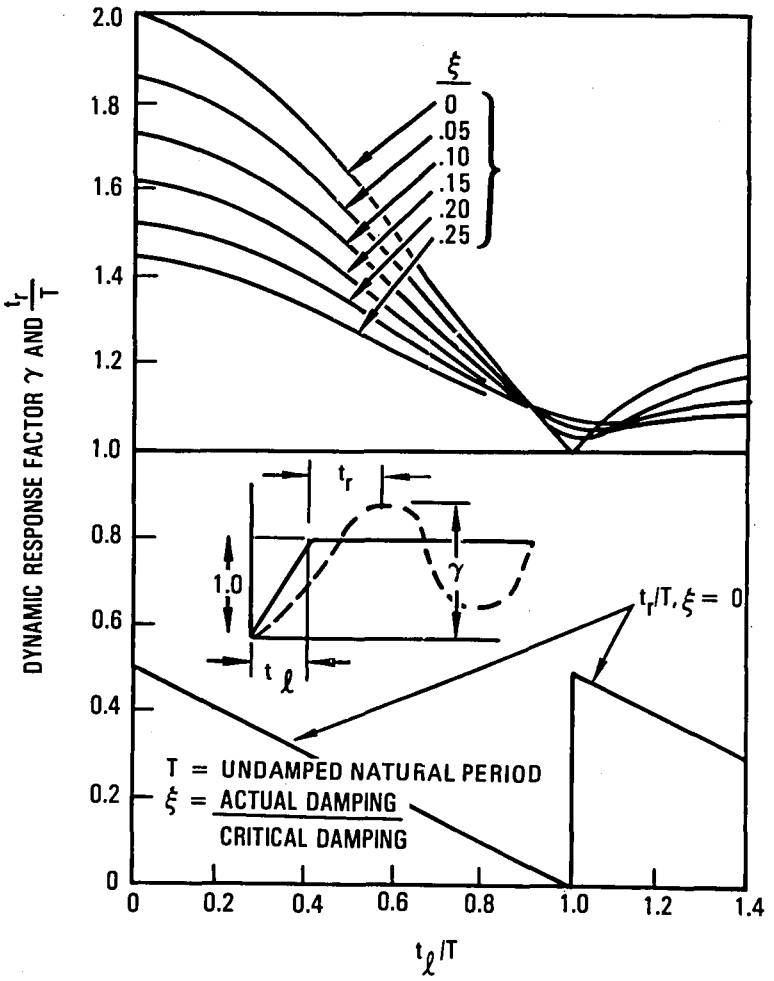

Figure 9-13. Dynamic Response Factor Curves for Ramped Step Pulse

9.8 Limitations of Analyses

The results of the various analyses are presented in Sections 4 through 8. In evaluating the validity of the analytical results it is important to understand the range of assumptions and the possible consequences of such assumptions. The following is a description of the pertinent assumptions which were used.

- The L-1649 six-degree slope impact test results are matched in the longitudinal direction in the passenger region. However, unless ground flexibility is assumed, the vertical responses appear high. Ground flexibility has the same effect as increased crushing distance on reducing vertical responses.

- The response of the airframe and floor, particularly in the vertical direction is significantly affected by the crushing characteristics of the structure. The current models assume that the loads from the impact point at the base of the fuselage underside are transmitted to the passenger floor via the floor posts, which are flexible and the airframe shell, which does not deform. Wherein loads can be high the shell lower sidewall might deform, absorbing energy and reducing load. A model which could account for shell deformation is shown below.

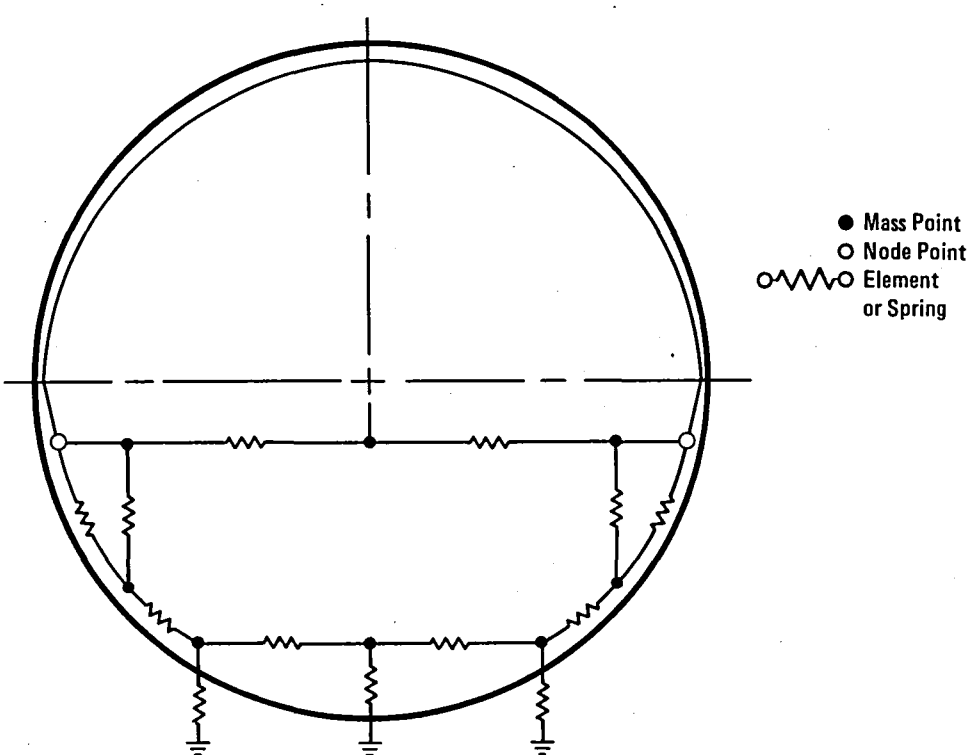

Obviously, this level of detail at several locations would enlarge the modeling requirements significantly. Vertical impact tests, using available sections, could prove valuable in assessing whether additional modeling detail is required. If significant shell deformation occurs one can expect that the peak accelerations obtained with a linear fuselage shell representation may be on the high side.

- The stub-wing model and rigid ground assumption used in the trend analyses simplify the KRASH model and allows for a comparison of results based solely on fuselage characteristics. If flexible ground were included, the results could be masked depending on the characteristics of the ground. The assumptions used to scale the aircraft math models are premises only and have not been verified with experimental data.

- Fuselage failure potential in the current analyses is based on exceedance of either a maximum shear or bending load. In reality a combination of simultaneous shear and bending will induce plastic deformation and/or failure. The incorporation of combined loads failure criteria in KRASH, as recommended in Reference 1, will enhance representations of combined loading conditions.

- The lift condition for wide-body analyses assumes a uniform 1G distribution. The actual aerodynamic lift condition is different and could influence some results. The inclusion of an improved KRASH IC subroutine, recommended in Reference 1, will allow this factor to be fully evaluated in a straightforward cost-effective manner, as well as enhance representations of test conditions in which initial loads or deformations (i.e. floor pitch and roll) are acting.

- The KRASH seat-occupant analytical models represent the occupant in a rudimentary fashion. The analytical results appear to compare favorably with regard to seat loads and can show occupant fold-over motion. However, without additional refinements occupant motion can not be expected to be depicted in total as a detailed occupant model would. Extending or combining KRASH capability with detailed occupant models for calibration with test data is both feasible and desirable.

9.9 Proposed Verification Program

Based on the evaluation of the FAA-CAMI transport seat tests, available floor pulse data and current candidate crash scenario analyses, a verification program is proposed. The salient features of the program outlined in Figure 9-14 are as follows:

- Perform drop tests of sections typical of several airplane categories to obtain crush characteristics which, in turn, can be utilized in a refined KRASH analysis of the crash scenarios. Include representatively loaded floor sections to ascertain transmissibility from the airframe, as well as obtain measureable pulses. Refine the KRASH model as

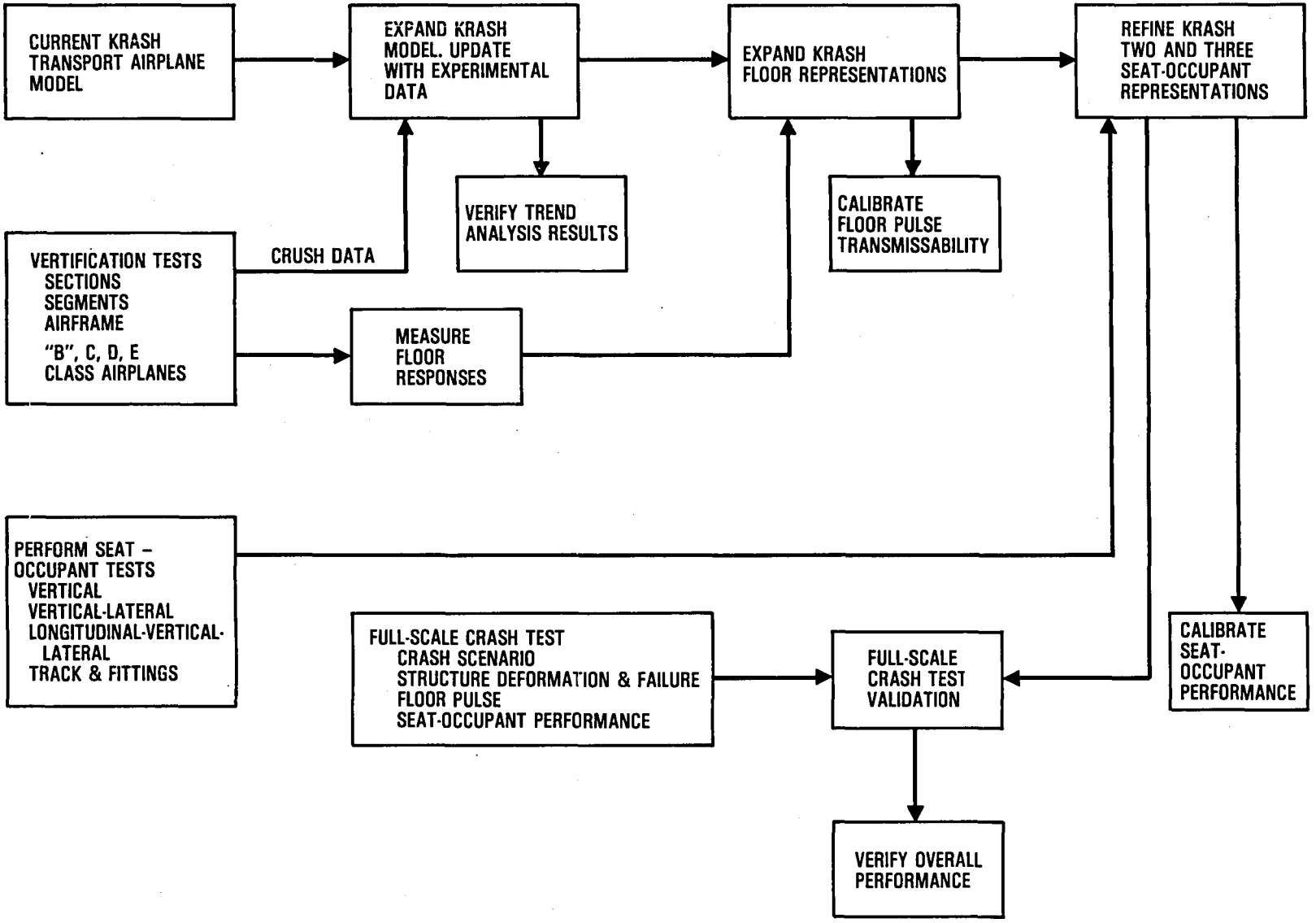

Figure 9-14. Flow Diagram - Proposed Verification Program

required to obtain floor pulses which are consistent with measured data. For each category of aircraft structure, 3 tests may be required to cover the range of sink speeds from 10 ft/sec to 20 ft/sec to 30 ft/sec.

- Perform seat-occupant tests to validate analytical models and complement the recent FAA-CAMI transport seat tests. As a minimum, the following tests are necessary.

  1. G_z vertical (upward) forces static and ramp accelerations dynamic, covering the range from 3 to 9 G's in intervals of 3G's and varying the ramp rate from .01 to .10 seconds. The data from these tests are to be used to verify seat stiffness properties on static and dynamic conditions and facilitate combined loading analyses.

  2. Combined $-G_z$ vertical (headward) and $-G_x$ longitudinal (spineward) decelerations with the following combinations.

$-G_x$	$-G_z$			
	3	4.5	6	9
3	•	•	•	•
4.5	•	•	•	•
6	•	•	•	•
9	•	•	•	•

  3. Combined Longitudinal-Vertical-lateral tests with G_y @ ±1.5 and ±3.0 in the following combinations:

	$-G_z$		
$-G_x$	3	4.5	6
3	•	•	•
4.5	•	•	•
6	•	•	•
9	•	•	•

  4. Investigate track and fitting integrity for side and combined loading conditions.

The results of all seat tests shall be used to form an envelope of performance such as illustrated below:

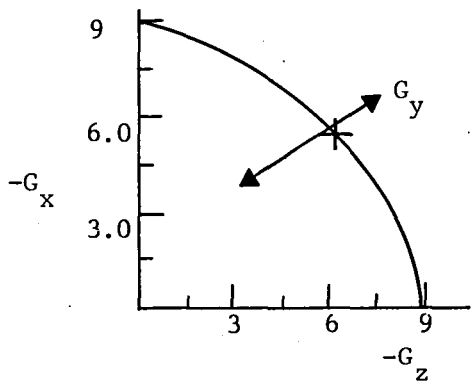

$G_y = 0, \pm 1.5, \pm 3.0$

The seat test results should be used to validate analytical models so that crash analysis pulses can be equated to equivalent ramp pulses. Measured parameters that can be used include:

1. Rear leg tension loads - longitudinal forces

2. Front and rear leg compression loads and deformation - vertical and combined loadings

3. Occupant $-G_z$ acceleration, Dynamic Response Index (DRI)-Vertical loading

4. Seat belt loads, - occupant G_x accelerations, - longitudinal loading

5. Track and fitting failure and deformation - lateral loading, combined loading

For tension failures, such as in pure longitudinal loading conditions, a static equivalence to a dynamic acceleration exists. In the case of a ramped acceleration pulse, the static equivalence is approximately 1.5 to 2.0 times the dynamic value. For compression failures the effect of dynamic instability, such as column buckling, as a function of rate of loading has to be determined in order to assess whether a static equivalence can be applied. For combined loading conditions, the determination of the predominant directional force or combination of forces which result in failure is needed.

- Perform airplane full-scale tests to verify analytical procedures. The test condition ideally should encompass at least one candidate crash scenario, result in fuselage underside crushing, floor damage, seat failure and possibly occupant injury. A Ground-To-Ground impact onto a 6° slope at 100 knots forward velocity would appear to be severe

enough to provide significant damage and cause occupant injury. This test condition is similar to the L1649 crash test impact conditions. However, this type of test requires protrusions such as pole or mound to ensure fuel spillage and breakaway of the landing gears prior to slope impact. An alternative test impact condition is an air-to-ground accident type. It would appear that a flight velocity $\geq$126 knots and a sink speed in excess of 20 ft/sec with a nose-up pitch attitude ($\geq 6^{\circ}$) could be extremely severe on the aircraft. Of concern on this test are 1) the failure mode of the landing gear, 2) the potential for fuselage breakup and 3) a need to induce fuel tank rupture. As noted in the air-to-ground hard landing analyses, this type of impact condition may not induce significant longitudinal loads. Thus, an overrun onto a sloped embankment while the airplane still has substantial forward velocity will most likely be necessary. Prior to the test, the potential impact conditions should be analyzed and parameterized to bracket anticipated results and, if necessary, alter the planned impact conditions.

Of prime importance is the need for a procedure to relate the crash environment pulse to seat test procedures. The results of this study illustrate a viable approach which utilizes state-of-the-art airframe analysis methodology combined with test results from an easily defineable test pulse. That procedure in step-by-step form is:

1. Obtain seat failure modes from a test process

2. Calibrate an analytical seat model with test data

3. Perform analysis to produce crash environment pulses

4. Analyze crash pulses using calibrated seat model to determine failure potential of occupied seat (1 cg attachment tension/compression, seat pan deformation, excessive lap belt load, occupant motion)

5. Use calibrated model results to equate to a standard pulse; i.e., step, triangular, trapezoid, etc.

In this manner, a series of arbitrary pulses each with a different peak G and shape can be compared with regard to critical behavior as produced by the standard pulse.

SECTION 10

CONCLUSIONS AND RECOMMENDATIONS

CONCLUSIONS

1. Crash Environment Analyses

   A. Floor pulses obtained from candidate crash scenarios range in direction, magnitude and duration as a consequence of variations in impact conditions and response locations.

   B. L1649 crash test floor pulses in the longitudinal aft direction (forward inertia) are less than 9g static and equivalent to $\leq$5g dynamic step pulse. The longitudinal forward (aft inertia) direction floor pulses are small (<3g transient). The equivalences for vertical-only or combined loading conditions need to be determined.

   C. The larger wide-body aircraft are expected to show floor pulses with magnitudes which are lower than the corresponding pulses for the smaller narrow-body aircraft. The actual amplitudes for floor response are strongly related to the amount of fuselage underside crush and ground flexibility or friction.

   D. The floor pulse shape, in addition to the peak acceleration value influences seat-occupant performance.

   E. Floor pulses for seat test requirements should be determined for conditions which preclude fuselage breakup and separation.

2. Seat-Occupant Performance

   A. The differences between static and dynamic test results obtained during the FAA-CAMI transport seat test program were primarily due to differences between static body block and anthropomorphic dummy designs.

   B. For the longitudinal-only ($-G_x$) loading condition, the primary failure mode is that of rear leg tension. This type of failure should not be affected by rate of loading. Thus, a static equivalence for $-G_x$ loading is appropriate for this condition, provided body block design improvements are achieved.

C. Performance of seats under combined longitudinal-lateral and longitudinal-vertical-lateral loading is degraded primarily as a result of track failure or leg pull-out from the track due to the introduction of side loads. Floor warpage is less significant than side loads in degrading seat performance, and more difficult to quantify.

D. Validation and calibration of analytical transport seat-occupant models with test data are feasible and practical approaches with which to assess seat-occupant performance during the crash environment. However, additional test data are needed to bracket seat performance and calibrate analytical models.

Figures 10-1 and 10-2 illustrate some of the salient conclusions.

RECOMMENDATIONS

1. Analyses

- Refine KRASH analytical methodology to enhance the treatment of all aspects of candidate crash scenarios including columnar impacts, combined loading effects and initialized aerodynamic loading.

- Investigate the refinement of transport airplane KRASH analytical modeling with regard to optimum fuselage mass segment representation as a function of airplane size, scaling parameters, airframe shell deformation and floor warpage.

- Validate KRASH two and three-seat/occupant representations with test data. Combine with an existing validated occupant model to improve occupant motion simulation.

- Extend KRASH analysis of candidate crash scenarios utilizing section, segment or airframe data and with measurements from a full-scale crash test.

2. Experimental Verification

- Perform substructure, section and/or airframe tests to provide substantiation of mass/size scaling trend premises and extend validity of crash scenario analyses.

- Perform additional seat tests to

  a) Develop a complete envelope of seat performance for a standard pulse

CRASH ENVIRONMENT ANALYSES

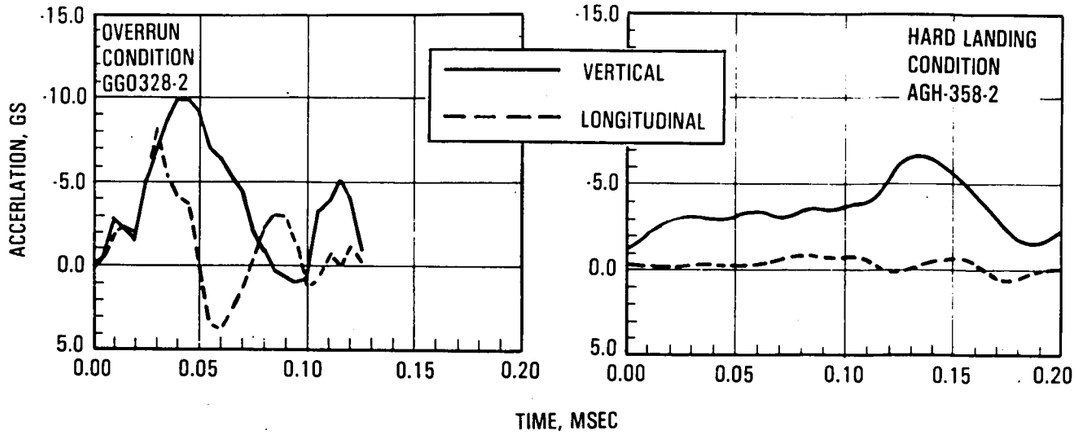

A. FLOOR PULSES RANGE IN DIRECTION, MAGNITUDE AND DURATION DEPENDING ON CRASH CONDITION

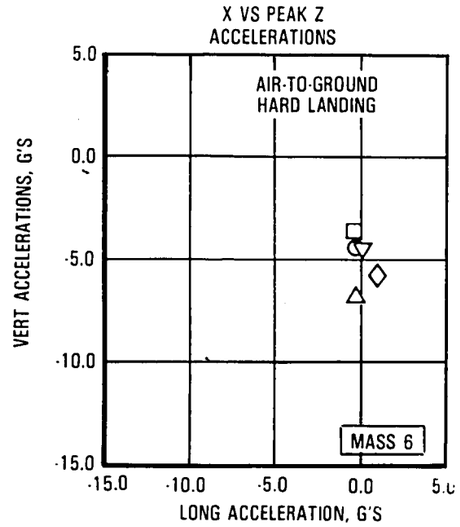

E. FLOOR PULSES FOR SEAT TEST REQUIREMENTS SHOULD BE DETERMINED FOR CONDITIONS WHICH PRECLUDE FUSELAGE BREAKUP AND SEPARATION

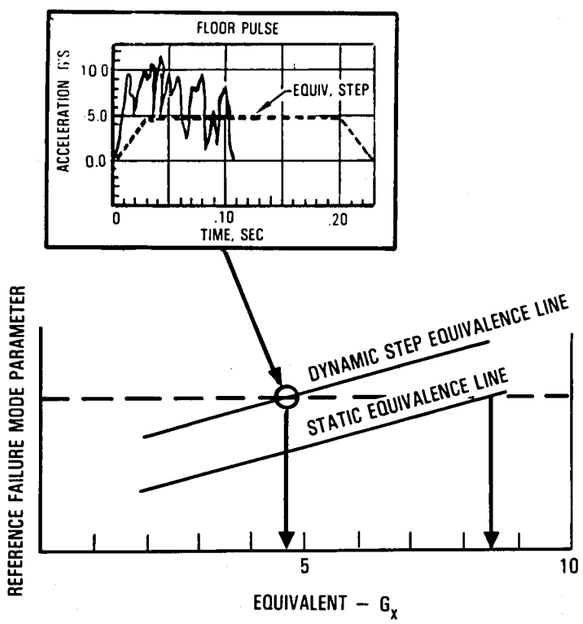

B. L1649 CRASH TEST FLOOR PULSES IN THE LONGITUDINAL AFT DIRECTION (FORWARD INERTIA) ARE LESS THAN 9G STATIC AND EQUIVALENT TO ≤ 5G DYNAMIC STEP PULSE

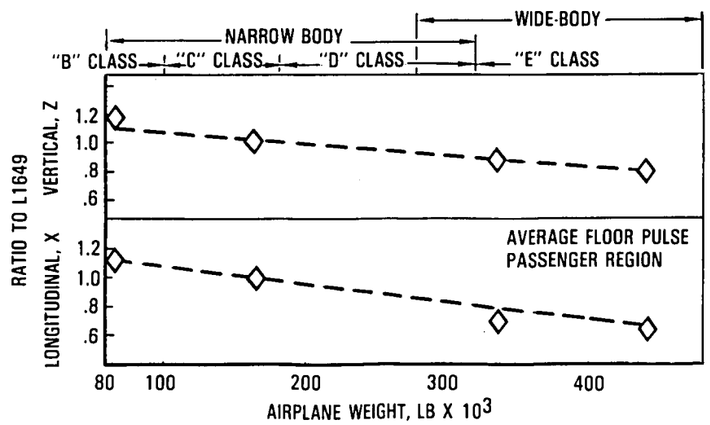

C. THE LARGER WIDE-BODY AIRPLANE ARE EXPECTED TO SHOW FLOOR PULSES WITH MAGNITUDES EQUAL OR LESS THAN CORRESPONDING PULSES FOR THE SMALLER NARROW-BODY AIRPLANES

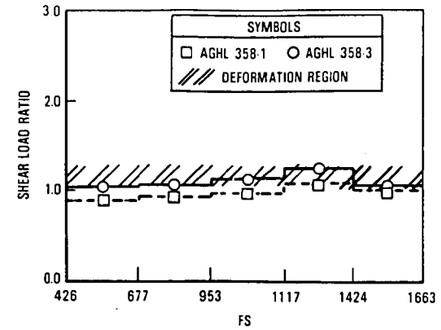

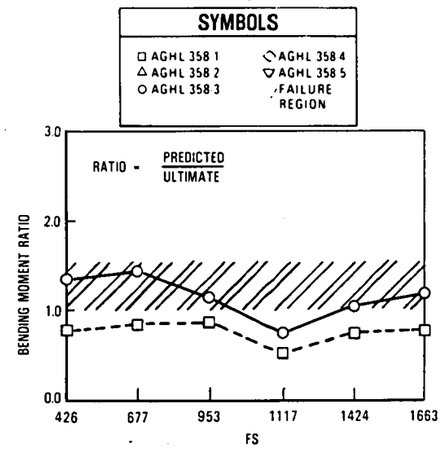

RESPONSE	-Gx PEAK	ΔV FT SEC	EQUIV STEP-Gx
MASS 3	7.6	11	3.3
MASS 6	7.5	11	4.8

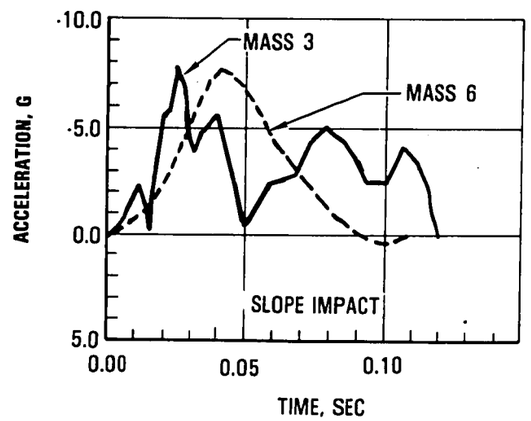

D. THE FLOOR PULSE SHAPE IN ADDITION TO THE PEAK ACCELERATION VALUE INFLUENCES SEAT OCCUPANT PERFORMANCE

Figure 10-1. Crash Environment Analyses Conclusions.

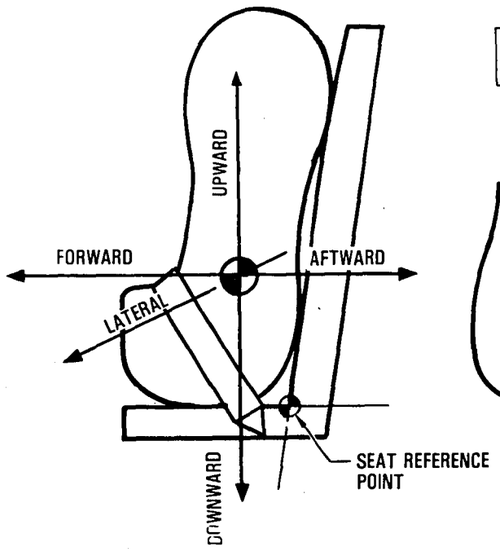

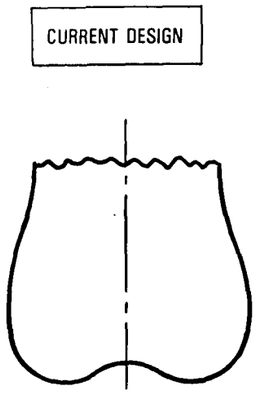

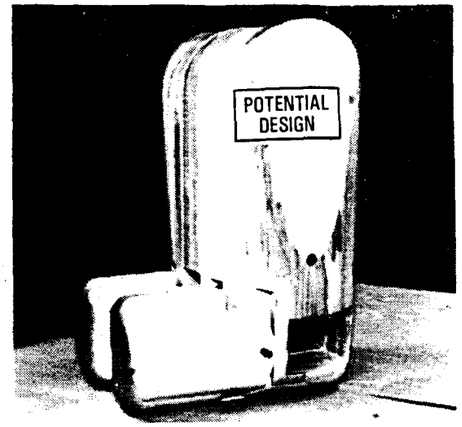

A. DIFFERENCE BETWEEN STATIC AND DYNAMIC TEST RESULTS FOR LONGITUDINAL ONLY LOADING CONDITION IS RELATED DIFFERENCES BETWEEN BODY BLOCK AND AND ANTHROPOMORPHIC DUMMY DESIGNS

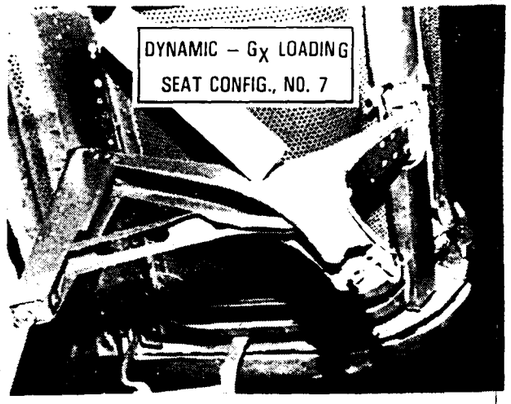

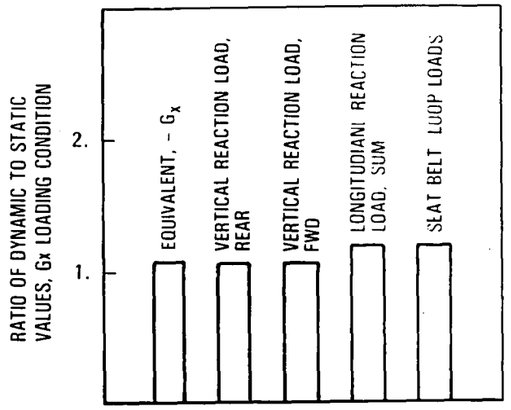

B. FOR LONGITUDINAL ONLY (-Gx) CONDITION A PRIMARY FAILURE MODE IS HIGH REAR LEG TENSION LOAD. STATIC DYNAMIC EQUIVALENCES CAN BE RELATED TO THIS TYPE OF FAILURE

SEAT – OCCUPANT PERFORMANCE

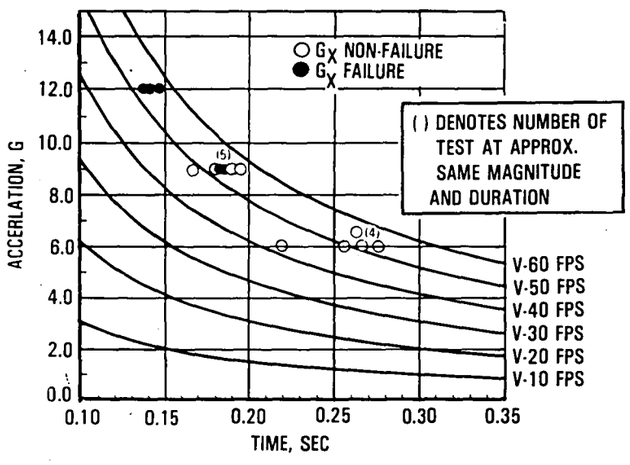

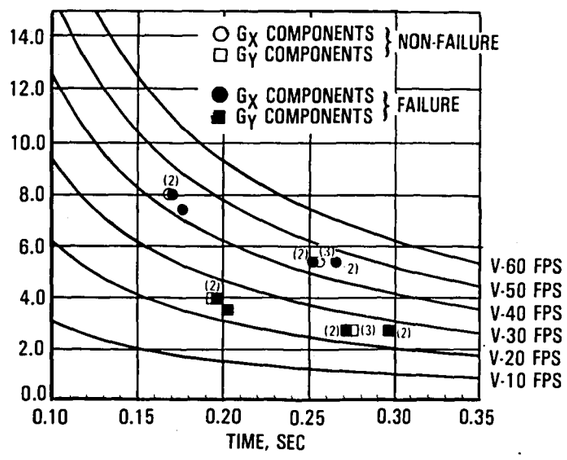

C. COMBINED LOADING CAN DEGRADE THE PERFORMANCE OF TRANSPORT AIRPLANE SEATS

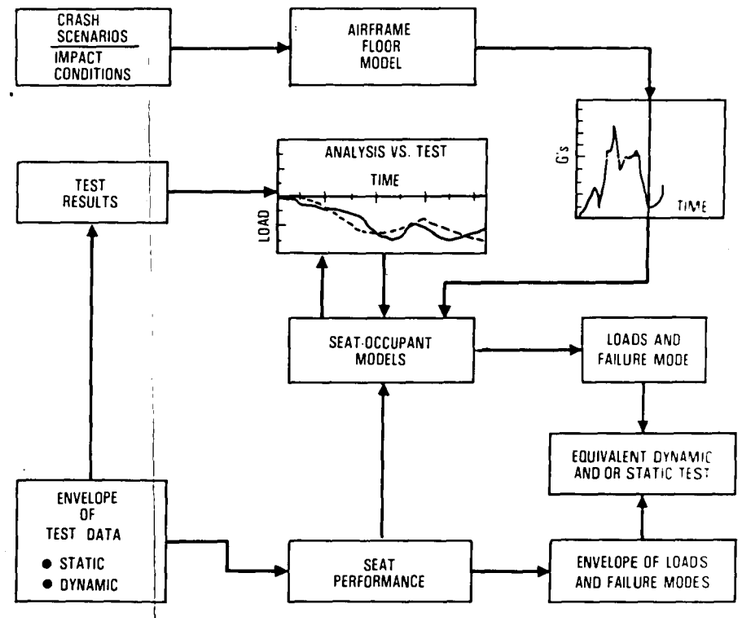

D. USE OF CALIBRATED VALIDATED ANALYTICAL SEAT OCCUPANT MODELS IS PRACTICAL FOR ASSESSING PERFORMANCE IN A CRASH ENVIRONMENT

Figure 10-2. Seat - Occupant Performance Conclusions

b) Validate and calibrate analytical seat-occupant representation

c) Perform complete evaluation of crash environment floor pulse severity envelope.

- Perform full-scale crash testing to verify analytical capability with regard to impact environment, airframe integrity, floor response and seat-occupant performance.

REFERENCES

1. Wittlin G.; Gamon, M.A.; and Shycoff, D.: "Transport Crash Dynamics," NASA CR-165851, DOT/FAA/CT-82/69, Lockheed-California Co., March 1982.

2. Federal Aviation Regulations, "FAR 25-Airworthiness Standards: Transport Category Airplanes," June 1974 (Amendments thru April 1982).

3. NACA Conference on Airplane Crash-Impact Loads, Crash Injuries and Principles of Seat Design for Crashworthiness, April 1956.

4. Reed, W. H., et al "Full-Scale Dynamic Crash Test of a Douglas DC-7 Aircraft, Aviation Safety Engineering and Research," FAA Technical Report ADS-37, Federal Aviation Administration, Washington D.C., April 1965.

5. Reed, W. H., et al "Full-Scale Dynamic Crash Test of a Lockheed Constellation Model 1649 Aircraft, Aviation Safety Engineering and Research," FAA Technical Report ADS-38, Federal Aviation Administration, Washington D.C., October 1965.

6. Wittlin, G. and Gamon, M. A., "Experimental Program for the Development of Improved Helicopter Structural Crashworthiness Analytical and Design Techniques," Lockheed-California Co., USAAMRDL-TR-72-72, May 1973.

7. Wittlin, G. and Gammon, M. A., "Full Scale Crash Test Experimental Verification of Method of Analysis for General Aviation Airplane Structural Crashworthiness," FAA-RD-77-188, Federal Aviation Administration, Washington D.C., February 1978.

8. "Light Fixed-Wing and Rotary Wing Aircraft Crashworthiness," MIL-STD-1290, January 1974.

9. "L-1011 Crashworthiness Studies of 5 FPS Landings with One or More Gears Retracted," LR 24664, Lockheed-California Co., Burbank, California, February 1974.

10. Chandler, R. F., Gowdy, R. V., "Loads Measured During Passenger Seat Tests" Civil Aeromedical Institute, Federal Aviation Administration, Oklahoma City, Oklahoma, Draft Report January 1982.

1. Report No. FAA Report DOT/FAA/CT-83-23 NASA CR-166089	2. Government Accession No.	3. Recipient's Catalog No.
4. Title and Subtitle ANALYTICAL MODELING OF TRANSPORT AIRCRAFT CRASH SCENARIOS TO OBTAIN FLOOR PULSES		5. Report Date April 1983 6. Performing Organization Code
7. Author(s) Gil Wittlin, Dave Lackey		8. Performing Organization Report No. LR 30141 10. Work Unit No.
9. Performing Organization Name and Address Lockheed-California Company Burbank, CA 91520		11. Contract or Grant No. NAS1-16083 13. Type of Report and Period Covered Nov. 1981 - July 1982
12. Sponsoring Agency Name and Address o U.S. Dept. of Transportation, Federal Aviation Admin. Systems Research & Devel. Service, Wash. D.C. 20590 o National Aeronautics & Space Admin., Wash. D.C. 20546		14. Sponsoring Agency Code FAA, NASA

15. Supplementary Notes

FAA Technical Monitor - C. Caiafa
NASA Technical Monitor - Dr. R. G. Thomson

16. Abstract

Transport aircraft candidate crash scenarios were analyzed with Program KRASH. Aircraft floor pulses and seat/occupant responses are presented. The study included 1) an evaluation of L1649 measured floor pulses during a six-degree slope impact test, 2) an assessment of mass and size effects on the peak responses, 3) analyses to determine responses of wide-body aircraft candidate crash scenarios, 4) an evaluation of FAA-CAMI passenger seat test results and, 5) an assessment of seat performance during potential crash environments.

Results of the study showed that: 1) Longitudinal-only pulses can be represented by equivalent step inputs and/or static requirements, 2) the L1649 crash test floor longitudinal pulse for the aft direction (forward inertia) is less than 9g static or an equivalent 5g step pulse. Aft inertia accelerations are extremely small (<3g transient) for representative crash scenarios, 3) a viable procedure to relate crash scenario floor pulses to standard laboratory dynamic and static test data using current state-of-the-art analysis and test procedures has been demonstrated. Floor transient acceleration pulses in the vertical, lateral and combined loading directions need to be analyzed with regard to seat-occupant performance using calibrated analytical models, and 4) floor pulse magnitudes are expected to be lower for wide-body aircraft than for smaller narrow-body aircraft.

Recommendations are presented with regard to extending current analysis capability and performing additional tests to support and verify analytical methodology.

17. Key Words (Suggested by Author(s))	18. Distribution Statement
Crashworthiness, Traneport Aircraft, Crash Dynamics, Analysis, Math Model, Floor Pulse, Seat-Occupant Response, Seat Test/Analysis	Document is available to the public through the National Technical Information Service, Springfield, VA 22161

19. Security Classif. (of this report)	20. Security Classif. (of this page)	21. No. of Pages	22. Price
Unclassified	Unclassified	193	

End of Document